Compositional diversity and thermal evolution of the Paleoarchean felsic crust: geochemical constraints from supracrustal zircons, apatites and rutiles from the Barberton Greenstone Belt, eastern Kaapvaal Craton.

by

Jean-Baptiste COMBAZ

*Dissertation presented for the degree of Doctor of Philosophy in the Faculty of Science at **Stellenbosch University** and **Université Toulouse III Paul Sabatier**, France, as part of the **cotutelle** agreement.*

The financial assistance of the National Research Foundation (NRF), the Centre National de la Recherche Scientifique (CNRS) and the EUR-TESS booster grant EUR TESS N°ANR-18-EURE-0018 in the framework of the Programme des Investissements d'Avenir towards this research is hereby acknowledged. Opinions expressed and conclusions arrived at, are those of the author and are not necessarily to be attributed to the different Research Funding institutions.

Supervisor: Professor Gary STEVENS (SU)
Co-supervisor: Doctor Oscar LAURENT (UT3)

March 2026

Declaration

By submitting this dissertation electronically, I declare that the entirety of the work contained therein is my own, original work, that I am the sole author thereof (save to the extent explicitly otherwise stated), that reproduction and publication thereof by Stellenbosch University will not infringe any third party rights and that I have not previously in its entirety or in part submitted it for obtaining any qualification. The present dissertation contains one article submitted to a peer-reviewed journal and two unpublished research manuscripts. The writing and development of the thesis were the principal responsibilities of myself and, where this is not the case, a declaration is included in the dissertation indicating the nature and extent of the contributions of co-authors.

Date: March 2026

Abstract

Historically, felsic crust formation and thermal evolution in the Archean have been mainly approached through the study of tonalite-trondhjemite-granodiorite rocks (TTGs). These Na-rich granitoids are deemed to represent up to 80% of the > 3.0 Ga Archean geological record and their petrogenesis has fed intense controversies over the existence of uniformitarian and/or non-uniformitarian tectonic settings at this time. However, several lines of evidence suggest that the apparently TTG-dominated felsic crust might not actually reflect the compositional diversity of the > 3.0 Ga continental crust, due to preservation biases.

To track potential missing components of the crust and better investigate its formation and evolution mechanisms, this study has focused on the detrital record of accessory minerals, namely zircon, apatite and rutile, deposited in ca. 3.55 to 3.21 Ga volcano-sedimentary to siliciclastic successions of the Barberton Granitoid-Greenstone Terrane (BGGT) in South Africa. Detrital zircons have comparable Pb-Pb ages, yet different trace elements, and for a significant proportion of them, Hf isotopic compositions, than igneous zircons of the Barberton TTGs. Indeed, ca. 40% of detrital zircons from the ca. 3.21 Ga Moodies Group show Hf isotope patterns like zircons of seemingly minor, granitic/rhyolitic clasts deposited in the Moodies Basal Conglomerate, sampling a K-rich silicic upper crustal component that is currently under-represented in the preserved granitoid-gneiss basement. Additionally, TTG apatites from all three magmatic events of the BGGT (ca. 3.55, 3.45 and 3.2 Ga) are compositionally different from > 3.25 Ga and > 3.43 Ga detrital apatites (from the Fig Tree and Onverwacht Groups, respectively), which show that the latter must have crystallized in a non-TTG source, resembling late-Archean sanukitoid suites. Lastly, the preservation of ca. 3.47 Ga Pb-Pb ages in metamorphic rutile grains of felsic schists that went to P-T conditions of ca 8 kbar and 660°C at ca. 3.23 Ga requires rapid heating and cooling of the Southern BGGT at rates (20-50 °C/Myr) approximating those encountered in the late stages of exhumation of Phanerozoic metamorphic core complexes.

Collectively, evidence gathered from the inventory of supracrustal accessory minerals of the BGGT suggests that 1) as documented in several other Archean terranes, the BGGT is affected by strong preservation biases; 2) models describing the chemical transition from TTG to compositionally diverse granitoids from 3.0 to 2.5 Ga do not account for these preservation biases, as rocks of sanukitoid-like and granitic composition already existed as early as ca 3.43 Ga ago, but got poorly preserved; and 3) the BGGT behaved as a strong, cold and rigid block (stabilized by a buoyant lithospheric mantle depleted early) and experienced fast tectonic rates akin to those of modern orogenic systems. The data collected here finally stresses out the importance of detrital accessory minerals in reconstructing the history of Earth's earliest continents.

Résumé

Historiquement, la question de la formation de la croûte siliceuse à l'Archéen et de son évolution thermique ont été l'objet d'études centrées sur les roches de type tonalite-trondhjémite-granodiorite (TTGs). Ces granitoïdes riches en Na représentent jusqu'à 80% de l'enregistrement géologique archéen d'âge supérieur à 3.0 Ga et leur pétrogenèse a souvent nourri des discussions sur l'existence de processus tectoniques actualistes et/ou non-actualistes dans la Terre primitive. Cependant, un certain nombre d'indices récents semblent suggérer que le caractère dominant des TTG dans la croûte archéenne préservée ne reflèterai pas la diversité des lithologies initialement présentes il y a plus de 3.0 Ga et ce, en raison de biais de préservation.

Afin de tracer l'existence de composants manquants de la croûte et mieux comprendre les mécanismes de sa formation et de son évolution, la présente étude s'est penchée sur les minéraux accessoires, zircon, apatite et rutile déposés dans des séries volcano-sédimentaires d'âge ca. 3.55 à 3.2 Ga des terrains granitiques-et-roches vertes de Barberton (BGGT) en Afrique du Sud. Les zircons détritiques présentent des âges Pb-Pb comparables mais des caractéristiques en éléments traces et, pour une grande proportion d'entre eux, un signal isotopique en Hf différents des zircons magmatiques cristallisées dans les TTGs de Barberton. En effet, près de 40% des zircons détritiques déposés dans le groupe de Moodies (âge de dépôt de ca. 3.21 Ga) montrent une composition isotopique en Hf ressemblant à celle observée dans les zircons de clastes granitiques/rhyolitiques déposés dans le conglomérat basal de Moodies, celui-ci échantillonnant une croûte supérieure siliceuse riche en K qui n'est pas représentée dans le socle granito-gneissique parvenu jusqu'à nous. De plus, les apatites des TTG ayant cristallisé lors des trois principaux évènements magmatiques de la BGGT (ca. 3.55, 3.45 et 3.2 Ga) présentent des compositions chimiques différentes de celles des apatites détritiques d'âges supérieur à 3.25 Ga et 3.43 Ga (des groupes de Fig Tree et Onverwacht respectivement), ce qui laisse suggérer que ces dernières ont cristallisé dans un magma chimiquement différent des TTG présents à l'affleurement mais pouvant ressembler aux granites archéens tardifs connus sous le nom de sanukitoïdes. Enfin, la préservation d'âges Pb-Pb autour de ca. 3.47 Ga dans des rutiles métamorphiques

cristallisés dans des schistes siliceux passés dans le facies amphibolites (conditions P-T de 8 kbar-660°C) à ca. 3.23 Ga, nécessite un chauffage suivi d'un refroidissement rapide du sud de la BGGT à des vitesses comprises entre 20 et 50°C/Ma. Ces vitesses de refroidissement sont communément observées lors des étapes finales de l'exhumation des métamorphic core complexes d'âge Phanérozoïque.

Prises ensemble, les éléments rassemblés à partir de l'inventaire des minéraux accessoires supra-crustaux de Barberton laissent suggérer que 1) de la même façon que les autres terrains Archéens, la ceinture de Barberton est sujette à un biais de préservation conséquent ; 2) les modèles décrivant la transition chimique des TTG aux granitoïdes archéens tardifs plus diversifiés (et riches en K) entre 3.0 et 2.5 Ga ne tiennent pas compte de ces biais de préservation de la croûte paléoarchéenne puisque des traces de ces granitoïdes diversifiées subsistent dans les zircons et apatites détritiques d'âges supérieur à 3.43 Ga ; 3) la ceinture granito-gneissique-roches vertes de Barberton représente un block tectonique froid et rigide stabilisé par un manteau lithosphérique précoce et ayant pu subir des taux d'enfouissement et d'exhumation tectoniques proches de ceux observés dans les contextes orogéniques récents. Les données récoltées dans cette étude soulignent l'importance des minéraux accessoires détritiques dans la reconstruction de l'histoire des premiers continents de la Terre.

Acknowledgements

I dedicate this work to my Highschool teacher Madame Sylvie-DULBECCO-CHORON who ignited my interest in Earth Sciences during the mind-blowing and fantastic courses that she gave at the Lycée Buffon, Paris 15ème Arrondissement and the field trip that she organized at the Chenaillet Ophiolites in September 2016, nearly ten years ago. I figured out now that this PhD journey started right there, in the middle of the Alps, when I listened to my SVT teacher telling the class about how the gabbros we were sitting on were just remnants of a former Alpine Ocean now mainly lost to subduction. This is the place and time where I realized that I wanted to become a geologist. Without your passion and utmost dedication to your students, dear Sylvie DULBECCO, this PhD would never have been done. You played a significant role in my motivation and determination to become a geologist, and I wanted to thank you for that.

I want to thank my family, my parents Hervé and Christine COMBAZ who supported me during this adventure between two continents. They never stopped believing that I could do this despite the great distance that came to separate us when I went to South Africa. My sisters Alix and Clémentine are also among the people who played a pivotal role in the realization of this project through their sense of humor, love and affection even though I still cannot figure out a simple way to make them understand that rocks are not just “stones and pebbles” but can reveal fantastic stories. I say thank you to my great friends Mattéo GENAR, Antonin ABILLON, Hugo VARIN, Denis PEHLIC, Adam HERZOG, Hippolyte DE BUE and Paul WERLE without the emotional, brotherly support of whom the successful accomplishment of this work would have been exceedingly difficult.

My supervisors Professor Gary STEVENS and Doctor Oscar LAURENT are warmly thanked for their constructive and helpful supervision. As I often said to my colleagues and co-workers during the hard times associated with PhD work (and which were many here!), it was always impressive to me how they had solutions for almost any problems. Oscar, you have this intrinsic ability to restore motivation to me no matter how desperate I was. I often say to my co-workers and friends that no matter how bad you feel your PhD is going, if you spend 20 minutes discussing with Oscar you will feel like you can conquer the world again. This is not pure flattery Oscar. It truly reflects how I felt during these hard times when everything was going sideways, and you were there to bring motivation back up and find solutions to any problems. It is incredible.

I want to give a special recognition to my friends from Brazil whom I met during my travels between the GET in Toulouse and Stellenbosch University. First comes Dr. Marcel Vinicius SANTOS LEANDRO, the first person whom I met right when coming out of the bus to Crozierhof in September 2022. Marcel, you were an inspiration throughout this journey, and I enjoyed every single time that we spent working and hanging out together. You came with me to the field in Barberton at a time when little of the regional geology was familiar to me and you helped me with my samples and then with the processing and data interpretation and so many things afterwards. Saying “Thank you” is not enough my man, but this is what I will say here. Second comes Dr. Ariela Oliveira MAZOZ, the “old lady”, who taught me a lot about apatite and monazite profiling from her arrival to Stellenbosch in October 2022 to the time in Plettenberg’s Bay in June 2023, to the Goldschmidt Conference in Prague in July 2025. You are a great friend to me Ariela and your support has not gone unnoticed. Third, I want to give a warm thank you to Dr. Calimeria PASSOS DO CARMO from the GET whom I met during the pre-conference field trip of the Hutton in September 2023. Cali, you really helped me “fit in” at the GET and in Toulouse during my stay there. Your support (and that of Antoine Colmet-Daage, your husband) during the transitional times when I had nowhere to stay before taking the plane back to South Africa and when I was still searching for a place in Toulouse, really helped me. Lastly, my friend from Porto Alegre, Henrique ZUCHETTI FERRARI, is warmly thanked as he was always there to share some drink and go to Burger’N Co at Saint-Aubin in Toulouse and I had the pleasure to meet him in his country during a holiday time in June 2025 at Cambara do Sul. Henrique, you are a loyal friend and

I still cannot figure out how you never complain about anything. This, for a Frenchman like me, is harder to explain than zircon Hf isotopic tracking of crustal growth in the Archean for sure. 100%. Obrigado Irmaõ. Before I started this PhD, I did not know any Brazilian but now, thanks to Marcel, Ariela, Cali and Henrique, I feel like I have been living in Brazil for 10 years.

My Southern African friends from the Earth Science Department at SU Dr. Tahnee OTTO (South Africa), Dr. Steve CHINGWARU (South Africa-Zimbabwe), Dr. Josiah SHILUNGA "PJ" (Namibia), Rowin MARAIS (South Africa), Daniel FERREIRA (South Africa) and Helena FEST (Germany-South Africa) from SU are warmly thanked for their help and support that they gave me throughout this PhD time. I enjoyed explaining the story of Archean zircons to you guys and sharing a beer at Bohos occasionally. I still remember that 21st of June 2024 when we all went to Haute Cabrière Wine Farm in Frankshoek for my birthday. I am glad you enjoyed the croissants and pain au chocolat that they make here. Jaco DELPORT and Jean-Pierre NEL from the University of Pretoria, Stoneman Building, deserve a special acknowledgment of their effort in teaching me the right way to make a clean mineral separation through SELFRAG-sieving-shaking table and hand panning. Your contribution to the realization of this work is far from being minor guys. Jaco, I also want to give you a special recognition in that camping trip to Barberton which you organized with the students of UP to look at the sedimentary successions. It was a challenging moment for me to be in the position to explain my research on the field to second year students for whom making the connection between microscale and macroscale processes might be difficult, but it was good training, and I enjoyed it beyond description. I did not forget those times at night when you braaied for us all under a heavy rain and I will always say that you are the braai specialist everywhere I go afterwards. That time at 5 am at the Boer Market in Pretoria is also not forgotten even though I do not recall having been more tired in my life than that morning.

My French friends from the GET in Toulouse also deserve some recognition of their contribution to the making of that project. Hugo RAFFET, among them, needs a special acknowledgement since he hosted me for a few weeks in September 2023 at his place, rue de la Chaine in Toulouse, when I was searching for accommodation. My friends Marius ALLEBE and César DYSON also contributed to this success. I want to thank you guys for the incredible time we spent at the Aéroconstellation in Toulouse and then at the MNHN in Paris in September 2025. Matteo GIACCARI, Chloé VALENTI, Christine BOFFOUO, Thomas KONE, Loren TESSIER, Adda ABBOUD, Malissa BAKOUCHE with whom I enjoyed taking bus 27 to Minîmes at night, David GUIMARAES, Matheus TRAVERS are warmly thanked for their support and the good times we spent hanging around Toulouse during my stay here. The technical guidance of Françoise MAUBE for operating the Tescan SEM at the GET and of Sandrine CHOY for preparing mounts is warmly acknowledged.

The support of my Co-authors Dr. Nadja DRABON, Dr. Emilie BRUAND, Dr. Sarah GLYNN, Dr. Frédéric COUFFIGNAL, Dr. Philippe DE PARSEVAL through the writing of the different manuscripts of this PhD thesis is also acknowledged. Finally, I want to thank Prof. Jean-François MOYEN and Prof. Alain CHAUVET for their guidance on my second field trip to Baadplas and the southern Barberton Belt. I enjoyed discussing petro-structural processes shaping the syenites and various aplitic/phonolitic veins and sharing a drink with you at night.

Table of Contents

List of Figures

List of Tables

«The result, therefore, of this physical inquiry is, that we find no vestige of a beginning—no prospect of an end."

James Hutton, *The Theory of the Earth*

«We are like a judge confronted by a defendant who declines to answer, and we must determine the truth from the circumstantial evidence."

Alfred Wegener, *The Origin of Continents and Oceans*

« Nature is to be found in her entirety nowhere more than in her smallest creatures. »

Caius Plinius Secundus, « Pliny the Elder", *Historia Naturalis*

« Descends dans le cratère du Yocul de Sneffels que l'ombre du Scartaris vient caresser avant les calendes de Juillet, voyageur audacieux, et tu parviendras au centre de la Terre. Ce que j'ai fait. Arne Saknussemm. »

Jules Verne, *Voyage au Centre de la Terre*.

1. Chapter 1: General Introduction

1.1. The Continental Crust: what? where? and when?

The Earth's lithosphere comprises two different crusts of contrasting compositions, densities and thickness. The oceanic crust consists of basaltic-gabbroic rocks formed at mid-oceanic ridges which seldom reach more than 7 km in thickness. The continental crust, on the other hand, has a mean composition of andesite (SiO_2 between 57 to 63% Rudnick & Fountain, 1995; Taylor & McLennan, 1995) and reaches thicknesses up to 80 km in orogenic plateaus (Cawood & Hawkesworth, 2019; Chopin, 2003; Jaupart et al., 2016; Zhang et al., 2011). Both type of crusts experience drastically different processes with the oceanic crust being recycled into the mantle every ca. 200 Ma at subduction zones (except for ophiolites obducted during orogenesis; Dilek & Furnes, 2014; Miyashiro, 1975) while the continental crust, due to its lower density and higher buoyancy, remains at the surface for billions of years and thus acts as an archive of geological events that have affected the Earth's surface since its formation (C. Hawkesworth et al., 2024; C. J. Hawkesworth et al., 2017).

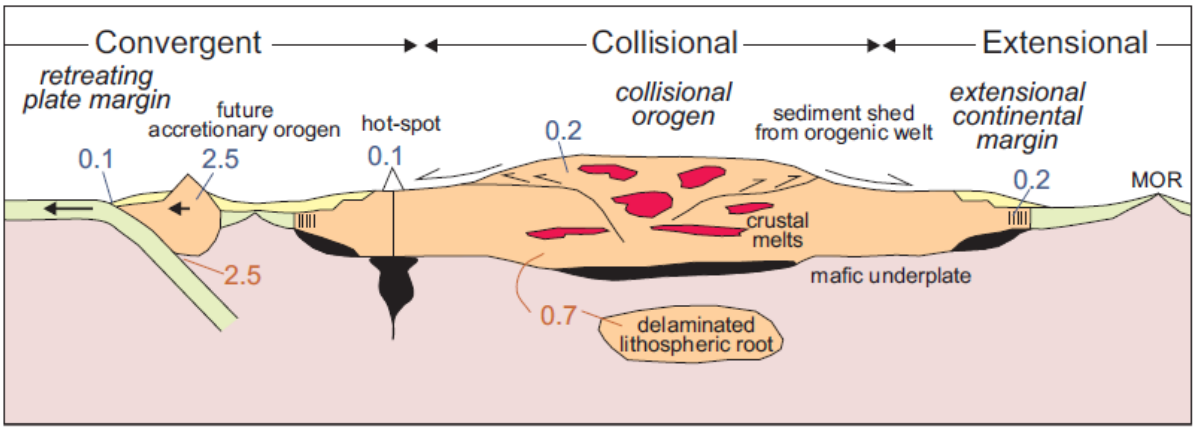

Figure 1-1 : Schematic representation from Cawood et al., 2013 illustrating the balance between volumes of juvenile additions (growth) vs volumes of recycled materials (recycling) to/from the modern continental crust.

The volume of continental crust present on Earth at any time of its history is a function of three time-integrated parameters: growth, recycling and reworking.

Continental crustal growth in the modern Earth mainly occurs at continental and island arcs through partial melting of mantle peridotite metasomatized by slab-derived fluids, which produces

basaltic/andesitic magmas that further extrude or differentiate within or at the base of the overlying crust (Castro et al., 2013; Jagoutz & Kelemen, 2015; Reubi & Müntener, 2022). Crustal recycling of continental material into the mantle does occur though through 1) delamination of lower crustal material (**Figure 1-1**, Beall et al., 2017; Johnson et al., 2014; Lustrino, 2005) in collisional settings, through "dripping" of cold garnet-rich residue (after the extraction of significant amounts of granitic melts, see Wolf & Wyllie, 1993) that is denser than the surrounding mantle peridotites and 2) erosion of exposed landmasses and subsequent subduction of terrigenous sediments at convergent margins (**Figure 1-1**, Scholl & Huene, 2009; C. R. Stern, 2011). It is estimated that, on the modern Earth, the volumes of juvenile continental crust generated at continental and island arcs are nearly compensated by the volumes of continental crust recycled into the mantle every year (**Figure 1-1** Cawood et al., 2013). Additionally, the continental crust experiences processes of intracrustal reworking which "*involves the remobilization of pre-existing crust by partial melting and/or erosion and sedimentation*" (definition from Cawood et al., 2013; C. J. Hawkesworth et al., 2010). This produces the hallmark vertical zonation of the continental crust into 1) an upper crust made of terrigenous sediments deposited on a granitic basement, 2) a middle crust made of amphibolite and lower granulite facies orthogneisses and paragneisses and 3) a lower crust that contains felsic and mafic granulites as well as mafic intrusive rocks (also see more nuanced interpretations in Hacker et al., 2011, 2015) (**Figure 1-2**). Partial melting of lower crustal rocks (termed "anatexis", Brown, 2007a; Harris & Massey, 1994; Raia & Spera, 1997; Sawyer, 2020) is partly responsible for the generation of granitic magmas that rise to the upper crust (through dykes, see Vigneresse & Clemens, 1999) and represent the dominant process of crustal reworking in the modern Earth. **Figure 1-2** (from Cawood et al., 2022) represents a schematic vertical cross-section of the different lithologies and metamorphic facies shaping the modern continental crust. A key question among geoscientists for the past 20 years has been to understand the evolution of the continental crust in terms of composition, structure and thermal behavior since the Archean (4.0 to 2.5 Ga), a period for which those three parameters are less well constrained.

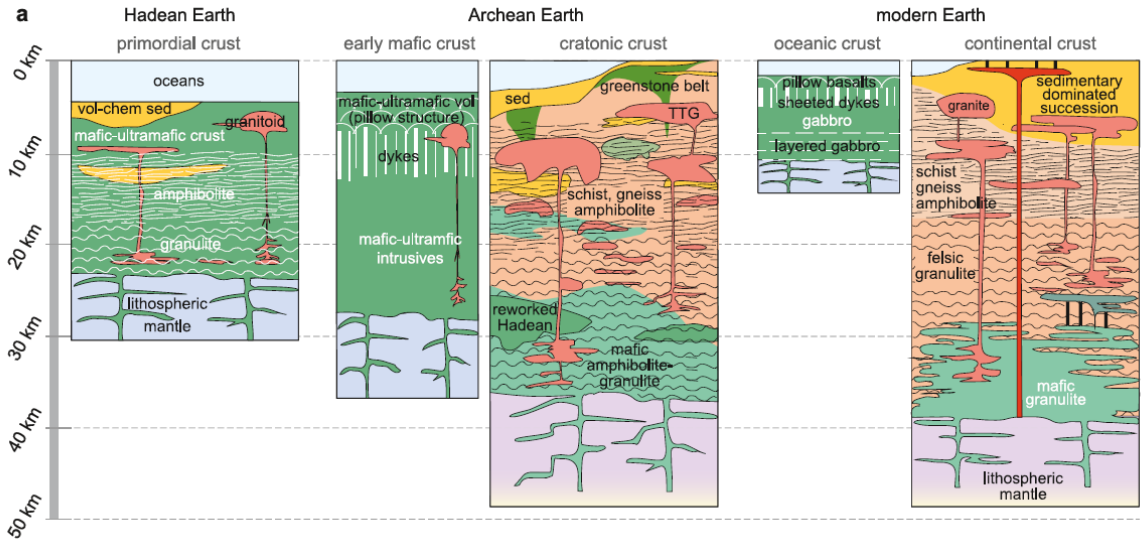

Figure 1-2 : Changing vertical structure of the continental crust from Hadean to present (from Cawood et al., 2022). Note the transition from TTG-granitoid magmatism in the Archean crust to a granite-dominated modern upper continental crust. Questions about the exact amount of felsic crust in Hadean and Archean time are still not fully answered. Explanation in the main text.

Terranes comprising old felsic rocks are localized in tectonically stable areas of the continental lithosphere and are referred to as cratons. Geologists can track the existence of evolved rocks of "continental" affinity, mostly in the form of tonalitic gneisses, to the 4.0 Ga orthogneisses of the Acasta Gneiss Complex in the Slave Craton, Canada (Bowring & Williams, 1999), while the oldest indirect evidence for exposure of felsic rocks to surface alteration comes from the discovery of 4.4 Ga detrital zircons in the Jack Hills metaconglomerates in the Yilgarn Craton, Australia (Cavosie et al., 2004; Wilde et al., 2001). Given the close association of felsic magmatism with subduction processes on the modern Earth, the high antiquity of these felsic rocks/minerals has often led geologist to propose that the classical subduction processes had operated back then (Hopkins et al., 2008) in similar ways as that documented in modern continental arcs. However, some controversy exists over the timing of the onset of a globally interconnected network of horizontally-moving lithospheric plates (see recent review from Harrison, 2024; Palin et al., 2020). Indeed, the formation of the Earth's earliest felsic crust in the Archean (period from 4.0 to 2.5 Ga) is also sometimes attributed to non-uniformitarian processes involving the partial melting of a magmatically overthickened, MgO-rich ultramafic crust at depth greater than c.a. 45 km (J. H. Bédard, 2018; Johnson et al., 2014, 2017; Palin et al., 2016; Smithies et

al., 2019) that produces melts of basaltic composition which, after crystallization, partially melt to produce the diagnostic continental rocks of the Archean i.e. tonalite-trondhjemite-granodiorite (TTG). In these models, the magmatic thickening of an ultramafic crust is a consequence of the higher degrees of melting of mantle peridotites, as a result of the higher mantle potential temperatures in the Archean (Herzberg et al., 2010; Korenaga, 2018). Such an allegedly higher mantle heat flow would have made the Archean continental lithosphere rheologically weaker and unable to sustain high topography (Korenaga, 2021; Rey et al., 2024; Rey & Houseman, 2006). Additionally, a higher mantle and crustal geotherm would prevent the burial of crustal material to eclogite facies conditions, which would explain the absence of the latter from the Archean geological record (Bjørnerud & Austrheim, 2004; Brown et al., 2020; Brown & Johnson, 2018; Gerya, 2014; Sizova et al., 2014). Transition to modern plate-tectonic processes is assumed by most geologists to happen diachronously from one craton to another, i.e. between 3.0 Ga and 2.5 Ga (C. J. Hawkesworth et al., 2017; Laurent et al., 2014, for more extreme opinions see Stern, 2005) and to be reflected in the evolution of the composition of felsic rocks preserved in Archean cratons, as will be better explained in the following subsection.

1.2. The evolution of the Archean continental crust

The petrological-geochemical study of the Archean geological record has been feeding intense debates about the timing of the onset of plate-tectonic processes for more than 40 years In particular, as detailed in this section, the Neoarchean period (ca. 2.9 to 2.5 Ga) represents the time when the upper felsic crust experienced a geochemical transition from a Na-rich composition towards a K-rich composition, which is often interpreted as marking the onset of modern plate-tectonics on Earth (Chowdhury et al., 2025; Condie, 2018; C. Hawkesworth et al., 2024; Laurent et al., 2014).

1.2.1. Before 3.0 Ga: greenstone belts and tonalite-trondhjemite-granodiorite plutons (TTG)

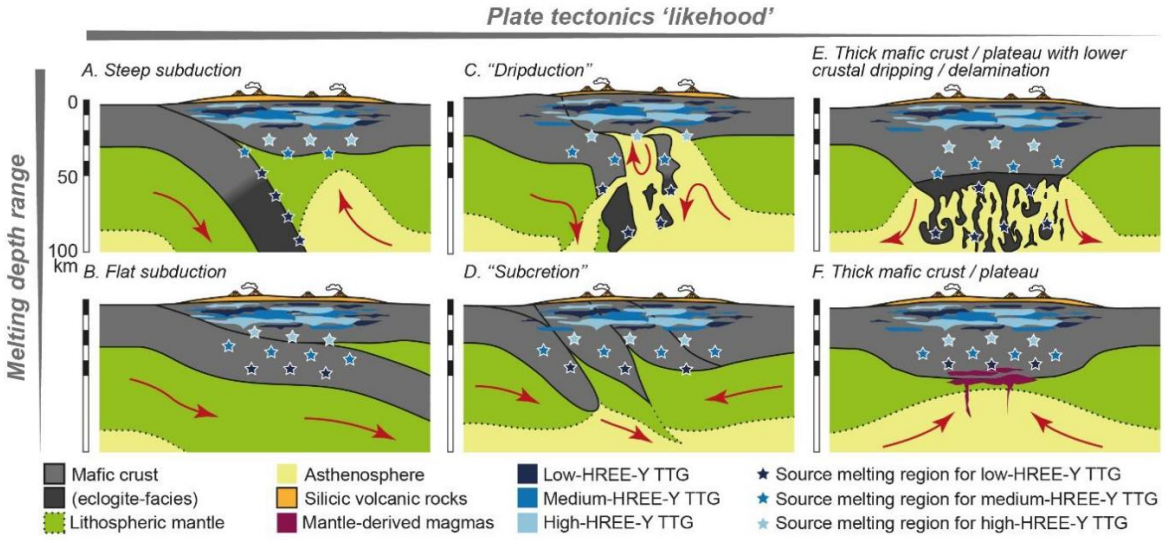

Figure 1-3 : The range of plausible tectonic environments that could produce Archean TTGs, from "uniformitarian" (left) to "non-uniformitarian" (right) and depending on the melting depth range considered, i.e. a wide pressure window of 0.5-2.5 GPa (top) or a more restricted one, i.e. ≤1.5 GPa (bottom) (from Laurent et al., 2024).

Before 3.0 Ga, the dominant granitoid component of cratons are Na-rich granitoids belonging to the Tonalite-Trondhjemite-Granodiorite (TTG) series (Jahn et al., 1981; Laurent et al., 2024; J.-F. Moyen, 2011; J.-F. Moyen & Martin, 2012). These sodium-rich granitoids represent from 50 to 80% of the volume of the preserved Archean crust older than 3.0 Ga (Bleeker, 2003; J.-F. Moyen, 2011; Polat, 2012). Closely associated with the TTGs and occurring as syn-formal keels or fold-and-thrust belts sandwiched between the plutons (like in the Barberton Granitoid-Greenstone Terrane, see section 1.5. below), are a mixture of ultramafic-basaltic volcanic rocks, chemical sediments such as the Banded Iron Formations (BIF) and minor clastic sediments. These are all grouped under the terminology of "greenstone belts", as a result of the greenish colors displayed by these supracrustal rocks (mostly due to the occurrence of greenschist facies mineral phases like chlorite or epidote, see Anhaeusser, 2014; Condie, 1981).

The geochemical properties of TTGs (Na_2O content > 4 wt%, enrichment in LILE, fractionation of their REE spectra with variable depletion in HREE, absence of Eu anomaly, cf Laurent et al., 2024; Martin, 1986; J.-F. Moyen & Martin, 2012), combined with their rare occurrence in the Phanerozoic

crust with respect to K-rich granitoids, have been related to a range of tectonic contexts of magma production either resembling modern-day subduction processes or being drastically different and non-uniformitarian (**Figure 1-3**). Some studies advocated the formation of TTG-like melts through either partial melting of basaltic crust (e.g. Bédard, 2006) or fractionation of mafic melt derived from a LILE-enriched lithospheric mantle (e.g. Johnson et al., 2014; Smithies et al., 2019), both taking place mainly within the lower crustal roots of an overthickened oceanic plateau (**Figure 1-3E-F**). In contrast, other authors (Martin et al., 2005, 2014; J.-F. Moyen & Martin, 2012) supported the petrogenesis of TTG-like magma being a consequence of partial melting of a LILE-enriched Archean tholeiite tectonically buried at high depth in the mantle, i.e. a process more akin to modern convergent margin settings (**Figure 1-3A-B**). Intermediate tectonic contexts such as dripduction (Nebel et al., 2018) or subcretion of mafic crust (Hiess et al., 2009) (**Figure 1-3C-D**) are equally viable scenario for the genesis of Archean TTGs, as reviewed by (Laurent et al., 2024). However, these tectonic models are largely based on the assumption that TTG bulk rock chemistry is representative of that of the melt and, thus, can be used to infer P-T conditions (hence tectonic settings) in which this melt was produced. Recent work from (Kendrick et al., 2021; Laurent et al., 2020; Rollinson, 2021) suggest that TTG, instead, might represents end products of significant differentiation of a tonalitic magma, the latter produced in a more limited P-T range than previously thought. As pointed out by (J. H. Bédard, 2018; Laurent et al., 2024) it is also rather likely that many of these local tectonic settings could have coexisted in the >3.0 Ga Archean Earth, with some sections of the lithosphere experiencing steep or shallow subduction and others producing oceanic plateaus. During that time, the alleged higher crustal temperatures (and associated ductile mechanical behavior, Korenaga, 2018, 2021; Mai & Korenaga, 2022) would have made amalgamation of different TTG-like micro-continents incapable to reach thicknesses akin to modern orogenic belts.

1.2.2. After 3.0 Ga: the onset of granitic magmatism

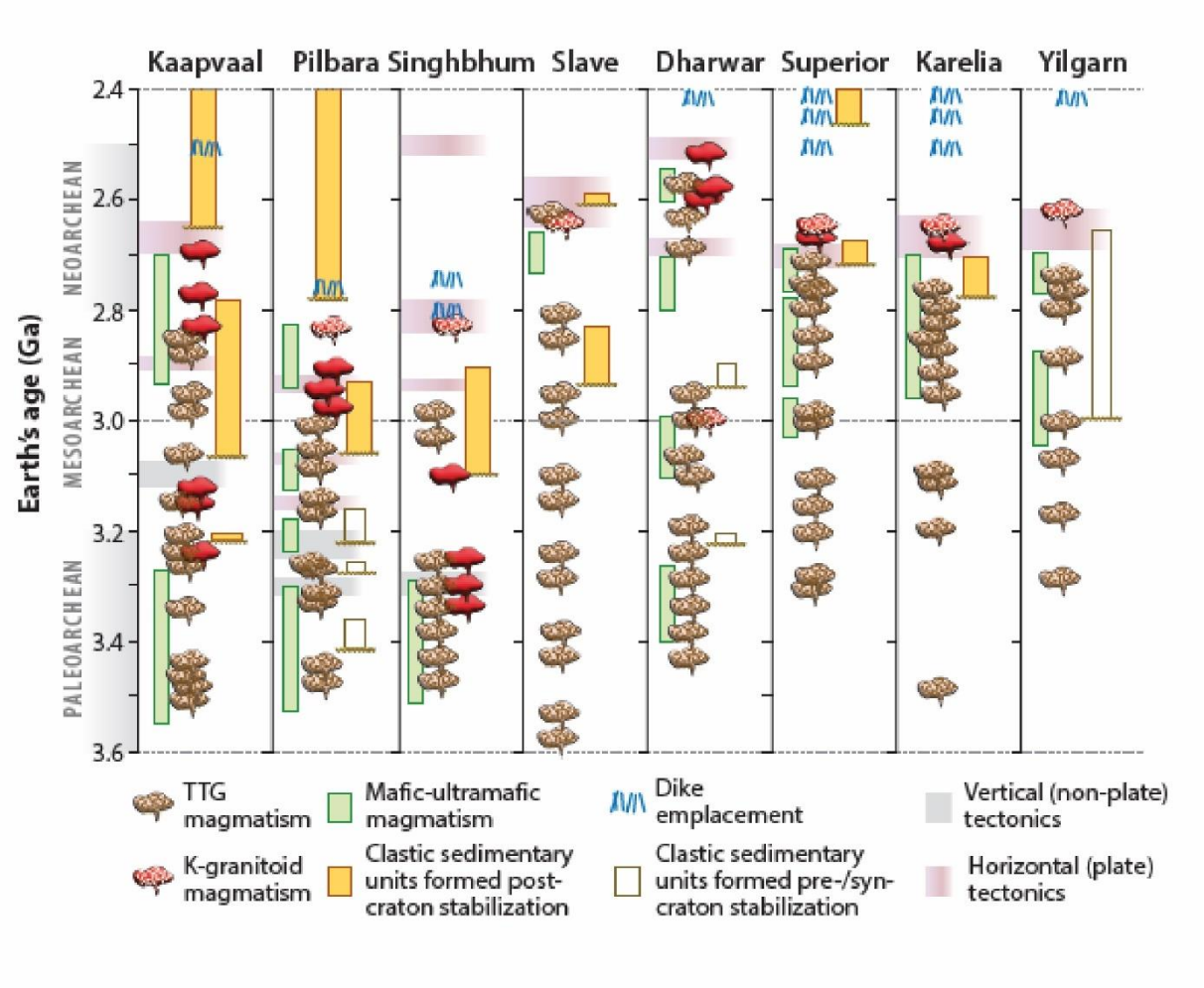

Figure 1-4 : Diachronous transition from TTG-dominated continental crust to K-rich magmatism in different Archean cratons (from Chowdhury et al., 2025).

At ages between ca. 3.0 Ga to ca. 2.5 Ga, the Archean rock record witnesses a gradual transition, and diachronous from craton to craton, towards K-rich magmatism, with the rise of more diversified granitoids in the felsic crust (Cassidy et al., 2006; Laurent et al., 2014; J. F. Moyen et al., 2021; Nebel et al., 2018; R. A. Stern et al., 1989) (**Figure1-4**). As a result, rocks of the TTG series become proportionately less dominant in the preserved volume of continental crust and give way to compositionally different granitoids (**Figure 1-4**). These chemically diverse granitoids are, with regional variations across cratons (**Figure 1-4**): 1) calk-alkaline, metaluminous, K-Cr-Ni-Mg rich granodiorites termed “sanukitoids” (L. P. Bédard, 1996; Cassidy et al., 2006; Champion & Smithies, 2001; de Oliveira et al., 2010; Fowler & Rollinson, 2012a; Halla, 2005; Jayananda et al., 2020; Jiang et

al., 2016; Martin et al., 2009; Shirey & Hanson, 1984; SMITHIES et al., 2004; Smithies et al., 2019; R. A. Stern et al., 1989); 2) slightly to moderately peraluminous, biotite (and subordinate two-mica) granites, arguably the second most abundant basement lithology in the Archean record after TTGs (Almeida et al., 2013; Feng & Kerrich, 1992; Frost et al., 1998; Jayananda et al., 2006; Liu et al., 2004; Meyer et al., 1994); and 3) hybrid granitoids intermediate in composition between TTGs, sanukitoids and biotite-/two-mica granites (Jayananda et al., 2006; J.-F. Moyen et al., 2003). These chemically diverse granitoids are interpreted as reflecting the onset of processes that are diagnostic of syn-to-post-collisional stages of modern orogens (**Figure 1-5**):

1) Sanukitoids, through their enrichment in both lithophile (K, Ba, Sr, REE) and "mantle-like" (Cr, Ni, Mg) elements, require involvement of felsic (crustal) and ultramafic (mantle) components in the magma source, interpreted to be a felsic melt (most often of TTG affinity) and a mantle peridotite.(Bibikova et al., 2005; Fowler & Rollinson, 2012b; Jayananda et al., 2020; Jiang et al., 2016; Martin et al., 2009). This dual origin and the calk-alkaline nature of sanukitoids suggests burial of basaltic + sedimentary rocks to P-T conditions high enough for them to start melting, a configuration that is more easily replicated in subduction-collision settings than in intraplate settings where magmas are dominantly alkaline (**Figure 1-5** Bonin, 2004; Clemens et al., 2009). Thus, sanukitoids mark the beginning of crustal growth through mantle wedge melting which is observed in modern continental and island arcs.
2) Biotite (and two-mica) granites represent peraluminous magmas enriched in K, which would derive from the partial melting of a TTG-like crust and/or sedimentary lithologies such as greywackes (Patiño-Douce & Beard., 1995; Watkins et al., 2007). While intracrustal reworking processes already existed long before 3.0 Ga (as evidenced by Hf isotope record in zircon, see section 1.3.) this is mainly interpreted as melting of a mafic crust to produce felsic rocks of the TTG series. From 3.0 Ga however, the production of peraluminous, K-rich granites shows that the felsic, TTG-sediments-like crust is now being internally reprocessed. This, as a result, marks the onset of intracrustal reworking of felsic crust that was described in section 1.1 (**Figure 1-5**).

3) Lastly, hybrid granites with chemical patterns intermediate between those of TTG, sanukitoids and two-mica granites are thought to derive from a mixing of the previous two magmatic components (Laurent et al., 2014) (**Figure 1-5**).

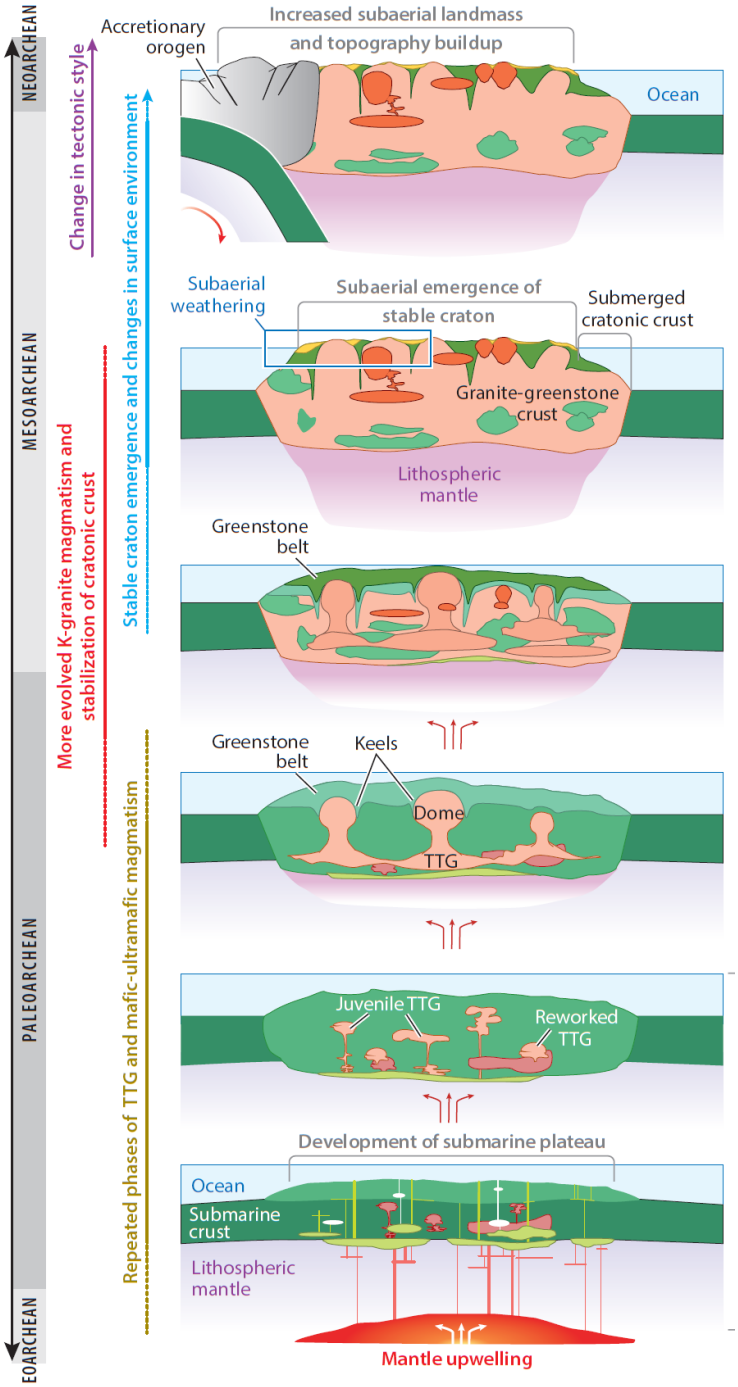

Figure 1-5 : Two-stage magmatic evolution of the Archean continental crust (from Chowdhury et al., 2025). The Archean geological record documents a chemical transition from TTGs towards a more diverse K-rich continental crust (sanukitoids, two-mica granites and hybrid granitoids) around 3.0-2.5 Ga. The formation of sanukitoids implies a growing contribution from metasomatized mantle peridotite that mixes with a TTG-like melt (onset of mantle wedge melting) whereas the formation of two-mica granites requires intracrustal reworking of TTGs with buried sediments similar to greywackes (onset of felsic crust reworking). This chemical diversification of the crust resembles the granitoid diversity observed in syn-to-post orogenic contexts of Phanerozoic orogens.

Again, not all these lithologies are expressed in every Archean craton. However, the same transition from Na-rich, TTG dominated crust to K-rich, to a compositionally diverse crust is documented in every craton across the world, albeit at different time (e.g. earlier for the Pilbara Craton, cf Smithies et al., 2004, later for the North China craton, cf Jiang et al., 2016 see **Figure 1-4**) suggesting that the stabilization and cratonization of the Continental lithosphere was a diachronous process. Also,

the comparable chemical affinities and diversity of Late-Archean granitoids with granitoids forming during syn-to-post-orogenic stages of modern orogenic cycles, is interpreted as a signature of the establishment of plate tectonics on a more global scale. This would result from the secular cooling of the Earth (Brown et al., 2022; Brown & Johnson, 2018; Palin et al., 2020) making the continental lithosphere rheologically stronger. In turn, a mechanically strong continental crust would allow the formation of linear suture zones between juxtaposed microcontinents (such as the Colesberg lineament between the Pietersburg block and the Northern edge of the Kaapvaal craton Eglington & Armstrong, 2004; Schoene et al., 2009) translating into changing structural grain from a dome-and-keel architecture of >3.0 Ga Archean granite-greenstone terranes to a more linear/accretionary orogenic one. Lastly, the stabilization of the Neoarchean continental lithosphere is supported by the formation of a depleted lithospheric mantle which, due to its higher buoyancy compared to ambient convective mantle, keeps the continental landmasses above sea level, enabling the erosion and deposition of thick terrigenous sedimentary layers (Flament et al., 2013; Korenaga, 2018, 2021; Mai & Korenaga, 2022; Rey et al., 2024; Schoene et al., 2009).

1.3. Geological evidence for pre-Neoarchean stabilization of continental lithosphere.

The scenario presented above, while shedding lights on the changing upper crustal composition at c.a. 3.0-2.5 Ga, suffers from some intrinsic inconsistencies that will be discussed in detail below:

1) The global record of Hf isotopes in zircons (i.e. from 4.4 to 3.0 Ga) shows evidence for an early transition in tectonic regime, interpreted as reflecting stabilization of the first cratonic nuclei between 3.8 to 3.6 Ga., ca. 1 Gyr before its documented involvement according to the whole-rock record.
2) The geological record of some Archean terranes show evidence for an earlier stabilization of the local continental crust as early as the Paleo-/Meso-Archean.

3) The geological record may not accurately represent the lithological diversity of the crust at the time of its formation.

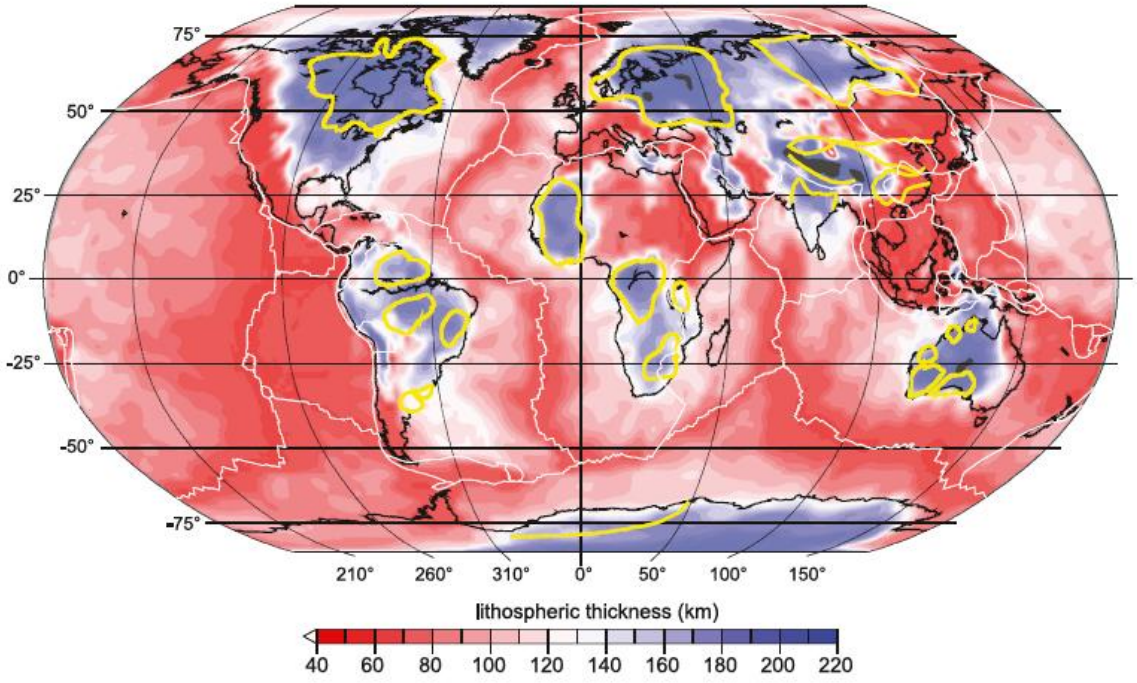

Figure 1-6 : Lithospheric thickness model with position of cratons outlined with yellow contours (map from Cawood et al., 2022; Priestley et al., 2018). Note the relatively minor proportion represented by exposures of Precambrian cratons in the continental lithosphere with respect to Phanerozoic continental rock.

Additionally, one must remember that the surface area of continental rocks that is older than 2.5 Ga represents less than 14% of the total surface of exposed and buried continental rocks (Goodwin, 1996) (**Figure 1-6**) while the total surface of continental rocks older than 3.0 Ga represents less than 5% of the total surface of the exposed continental crust (Goodwin, 1996; C. J. Hawkesworth et al., 2017) (**Figure 1-6**). Connected with the commonly held view that between 60 to 80% of the present volume of the continental crust was extracted by 3.0 Ga (Dhuime et al., 2012, 2015), a trivial conclusion is that most of the pre 2.5 Ga felsic rocks were recycled or reworked after their initial crystallization/deposition, supporting the idea of a significant preservation bias of the Archean rock record. An important question that geologists ask is what these missing rocks looked like and are the preserved rocks representative of them.

1.3.1. The global record of Hf isotopes in zircons: evidence for formation of cratonic nuclei at the Eo-Paleoarchean transition (ca. 3.8-3.6 Ga)

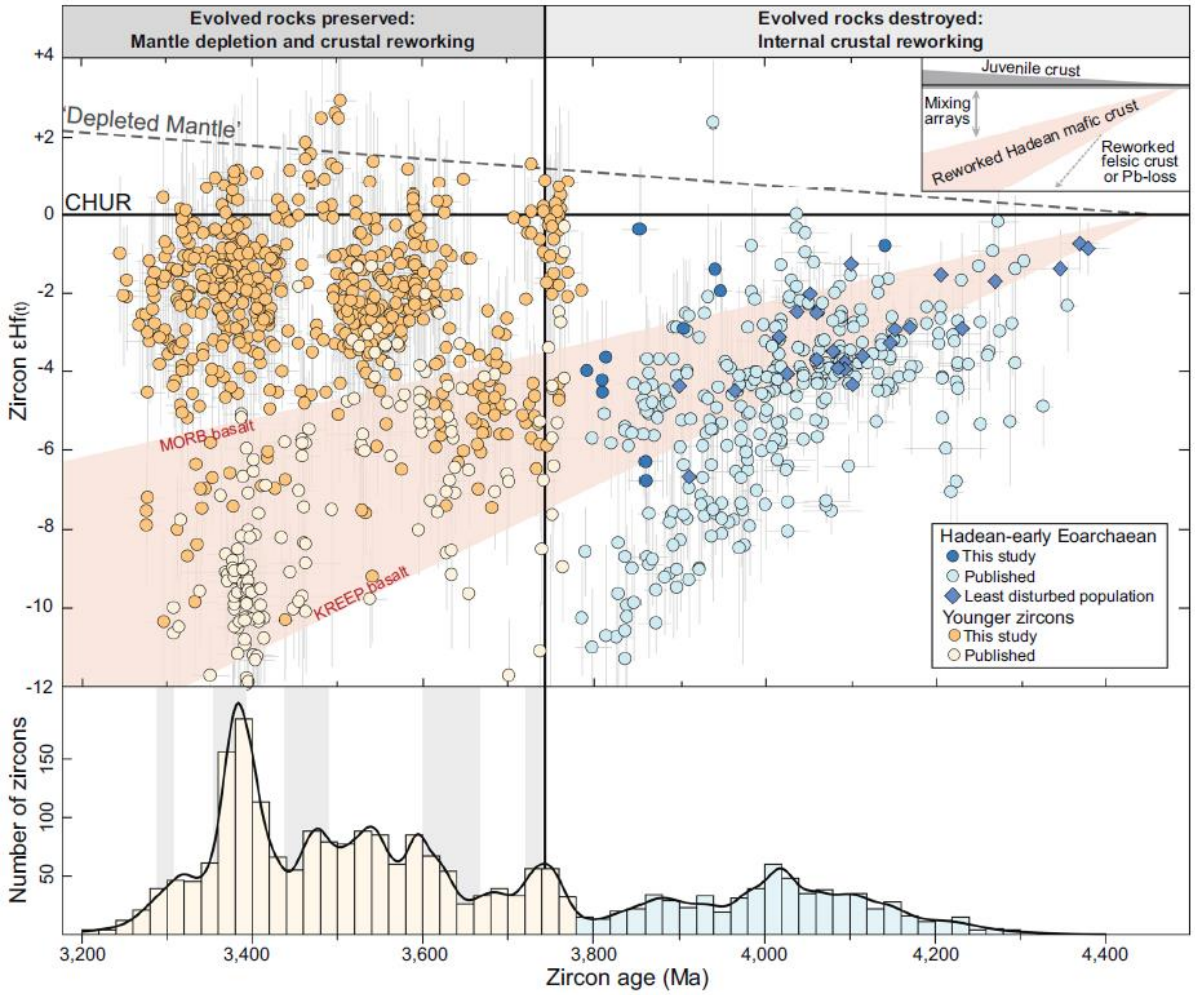

Figure 1-7 : Zircon $\varepsilon Hf_{(t)}$ vs age (Ma) graph from Mulder et al., 2021 illustrating the evolution of crust-mantle interactions from Hadean to the end of the Paleoarchean. Zircon with $\varepsilon Hf_{(t)} > 0$ crystallized in a source that was recently extracted from the Mantle and/or with a high Lu/Hf ratio, translating into a more radiogenic Hf isotopic composition than the CHondrite Uniform Reservoir (CHUR). Zircon with $\varepsilon Hf_{(t)} < 0$ crystallized in a source that was extracted from the mantle a long time before the crystallization of the mineral and show low Lu/Hf ratio, resulting in less radiogenic Hf isotopic composition than the CHUR

Zircon possesses a very strong affinity for Hf^{4+} which it incorporates to levels up to 1.5 wt% as a result of simple chemical substitution with Zr^{4+}(Hoskin & Schaltegger, 2003; Payne et al., 2016; Spencer et al., 2020; Watson & Harrison, 1983). In contrast, while having a strong affinity for HREE like Lu, the concentration of the latter in zircon is much lower compared with Hf (Belousova et al., 2002; Grimes et al., 2015). As a result, the $^{176}Hf/^{177}Hf$ ratio of zircon at the time of crystallization is

virtually not modified through radioactive decay of parent ^{176}Lu and remains nearly constant (at least within our analytical uncertainties) for billions of years (Fisher et al., 2014; Payne et al., 2016; Spencer et al., 2020). This property enables geologists to identify the $^{176}Hf/^{177}Hf$ ratio of the melt zircon crystallized from, which, at first order, depends on the proportion of crustal-derived vs mantle-derived components in the magma source (Amelin et al., 2000; Guitreau et al., 2012; Zeh et al., 2013). Due to the incompatible behavior of Hf during partial melting of mantle rocks, this element eventually concentrates into the crust whereas Lu being more compatible with mantle solid residuum remains in the mantle. Over billions of years of separate crust-mantle evolution, the Hf isotopic signature of both reservoirs diverge, with mantle rocks being strongly radiogenic ($\varepsilon Hf_{(t)}$ > CHUR line, **Figure 1-7**) whereas crustal rocks evolve to systematically non-radiogenic signature ($\varepsilon Hf_{(t)}$ < CHUR line, **Figure 1-7**).

The global compilations of Hf isotopic signature of Paleoarchean to Hadean igneous and detrital zircons from (Bauer et al., 2020; Mulder et al., 2021) documents a two-stage history of crust-mantle interaction from 4.4 Ga to ca. 3.2 Ga (**Figure 1-7**). From 4.4 Ga to 3.8 Ga, the zircon Hf isotopic composition becomes increasingly negative (**Figure 1-7**) outlining zircon crystallization in crust-derived melts, with little mixing with mantle-derived magmas. This is interpreted as reflecting intracrustal reworking of mafic crust. From 3.8 to 3.6 Ga, the global Hf isotope record shifts to radiogenic, chondritic to supra-chondritic values, a phenomenon that is present in all cratons but happens with different timing (more around ca. 3.2 Ga for SW Greenland, see Kirkland et al., 2021; Næraa et al., 2012) (**Figure 1-7**). This hallmarks the onset of substantial contribution of mantle melting to the formation of felsic crust (i.e. crustal growth), the latter hence carrying along the radiogenic, ^{176}Hf-enriched signature of its mantle source (i.e. positive $\varepsilon Hf_{(t)}$). Therefore, the works of (Bauer et al., 2020; Kirkland et al., 2021; Mulder et al., 2021; Næraa et al., 2012) document the coupled mantle melting and juvenile crust formation from ca. 3.8 to 3.6 Ga, generating buoyant cratonic nuclei.. Therefore, if one believes the global zircon Hf isotopic record, the formation of a buoyant continental lithosphere and the associated stabilization of the earliest cratons happened at ca. 3.8-3.6 Ga, some 600 Ma to 1 Ga

earlier than what was proposed before based on the appearance and diversification of K-rich magmatism in the rock-record.

1.3.2. Lithological evidence for a more diverse, >3 Ga felsic crust?

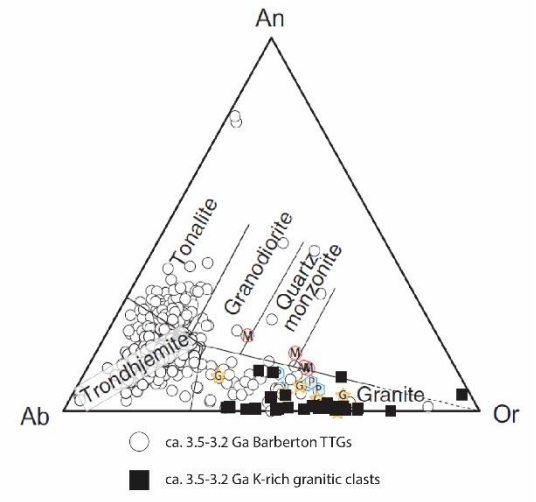

Figure 1-8 : Ternary plot showing the felsdspar K-rich composition of granitic clasts deposited in the Moodies Basal Conglomerate (modified after Sanchez-Garrido et al., 2011).

As outlined in (J.-F. Moyen, 2011)'s contribution, the dominant felsic rocks of the Archean Eon have often experienced intense strain and metamorphism after their crystallization, such that they become "grey gneisses" that are not always chemically identical to TTGs. In fact, grey gneisses represent either a mixture of TTG + infolded (meta-)sediments + felsic (meta-)volcanic rocks + greenstones, all of which being metamorphosed to amphibolite facies; or TTG *sensu stricto* (s.s), which are pristine TTG orthogneisses not mixed with other lithologies. The further back in time one goes, the harder it becomes to find TTGs retaining a pristine magmatic fabric and most Eoarchean (from 4.0 to 3.6 Ga) felsic rocks are thus generally characterized as "grey gneisses", although some exceptions occur. It follows that while TTGs are often strained, mixed with other lithologies and deformed to grey gneisses, particularly for Eo-to-Paleoarchean times, grey gneisses are not always chemical equivalents of TTG s.s. Indeed, the widespread occurrence of a gneissic fabric in Eoarchean felsic rocks could have made the identification of meta-igneous rocks of potentially different compositions than TTG more difficult and thus, strengthen the conception of a TTG-dominated, >3.0 Ga Archean felsic crust.

The Acasta Gneiss Complex in Canada offers some interesting insights on these matters. The study of (Reimink et al., 2014) identified some tonalitic gneisses at Idiwhaa in the Acasta Gneiss Complex

that have major and trace element composition different than that of TTG s.s from (J.-F. Moyen, 2011), notably a higher Fe content. These gneisses also produced a REE pattern that bears similarities to that of volcanic rocks called icelandites, which was interpreted by the authors as indicating that the Acasta felsic crust formed in settings similar to modern Iceland (hot spot/mid oceanic ridge interaction). This observation is not an isolated pattern. Indeed, hints of a higher felsic crust diversity in the preserved Archean rock record also occurs in Eastern Hebei, North China Craton where ~ 3.7 Ga K_2O-rich granites and quartz monzonites were recently found in enclaves preserved in 2.5 Ga potassic granites (Dong et al., 2024). The same findings were described in the Barberton Granitoid-Greenstone Terrane (BGGT), South Africa where (Kröner et al., 2018; Kröner & Compston, 1988; Reimer et al., 1985; Sanchez-Garrido et al., 2011) documented 3.2- to 3.5 Ga-old granitic-rhyolitic clasts in ca. 3.2 Ga conglomerates (**Figure 1-8**), with K_2O contents between 3.7 to 9.0 wt%, much higher than TTGs (mean K_2O content ~ 1.7 wt%, see J.-F. Moyen & Martin, 2012), although these clasts do not have equivalents in the exposed plutonic record. The parallel crystallization age distribution of these granitic/rhyolitic clasts with those of the local Barberton TTGs was used to argue that these clasts could represent remnants of a potassium-rich upper crust formed coevally with TTGs but mainly lost to crustal recycling. Furthermore, the study of Vezinet et al., 2025, focusing on two ca. 3.2-3.1 Ga tonalitic plutons of the BGGT in South Africa has conducted trace element profiling of magmatic apatites and identified a LREE-enrichment within the grains, a feature that resembles that of apatites crystallized within <2.9 Ga Sanukitoids and Phanerozoic I-type granites. This suggests that these tonalites, though part of the TTG series on a major element basis, have apatite REE patterns typical of sanukitoids. Consistent metamorphic and structural studies conducted in the BGGT for the past ~ 20 years (K. A. Cutts et al., 2014; J. F. Diener et al., 2005; J. F. A. Diener & Dziggel, 2021; Dziggel et al., 2002, 2005, 2006; Kato et al., 2018; Kisters et al., 2003; J.-F. Moyen et al., 2006) which document linear, thrust-like faults accommodating a NW-SE horizontal shortening of the granitoid-greenstone terrane at ca. 3.2 Ga, also support a Meso-Archean cratonization of the BGGT i.e. earlier than the global geological record suggests. Obviously, the present-day aerial extent of these Eoarchean icelandites, granitic enclaves/clasts, and sanukitoid-like rocks is limited, so these observations apparently do not challenge the view that TTGs represent up to 80% of the preserved > 3.0 Ga Archean crustal volume (J.-F. Moyen,

2011; Polat, 2012). Nevertheless, this shows that a better assessment of grey gneisses protolith lithologies is required. Furthermore, as the next section will illustrate, the proportions of TTG vs non-TTG rocks in the preserved geological record might not accurately represent the lithological diversity of the Archean felsic crust at the time it was formed.

1.3.3. Preservation biases recorded by decoupling of the detrital and plutonic zircon O isotope record

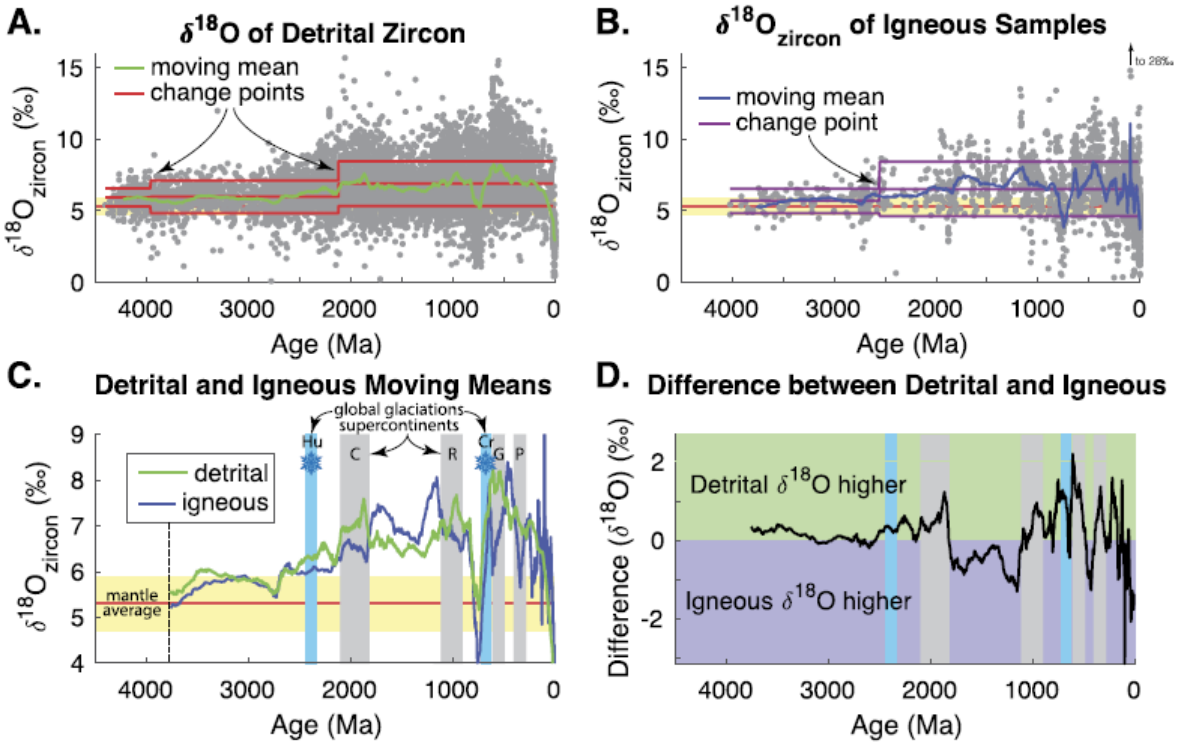

Figure 1-9 : Differences between $\delta^{18}O$ of igneous zircons and that of detrital zircons (from Spencer et al., 2022).

Oxygen isotopes in zircons (notably the $\delta^{18}O$ value, i.e. deviation of the $^{18}O/^{16}O$ ratio from that of an international standard, usually the Standard Mean Ocean Water [SMOW]) are used to track the presence of surface weathered material in the source of their parent magmas. It follows that a zircon $\delta^{18}O_{SMOW} > 7.0$ ‰ indicates a magma source that contained material that interacted with water at the surface (i.e. sedimentary rocks) whereas a $\delta^{18}O_{SMOW}$ of 5.3 ± 0.1 (1σ) ‰ indicates a mantle-derived magma source at first order (Valley et al., 1998, 2005). The identification of $\delta^{18}O_{SMOW}$ reaching values up to 15.0 ± 0.4 ‰ in Hadean detrital zircons of the Jack Hills meta-conglomerates has enabled

scientists to suggests that liquid water was present as early as 4.4 Ga on Earth, thereby suggesting cooling from a magma ocean to surface conditions allowing the presence of liquid water in less than 150 Ma (Harrison et al., 2008; Mojzsis et al., 2001; Wilde et al., 2001).

However, when comparing global records of detrital/sedimentary zircon $\delta^{18}O_{SMOW}$ with zircon $\delta^{18}O_{SMOW}$ from preserved igneous rocks, Spencer et al., 2022 discovered that, over 4.4 Ga of crustal evolution and maturation, the former are systematically higher than the latter for the Archean period (**Figure 1-9**). This suggests that the preserved geological record from Archean time does not faithfully represent the diversity of lithologies that produced the detrital zircons of similar age. This also suggests a vertical oxygen isotopic stratification of the continental crust at this time, with the upper crust consisting of higher proportions of igneous rocks derived from sediment-derived melting, preferentially feeding the high $\delta^{18}O_{SMOW}$ detrital zircons to clastic sediments, and the lower crust with a higher proportion of mantle-derived igneous rocks (i.e. lower $\delta^{18}O_{SMOW}$). The fact that high $\delta^{18}O_{SMOW}$ detrital zircons have a slightly different proportion of sources than what is preserved in the igneous record raises question about the potentially significant erosional bias that affects the Archean geological record and the possibility that some voluminous rock components were recycled and/or eroded away.

Therefore, while the 3.0 to 2.5 Ga period might represent a global transition to modern tectonics, evidence gathered from the occurrence of seemingly minor granitoid types at earlier times, as well as the zircon O and Hf isotopic records, rather suggest that the > 3.0 Ga evolution was not as simple and non-uniformitarian as conventionally considered. The key question is thus to know how much of the ancient Archean felsic crust these non-TTG rocks actually represent with respect to the small volumes preserved today. Accessing these missing crustal components can benefit from a comparison between the detrital and igneous record of a well characterized Archean terrane as the next two sections will illustrate.

1.4. Detrital accessory minerals as key tools to constrain the evolution of > 3.0 Ga Archean crust

1.4.1. Zircon: a tracer of crust-mantle evolution through time

The studies that have utilized zircon as a tracer of felsic crustal evolution in Hadean to Archean contexts are beyond numbers (Amelin et al., 2000; Bauer et al., 2020; Bell et al., 2015; Blichert-Toft & Albarède, 2008; Bruand et al., 2016; Cavosie et al., 2004; Compston & Pidgeon, 1986; Drabon et al., 2021; Harrison et al., 2008; Hopkins et al., 2008; Reimink et al., 2020; Valley et al., 2005; Wilde et al., 2001, to mention a few). To briefly summarize, zircon is a robust accessory mineral that crystallizes in intermediate to acidic melts (whole rock SiO_2 > 60%, Boehnke et al., 2013; Hoskin & Schaltegger, 2003; Watson & Harrison, 1983) and incorporates significant amounts of U (due to chemical substitution with Zr in the $ZrSiO_4$ formula, cf. Hoskin & Schaltegger, 2003) but little to no Pb during crystallization, making it a good geochronometer. Additionally, zircon can preserve the original Hf isotopic composition of its parent magma (see section 1.3.2) which depends on the respective importance of mantle vs crustal components in the magma source of the latter (Couzinié et al., 2016; C. J. Hawkesworth & Kemp, 2006b; Vervoort & Kemp, 2016). Furthermore, as explained in section 1.3.4, zircon O isotope signature provides a robust proxy of prior magma source interaction with seawater (Payne et al., 2016; Valley et al., 2005). The Ti content of zircon provides estimates of the crystallization temperature of the mineral (Ferry & Watson, 2007; Fonseca Teixeira et al., 2023; Schiller & Finger, 2019) and, despite some recent revisions of the meaning of geochemical proxies such as the Eu anomaly and Th/U ratio (Yakymchuk et al., 2018, 2023), the general trace element signature of zircon can, to some extent, distinguish magma sources from one another, in particular in geological periods for which the operation of plate tectonics is certain (Belousova et al., 2002; Grimes et al., 2007, 2015). Also, trace element-in-zircons have been increasingly used to filter grains that experienced hydrothermal alteration and precipitation of secondary zirconolite compounds (Bell et al., 2016, 2019; Bolhar et al., 2021; Kitajima et al., 2012). Finally, these isotopic, chronological and chemical data retained in zircon are wonderfully preserved and suffer little modification due to the mineral's inherent resistance to surface weathering and transport in clastic sedimentary systems (Dryden & Dryden, 1946;

A. Morton, 2012; A. C. Morton & Hallsworth, 1999). This enables zircon to survive multiple sedimentary cycles for billions of years largely unaffected, a property that becomes interesting when applied to a context for which little igneous rocks have survived such as the Archean.

However, the above summary of the zircon "toolbox" does not rule out inherent biases associated with zircon-centered studies. Indeed, zircon is not a ubiquitous mineral, since it mainly forms in magmas with SiO_2 content above 60% (intermediate to acidic, cf C. J. Hawkesworth & Kemp, 2006a) and thus, when used out of context (i.e. detrital grains), necessarily biases the study to the record of felsic crust components. Also, while trace elements in zircons are a powerful tool to distinguish very different (and somewhat uncommon) magma types (e.g. alkaline, mafic, carbonatitic vs granitic zircons; Belousova et al., 2002) or strikingly distinct geological environments (Grimes et al., 2007, 2015) zircon incorporates trace elements (HREE, Hf, U, Th, Y) that show little variability between very different granitoid types (J.-F. Moyen et al., 2017) resulting in zircons having similar trace element patterns across a range of compositions and petrogenetic mechanisms. Also, its application to discriminate magma types formed during a period of Earth's history for which the operation of plate-tectonics is not certain remains debated (Grimes et al., 2015). Finally, zircon has a high closure temperature for Pb diffusion (Cherniak et al., 1991) which represents a key advantage for dating the crystallization of the mineral (at notably lower temperature than T_c for Pb diffusion in zircon) but offers little prospects of constraining its thermal evolution after initial crystallization. Yet, constraining the thermal evolution of felsic rocks after their crystallization or deposition has major implications on the cooling rate of sedimentary units that went to lower crustal P/T conditions which connects with the local tectonic setting (J. A. Cutts et al., 2019; Ivan et al., 2022).

Therefore, zircon cannot be used alone, and geologists must combine zircon data with more ubiquitous and compositionally variable minerals to gain a better understanding of the compositional diversity of missing crustal components and the thermal evolution of crustal rocks, and particularly Archean terranes.

1.4.2. Apatite as a more faithful recorder of magma compositions

Recent studies have shed light on the importance of apatite as a tracer of missing crustal rocks and crustal evolution (Antoine et al., 2020; Bruand et al., 2016, 2020; Chew et al., 2021; Henrichs et al., 2019; Kieffer et al., 2024; Kirkland et al., 2017; Miyake et al., 2024; O'Sullivan et al., 2020; Vezinet et al., 2025). Apatite is, indeed, a much more ubiquitous accessory phase than zircon and crystallizes in a broader range of magma compositions, i.e. from mafic to felsic (Belousova et al., 2002; Chakhmouradian et al., 2017; O'Sullivan et al., 2020). Therefore, its trace and REE chemistry may help to reduce the biases resulting from a detrital zircon study alone.

In addition, apatite trace element contents are much more sensitive than zircons to the composition of the magma it crystallized from. As an example, the study of (Bruand et al., 2016) has shown the Sr content of apatite to be negatively correlated to the SiO_2 content of the parent magma and thus provides a proxy of the degree of chemical differentiation of the source rock. Additionally, the LREE content of apatite shows a strong negative correlation with the ASI of the parent melt as demonstrated in earlier studies (Montel, 1986; Piccoli & Candela, 2002; Pichavant et al., 1992). More recently, the study of (Kieffer et al., 2024) has established a workflow that filters apatites of different origins (i.e. metasomatic vs magmatic, felsic vs mafic, S-type vs I-type granite, etc.), a powerful tool in the case of apatite populations for which the original context is not known (detrital). The halogen (F and Cl) content of apatite also enables to filter out grains that experienced hydrothermal alteration from magmatic ones (high F, low Cl, cf Harlov, 2015) as well as mafic vs felsic parent melts (Kendall-Langley et al., 2021).

As a result of its ubiquity and chemical composition being more sensitive to magmatic processes, apatite offers a viable alternative to the limits of zircon-tracking of missing components mentioned above. While few studies document apatite trace element signatures in Archean TTGs and grey gneisses (Antoine et al., 2020; Miyake et al., 2024; Vezinet et al., 2025), little has been published about detrital apatites from sedimentary successions and most of these are concerned with thermochronological aspects (Clarke et al., 2023) rather than chemical tracing. This lack of data for

detrital grains mainly reflects the low survivability of apatite during sedimentary cycles, due to the inherent higher sensitivity of apatite to fluid alteration and capacity to dissolve and reprecipitate (A. Morton, 2012; A. C. Morton & Hallsworth, 1999), the more so for prolonged periods of alluvial storage such as is expected for Archean sediments (Chew et al., 2020; A. C. Morton & Hallsworth, 2007). Although recovering apatites in Archean clastic sediments can thus become a challenge, its rare occurrence can shed light on the composition of upper crustal rock much more precisely than zircon.

1.4.3. Rutile: a good recorder of the thermal evolution of the crust

Rutile, like apatite, is becoming a mineral of a wider interest in the scientific community, particularly due to its inherent retention of cooling ages. Indeed, rutile possesses a closure temperature for Pb diffusion of ~ 500-600°C (Bracciali et al., 2013; Cherniak, 2000; Kooijman et al., 2010; Meinhold, 2010; Mezger et al., 1989, 1991). In addition, rutile crystallizes predominantly in high-grade metamorphic rocks, commonly above amphibolite facies conditions, so its occurrence provides an insight into lower crustal processes (Pereira et al., 2021; Pereira & Storey, 2023). In particular, the Zr content of rutile is highly temperature-dependent and allows for calculation of temperature of crystallization or metamorphic equilibration of the mineral under specific set of conditions (Ferry & Watson, 2007; Kohn, 2020; Zack, Moraes, et al., 2004; Zack & Kooijman, 2017). In the case of metamorphic grains, assuming a certain pressure of equilibration and the coexistence with quartz and zircon, Zr-in-rutile temperature can provide insights into paleo-thermal gradients of the continental crust (Pereira et al., 2021). These properties collectively enable both to characterize the conditions of high-grade metamorphism and date the time when the resulting rocks were exhumed to mid-crustal temperatures. Additionally, rutile can also crystallize in magmatic-hydrothermal systems and discriminating those from metamorphic grains benefits from recent developments on rutile trace element chemistry (Schirra & Laurent, 2021).

A series of recent studies have emphasized the importance of rutile in determining provenance of clastic sediments, with the development of chemical proxies filtering between metamorphic vs hydrothermal vs magmatic grains and, to a lesser extent, mafic vs pelitic grains (Agangi et al., 2020; Luvizotto et al., 2009; Meinhold, 2010; Triebold et al., 2007, 2012; Zack, von Eynatten, et al., 2004; Zeh et al., 2018). This is a powerful tool in a context where the source might be difficult to identify, such as the Archean, or even lost by crustal reworking/recycling. However, while some recent work on Proterozoic-Phanerozoic settings have utilized rutile as a tracer of exhumation processes of eclogitic-granulitic rocks (Agangi et al., 2020; Bonnet et al., 2022; Byrne et al., 2024; J. A. Cutts et al., 2019), similar studies are lacking for Archean terranes. Yet, enlightening the cooling rate at which high-grade Archean metamorphic rocks were exhumated might help to discriminate possible tectonic settings, as fast cooling rates generally reflects tectonic-denudation of orogenic cores (Scibiorski et al., 2015) whereas slow cooling rates are more peculiar of the orogenic collapse (gravity-driven) of an overthickened crust that retard cooling (the "Large Hot Orogens" of Jamieson & Beaumont, 2013).

1.5. Case study: the Barberton-Granitoid-Greenstone Terrane (BGGT)

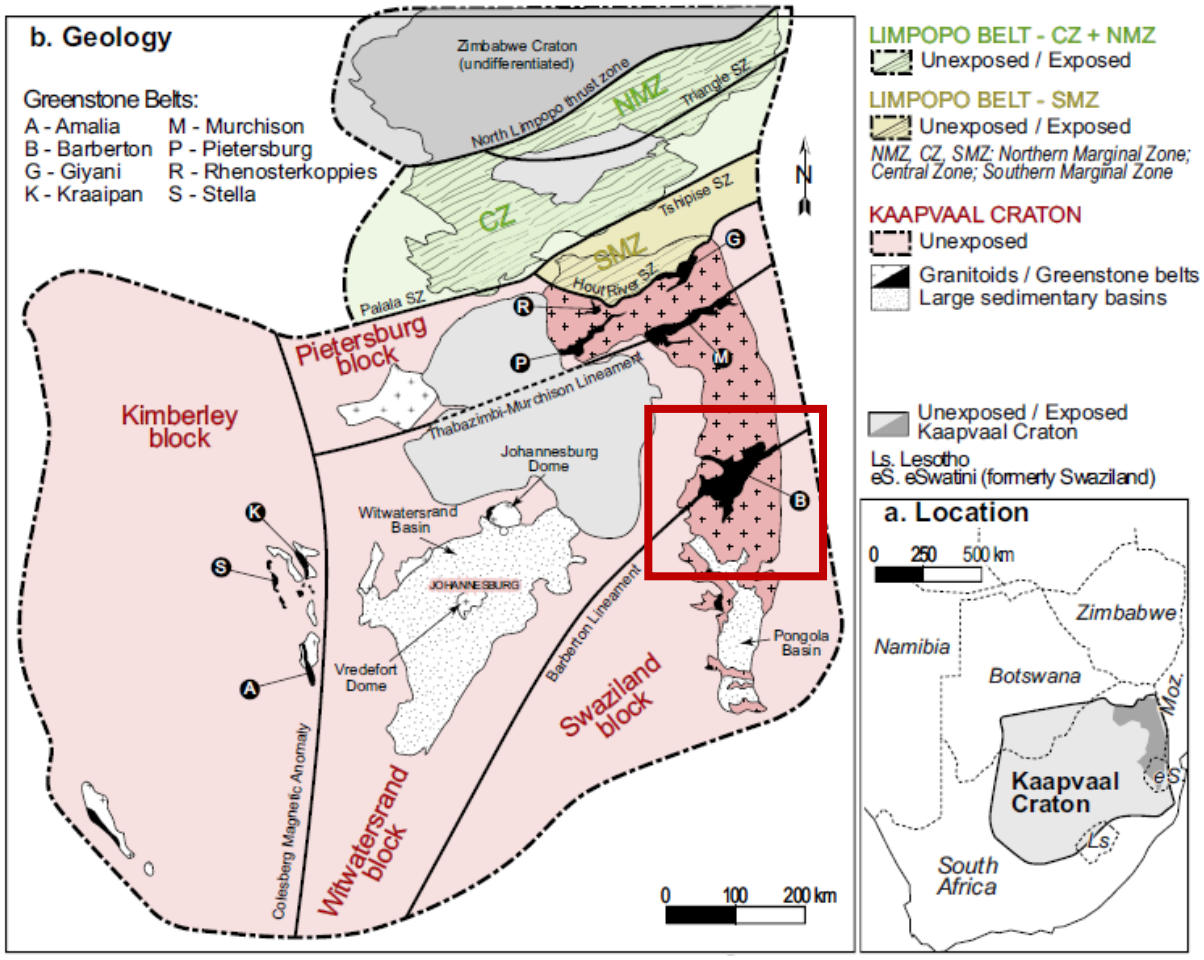

Figure 1-10 : Simplified structural map of the Kaapvaal Craton in Southern Africa showing the different tectonic blocks accreted along suture zones during the Neo-Archean (from Moyen et al., 2024). The BGGT (red box) lies at the border between the Swaziland block and the Witwatersrand block i.e. the cratonic nucleus of the craton. Both blocks were accreted at ca. 3.1-3.0 Ga along the Barberton Lineament.

The BGGT in eastern Mpumalanga, South Africa, is part of the Eastern Kaapvaal Craton and lies at the junction between the Witwatersrand Block and Swaziland Block (**Figure 1-10**), which form the nucleus of the craton. Other granitoid-greenstone terranes (notably the Pietersburg Block, cf. Laurent et al., 2019; J. F. Moyen et al., 2024 **Figure 1-10**) are present and show a younging in age the further to the NW, perpendicular to the structural grain of the BGGT (NE-SW extension, see (Eglington & Armstrong, 2004; JAGUIN et al., 2012; J. F. Moyen et al., 2024; Poujol, 2001). This pattern is interpreted as marking the sequential, lateral accretion and tectonic collage of the craton from 3.1 to ca. 2.6 Ga (Eglington & Armstrong, 2004; Laurent et al., 2019; Zeh et al., 2009).

The BGGT is an ideal framework to bring new constraints on the nature of lithologies, structure and thermal-tectonic evolution of the Earth's earliest crust by looking at the supracrustal record and connecting it to the igneous/plutonic record. Indeed, it is one of the best preserved Paleo-to-Mesoarchean greenstone terrane, for which the stratigraphic-structural relationships of the main supracrustal units and associated granitoid-gneisses have been well constrained since the late 1960s (Anhaeusser, 1969, 1976; Anhaeusser et al., 1981; Heubeck & Lowe, 1994; Kisters et al., 2003; Lowe, 1999; Lowe & Byerly, 2007) (**Figure 1-11**). To summarize these previous studies, the Barberton Greenstone Belt (BGB) represents the three main stratigraphic groups that, together with the concomitantly developed TTG-like basement, form the BGGT. These groups, from older to younger, are the Onverwacht Group (ca. 3.55 to 3.26 Ga), the Fig Tree Group (ca. 3.26 to 3.23 Ga) and the Moodies Group (ca. 3.23 to 3.21 Ga).

The Onverwacht Group is dominantly composed of ultramafic and mafic rocks, some of which belonging to the komatiite series (Parman et al., 1997), with some minor volcano-clastic to clastic sediments (De Wit et al., 1987a; de Wit et al., 2011; Dziggel et al., 2006; Grosch et al., 2011; Kröner et al., 2016). The group was deposited diachronously across the belt (Lowe, 1999; Lowe & Byerly, 2007) and it represents the thickest part of the BGB stratigraphy. The Fig Tree Group consists of volcanic rocks, chemical and clastic sediments (Anhaeusser, 1983; Hofmann, 2005; Stevens et al., 2002), which are overlain by the up to ca. 4 km thick clastic-tuffaceous silicic rocks of the Moodies Group (Heubeck, 2019; Heubeck et al., 2022) (**Figure 1-11**). These supracrustal rocks have been intruded by TTG magmas (now forming granitoids-gneisses) during three main episodes, i.e. 3.52-3.51 Ga, 3.46-3.44 Ga and 3.23-3.21 Ga (Kamo & Davis, 1994; Kröner et al., 1996; Laurent et al., 2020; J.-F. Moyen et al., 2007; Robb et al., 1986; Schoene et al., 2009; Yearron et al., 2003; Zeh et al., 2009). The TTGs are followed from ca. 3.12 Ga by the emplacement of the weakly- to undeformed, granitic-monzonitic-syenitic (GMS) granitoids, which truncate the >3.2 Ga basement and supracrustal rocks (Santos Leandro et al., s. d.).

The BGGT is divided into two separate terranes that are tectonically juxtaposed along the Saddleback-Inyoka-Fault System (SIFS, see **Figure 1-11 A**), a NE-SW trending reverse fault that act

as a suture zone between both tectonic blocks (i.e. the Northern Terrane located NW of the SIFS and the Southern Terrane located SE of SIFS, sensu Zeh et al., 2009 see also recent review from J. F. Moyen et al., 2024). This collision of both terranes along the SIFS happened at ca. 3.2 Ga as a result of convergent processes presumably accommodated by subduction and was responsible for the burial of the Stolzburg Terrane (**Figure 1-11 B**) to high grades and its subsequent exhumation to amphibolite facies conditions (J. F. Diener et al., 2005; Dziggel et al., 2002; J.-F. Moyen et al., 2006). Additionally, collision along the SIFS is responsible for the structural style of the greenstone belt, i.e. a linear belt in an accretionary wedge thrust against the more competent plutonic blocks of the BGGT with strain localized along the SIFS, quite different to dome-and-keel architecture that geologists observe in other cratons (e.g. the East Pilbara Terrane i.e. Champion & Smithies, 2001; François et al., 2014).

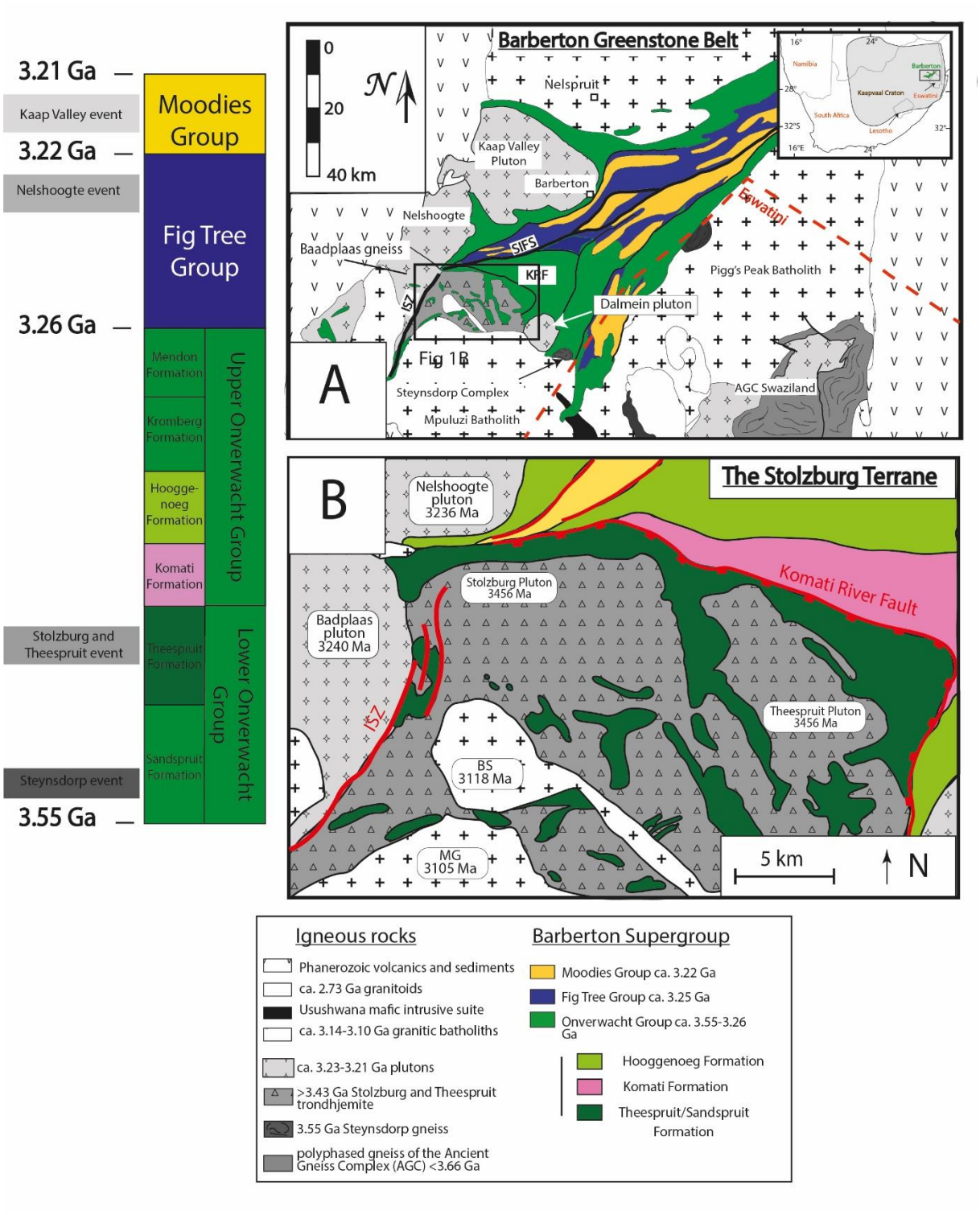

Figure 1-11 : Simplified geological map of the Barberton Greenstone Belt (A) and the Stolzburg Terrane (B) with a sketch stratigraphic log indicating the ages of the main TTG emplacement events (grey boxes).

1.5.1. Previous work on sediment provenance in the BGGT

In addition to being well characterized from a whole-rock and tectono-metamorphic aspect, the BGGT has also benefited from a number of studies discussing the provenance of clastic sediments through detrital zircon analysis (Byerly et al., 2018; Drabon et al., 2017, 2021, 2022, 2024; Hoffmann et al., 2016; Kröner et al., 2014; Lowe et al., 2021; Wang et al., 2022; Zeh et al., 2013, 2014). This was mainly achieved by comparing age, chemical and isotopic signatures between detrital zircons and plutonic zircons of the Barberton TTGs to assess the potential source-to-sink relationship between either. The results of these studies can be summarized as follows:

1) Zircons crystallized in the Barberton TTGs have an $\varepsilon Hf_{(t)}$ that is supra-chondritic (i.e. radiogenic zircons). This applies to TTG plutons and gneisses of the BGGT itself and those of the AGC (**Figure 1-11A**) (Hoffmann et al., 2016; Kröner et al., 2014; Laurent et al., 2020; Zeh et al., 2009, 2011). Only TTG plutons of the Southern BGGT (i.e. Theespruit and Stolzburg plutons, cf **Figure 1-11B**) had their zircon characterized for trace elements by (Laurent et al., 2022). The authors notably documented the unusually low Ti content of these zircons.
2) Detrital zircons deposited in clastic volcano-sediments from Upper Onverwacht to Moodies Groups have a U-Pb age distribution that largely resemble that of TTG zircons, although some minor age components at ca. 3.3 Ga and 3.6 Ga do not have an exposed magmatic equivalent (Drabon et al., 2024; Zeh et al., 2013). Lastly, some seemingly minor clastic sedimentary deposits contain a high concentration of zircons as old as ca. 4.2 Ga, which also do not have any magmatic equivalent in the exposed rock record and presumably derived from a different, older terrane through impact-related reworking and wind transport (Byerly et al., 2018; Drabon et al., 2017; Lowe et al., 2021).
3) Sedimentological work conducted in the Moodies Group by (Heubeck, 2019; Heubeck et al., 2022) shows that facies analysis and sandstone composition indicate provenance of sedimentary material from the Southern BGGT. However (**Figure 1-11A**). The absence of

high-grade, transport-resistant minerals like staurolite and garnet in Moodies sandstones also excludes possible sourcing of the sediments from the high-grade gneisses of the AGC.

The sourcing of clastic sediments of the BGB, in particular those of the Moodies Group, is currently mainly attributed to intraformational reworking of older sedimentary strata (Heubeck et al., 2022). For example, the similar trace element patterns observed in Moodies and Fig Tree zircons by (Drabon et al., 2024) drove the authors to suggest that the Moodies zircons are second-cycles grains eroded from underlying Fig Tree age strata, themselves containing igneous and detrital zircon corresponding to the main magmatic events of the BGGT. However, it must be noted that a significant fraction of the BGB detrital zircons have negative $\varepsilon Hf_{(t)}$, which require a magmatic source with a non-radiogenic Hf isotopic pattern, which cannot be represented by the (dominantly positive- $\varepsilon Hf_{(t)}$) TTGs or their volcanic equivalents. Furthermore, some seemingly small felsic rock units were poorly investigated as possible sources, like the felsic volcanic rocks of the Lower Onverwacht Group (Agangi et al., 2018) and now unpreserved magmatic units as represented by the granitic clasts deposited in the Moodies Basal Conglomerate (Sanchez-Garrido et al., 2011).

1.5.2. Previous work on the metamorphic evolution of the BGGT

Due to the presence of Al-rich clastic sediments of very old ages (ca. 3.5 Ga, see Anhaeusser, 1980; De Wit et al., 1987b; Dziggel et al., 2006) unconformably overlying the Stolzburg and Theespruit plutons in the Stolzburg Terrane (**Figure 1-11**), the BGGT has sparkled considerable interest to investigate the P-T-deformation path of Archean high-grade rocks. Numerous studies have now better characterized the tectono-metamorphic history of the Stolzburg Terrane and their results are briefly summarized here:

1) The age of metamorphism has been constrained to ca. 3230-3190Ma from dating of different accessory minerals (monazite, garnet, titanite) sampled from supracrustal sequences of the Theespruit-Sandspruit Formation (**Figure 1-11**) (K. A. Cutts et al., 2014; J. F. Diener et al., 2005; Dziggel et al., 2005; Kamo & Davis, 1994). An older age of metamorphism at ca. 3436

± 18 Ma is documented from monazites preserved within amphibolite felsic schists, outlining different metamorphic episodes affecting the Southern BGGT (K. A. Cutts et al., 2014).

2) Regarding the ca. 3230 Ma metamorphic event, peak metamorphic conditions increase from schists located close to the Komati River Fault (KRF, **Figure 1-11**) to supracrustal rocks in the South where they reach those of the amphibolite facies (i.e. from ca. 5 kbar-490°C to ca. 11 kbars-700°C, J. F. Diener et al., 2005; Dziggel et al., 2002; Kisters et al., 2003; J.-F. Moyen et al., 2006). The diagnostic amphibolite facies parageneses is present within the S-C fabric of amphibolitized felsic schists, suggesting that peak P-T conditions were reached during exhumation of the rocks (J. F. Diener et al., 2005).
3) Amphibolite-facies supracrustal rocks of the Stolzburg Terrane are included as cold enclaves within the shallow-level, ca. 3203 Ma Dalmein granodioritic pluton, suggesting that cooling from amphibolite-facies conditions was largely terminated at the time of intrusion (Lana et al., 2010).
4) The high-grade, amphibolite-facies supracrustal rock sequences of the Stolzburg Block are tectonically juxtaposed against the lower-grade (greenschist-facies) units of the overlying Komati Formation along a major structural break, the Komati River Fault (KRF) (**Figure 1-11**, Cloete, 1999; Grosch, 2019). This fault acts as a detachment system along which rocks of the Stolzburg Terrane were exhumated after reaching peak conditions at ca. 3230 Ma (Kisters et al., 2003).
5) U-Pb thermochronological ages of apatites from the Stolzburg pluton revealed the incomplete resetting of the U-Pb system, with apatite cores recording the ca. 3456 Ma crystallization ages over a large scale (see Mühlberg et al., 2021). This shows that the Stolzburg Terrane behaved as a coherent, cold rigid block during metamorphism and that cooling must have been fast enough to keep the U-Pb clock unaffected.

Whereas the metamorphic and tectonic conditions of the southern BGGT are well constrained, there has been few attempts to constrain the rate at which the Stolzburg Terrane was exhumed and the tectonic processes associated. Yet these have very strong implication on the regional tectonics (Brown

et al., 2022; Collins, 2002; Jamieson & Beaumont, 2013; Scibiorski et al., 2015; Vanderhaeghe et al., 2003) and can help to strengthen conclusions derived from geothermobarometric studies.

1.5.3. Knowledge gaps

While being extensively characterized for TTG and detrital zircon patterns, the latter have not been compared in detail using combined age, O-Hf isotopic and trace element data, with zircons from either the TTG or the non-TTG, volumetrically minor granitic volcanic units. Additionally, while the trace element composition of TTG-hosted apatite in the BGGT is receiving increasing interest, particularly for the ca. 3.23-3.22 Ga generations of TTGs (Miyake et al., 2024; Vezinet et al., 2025), there is no systematic investigation yet of whether these compositions vary across the different TTG generations. Moreover, detrital apatites, which could ideally supplement information derived from zircon (see section 1.4.2), have not been investigated so far. Lastly, the thermal evolution of the local felsic crust, particularly during the well-constrained ca. 3.2 Ga metamorphic event (J. F. Diener et al., 2005; Dziggel et al., 2002, 2005; Kisters et al., 2003; J.-F. Moyen et al., 2006), would likely benefit from an investigation of thermo-chronometers such as rutile.

1.6. Objectives of this study

The main objective of this study is to employ mainly detrital accessory minerals to investigate the nature and diversity of lithologies composing the Archean crust before 3.2 Ga, and, in turn, its structure and geological evolution. To achieve this aim, it is first necessary to build a consistent inventory of the geochemical record of these different accessory minerals at the scale of the BGB. Then, it is necessary to integrate the detrital record with the igneous record, using both published results (for zircon) and newly obtained major and trace element data on TTG-hosted apatite. This will allow us to build a comprehensive comparison basis between igneous and supracrustal rock units in the BGGT. A second

objective is to characterize the thermal evolution of the BGGT by producing new U-Pb and trace element data on rutiles belonging to metamorphosed volcano-clastic sequences.

To achieve these objectives, I have collected samples of the clastic sediments interspersed through the stratigraphy which I processed using conventional accessory mineral separation. Zircons, apatites and rutiles were characterized at the SEM using either cathodoluminescence (CL) imagery (zircon and apatite) or back-scattered-electron images (BSE) (rutile). Apatite's halogen composition was analyzed using electron probe micro-analyser (EPMA). Then all three mineralogies were analyzed using mass spectrometry techniques that will be described in greater details in the following chapters. The data collected allowed me to reassess previous models of sedimentary sources proposed for the BGB and shed a new light on the compositional diversity of the > 3.2 Ga Archean felsic crust.

1.7. Structure of the thesis

This thesis comprises six chapters. The first chapter introduces the topic of accessory mineral use and connects with the discussion on continental crust formation and evolution (present introduction). The second chapter presents a research article manuscript on detrital zircons of the BGB which was submitted to *Precambrian Research*, received acceptance pending major corrections and is currently under the second round of peer-review. Chapter 3 is a research article manuscript that described trace element patterns in two samples of detrital apatites and five samples of TTG apatites and is currently getting ready for submission to *Geochemica et Cosmochemica Acta*. Chapter 4 is a research article manuscript that describes the thermal evolution of two samples of the Onverwacht Group containing metamorphic rutiles and is currently in preparation for submission to *Lithos*. Chapter 5 presents the general implications and conclusions derived from the entire dataset. Chapter 6 corresponds to the elemental, isotopic and geochronological datasets produced in this study as well as links to online repositories.

1.8. References Chapter 1

Agangi, A., Hofmann, A., & Elburg, M. A. (2018). A review of Palaeoarchaean felsic volcanism in the eastern Kaapvaal craton : Linking plutonic and volcanic records. *Geoscience Frontiers*, *9*(3), 667-688.

Agangi, A., Plavsa, D., Reddy, S. M., Olierook, H., & Kylander-Clark, A. (2020). Compositional modification and trace element decoupling in rutile : Insight from the Capricorn Orogen, Western Australia. *Precambrian Research*, *345*, 105772.

Almeida, J. de A. C. de, Dall'Agnol, R., & Leite, A. A. da S. (2013). Geochemistry and zircon geochronology of the Archean granite suites of the Rio Maria granite-greenstone terrane, Carajás Province, Brazil. *Journal of South American Earth Sciences*, *42*, 103-126. https://doi.org/10.1016/j.jsames.2012.10.008

Amelin, Y., Lee, D.-C., & Halliday, A. N. (2000). Early-middle Archaean crustal evolution deduced from Lu-Hf and U-Pb isotopic studies of single zircon grains. *Geochimica et Cosmochimica Acta*, *64*(24), 4205-4225.

Anhaeusser, C. R. (1969). *The stratigraphy, structure, and gold mineralization of the Jamestown and Sheba Hills areas of the Barberton Mountain Land* [PhD Thesis]. https://wiredspace.wits.ac.za/bitstreams/01ac4533-4225-480c-b19e-ec3dc038be27/download

Anhaeusser, C. R. (1976). Archean metallogeny in southern Africa. *Economic Geology*, *71*(1), 16-43.

Anhaeusser, C. R. (1980). A geological investigation of the Archaean granite-greenstone terrane south of the Boesmanskop syenite pluton, Barberton Mountain Land. *South African Journal of Geology*, *83*(1), 93-106.

Anhaeusser, C. R. (1983). *The geology of the Schapenburg greenstone remnant and surrounding Archaean granitic terrane south of Badplaas, Eastern Transvaal*. https://pascal-francis.inist.fr/vibad/index.php?action=getRecordDetail&idt=6522482

Anhaeusser, C. R. (2014). Archaean greenstone belts and associated granitic rocks–a review. *Journal of African Earth Sciences*, *100*, 684-732.

Anhaeusser, C. R., Robb, L. J., & Viljoen, M. J. (1981). *Provisional geological map of the Barberton greenstone belt and surrounding granitic terrane, eastern Transvaal and Swaziland*. https://scholar.google.com/scholar?cluster=5265688940629013284&hl=en&oi=scholarr

Antoine, C., Bruand, E., Guitreau, M., & Devidal, J. -L. (2020). Understanding Preservation of Primary Signatures in Apatite by Comparing Matrix and Zircon-Hosted Crystals From the Eoarchean Acasta Gneiss Complex (Canada). *Geochemistry, Geophysics, Geosystems*, *21*(7), e2020GC008923. https://doi.org/10.1029/2020GC008923

Bauer, A. M., Reimink, J. R., Chacko, T., Foley, B. J., Shirey, S. B., & Pearson, D. G. (2020). Hafnium isotopes in zircons document the gradual onset of mobile-lid tectonics. *Geochemical Perspectives Letters*, *14*, 1-6.

Beall, A. P., Moresi, L., & Stern, T. (2017). Dripping or delamination? A range of mechanisms for removing the lower crust or lithosphere. *Geophysical Journal International*, *210*(2), 671-692. https://doi.org/10.1093/gji/ggx202

Bédard, J. H. (2018). Stagnant lids and mantle overturns : Implications for Archaean tectonics, magmagenesis, crustal growth, mantle evolution, and the start of plate tectonics. *Geoscience Frontiers*, *9*(1), 19-49.

Bédard, L. P. (1996). Archean high-Mg quartz-monzodiorite suite : A re-evaluation of the parental magma and differentiation. *The Journal of Geology*, *104*(6), 713-728.

Bell, E. A., Boehnke, P., Barboni, M., & Harrison, T. M. (2019). Tracking chemical alteration in magmatic zircon using rare earth element abundances. *Chemical Geology*, *510*, 56-71.

Bell, E. A., Boehnke, P., & Harrison, T. M. (2016). Recovering the primary geochemistry of Jack Hills zircons through quantitative estimates of chemical alteration. *Geochimica et Cosmochimica Acta*, *191*, 187-202.

Bell, E. A., Boehnke, P., Hopkins-Wielicki, M. D., & Harrison, T. M. (2015). Distinguishing primary and secondary inclusion assemblages in Jack Hills zircons. *Lithos*, *234*, 15-26.

Belousova, E., Griffin, W., O'Reilly, S. Y., & Fisher, N. (2002). Igneous zircon : Trace element composition as an indicator of source rock type. *Contributions to Mineralogy and Petrology*, *143*(5), 602-622. https://doi.org/10.1007/s00410-002-0364-7

Bibikova, E. V., Petrova, A., & Claesson, S. (2005). The temporal evolution of sanukitoids in the Karelian Craton, Baltic Shield : An ion microprobe U–Th–Pb isotopic study of zircons. *Lithos*, *79*(1-2), 129-145.

Bjørnerud, M. G., & Austrheim, H. (2004). Inhibited eclogite formation : The key to the rapid growth of strong and buoyant Archean continental crust. *Geology*, *32*(9), 765-768. https://doi.org/10.1130/G20590.1

Bleeker, W. (2003). The late Archean record : A puzzle in ca. 35 pieces. *Lithos*, *71*(2-4), 99-134.

Blichert-Toft, J., & Albarède, F. (2008). Hafnium isotopes in Jack Hills zircons and the formation of the Hadean crust. *Earth and Planetary Science Letters*, *265*(3-4), 686-702.

Boehnke, P., Watson, E. B., Trail, D., Harrison, T. M., & Schmitt, A. K. (2013). Zircon saturation re-revisited. *Chemical Geology*, *351*, 324-334.

Bolhar, R., Hofmann, A., Allen, C. M., & Maas, R. (2021). A LA-ICPMS zircon record of magmatic crystallization and compositional alteration in meta-igneous rocks of the eastern Kaapvaal Craton. *South African Journal of Geology*, *124*(3), 761-782. https://doi.org/10.25131/sajg.124.0042

Bonin, B. (2004). Do coeval mafic and felsic magmas in post-collisional to within-plate regimes necessarily imply two contrasting, mantle and crustal, sources? A review. *Lithos*, *78*(1), 1-24. https://doi.org/10.1016/j.lithos.2004.04.042

Bonnet, G., Chopin, C., Locatelli, M., Kylander-Clark, A. R. C., & Hacker, B. R. (2022). Protracted Subduction of the European Hyperextended Margin Revealed by Rutile U-Pb Geochronology Across the Dora-Maira Massif (Western Alps). *Tectonics*, *41*(4), e2021TC007170. https://doi.org/10.1029/2021TC007170

Bowring, S. A., & Williams, I. S. (1999). Priscoan (4.00–4.03 Ga) orthogneisses from northwestern Canada. *Contributions to Mineralogy and Petrology*, *134*(1), 3-16. https://doi.org/10.1007/s004100050465

Bracciali, L., Parrish, R. R., Horstwood, M. S., Condon, D. J., & Najman, Y. (2013). UPb LA-(MC)-ICP-MS dating of rutile : New reference materials and applications to sedimentary provenance. *Chemical Geology*, *347*, 82-101.

Brown, M. (2007). Crustal melting and melt extraction, ascent and emplacement in orogens : Mechanisms and consequences. *Journal of the Geological Society*, *164*(4), 709-730. https://doi.org/10.1144/0016-76492006-171

Brown, M., & Johnson, T. (2018). Secular change in metamorphism and the onset of global plate tectonics. *American Mineralogist*, *103*(2), 181-196. https://doi.org/10.2138/am-2018-6166

Brown, M., Johnson, T., & Gardiner, N. J. (2020). Plate Tectonics and the Archean Earth. *Annual Review of Earth and Planetary Sciences*, *48*(1), 291-320. https://doi.org/10.1146/annurev-earth-081619-052705

Brown, M., Johnson, T., & Spencer, C. J. (2022). Secular changes in metamorphism and metamorphic cooling rates track the evolving plate-tectonic regime on Earth. *Journal of the Geological Society*, *179*(5), jgs2022-050. https://doi.org/10.1144/jgs2022-050

Bruand, E., Fowler, M., Storey, C., Laurent, O., Antoine, C., Guitreau, M., Heilimo, E., & Nebel, O. (2020). Accessory mineral constraints on crustal evolution : Elemental fingerprints for magma discrimination. *Geochemical Perspectives Letters*, *13*, 7-12.

Bruand, E., Storey, C., & Fowler, M. (2016). An apatite for progress : Inclusions in zircon and titanite constrain petrogenesis and provenance. *Geology*, *44*(2), 91-94.

Byerly, B. L., Lowe, D. R., Drabon, N., Coble, M. A., Burns, D. H., & Byerly, G. R. (2018). Hadean zircon from a 3.3 Ga sandstone, Barberton greenstone belt, South Africa. *Geology*, *46*(11), 967-970.

Byrne, T., Chojnacki, M., Lewis, J., Lee, J.-C., Ho, G.-R., Yeh, E.-C., Lee, Y.-H., Tsai, C.-H., Evans, M., & Webb, L. (2024). Tectonic exhumation of a metamorphic core in an arc-continent collision during oblique convergence, Taiwan. *Progress in Earth and Planetary Science*, *11*(1), 23. https://doi.org/10.1186/s40645-024-00627-w

Cassidy, K. F., Champion, D. C., & Smithies, R. H. (2006). Origin of Archean late potassic granites : Evidence from the Yilgarn and Pilbara cratons. *Geochimica et Cosmochimica Acta Supplement*, *70*(18), A88-A88.

Castro, A., Vogt, K., & Gerya, T. (2013). Generation of new continental crust by sublithospheric silicic-magma relamination in arcs : A test of Taylor's andesite model. *Gondwana Research*, *23*(4), 1554-1566. https://doi.org/10.1016/j.gr.2012.07.004

Cavosie, A. J., Wilde, S. A., Liu, D., Weiblen, P. W., & Valley, J. W. (2004). Internal zoning and U–Th–Pb chemistry of Jack Hills detrital zircons : A mineral record of early Archean to Mesoproterozoic (4348–1576 Ma) magmatism. *Precambrian Research*, *135*(4), 251-279.

Cawood, P. A., Chowdhury, P., Mulder, J. A., Hawkesworth, C. J., Capitanio, F. A., Gunawardana, P. M., & Nebel, O. (2022). Secular Evolution of Continents and the Earth System. *Reviews of Geophysics*, *60*(4), e2022RG000789. https://doi.org/10.1029/2022RG000789

Cawood, P. A., & Hawkesworth, C. J. (2019). Continental crustal volume, thickness and area, and their geodynamic implications. *Gondwana Research*, *66*, 116-125. https://doi.org/10.1016/j.gr.2018.11.001

Cawood, P. A., Hawkesworth, C. J., & Dhuime, B. (2013). The continental record and the generation of continental crust. *GSA Bulletin*, *125*(1-2), 14-32. https://doi.org/10.1130/B30722.1

Chakhmouradian, A. R., Reguir, E. P., Zaitsev, A. N., Couëslan, C., Xu, C., Kynickỳ, J., Mumin, A. H., & Yang, P. (2017). Apatite in carbonatitic rocks : Compositional variation, zoning, element partitioning and petrogenetic significance. *Lithos*, *274*, 188-213.

Champion, D. C., & Smithies, R. H. (2001). Archaean granites of the Yilgarn and Pilbara cratons, Western Australia. *KF Cassidy, JM Dunphy and MJ Van Kranendonk (Eds.)*, *4*, 134-136.

Cherniak, D. J. (2000). Pb diffusion in rutile. *Contributions to Mineralogy and Petrology*, *139*(2), 198-207. https://doi.org/10.1007/PL00007671

Cherniak, D. J., Lanford, W. A., & Ryerson, F. J. (1991). Lead diffusion in apatite and zircon using ion implantation and Rutherford backscattering techniques. *Geochimica et cosmochimica acta*, *55*(6), 1663-1673.

Chew, D., Drost, K., Marsh, J. H., & Petrus, J. A. (2021). LA-ICP-MS imaging in the geosciences and its applications to geochronology. *Chemical Geology*, *559*, 119917.

Chew, D., O'Sullivan, G., Caracciolo, L., Mark, C., & Tyrrell, S. (2020). Sourcing the sand : Accessory mineral fertility, analytical and other biases in detrital U-Pb provenance analysis. *Earth-Science Reviews*, *202*, 103093. https://doi.org/10.1016/j.earscirev.2020.103093

Chopin, C. (2003). Ultrahigh-pressure metamorphism : Tracing continental crust into the mantle. *Earth and Planetary Science Letters*, *212*(1), 1-14. https://doi.org/10.1016/S0012-821X(03)00261-9

Chowdhury, P., Cawood, P. A., & Mulder, J. A. (2025). Subaerial Emergence of Continents on Archean Earth. *Annual Review of Earth and Planetary Sciences*, *53*(Volume 53, 2025), 443-478. https://doi.org/10.1146/annurev-earth-040722-093345

Clarke, A. J. I., Kirkland, C. L., Glorie, S., Gillespie, J., & Kinny, P. D. (2023). The unroofing of Archean crustal domes as recorded by detrital zircon and apatite. *Precambrian Research*, *395*, 107132. https://doi.org/10.1016/j.precamres.2023.107132

Clemens, J. D., Darbyshire, D. P. F., & Flinders, J. (2009). Sources of post-orogenic calcalkaline magmas : The Arrochar and Garabal Hill–Glen Fyne complexes, Scotland. *Lithos*, *112*(3), 524-542. https://doi.org/10.1016/j.lithos.2009.03.026

Cloete, M. (1999). *Aspects of volcanism and metamorphism of the Onverwacht group lavas in the South-Western portion of the Barberton greenstone belt.* [PhD Thesis]. https://wiredspace.wits.ac.za/items/cd520741-8d50-41a3-851e-bbc95bf82b2b

Collins, W. J. (2002). Hot orogens, tectonic switching, and creation of continental crust. *Geology*, *30*(6), 535-538. https://doi.org/10.1130/0091-7613(2002)030%253C0535:HOTSAC%253E2.0.CO;2

Compston, W., & Pidgeon, R. T. (1986). Jack Hills, evidence of more very old detrital zircons in Western Australia. *Nature*, *321*(6072), 766-769.

Condie, K. C. (1981). *Archean greenstone belts* (Vol. 3). Elsevier. https://books.google.com/books?hl=fr&lr=&id=6LkEpT_nlOAC&oi=fnd&pg=PP1&dq=Condie.+1981+greenstone&ots=hree9KwIBD&sig=7UDlC2znn7-ELP9jVJhBV46josw

Condie, K. C. (2018). A planet in transition : The onset of plate tectonics on Earth between 3 and 2 Ga? *Geoscience Frontiers*, *9*(1), 51-60. https://doi.org/10.1016/j.gsf.2016.09.001

Couzinié, S., Laurent, O., Moyen, J.-F., Zeh, A., Bouilhol, P., & Villaros, A. (2016). Post-collisional magmatism : Crustal growth not identified by zircon Hf–O isotopes. *Earth and Planetary Science Letters*, *456*, 182-195. https://doi.org/10.1016/j.epsl.2016.09.033

Cutts, J. A., Smit, M. A., Kooijman, E., & Schmitt, M. (2019). Two-Stage Cooling and Exhumation of Deeply Subducted Continents. *Tectonics*, *38*(3), 863-877. https://doi.org/10.1029/2018TC005292

Cutts, K. A., Stevens, G., Hoffmann, J. E., Buick, I. S., Frei, D., & Münker, C. (2014). Paleo-to Mesoarchean polymetamorphism in the Barberton Granite-Greenstone Belt, South Africa : Constraints from U-Pb monazite and Lu-Hf garnet geochronology on the tectonic processes that shaped the belt. *Bulletin*, *126*(3-4), 251-270.

De Wit, M. J., Armstrong, R., Hart, R. J., & Wilson, A. H. (1987a). Felsic igneous rocks within the 3.3- to 3.5-Ga Barberton Greenstone Belt : High crustal level equivalents of the surrounding Tonalite-Trondhjemite Terrain, emplaced during thrusting. *Tectonics*, *6*(5), 529-549. https://doi.org/10.1029/TC006i005p00529

De Wit, M. J., Armstrong, R., Hart, R. J., & Wilson, A. H. (1987b). Felsic igneous rocks within the 3.3- to 3.5-Ga Barberton Greenstone Belt : High crustal level equivalents of the surrounding Tonalite-Trondhjemite Terrain, emplaced during thrusting. *Tectonics*, *6*(5), 529-549. https://doi.org/10.1029/TC006i005p00529

de Oliveira, M. A., Dall'Agnol, R., & Scaillet, B. (2010). Petrological constraints on crystallization conditions of Mesoarchean sanukitoid rocks, southeastern Amazonian craton, Brazil. *Journal of Petrology*, *51*(10), 2121-2148.

de Wit, M. J., Furnes, H., & Robins, B. (2011). Geology and tectonostratigraphy of the Onverwacht Suite, Barberton greenstone belt, South Africa. *Precambrian Research*, *186*(1-4), 1-27.

Dhuime, B., Hawkesworth, C. J., Cawood, P. A., & Storey, C. D. (2012). A Change in the Geodynamics of Continental Growth 3 Billion Years Ago. *Science*, *335*(6074), 1334-1336. https://doi.org/10.1126/science.1216066

Dhuime, B., Wuestefeld, A., & Hawkesworth, C. J. (2015). Emergence of modern continental crust about 3 billion years ago. *Nature Geoscience*, *8*(7), 552-555. https://doi.org/10.1038/ngeo2466

Diener, J. F. A., & Dziggel, A. (2021). Can mineral equilibrium modelling provide additional details on metamorphism of the Barberton garnet amphibolites? *South African Journal of Geology*, *124*(1), 211-224. https://doi.org/10.25131/sajg.124.0003

Diener, J. F., Stevens, G., Kisters, A. F., & Poujol, M. (2005). Metamorphism and exhumation of the basal parts of the Barberton greenstone belt, South Africa : Constraining the rates of Mesoarchaean tectonism. *Precambrian Research*, *143*(1-4), 87-112.

Dilek, Y., & Furnes, H. (2014). Ophiolites and their origins. *Elements*, *10*(2), 93-100.

Dong, C., Liu, S., Nutman, A. P., Li, P., Xie, H., Li, Y., Liu, D., & Wan, Y. (2024). New discovery of 3.84–3.64 Ga diverse granitoids in eastern Hebei, North China Craton : Petrogenesis and significance. *Geological Society of America Bulletin*, *136*(11-12), 5249-5261.

Drabon, N., Byerly, B. L., Byerly, G. R., Wooden, J. L., Keller, C. B., & Lowe, D. R. (2021). Heterogeneous Hadean crust with ambient mantle affinity recorded in detrital zircons of the Green Sandstone Bed, South Africa. *Proceedings of the National Academy of Sciences*, *118*(8), e2004370118.

Drabon, N., Byerly, B. L., Byerly, G. R., Wooden, J. L., Wiedenbeck, M., Valley, J. W., Kitajima, K., Bauer, A. M., & Lowe, D. R. (2022). Destabilization of Long-Lived Hadean Protocrust and the Onset of Pervasive Hydrous Melting at 3.8 Ga. *AGU Advances*, *3*(2), e2021AV000520. https://doi.org/10.1029/2021AV000520

Drabon, N., Kirkpatrick, H. M., Byerly, G. R., & Wooden, J. L. (2024). Trace elements in zircon record changing magmatic processes and the multi-stage build-up of Archean proto-continental crust. *Geochimica et Cosmochimica Acta*, *373*, 136-150.

Drabon, N., Lowe, D. R., Byerly, G. R., & Harrington, J. A. (2017). Detrital zircon geochronology of sandstones of the 3.6–3.2 Ga Barberton greenstone belt : No evidence for older continental crust. *Geology*, *45*(9), 803-806.

Dryden, A. L., & Dryden, C. (1946). Comparative rates of weathering of some common heavy minerals. *Journal of Sedimentary Research*, *16*(3), 91-96. https://doi.org/10.1306/D426926A-2B26-11D7-8648000102C1865D

Dziggel, A., Armstrong, R. A., Stevens, G., & Nasdala, L. (2005). Growth of zircon and titanite during metamorphism in the granitoid-gneiss terrane south of the Barberton greenstone belt, South Africa. *Mineralogical Magazine*, *69*(6), 1019-1036.

Dziggel, A., Stevens, G., Poujol, M., Anhaeusser, C. R., & Armstrong, R. A. (2002). Metamorphism of the granite–greenstone terrane south of the Barberton greenstone belt, South Africa : An insight into the tectono-thermal evolution of the 'lower'portions of the Onverwacht Group. *Precambrian Research*, *114*(3-4), 221-247.

Dziggel, A., Stevens, G., Poujol, M., & Armstrong, R. A. (2006). *Contrasting source components of clastic metasedimentary rocks in the lowermost formations of the Barberton greenstone belt*.

Eglington, B. M., & Armstrong, R. A. (2004). The Kaapvaal Craton and adjacent orogens, southern Africa : A geochronological database and overview of the geological development of the craton. *South African Journal of Geology*, *107*(1-2), 13-32.

Feng, R., & Kerrich, R. (1992). Geochemical evolution of granitoids from the Archean Abitibi Southern Volcanic Zone and the Pontiac subprovince, Superior Province, Canada : Implications for tectonic history and source regions. *Chemical Geology*, *98*(1), 23-70. https://doi.org/10.1016/0009-2541(92)90090-R

Ferry, J. M., & Watson, E. B. (2007). New thermodynamic models and revised calibrations for the Ti-in-zircon and Zr-in-rutile thermometers. *Contributions to Mineralogy and Petrology*, *154*(4), 429-437. https://doi.org/10.1007/s00410-007-0201-0

Fisher, C. M., Vervoort, J. D., & Hanchar, J. M. (2014). Guidelines for reporting zircon Hf isotopic data by LA-MC-ICPMS and potential pitfalls in the interpretation of these data. *Chemical geology*, *363*, 125-133.

Flament, N., Coltice, N., & Rey, P. F. (2013). The evolution of the 87Sr/86Sr of marine carbonates does not constrain continental growth. *Precambrian Research*, *229*, 177-188. https://doi.org/10.1016/j.precamres.2011.10.009

Fonseca Teixeira, L. M., Troch, J., & Bachmann, O. (2023). The dynamic nature of aTiO2 : Implications for Ti-based thermometers in magmatic systems. *Geology*, *52*(1), 92-96. https://doi.org/10.1130/G51587.1

Fowler, M., & Rollinson, H. (2012a). Phanerozoic sanukitoids from Caledonian Scotland : Implications for Archean subduction. *Geology*, *40*(12), 1079-1082.

Fowler, M., & Rollinson, H. (2012b). Phanerozoic sanukitoids from Caledonian Scotland : Implications for Archean subduction. *Geology*, *40*(12), 1079-1082.

François, C., Philippot, P., Rey, P., & Rubatto, D. (2014). Burial and exhumation during Archean sagduction in the East Pilbara granite-greenstone terrane. *Earth and Planetary Science Letters*, *396*, 235-251.

Frost, C. D., Frost, B. R., Chamberlain, K. R., & Hulsebosch, T. P. (1998). The Late Archean history of the Wyoming province as recorded by granitic magmatism in the Wind River Range, Wyoming. *Precambrian Research*, *89*(3), 145-173. https://doi.org/10.1016/S0301-9268(97)00082-X

Gerya, T. (2014). Precambrian geodynamics : Concepts and models. *Gondwana Research*, *25*(2), 442-463.

Goodwin, A. M. (1996). *Principles of Precambrian Geology*. Elsevier.

Grimes, C. B., John, B. E., Kelemen, P. B., Mazdab, F. K., Wooden, J. L., Cheadle, M. J., Hanghøj, K., & Schwartz, J. J. (2007). Trace element chemistry of zircons from oceanic crust : A method for distinguishing detrital zircon provenance. *Geology*, *35*(7), 643-646.

Grimes, C. B., Wooden, J. L., Cheadle, M. J., & John, B. E. (2015). "Fingerprinting" tectono-magmatic provenance using trace elements in igneous zircon. *Contributions to Mineralogy and Petrology*, *170*(5-6), 46. https://doi.org/10.1007/s00410-015-1199-3

Grosch, E. G. (2019). Metamorphic processes preserved in early Archean supracrustal rocks of the Barberton Greenstone Belt, South Africa. *Geological Society, London, Special Publications*, *478*(1), 315-334. https://doi.org/10.1144/SP478.15

Grosch, E. G., Kosler, J., McLoughlin, N., Drost, K., Slama, J., & Pedersen, R. B. (2011). Paleoarchean detrital zircon ages from the earliest tectonic basin in the Barberton Greenstone Belt, Kaapvaal craton, South Africa. *Precambrian Research*, *191*(1-2), 85-99.

Guitreau, M., Blichert-Toft, J., Martin, H., Mojzsis, S. J., & Albarède, F. (2012). Hafnium isotope evidence from Archean granitic rocks for deep-mantle origin of continental crust. *Earth and Planetary Science Letters*, *337-338*, 211-223. https://doi.org/10.1016/j.epsl.2012.05.029

Hacker, B. R., Kelemen, P. B., & Behn, M. D. (2011). Differentiation of the continental crust by relamination. *Earth and Planetary Science Letters*, *307*(3), 501-516. https://doi.org/10.1016/j.epsl.2011.05.024

Hacker, B. R., Kelemen, P. B., & Behn, M. D. (2015). Continental Lower Crust. *Annual Review of Earth and Planetary Sciences*, *43*(Volume 43, 2015), 167-205. https://doi.org/10.1146/annurev-earth-050212-124117

Halla, J. (2005). Late Archean high-Mg granitoids (sanukitoids) in the southern Karelian domain, eastern Finland : Pb and Nd isotopic constraints on crust- mantle interactions. *Lithos*, *79*(1-2), 161-178.

Harlov, D. E. (2015). Apatite : A fingerprint for metasomatic processes. *Elements*, *11*(3), 171-176.

Harris, N., & Massey, J. (1994). Decompression and anatexis of Himalayan metapelites. *Tectonics*, *13*(6), 1537-1546. https://doi.org/10.1029/94TC01611

Harrison, T. M. (2024). We don't know when plate tectonics began. *Journal of the Geological Society*, *181*(4), jgs2023-212. https://doi.org/10.1144/jgs2023-212

Harrison, T. M., Schmitt, A. K., McCulloch, M. T., & Lovera, O. M. (2008). Early (≥ 4.5 Ga) formation of terrestrial crust : Lu–Hf, δ18O, and Ti thermometry results for Hadean zircons. *Earth and Planetary Science Letters*, *268*(3), 476-486. https://doi.org/10.1016/j.epsl.2008.02.011

Hawkesworth, C., Cawood, P. A., Dhuime, B., & Kemp, T. (2024). Tectonic processes and the evolution of the continental crust. *Journal of the Geological Society*, *181*(4), jgs2024-027. https://doi.org/10.1144/jgs2024-027

Hawkesworth, C. J., Cawood, P. A., Dhuime, B., & Kemp, T. I. S. (2017). Earth's Continental Lithosphere Through Time. *Annual Review of Earth and Planetary Sciences*, *45*(1), 169-198. https://doi.org/10.1146/annurev-earth-063016-020525

Hawkesworth, C. J., Dhuime, B., Pietranik, A. B., Cawood, P. A., Kemp, A. I. S., & Storey, C. D. (2010). The generation and evolution of the continental crust. *Journal of the Geological Society*, *167*(2), 229-248. https://doi.org/10.1144/0016-76492009-072

Hawkesworth, C. J., & Kemp, A. I. S. (2006a). Evolution of the continental crust. *Nature*, *443*(7113), 811-817.

Hawkesworth, C. J., & Kemp, A. I. S. (2006b). Using hafnium and oxygen isotopes in zircons to unravel the record of crustal evolution. *Chemical Geology*, *226*(3-4), 144-162.

Henrichs, I. A., Chew, D. M., O'Sullivan, G. J., Mark, C., McKenna, C., & Guyett, P. (2019). Trace Element (Mn-Sr-Y-Th-REE) and U-Pb Isotope Systematics of Metapelitic Apatite During Progressive Greenschist- to Amphibolite-Facies Barrovian Metamorphism. *Geochemistry, Geophysics, Geosystems*, *20*(8), 4103-4129. https://doi.org/10.1029/2019GC008359

Herzberg, C., Condie, K., & Korenaga, J. (2010). Thermal history of the Earth and its petrological expression. *Earth and Planetary Science Letters*, *292*(1-2), 79-88.

Heubeck, C. (2019). The Moodies Group—A High-Resolution Archive of Archaean Surface Processes and Basin-Forming Mechanisms. In A. Kröner & A. Hofmann (Éds.), *The Archaean Geology of the Kaapvaal Craton, Southern Africa* (p. 133-169). Springer International Publishing. https://doi.org/10.1007/978-3-319-78652-0_6

Heubeck, C., Drabon, N., Byerly, G., Leisgang, I., Linnemann, U., Lowe, D., Mertz-Kraus, R., Gonzalez-Pinzon, A., Thomsen, T. B., & Zeh, A. (2022). Detrital zircon provenance of the Archean Moodies Group, Barberton Greenstone Belt, South Africa and Eswatini. *American Journal of Science*, *322*(2), 65-107.

Heubeck, C., & Lowe, D. R. (1994). Late syndepositional deformation and detachment tectonics in the Barberton Greenstone Belt, South Africa. *Tectonics*, *13*(6), 1514-1536. https://doi.org/10.1029/94TC01809

Hiess, J., Bennett, V. C., Nutman, A. P., & Williams, I. S. (2009). In situ U–Pb, O and Hf isotopic compositions of zircon and olivine from Eoarchaean rocks, West Greenland : New insights to making old crust. *Geochimica et Cosmochimica Acta*, *73*(15), 4489-4516. https://doi.org/10.1016/j.gca.2009.04.019

Hoffmann, J. E., Kröner, A., Hegner, E., Viehmann, S., Xie, H., Iaccheri, L. M., Schneider, K. P., Hofmann, A., Wong, J., & Geng, H. (2016). Source composition, fractional crystallization and magma mixing processes in the 3.48–3.43 Ga Tsawela tonalite suite (Ancient Gneiss Complex, Swaziland)–Implications for Palaeoarchaean geodynamics. *Precambrian Research*, *276*, 43-66.

Hofmann, A. (2005). The geochemistry of sedimentary rocks from the Fig Tree Group, Barberton greenstone belt : Implications for tectonic, hydrothermal and surface processes during mid-Archaean times. *Precambrian Research*, *143*(1), 23-49. https://doi.org/10.1016/j.precamres.2005.09.005

Hopkins, M., Harrison, T. M., & Manning, C. E. (2008). Low heat flow inferred from >4 Gyr zircons suggests Hadean plate boundary interactions. *Nature*, *456*(7221), Article 7221. https://doi.org/10.1038/nature07465

Hoskin, P. W., & Schaltegger, U. (2003). The composition of zircon and igneous and metamorphic petrogenesis. *Reviews in mineralogy and geochemistry*, *53*(1), 27-62.

Ivan, Z., Anthony I S, K., R Hugh, S., Daniela, R., Fawna, K., Johannes, H., Tim E, J., Klaus, G., Roberto F, W., Jeff D, V., Laure, M., & Sandra S, R. (2022). Greenstone burial–exhumation cycles at the late Archean transition to plate tectonics. *Nature Communications*, *13*(1), 7893. https://doi.org/10.1038/s41467-022-35208-2

Jagoutz, O., & Kelemen, P. B. (2015). Role of Arc Processes in the Formation of Continental Crust. *Annual Review of Earth and Planetary Sciences*, *43*(Volume 43, 2015), 363-404. https://doi.org/10.1146/annurev-earth-040809-152345

JAGUIN, J., GAPAIS, D., POUJOL, M., BOULVAIS, P., & MOYEN, J.-F. (2012). THE MURCHISON GREENSTONE BELT (SOUTH AFRICA) : A GENERAL TECTONIC FRAMEWORK. *South African Journal of Geology*, *115*(1), 65-76. https://doi.org/10.2113/gssajg.115.1.65

Jahn, B.-M., Glikson, A. Y., Peucat, J. J., & Hickman, A. H. (1981). REE geochemistry and isotopic data of Archean silicic volcanics and granitoids from the Pilbara Block, Western Australia : Implications for the early crustal evolution. *Geochimica et Cosmochimica Acta*, *45*(9), 1633-1652. https://doi.org/10.1016/S0016-7037(81)80002-6

Jamieson, R. A., & Beaumont, C. (2013). On the origin of orogens. *GSA Bulletin*, *125*(11-12), 1671-1702. https://doi.org/10.1130/B30855.1

Jaupart, C., Mareschal, J.-C., & Iarotsky, L. (2016). Radiogenic heat production in the continental crust. *Lithos*, *262*, 398-427.

Jayananda, M., Aadhiseshan, K. R., Kusiak, M. A., Wilde, S. A., Sekhamo, K., Guitreau, M., Santosh, M., & Gireesh, R. V. (2020). Multi-stage crustal growth and Neoarchean geodynamics in the Eastern Dharwar Craton, southern India. *Gondwana Research*, *78*, 228-260.

Jayananda, M., Chardon, D., Peucat, J.-J., & Capdevila, R. (2006). 2.61 Ga potassic granites and crustal reworking in the western Dharwar craton, southern India : Tectonic, geochronologic and geochemical constraints. *Precambrian Research*, *150*(1), 1-26. https://doi.org/10.1016/j.precamres.2006.05.004

Jiang, N., Guo, J., Fan, W., Hu, J., Zong, K., & Zhang, S. (2016). Archean TTGs and sanukitoids from the Jiaobei terrain, North China craton : Insights into crustal growth and mantle metasomatism. *Precambrian Research*, *281*, 656-672.

Johnson, T. E., Brown, M., Gardiner, N. J., Kirkland, C. L., & Smithies, R. H. (2017). Earth's first stable continents did not form by subduction. *Nature*, *543*(7644), 239-242.

Johnson, T. E., Brown, M., Kaus, B. J. P., & VanTongeren, J. A. (2014). Delamination and recycling of Archaean crust caused by gravitational instabilities. *Nature Geoscience*, *7*(1), 47-52. https://doi.org/10.1038/ngeo2019

Kamo, S. L., & Davis, D. W. (1994). Reassessment of Archean crustal development in the Barberton Mountain Land, South Africa, based on U-Pb dating. *Tectonics*, *13*(1), 167-192. https://doi.org/10.1029/93TC02254

Kato, D., Aoki, K., Komiya, T., Yamamoto, S., Sawaki, Y., Asanuma, H., Sato, T., Tsuchiya, Y., Shozugawa, K., & Matsuo, M. (2018). Constraints on the P–T conditions of high-pressure metamorphic rocks from the Inyoni shear zone in the mid-Archean Barberton Greenstone Belt, South Africa. *Precambrian Research*, *315*, 1-18.

Kendall-Langley, L. A., Kemp, A. I. S., Hawkesworth, C. J., Craven, J., Talavera, C., Hinton, R., Roberts, M. P., & EIMF. (2021). Quantifying F and Cl concentrations in granitic melts from apatite inclusions in zircon. *Contributions to Mineralogy and Petrology*, *176*(7), 58. https://doi.org/10.1007/s00410-021-01813-5

Kendrick, J., Duguet, M., & Yakymchuk, C. (2021). Diversification of Archean tonalite-trondhjemite-granodiorite suites in a mushy middle crust. *Geology*, *50*(1), 76-80. https://doi.org/10.1130/G49287.1

Kieffer, M. A., Dare, S. A., & Gendron, M. (2024). Trace element discrimination diagrams to identify igneous apatite from I-, S-and A-type granites and mafic intrusions : Implications for provenance studies and mineral exploration. *Chemical Geology*, *649*, 121965.

Kirkland, C. L., Hartnady, M. I. H., Barham, M., Olierook, H. K. H., Steenfelt, A., & Hollis, J. A. (2021). Widespread reworking of Hadean-to-Eoarchean continents during Earth's thermal peak. *Nature Communications*, *12*(1), 331. https://doi.org/10.1038/s41467-020-20514-4

Kirkland, C. L., Hollis, J., Danišík, M., Petersen, J., Evans, N. J., & McDonald, B. J. (2017). Apatite and titanite from the Karrat Group, Greenland; implications for charting the thermal evolution of crust from the U-Pb geochronology of common Pb bearing phases. *Precambrian Research*, *300*, 107-120.

Kisters, A. F. M., Stevens, G., Dziggel, A., & Armstrong, R. A. (2003). Extensional detachment faulting and core-complex formation in the southern Barberton granite–greenstone terrain, South Africa : Evidence for a 3.2 Ga orogenic collapse. *Precambrian Research*, *127*(4), 355-378. https://doi.org/10.1016/j.precamres.2003.08.002

Kitajima, K., Ushikubo, T., Kita, N. T., Maruyama, S., & Valley, J. W. (2012). Relative retention of trace element and oxygen isotope ratios in zircon from Archean rhyolite, Panorama Formation, North Pole Dome, Pilbara Craton, Western Australia. *Chemical Geology*, *332*, 102-115.

Kohn, M. J. (2020). A refined zirconium-in-rutile thermometer. *American Mineralogist*, *105*(6), 963-971. https://doi.org/10.2138/am-2020-7091

Kooijman, E., Mezger, K., & Berndt, J. (2010). Constraints on the U–Pb systematics of metamorphic rutile from in situ LA-ICP-MS analysis. *Earth and Planetary Science Letters*, *293*(3-4), 321-330.

Korenaga, J. (2018). Crustal evolution and mantle dynamics through Earth history. *Philosophical Transactions of the Royal Society A: Mathematical, Physical and Engineering Sciences*, *376*(2132), 20170408.

Korenaga, J. (2021). Was there land on the early Earth? *Life*, *11*(11), 1142.

Kröner, A., Anhaeusser, C. R., Hoffmann, J. E., Wong, J., Geng, H., Hegner, E., Xie, H., Yang, J., & Liu, D. (2016). Chronology of the oldest supracrustal sequences in the Palaeoarchaean Barberton Greenstone Belt, South Africa and Swaziland. *Precambrian Research*, *279*, 123-143.

Kröner, A., & Compston, W. (1988). Ion microprobe ages of zircons from early Archaean granite pebbles and greywacke, Barberton greenstone belt, southern Africa. *Precambrian Research*, *38*(4), 367-380.

Kröner, A., Hegner, E., Wendt, J. I., & Byerly, G. R. (1996). The oldest part of the Barberton granitoid-greenstone terrain, South Africa : Evidence for crust formation between 3.5 and 3.7 Ga. *Precambrian Research*, *78*(1-3), 105-124.

Kröner, A., Hoffmann, J. E., Xie, H., Münker, C., Hegner, E., Wan, Y., Hofmann, A., Liu, D., & Yang, J. (2014). Generation of early Archaean grey gneisses through melting of older crust in the eastern Kaapvaal craton, southern Africa. *Precambrian Research*, *255*, 823-846.

Kröner, A., Wong, J., & Xie, H. (2018). The oldest granite clast in the Moodies conglomerate, Barberton greenstone belt, South Africa, and its likely origin. *South African Journal of Geology*, *121*(1), 43-50.

Lana, C., Tohver, E., & Cawood, P. (2010). Quantifying rates of dome-and-keel formation in the Barberton granitoid-greenstone belt, South Africa. *Precambrian Research*, *177*(1), 199-211. https://doi.org/10.1016/j.precamres.2009.12.001

Laurent, O., Björnsen, J., Wotzlaw, J.-F., Bretscher, S., Pimenta Silva, M., Moyen, J.-F., Ulmer, P., & Bachmann, O. (2020). Earth's earliest granitoids are crystal-rich magma reservoirs tapped by silicic eruptions. *Nature Geoscience*, *13*(2), 163-169.

Laurent, O., Guitreau, M., Bruand, E., & Moyen, J.-F. (2024). At the dawn of continents : Archean tonalite-trondhjemite-granodiorite suites. *Elements*, *20*(3), 174-179.

Laurent, O., Martin, H., Moyen, J.-F., & Doucelance, R. (2014). The diversity and evolution of late-Archean granitoids : Evidence for the onset of "modern-style" plate tectonics between 3.0 and 2.5 Ga. *Lithos*, *205*, 208-235.

Laurent, O., Moyen, J.-F., Wotzlaw, J.-F., Björnsen, J., & Bachmann, O. (2022). Early Earth zircons formed in residual granitic melts produced by tonalite differentiation. *Geology*, *50*(4), 437-441.

Laurent, O., Zeh, A., Brandl, G., Vezinet, A., & Wilson, A. (2019). Granitoids and Greenstone Belts of the Pietersburg Block—Witnesses of an Archaean Accretionary Orogen Along the Northern Edge of the Kaapvaal Craton. In A. Kröner & A. Hofmann (Éds.), *The Archaean Geology of the Kaapvaal Craton, Southern Africa* (p. 83-107). Springer International Publishing. https://doi.org/10.1007/978-3-319-78652-0_4

Liu, S., Pan, Y., Xie, Q., Zhang, J., & Li, Q. (2004). Archean geodynamics in the Central Zone, North China Craton : Constraints from geochemistry of two contrasting series of granitoids in the Fuping and Wutai complexes. *Precambrian Research*, *130*(1), 229-249. https://doi.org/10.1016/j.precamres.2003.12.001

Lowe, D. R. (1999). *Geologic evolution of the Barberton Greenstone Belt and vicinity*. https://pubs.geoscienceworld.org/gsa/books/edited-volume/486/chapter-pdf/967261/i0-8137-2329-9-329-0-287.pdf

Lowe, D. R., & Byerly, G. R. (2007). An overview of the geology of the Barberton Greenstone Belt and vicinity : Implications for early crustal development. *Developments in Precambrian geology*, *15*, 481-526.

Lowe, D. R., Drabon, N., Byerly, G. R., & Byerly, B. L. (2021). Windblown Hadean zircons derived by erosion of impact-generated 3.3 Ga uplifts, Barberton Greenstone Belt, South Africa. *Precambrian Research*, *356*, 106111.

Lustrino, M. (2005). How the delamination and detachment of lower crust can influence basaltic magmatism. *Earth-Science Reviews*, *72*(1), 21-38. https://doi.org/10.1016/j.earscirev.2005.03.004

Luvizotto, G. L., Zack, T., Triebold, S., & Von Eynatten, H. (2009). Rutile occurrence and trace element behavior in medium-grade metasedimentary rocks : Example from the Erzgebirge, Germany. *Mineralogy and Petrology*, *97*(3-4), 233-249. https://doi.org/10.1007/s00710-009-0092-z

Mai, V. V., & Korenaga, J. (2022). What controlled the thickness of continental crust in the Archean? *Geology*, *50*(10), 1091-1095.

Martin, H. (1986). Effect of steeper Archean geothermal gradient on geochemistry of subduction-zone magmas. *Geology*, *14*(9), 753-756.

Martin, H., Moyen, J.-F., Guitreau, M., Blichert-Toft, J., & Le Pennec, J.-L. (2014). Why Archaean TTG cannot be generated by MORB melting in subduction zones. *Lithos*, *198*, 1-13.

Martin, H., Moyen, J.-F., & Rapp, R. (2009). The sanukitoid series : Magmatism at the Archaean–Proterozoic transition. *Earth and Environmental Science Transactions of the Royal Society of Edinburgh*, *100*(1-2), 15-33.

Martin, H., Smithies, R. H., Rapp, R., Moyen, J.-F., & Champion, D. (2005). An overview of adakite, tonalite–trondhjemite–granodiorite (TTG), and sanukitoid : Relationships and some implications for crustal evolution. *Lithos*, *79*(1), 1-24. https://doi.org/10.1016/j.lithos.2004.04.048

Meinhold, G. (2010). Rutile and its applications in earth sciences. *Earth-Science Reviews*, *102*(1-2), 1-28.

Meyer, F. M., Robb, L. J., Reimold, W. U., & de Bruiyn, H. (1994). Contrasting low- and high-Ca granites in the Archean Barberton Mountain Land, Southern Africa. *Lithos*, *32*(1), 63-76. https://doi.org/10.1016/0024-4937(94)90021-3

Mezger, K., Hanson, G. N., & Bohlen, S. R. (1989). High-precision UPb ages of metamorphic rutile : Application to the cooling history of high-grade terranes. *Earth and Planetary Science Letters*, *96*(1-2), 106-118.

Mezger, K., Rawnsley, C. M., Bohlen, S. R., & Hanson, G. N. (1991). U-Pb Garnet, Sphene, Monazite, and Rutile Ages : Implications for the Duration of High-Grade Metamorphism and Cooling

Histories, Adirondack Mts., New York. *The Journal of Geology*, *99*(3), 415-428. https://doi.org/10.1086/629503
Miyake, S., Aoki, K., Komiya, T., Aoki, S., Fukuyama, M., & Ogasawara, M. (2024). Geochemical Signatures of Igneous Zircon and Apatite : Generation of Archean TTGs in the Barberton Granitoid-Greenstone Terrain, South Africa. *Island Arc*, *33*(1). https://doi.org/10.1111/iar.12536
Miyashiro, A. (1975). Classification, Characteristics, and Origin of Ophiolites. *The Journal of Geology*, *83*(2), 249-281. https://doi.org/10.1086/628085
Mojzsis, S. J., Harrison, T. M., & Pidgeon, R. T. (2001). Oxygen-isotope evidence from ancient zircons for liquid water at the Earth's surface 4,300 Myr ago. *Nature*, *409*(6817), 178-181. https://doi.org/10.1038/35051557
Montel, J.-M. (1986). Experimental determination of the solubility of Ce-monazite in SiO2-Al2O3-K2O-Na2O melts at 800 C, 2 kbar, under H2O-saturated conditions. *Geology*, *14*(8), 659-662.
Morton, A. (2012). CHAPTER 8 : VALUE OF HEAVY MINERALS IN SEDIMENTS AND SEDIMENTARY ROCKS FOR PROVENANCE, TRANSPORT HISTORY AND STRATIGRAPHIC CORRELATION. In P. Sylvester (Éd.), *Quantitative Mineralogy and Microanalysis of Sediments and Sedimentary Rocks* (Vol. 42, p. 0). Mineralogical Association of Canada. https://doi.org/10.3749/9780921294825.ch08
Morton, A. C., & Hallsworth, C. (2007). Chapter 7 Stability of Detrital Heavy Minerals During Burial Diagenesis. In M. A. Mange & D. T. Wright (Éds.), *Developments in Sedimentology* (Vol. 58, p. 215-245). Elsevier. https://doi.org/10.1016/S0070-4571(07)58007-6
Morton, A. C., & Hallsworth, C. R. (1999). Processes controlling the composition of heavy mineral assemblages in sandstones. *Sedimentary geology*, *124*(1-4), 3-29.
Moyen, J. F., McCoy-West, A. J., Bruand, E., Millet, M. A., Nebel, O., Cawood, P. A., Saji, N., Ladwig, A., Klaver, M., & Elburg, M. (2024). Felsic crust development in the Kaapvaal Craton, South Africa : A reference sample collection to investigate a billion years of geological history. *Earth-Science Reviews*, *250*, 104680. https://doi.org/10.1016/j.earscirev.2024.104680
Moyen, J. F., Zeh, A., Cuney, M., Dziggel, A., & Carrouée, S. (2021). The multiple ways of recycling Archaean crust : A case study from the ca. 3.1 Ga granitoids from the Barberton Greenstone Belt, South Africa. *Precambrian Research*, *353*, 105998.
Moyen, J.-F. (2011). The composite Archaean grey gneisses : Petrological significance, and evidence for a non-unique tectonic setting for Archaean crustal growth. *Lithos*, *123*(1-4), 21-36.
Moyen, J.-F., Laurent, O., Chelle-Michou, C., Couzinié, S., Vanderhaeghe, O., Zeh, A., Villaros, A., & Gardien, V. (2017). Collision vs. subduction-related magmatism : Two contrasting ways of granite formation and implications for crustal growth. *Lithos*, *277*, 154-177. https://doi.org/10.1016/j.lithos.2016.09.018
Moyen, J.-F., & Martin, H. (2012). Forty years of TTG research. *Lithos*, *148*, 312-336.
Moyen, J.-F., Martin, H., Jayananda, M., & Auvray, B. (2003). Late Archaean granites : A typology based on the Dharwar Craton (India). *Precambrian Research*, *127*(1-3), 103-123.
Moyen, J.-F., Stevens, G., & Kisters, A. (2006). Record of mid-Archaean subduction from metamorphism in the Barberton terrain, South Africa. *Nature*, *442*(7102), 559-562.
Moyen, J.-F., Stevens, G., Kisters, A. F., & Belcher, R. W. (2007). TTG plutons of the Barberton granitoid-greenstone terrain, South Africa. *Developments in Precambrian Geology*, *15*, 607-667.
Mühlberg, M., Stevens, G., Moyen, J.-F., Kisters, A. F., & Lana, C. (2021). Thermal evolution of the Stolzburg Block, Barberton granitoid-greenstone terrain, South Africa : Implications for Paleoarchean tectonic processes. *Precambrian Research*, *359*, 106082.
Mulder, J. A., Nebel, O., Gardiner, N. J., Cawood, P. A., Wainwright, A. N., & Ivanic, T. J. (2021). Crustal rejuvenation stabilised Earth's first cratons. *Nature Communications*, *12*(1), 3535.
Næraa, T., Scherstén, A., Rosing, M. T., Kemp, A. I. S., Hoffmann, J. E., Kokfelt, T. F., & Whitehouse, M. J. (2012). Hafnium isotope evidence for a transition in the dynamics of continental growth 3.2 Gyr ago. *Nature*, *485*(7400), 627-630. https://doi.org/10.1038/nature11140
Nebel, O., Capitanio, F. A., Moyen, J.-F., Weinberg, R. F., Clos, F., Nebel-Jacobsen, Y. J., & Cawood, P. A. (2018). When crust comes of age : On the chemical evolution of Archaean, felsic continental crust by crustal drip tectonics. *Philosophical Transactions of the Royal Society A:*

Mathematical, Physical and Engineering Sciences, *376*(2132), 20180103. https://doi.org/10.1098/rsta.2018.0103

O'Sullivan, G., Chew, D., Kenny, G., Henrichs, I., & Mulligan, D. (2020). The trace element composition of apatite and its application to detrital provenance studies. *Earth-Science Reviews*, *201*, 103044.

Palin, R. M., Santosh, M., Cao, W., Li, S.-S., Hernández-Uribe, D., & Parsons, A. (2020). Secular change and the onset of plate tectonics on Earth. *Earth-Science Reviews*, *207*, 103172.

Palin, R. M., White, R. W., & Green, E. C. (2016). Partial melting of metabasic rocks and the generation of tonalitic–trondhjemitic–granodioritic (TTG) crust in the Archaean : Constraints from phase equilibrium modelling. *Precambrian Research*, *287*, 73-90.

Parman, S. W., Dann, J. C., Grove, T. L., & De Wit, M. J. (1997). Emplacement conditions of komatiite magmas from the 3.49 Ga Komati Formation, Barberton greenstone belt, South Africa. *Earth and Planetary Science Letters*, *150*(3-4), 303-323.

PATIÑO DOUCE, A. E., & BEARD, J. S. (1995). Dehydration-melting of Biotite Gneiss and Quartz Amphibolite from 3 to 15 kbar. *Journal of Petrology*, *36*(3), 707-738. https://doi.org/10.1093/petrology/36.3.707

Payne, J. L., McInerney, D. J., Barovich, K. M., Kirkland, C. L., Pearson, N. J., & Hand, M. (2016). Strengths and limitations of zircon Lu-Hf and O isotopes in modelling crustal growth. *Lithos*, *248-251*, 175-192. https://doi.org/10.1016/j.lithos.2015.12.015

Pereira, I., & Storey, C. D. (2023). Detrital rutile : Records of the deep crust, ores and fluids. *Lithos*, *438-439*, 107010. https://doi.org/10.1016/j.lithos.2022.107010

Pereira, I., Storey, C. D., Darling, J. R., Moreira, H., Strachan, R. A., & Cawood, P. A. (2021). Detrital rutile tracks the first appearance of subduction zone low T/P paired metamorphism in the Palaeoproterozoic. *Earth and Planetary Science Letters*, *570*, 117069.

Piccoli, P. M., & Candela, P. A. (2002). Apatite in igneous systems. *Reviews in Mineralogy and Geochemistry*, *48*(1), 255-292.

Pichavant, M., Montel, J.-M., & Richard, L. R. (1992). Apatite solubility in peraluminous liquids : Experimental data and an extension of the Harrison-Watson model. *Geochimica et Cosmochimica Acta*, *56*(10), 3855-3861.

Polat, A. (2012). Growth of Archean continental crust in oceanic island arcs. *Geology*, *40*(4), 383.

Poujol, M. (2001). U-Pb isotopic evidence for episodic granitoid emplacement in the Murchison greenstone belt, South Africa. *Journal of African Earth Sciences*, *33*(1), 155-163. https://doi.org/10.1016/S0899-5362(01)90096-X

Priestley, K., McKenzie, D., & Ho, T. (2018). A Lithosphere–Asthenosphere Boundary—A Global Model Derived from Multimode Surface-Wave Tomography and Petrology. In *Lithospheric Discontinuities* (p. 111-123). American Geophysical Union (AGU). https://doi.org/10.1002/9781119249740.ch6

Raia, F., & Spera, F. J. (1997). Simulations of crustal anatexis : Implications for the growth and differentiation of continental crust. *Journal of Geophysical Research: Solid Earth*, *102*(B10), 22629-22648. https://doi.org/10.1029/97JB01589

Reimer, T. O., Condie, K. C., Schneider, G., & Georgi, A. (1985). Petrography and geochemistry of granitoid and metamorphite pebbles from the early Archaean Moodies Group, Barberton Mountainland/South Africa. *Precambrian Research*, *29*(4), 383-404.

Reimink, J. R., Chacko, T., Stern, R. A., & Heaman, L. M. (2014). Earth's earliest evolved crust generated in an Iceland-like setting. *Nature Geoscience*, *7*(7), 529-533.

Reimink, J. R., Davies, J. H., Bauer, A. M., & Chacko, T. (2020). A comparison between zircons from the Acasta Gneiss Complex and the Jack Hills region. *Earth and Planetary Science Letters*, *531*, 115975.

Reubi, O., & Müntener, O. (2022). Making Andesites and the Continental Crust : Mind the Step When Wet. *Journal of Petrology*, *63*(6), egac044. https://doi.org/10.1093/petrology/egac044

Rey, P. F., Coltice, N., & Flament, N. (2024). Archean geodynamics underneath weak, flat, and flooded continents. *Elements*, *20*(3), 180-186.

Rey, P. F., & Houseman, G. (2006). Lithospheric scale gravitational flow : The impact of body forces on orogenic processes from Archaean to Phanerozoic. *Geological Society, London, Special Publications*, *253*(1), 153-167.

Robb, L. J., Barton Jr, J. M., Kable, E. J. D., & Wallace, R. C. (1986). Geology, geochemistry and isotopic characteristics of the Archaean Kaap Valley pluton, Barberton mountain land, South Africa. *Precambrian Research*, *31*(1), 1-36.

Rollinson, H. (2021). Do all Archaean TTG rock compositions represent former melts? *Precambrian Research*, *367*, 106448. https://doi.org/10.1016/j.precamres.2021.106448

Rudnick, R. L., & Fountain, D. M. (1995). Nature and composition of the continental crust : A lower crustal perspective. *Reviews of Geophysics*, *33*(3), 267-309. https://doi.org/10.1029/95RG01302

Sanchez-Garrido, C. J., Stevens, G., Armstrong, R. A., Moyen, J.-F., Martin, H., & Doucelance, R. (2011). Diversity in Earth's early felsic crust : Paleoarchean peraluminous granites of the Barberton Greenstone Belt. *Geology*, *39*(10), 963-966.

Santos Leandro, M. V., Stevens, G., Moyen, J.-F., Kisters, A., & Ferreira, A. (s. d.). Archean Syenites by Intracrustal Processes : The Boesmanskop Alkaline Complex, Eastern Kaapvaal Craton. *Eastern Kaapvaal Craton*. Consulté 16 mai 2025, à l'adresse https://papers.ssrn.com/sol3/papers.cfm?abstract_id=4972697

Sawyer, E. W. (2020). Petrogenesis of Secondary Diatexites and the Melt Budget for Crustal Reworking. *Journal of Petrology*, *61*(3), egaa039. https://doi.org/10.1093/petrology/egaa039

Schiller, D., & Finger, F. (2019). Application of Ti-in-zircon thermometry to granite studies : Problems and possible solutions. *Contributions to Mineralogy and Petrology*, *174*(6), 51. https://doi.org/10.1007/s00410-019-1585-3

Schirra, M., & Laurent, O. (2021). Petrochronology of hydrothermal rutile in mineralized porphyry Cu systems. *Chemical Geology*, *581*, 120407. https://doi.org/10.1016/j.chemgeo.2021.120407

Schoene, B., Dudas, F. O. L., Bowring, S. A., & De Wit, M. (2009). Sm–Nd isotopic mapping of lithospheric growth and stabilization in the eastern Kaapvaal craton. *Terra Nova*, *21*(3), 219-228. https://doi.org/10.1111/j.1365-3121.2009.00877.x

Scholl, D. W., & Huene, R. V. (2009). Implications of estimated magmatic additions and recycling losses at the subduction zones of accretionary (non-collisional) and collisional (suturing) orogens. In P. A. Cawood & A. Kröner (Éds.), *Earth Accretionary Systems in Space and Time* (Vol. 318, p. 0). Geological Society of London. https://doi.org/10.1144/SP318.4

Scibiorski, E., Tohver, E., & Jourdan, F. (2015). Rapid cooling and exhumation in the western part of the Mesoproterozoic Albany-Fraser Orogen, Western Australia. *Precambrian Research*, *265*, 232-248. https://doi.org/10.1016/j.precamres.2015.02.005

Shirey, S. B., & Hanson, G. N. (1984). Mantle-derived Archaean monozodiorites and trachyandesites. *Nature*, *310*(5974), 222-224.

Sizova, E., Gerya, T., & Brown, M. (2014). Contrasting styles of Phanerozoic and Precambrian continental collision. *Gondwana Research*, *25*(2), 522-545.

SMITHIES, R. H., CHAMPION, D. C., & SUN, S.-. S. (2004). Evidence for Early LREE-enriched Mantle Source Regions : Diverse Magmas from the c. 3·0 Ga Mallina Basin, Pilbara Craton, NW Australia. *Journal of Petrology*, *45*(8), 1515-1537. https://doi.org/10.1093/petrology/egh014

Smithies, R. H., Lu, Y., Johnson, T. E., Kirkland, C. L., Cassidy, K. F., Champion, D. C., Mole, D. R., Zibra, I., Gessner, K., Sapkota, J., De Paoli, M. C., & Poujol, M. (2019). No evidence for high-pressure melting of Earth's crust in the Archean. *Nature Communications*, *10*(1), 5559. https://doi.org/10.1038/s41467-019-13547-x

Spencer, C. J., Cavosie, A. J., Morrell, T. R., Lu, G. M., Liebmann, J., & Roberts, N. M. W. (2022). Disparities in oxygen isotopes of detrital and igneous zircon identify erosional bias in crustal rock record. *Earth and Planetary Science Letters*, *577*, 117248. https://doi.org/10.1016/j.epsl.2021.117248

Spencer, C. J., Kirkland, C. L., Roberts, N. M. W., Evans, N. J., & Liebmann, J. (2020). Strategies towards robust interpretations of in situ zircon Lu–Hf isotope analyses. *Geoscience Frontiers*, *11*(3), 843-853.

Stern, C. R. (2011). Subduction erosion : Rates, mechanisms, and its role in arc magmatism and the evolution of the continental crust and mantle. *Gondwana Research*, *20*(2), 284-308. https://doi.org/10.1016/j.gr.2011.03.006

Stern, R. A., Hanson, G. N., & Shirey, S. B. (1989). Petrogenesis of mantle-derived, LILE-enriched Archean monzodiorites and trachyandesites (sanukitoids) in southwestern Superior Province. *Canadian Journal of Earth Sciences*, *26*(9), 1688-1712.

Stern, R. J. (2005). Evidence from ophiolites, blueschists, and ultrahigh-pressure metamorphic terranes that the modern episode of subduction tectonics began in Neoproterozoic time. *Geology*, *33*(7), 557-560.

Stevens, G., Droop, G. T. R., Armstrong, R. A., & Anhaeusser, C. R. (2002). Amphibolite facies metamorphism in the Schapenburg schist belt : A record of the mid-crustal response to∼ 3.23 Ga terrane accretion in the Barberton greenstone belt. *South African Journal of Geology*, *105*(3), 271-284.

Taylor, S. R., & McLennan, S. M. (1995). The geochemical evolution of the continental crust. *Reviews of Geophysics*, *33*(2), 241-265. https://doi.org/10.1029/95RG00262

Triebold, S., von Eynatten, H., Luvizotto, G. L., & Zack, T. (2007). Deducing source rock lithology from detrital rutile geochemistry : An example from the Erzgebirge, Germany. *Chemical geology*, *244*(3-4), 421-436.

Triebold, S., von Eynatten, H., & Zack, T. (2012). A recipe for the use of rutile in sedimentary provenance analysis. *Sedimentary Geology*, *282*, 268-275.

Valley, J. W., Kinny, P. D., Schulze, D. J., & Spicuzza, M. J. (1998). Zircon megacrysts from kimberlite : Oxygen isotope variability among mantle melts. *Contributions to Mineralogy and Petrology*, *133*(1), 1-11. https://doi.org/10.1007/s004100050432

Valley, J. W., Lackey, J. S., Cavosie, A. J., Clechenko, C. C., Spicuzza, M. J., Basei, M. A. S., Bindeman, I. N., Ferreira, V. P., Sial, A. N., & King, E. M. (2005). 4.4 billion years of crustal maturation : Oxygen isotope ratios of magmatic zircon. *Contributions to Mineralogy and Petrology*, *150*, 561-580.

Vanderhaeghe, O., Teyssier, C., McDougall, I., & Dunlap, W. J. (2003). Cooling and exhumation of the Shuswap Metamorphic Core Complex constrained by 40Ar/39Ar thermochronology. *Geological Society of America Bulletin*, *115*(2), 200-216.

Vervoort, J. D., & Kemp, A. I. (2016). Clarifying the zircon Hf isotope record of crust–mantle evolution. *Chemical Geology*, *425*, 65-75.

Vezinet, A., Flores-Rojas, J., Sobolev, A. V., Léger, J., Chugunov, A. V., Batanova, V. G., Elburg, M. A., Hofmann, A., Balvay, M., & Paradis, N. (2025). Igneous apatite geochemistry indicates early cratonization of continents. *Precambrian Research*, *430*, 107927. https://doi.org/10.1016/j.precamres.2025.107927

Vigneresse, J. L., & Clemens, J. D. (1999). Granitic magma ascent and emplacement : Neither diapirism nor neutral buoyancy. In B. C. Vendeville, Y. Mart, & J.-L. Vigneresse (Éds.), *Salt, Shale and Igneous Diapirs in and around Europe* (Vol. 174, p. 0). Geological Society of London. https://doi.org/10.1144/GSL.SP.1999.174.01.01

Wang, H., Yang, J.-H., Zhu, Y.-S., Huang, C., Xu, L., Wu, S.-T., & Liu, Y. (2022). Archean crustal growth and reworking revealed by combined U-Pb-Hf-O isotope and trace element data of detrital zircons from ancient and modern river sediments of the eastern Kaapvaal Craton. *Geochimica et Cosmochimica Acta*, *320*, 79-104.

Watkins, J. M., Clemens, J. D., & Treloar, P. J. (2007). Archaean TTGs as sources of younger granitic magmas : Melting of sodic metatonalites at 0.6–1.2 GPa. *Contributions to Mineralogy and Petrology*, *154*(1), 91-110. https://doi.org/10.1007/s00410-007-0181-0

Watson, E. B., & Harrison, T. M. (1983). Zircon saturation revisited : Temperature and composition effects in a variety of crustal magma types. *earth and planetary science letters*, *64*(2), 295-304.

Wilde, S. A., Valley, J. W., Peck, W. H., & Graham, C. M. (2001). Evidence from detrital zircons for the existence of continental crust and oceans on the Earth 4.4 Gyr ago. *Nature*, *409*(6817), 175-178.

Wolf, M. B., & Wyllie, P. J. (1993). Garnet Growth during Amphibolite Anatexis : Implications of a Garnetiferous Restite. *The Journal of Geology*, *101*(3), 357-373. https://doi.org/10.1086/648229

Yakymchuk, C., Holder, R. M., Kendrick, J., & Moyen, J.-F. (2023). Europium anomalies in zircon : A signal of crustal depth? *Earth and Planetary Science Letters*, *622*, 118405. https://doi.org/10.1016/j.epsl.2023.118405

Yakymchuk, C., Kirkland, C. L., & Clark, C. (2018). Th/U ratios in metamorphic zircon. *Journal of Metamorphic Geology*, *36*(6), 715-737. https://doi.org/10.1111/jmg.12307

Yearron, L., Clemens, J., Stevens, G., & Anhaeusser, C. (2003). Geochemistry and petrogenesis of the granitoids of the Barberton Mountain Land, South Africa. *EGS-AGU-EUG Joint Assembly*, 2639. https://ui.adsabs.harvard.edu/abs/2003EAEJA.....2639Y/abstract

Zack, T., & Kooijman, E. (2017). Petrology and geochronology of rutile. *Reviews in Mineralogy and Geochemistry*, *83*(1), 443-467.

Zack, T., Moraes, R., & Kronz, A. (2004). Temperature dependence of Zr in rutile : Empirical calibration of a rutile thermometer. *Contributions to Mineralogy and Petrology*, *148*(4), 471-488. https://doi.org/10.1007/s00410-004-0617-8

Zack, T., von Eynatten, H., & Kronz, A. (2004). Rutile geochemistry and its potential use in quantitative provenance studies. *Sedimentary Geology*, *171*(1-4), 37-58.

Zeh, A., Cabral, A. R., Koglin, N., & Decker, M. (2018). Rutile alteration and authigenic growth in metasandstones of the Moeda Formation, Minas Gerais, Brazil – A result of Transamazonian fluid–rock interaction. *Chemical Geology*, *483*, 397-409. https://doi.org/10.1016/j.chemgeo.2018.03.007

Zeh, A., Gerdes, A., & Barton Jr, J. M. (2009). Archean accretion and crustal evolution of the Kalahari Craton—The zircon age and Hf isotope record of granitic rocks from Barberton/Swaziland to the Francistown Arc. *Journal of Petrology*, *50*(5), 933-966.

Zeh, A., Gerdes, A., & Heubeck, C. (2013). U–Pb and Hf isotope data of detrital zircons from the Barberton Greenstone Belt : Constraints on provenance and Archaean crustal evolution. *Journal of the Geological Society*, *170*(1), 215-223.

Zeh, A., Gerdes, A., & Millonig, L. (2011). Hafnium isotope record of the Ancient Gneiss Complex, Swaziland, southern Africa : Evidence for Archaean crust–mantle formation and crust reworking between 3.66 and 2.73 Ga. *Journal of the Geological Society*, *168*(4), 953-964. https://doi.org/10.1144/0016-76492010-117

Zeh, A., Stern, R. A., & Gerdes, A. (2014). The oldest zircons of Africa—Their U–Pb–Hf–O isotope and trace element systematics, and implications for Hadean to Archean crust–mantle evolution. *Precambrian Research*, *241*, 203-230.

Zhang, Z., Deng, Y., Teng, J., Wang, C., Gao, R., Chen, Y., & Fan, W. (2011). An overview of the crustal structure of the Tibetan plateau after 35 years of deep seismic soundings. *Journal of Asian Earth Sciences*, *40*(4), 977-989. https://doi.org/10.1016/j.jseaes.2010.03.010

2. Chapter 2: Presentation of research paper 1 - New U-Pb, trace element, Hf and O isotopic data from detrital zircons of the Barberton Greenstone Belt reveal missing sources to Archean clastic sediments.

This manuscript was submitted to *Precambrian Research,* went through major corrections after constructive comments by editor A. Kemp, R. Bohlar and two anonymous reviewers. It was re-submitted in late October 2025. Supplementary materials are available as an electronic link provided in Chapter 6.

Jean-Baptiste Combaz: Conceptualization, Methodology, Validation, Formal analysis, Investigation, Resources, Data Curation, Writing (original draft), Writing, Review and Editing, Visualization, Project administration, Funding acquisition **Oscar Laurent**: Conceptualization, Methodology, Validation, Resources, Writing-Review and Editing, Visualization, Project administration, Supervision, Funding acquisition **Gary Stevens**: Conceptualization, Validation, Writing-Review and Editing, Project administration, Supervision, Funding acquisition **Nadja Drabon**: Validation, Formal analysis, Resources, Writing-Review and Editing **Sarah Glynn**: Resources, Data Curation, Writing-Review and Editing **Frédéric Couffignal**: Resources, Data Curation, Writing-Review and Editing.

New U-Pb, trace element, Hf and O isotopic data from detrital zircons of the Barberton Greenstone Belt reveal missing sources to Archean clastic sediments.

COMBAZ Jean-Baptiste*[,a,b], LAURENT Oscar[b], STEVENS Gary[a] , DRABON Nadja[c], GLYNN Sarah[d,e], COUFFIGNAL Frédéric[d]

[a]Department of Geology, University of Stellenbosch, Private Bag X1, Matieland 7602, South Africa
[b]Géosciences Environnement Toulouse, CNRS-Université de Toulouse, 14 av. E. Belin, 31400, France
[c]Department of Earth and Planetary Sciences, Harvard University, Cambridge, MA, USA
[d]Helmholtz Centre Potsdam, GFZ German Research Centre for Geosciences, Germany
[e]University of the Witwatersrand, School of Geosciences, South Africa

*Corresponding author: jean-baptiste.combaz@orange.fr; https://orcid.org/0009-0007-1021-4052

Abstract

The formation of the Earth's earliest silicic crust has been largely addressed through the study of the dominant Archean felsic lithology, i.e. tonalite – trondhjemite – granodiorite (TTG) rocks. However, Archean terranes may have been affected by significant preservation biases, which have been overlooked so far. To address this issue, we have conducted a comprehensive study of U-Pb ages, Hf and O isotopic and trace element compositions of detrital zircons deposited over the entire sequence of clastic sediments of the Barberton Greenstone Belt (South Africa). Our study first reveals the importance of local sourcing of sedimentary successions at all stratigraphic levels, which highlights the importance of investigating supracrustal zircons from a large sample set, representative of the lithological diversity and stratigraphy in a given area. Second, our results point to significant biases in the preservation of the Paleoarchean crustal record. Zircons deposited in both the ca. 3.43 Ga Hooggenoeg Formation and the ca. 3.25 Ga Fig-Tree aged meta-greywackes (Schapenburg Schist Belt) revealed $^{207}Pb/^{206}Pb$ age populations and/or trace element compositions that do not have plutonic equivalents in the terranes from which the zircons were sourced. Additionally, compiling our results with datasets from previous work, 40% of all detrital zircons of the ca. 3.22 Ga Moodies Group, while having similar $^{207}Pb/^{206}Pb$ age distribution as that of igneous zircon from regionally exposed TTGs/gneisses, show distinct $\varepsilon Hf_{(t)}$ values (dominantly sub-chondritic) and trace element contents from those of igneous zircons (notably showing dominantly supra-chondritic $\varepsilon Hf_{(t)}$). This also applies to ca. 3.53-3.45 Ga, negative-$\varepsilon Hf_{(t)}$ zircons from two samples of felsic schists of the lower Onverwacht group (Theespruit Formation). We therefore interpret these non-radiogenic zircons to have been sourced from an unpreserved, isotopically evolved and non-TTG magma source, most likely similar to granitic/rhyolitic clasts of the Moodies Basal Conglomerate and the felsic volcanic sequences of the Theespruit Formation. The high proportion of these zircons in the Moodies Group strongly suggests that these granitic clasts are the relicts of a hitherto much more voluminous component of the Paleoarchean felsic crust.. This result calls for a reassessment of the lithological diversity and structure of the Earth's first silicic crust.

2.1. Introduction

The Formation of Earth's earliest stable continental crust played a fundamental role in shaping our planet's habitability (Korenaga, 2012; Spohn & Breuer, 2016; Stern, 2018). However, the mechanisms and geodynamic processes by which this first crust was formed remain controversial, due to the scarcity and ambiguity of the oldest (Hadean and Archean, i.e. 4.5 to 2.5 Ga ago) geological record (see reviews from Gerya, 2014; C. Hawkesworth et al., 2024; C. J. Hawkesworth et al., 2020;

Korenaga, 2018 and references therein). Archean terranes generally show the juxtaposition of two rock-types: 1) Na-rich plutonic or gneissic rocks ("grey gneisses") with a Tonalite-Trondhjemite-Granodiorite (TTGs) composition (Moyen, 2011; Moyen & Martin, 2012; Vezinet et al., 2018) and 2) volcano-sedimentary successions with (ultra)mafic lavas (including komatiites) and meta-sedimentary rocks of both chemical (e.g. Banded Iron Formations) and clastic origin, grouped together under the "greenstone" terminology ; Gorman et al., 1978).

As the earliest, apparently dominant volumetric component (Bleeker, 2003; Polat, 2012) of the Archean continental crust, rocks of the TTG suite have been extensively investigated over the past 50 years to constrain the geological mechanisms and tectonic settings of early felsic crust generation (see Barker & Arth, 1976; Bédard, 2006; Ferrero et al., 2022; Foley, 2008; Jahn et al., 1981; Johnson et al., 2017, 2019; Laurent et al., 2024; Martin, 1986; Moyen & Martin, 2012; Palin et al., 2016; Pourteau et al., 2020; Rollinson, 1996; Smithies, 2000). However, whether the dominance of the TTG suite truly reflects the character of Earth's earliest felsic crust or a preservational bias is increasingly being questioned (Large et al., 2018; Ptáček et al., 2020; Smit & Mezger, 2017; Spencer et al., 2022; Sun, 2018; Tang et al., 2016). Ancient (>3.5 Ga-old), granitoid rocks that do not classify as TTGs have been identified in various cratons, for instance in Isua supracrustal belt of Greenland (Nutman & Hiess, 2009) and in South Africa (Kröner et al., 2018; Sanchez-Garrido et al., 2011). Several recent studies have further shown that even the oldest, Hadean–Eoarchean terranes are characterized by diverse granitoid types, for instance in Eastern Hebei, North China Craton (Dong et al., 2024) and the Slave Craton (Reimink et al., 2014, 2016, 2020). Additionally, the study of Spencer et al., 2022 highlighted the importance of considering preservational bias when dealing with Archean terranes. These findings call for a better characterization of the diversity of earliest silicic crustal rocks and the implications of this for crust-forming processes on the early Earth.

As the present-day inventory of Archean lithologies may result from selective preservation during tectonic/surficial reworking and therefore, not be representative of the original crustal lithologies (C. Hawkesworth et al., 2009; C. J. Hawkesworth et al., 2017, 2020), it is important to learn what we can from accessory minerals in clastic sediments. In this respect, zircon is the mineral of choice

(Harrison et al., 2017). Although mostly crystallizing in intermediate to acidic melts an thus, not representing an entirely comprehensive record of the source material to the sediments which host them (Watson & Harrison, 1983), zircon populations, through their U-Pb magmatic ages (Hoskin & Schaltegger, 2003) and O and Lu-Hf isotopes (Fisher et al., 2011, 2014; C. J. Hawkesworth & Kemp, 2006; Spencer et al., 2020, 2022; Valley et al., 2005), provide essential information as to the age, crustal history and petrogenesis of their host rocks. Additionally, investigations of Archean detrital zircons have benefitted from developments on trace elements (E. Belousova et al., 2002; Grimes et al., 2007, 2015) and Ti thermometry (Ferry & Watson, 2007; Schiller & Finger, 2019) which, despite some inherent biases due to the limited trace element variability of zircon, enable to discriminate between different detrital zircon populations based on their likely source rocks.

The Barberton Greenstone Belt (BGB) of the eastern Kaapvaal Craton (South Africa and Eswatini), one of the best-preserved Paleoarchean (ca. 3.5 to 3.2 Ga-old) greenstone sequences (Anhaeusser, 1980, 1981; De Ronde & De Wit, 1994; Heubeck & Lowe, 1994; Kamo & Davis, 1994; Lowe, 1999; Lowe & Byerly, 2007), is an ideal target to investigate potential preservation biases in the Archean crustal record. The BGB indeed hosts clastic sedimentary rocks spanning over ca. 300 Ma of deposition history, including the 3-4 km-thick Moodies Group (Heubeck et al., 2022; Heubeck & Lowe, 1994, 1994) and thinner layers interspersed through the stratigraphy (Anhaeusser, 1981, 1983; de Wit et al., 2011; Grosch, 2019; Grosch et al., 2011, 2012; Stevens et al., 2002). Moreover, potential igneous sources of detrital material surrounding the BGB have been well characterized, both from a whole-rock geochemical (Anhaeusser, 1980; Moyen et al., 2007; Yearron et al., 2003) and zircon (Laurent et al., 2020, 2022; Zeh et al., 2009, 2011) perspectives. Previous studies showed that detrital zircons in the BGB mainly mimic the U-Pb age distribution of the regional TTG suites (ca. 3.55-3.50, 3.45-3.40 and 3.30-3.20 Ga) (Zeh et al. 2013, Wang et al. 2024, Drabon et al. 2024). Apart from a subordinate group with age distributions tailing up to Hadean dates (4.1-3.3 Ga) that must derive from an extraneous terrane representing reworking of Hadean crust (Drabon et al., 2022), the dominant population of BGB detrital zircon has been interpreted to be derived from local sources, i.e. regional TTGs and the associated Ancient Gneiss Complex (AGC), located to the south of the BGB (Wang et al., 2022; Zeh et

al., 2013); and/or various volcanic-sedimentary rocks from the BGB itself (e.g. Drabon et al., 2024; Heubeck et al., 2022). In particular, some tuffaceous and sedimentary layers of the Upper Onverwacht and Fig Tree Groups were suggested as potential sources of detrital zircons for Moodies strata located in the central BGB (Drabon et al., 2019, 2022, 2024) and Heubeck et al., 2022 highlighted the intra-Formational nature of Moodies sedimentation with most zircons having gone through several sedimentary cycles.

However, the respective contributions of these different lithologies in feeding the sedimentary layers from various stratigraphic levels of the BGB are still unknown as well as the applicability of intra-sedimentary recycling to the whole greenstone belt. Moreover, other potential rock types were so far poorly considered as potential sources, including the oldest (ca. 3.55 Ga) BGB silicic volcanic/volcaniclastic rocks (the Theespruit Formation) (Anhaeusser, 1980; de Wit, 1982; J. F. Diener et al., 2005; Drabon et al., 2024; Heubeck et al., 2022; Kröner et al., 1996, 2013, 2016) and >3.2 Ga K_2O-rich granites/rhyolites now found as clasts in the basal conglomerate of the Moodies group (Kröner et al., 2018; Reimer et al., 1985; Sanchez-Garrido et al., 2011).

The objective of this study is to fill these gaps through a detailed investigation of the provenance of detrital zircon and their host sedimentary rocks over the ca. 300 Ma of BGB history. For this purpose, we performed new U-Pb, Hf-O isotopic and trace element analyses on zircons from clastic meta-sedimentary rocks and volcaniclastic rocks at different levels covering the entire stratigraphy and combine these with existing literature data. Our results point to potential biases affecting both the detrital zircon and exposed lithological records. In particular, we highlight a significant contribution of non-TTG rocks to the detrital zircon record of the BGB, with implications for the diversity of plutonic/volcanic components of the Archean crust and its Formation mechanisms.

2.2. Geological setting

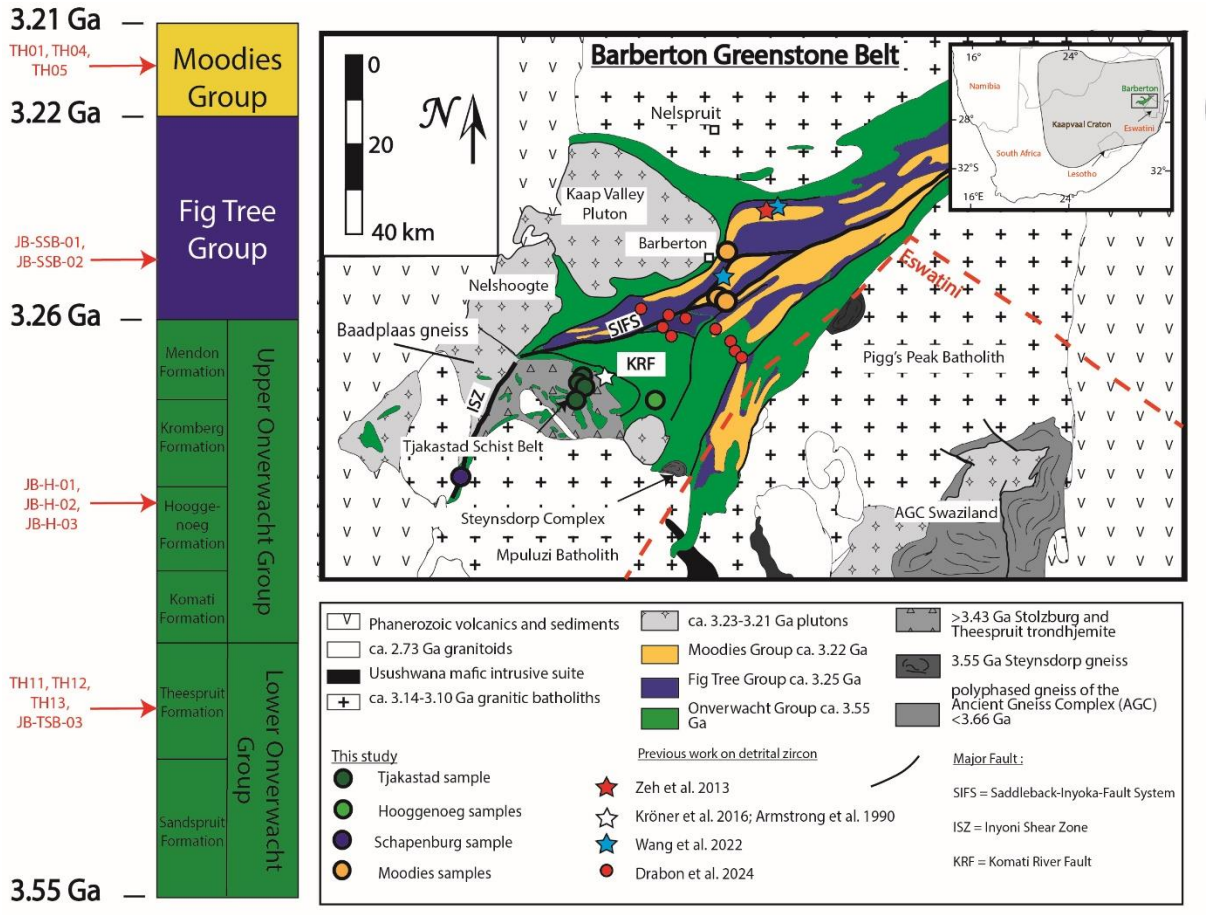

Figure 2-1 : Geological map of the Barberton Granitoid-Greenstone Terrane (after Anhaeusser 1980 and Schoene et al 2008) and synthetic, sketch stratigraphic log (left) of the Barberton Supergroup, showing sample locations (arrows on the log, circles or stars on the map) and their approximative stratigraphic positions.

The Barberton Greenstone Belt (BGB) (**Figure 2-1**) is located in the eastern Kaapvaal craton (South Africa and Eswatini) and is part of the Witwatersrand block (Eglington & Armstrong, 2004; Laurent et al., 2014; Schoene et al., 2008). The structural and stratigraphic characteristics of the belt have been investigated since the early 1960s (Anhaeusser, 1980, 1981, 2019; Condie et al., 1970; De Ronde & De Wit, 1994; De Wit, Armstrong, et al., 1987; de Wit, 1982; Kamo & Davis, 1994). The greenstone sequence is divided into three stratigraphic groups (see **Figure 2-1**), namely (from oldest to youngest) the Onverwacht Group, the Fig Tree Group and the Moodies Group. The 3.55-3.26 Ga Onverwacht Group is mostly made of mafic and ultramafic lavas with minor felsic volcanics and clastic sediments (Decker et al., 2015; Hofmann et al., 2013; Lowe, 1999; Lowe & Byerly, 2020; Trower & Lowe, 2016). The 3.26-3.22 Ga Fig Tree Group contains a greater proportion of sedimentary rocks (including BIF, chert, sandstones and shale) (Byerly et al., 1996; Drabon & Lowe, 2022; Hofmann,

2005; Hofmann et al., 2013; Kohler & Anhaeusser, 2002; Nocita & Lowe, 1990) and volcanic rocks of more silicic (dacitic to rhyolitic) composition (Byerly et al., 1996; Drabon & Lowe, 2022). Finally, the 3.22-3.21 Ga Moodies Group comprises a thick (ca. 3 to 4 km) pile of mature clastic sedimentary rocks (conglomerate, mudstone and sandstone) interlayered with meta-tuffs and felsic volcanic rocks (Heubeck, 2019; Heubeck et al., 2013, 2022).

The BGB is surrounded by silicic plutonic rocks, predominantly TTG gneisses and granitoids emplaced from ca. 3.55 and 3.21 Ga, i.e. broadly synchronously with the deposition of the Barberton Supergroup. The combination of these TTGs and the BGB "greenstones" defines the Barberton Granitoid-Greenstone Terrane (BGGT). The BGGT results from the assembly of two distinct crustal blocks at 3.23-3.22 Ga (e.g. De Ronde & De Wit, 1994; De Wit, Hart, et al., 1987; de Wit, 1982; Moyen et al., 2006, 2007; Stevens & Moyen, 2007; Zeh et al., 2009) along a suture zone represented by major NE-SW-trending structures, the Saddleback-Inyoka Fault system (SIFS) and Inyoni Shear Zone (ISZ) (**Figure 2-1**). The Southern terrane (sensu Zeh et al., 2009) is the oldest crustal block and is further divided into the high-grade (amphibolite-facies) Stolzburg Terrane, south of the Komati River Fault (KRF) (J. F. A. Diener et al., 2005; A. F. M. Kisters et al., 2003; Lowe & Byerly, 2007; Moyen et al., 2007; Stevens & Moyen, 2007) and a lower-grade (greenschist-facies) block north of the KRF (D. Cloete, 1993; M. Cloete, 1999; Grosch, 2019). The Stolzburg Terrane comprises the ca. 3.53 Ga felsic volcanic/volcaniclastic rocks of the Theespruit Formation (Kröner et al., 1996, 2013, 2016) and ca. 3.46-3.44 Ga Stolzburg and Theespruit trondhjemites and related plutonic rocks (Anhaeusser, 1980; Laurent et al., 2020; Moyen et al., 2007). The Stolzburg Terrane underwent ca. 3.23 Ga amphibolite-facies metamorphism (Stevens & Moyen, 2007) and is thought to represent lower crustal exposures of a tectonically overthickened continental crust (J. F. A. Diener et al., 2005; Dziggel et al., 2002, 2006a). North of the SIFS–ISZ suture, the Northern terrane consists largely of younger (and less well studied), ca. 3.29-3.21 Ga-old TTG gneiss units (Badplaas and Nelshoogte) and plutons (Kaap Valley tonalite) (Anhaeusser, 2019; A. F. Kisters et al., 2010; Matsumura, 2014; Moyen et al., 2007; Zeh et al., 2009).

2.3. Materials and methods

2.3.1. Sampling strategy

We collected samples of clastic sedimentary rocks at several levels of the Barberton Stratigraphy (**Figure 2-1**; **Table 2-1**). Three samples of sandstones were collected within Moodies-age strata, two samples of Fig Tree-age meta-greywackes from the Schapenburg Schist Belt (SSB), three samples within sedimentary rocks of the Upper Onverwacht group (corresponding to H6 layer of the Hooggenoeg Formation, the so-called Noisy Formation by de Wit et al., 2011; Grosch et al., 2011 and three samples of felsic schists/volcaniclastics in the Theespruit-age Tjakastad Schist Belt (TSB) in the South. **Figure S4 in supplementary material** show their outcrop patterns and petrography, respectively.

Sample name	Stratigraphic position	Location	Lithology	Latitude	Longitude	Number of O isotopes analyses	Number of U-Pb-trace elements analyses	Number of Lu-Hf analyses
TH01	Moodies Group	Western limb of the Eureka Syncline	Arkosic sandstone with minor conglomerate layers	-25.955	31.2475	0	141	50
TH04	Moodies Group	Dycedale Syncline	Arkosic massive sandstone	-25.999167	31.192	0	287	71
TH05	Moodies Group	Dycedale Syncline	Arkosic massive sandstone	-25.895556	31.192222	0	228	63
SSB-01	Fig Tree Group	Schapenburg Schist Belt	Amphibolitized cross-bedded meta-greywackes/turbidites	-26.18172	30.53802	108	205	46
SSB-02	Fig Tree Group	Schapenburg Schist Belt	Amphibolitized cross-bedded meta-greywackes/turbidites	-26.18109	30.54041	22	50	7
H-03	H6 layer, Upper Onverwacht Group	Eastern limb of the Onverwacht Anticline	Polymictitic volcano-clastic "diamictite"	-26.024619	30.988467	20	61	26
H-02	H6 layer, Upper Onverwacht Group	Eastern limb of the Onverwacht Anticline	Polymictitic volcano-clastic "diamictite"	-26.024619	30.988467	17	50	20
H-01	H6 layer, Upper Onverwacht Group	Eastern limb of the Onverwacht Anticline	Polymictitic volcano-clastic "diamictite"	-26.024483	30.988394	70	195	47
TH11	Theespruit Formation, Lower Onverwacht Group	Tjakastad Schist Belt	Amphibolite Felsic Schist	-25.04	30.994444	0	191	39
TH12	Theespruit Formation, Lower Onverwacht Group	Tjakastad Schist Belt	Amphibolite Felsic Schist	-25.049722	30.873333	0	133	20
TH13	Theespruit Formation, Lower Onverwacht Group	Tjakastad Schist Belt	AmphiboliteFelsic Schist	-25.223056	30.041667	0	280	65
TSB-03	Theespruit Formation, Lower Onverwacht Group	Tjakastad Schist Belt	Amphibolite Felsic Schist	-26.013972	30.783972	76	160	53

Table 2-1 : Summary of samples investigated in this study for detrital zircon studies.

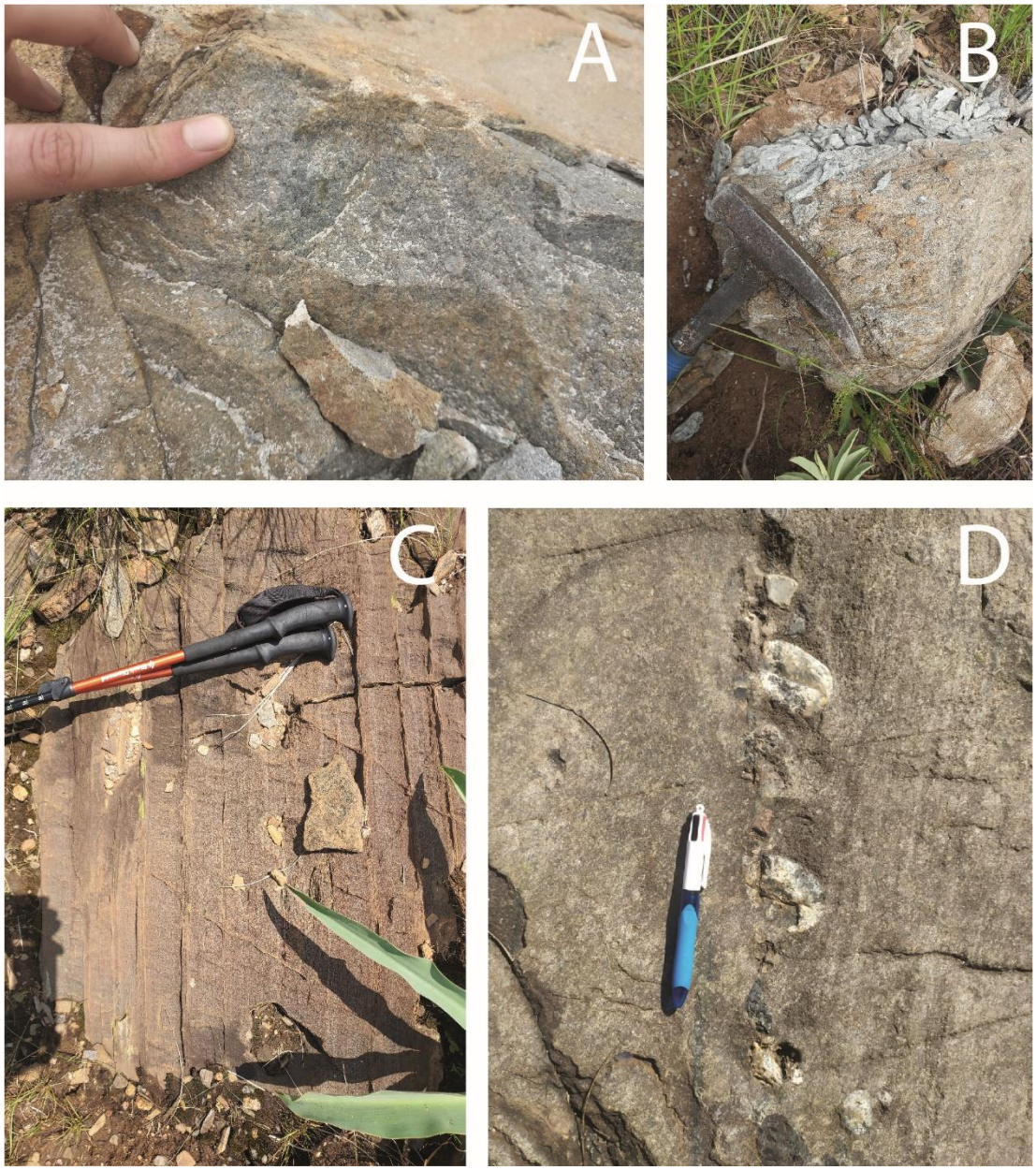

Figure 2-2: Representative pictures of outcrops from which selected samples from this study were collected. A) sample H-01: polymictic volcano-clastic "diamictite" (conglomerate) of the Onverwacht H6 layer (Noisy Formation, de Wit et al., 2011; Grosch et al., 2011). B) sample TSB-03: kyanite-bearing felsic schist of the Tjakastad Schist Belt (sampling site 62105 from Diener, 2004). C) sample SSB-01: planar-bedded meta-greywacke/arkose from the Schapenburg Schist Belt (locality described in Stevens et al., 2002). D) sample TH-01: sandstone with conglomeratic pebbles from the Moodies group in the western flank of the Eureka Syncline (unit MdQ1 of Heubeck et al., 2022).

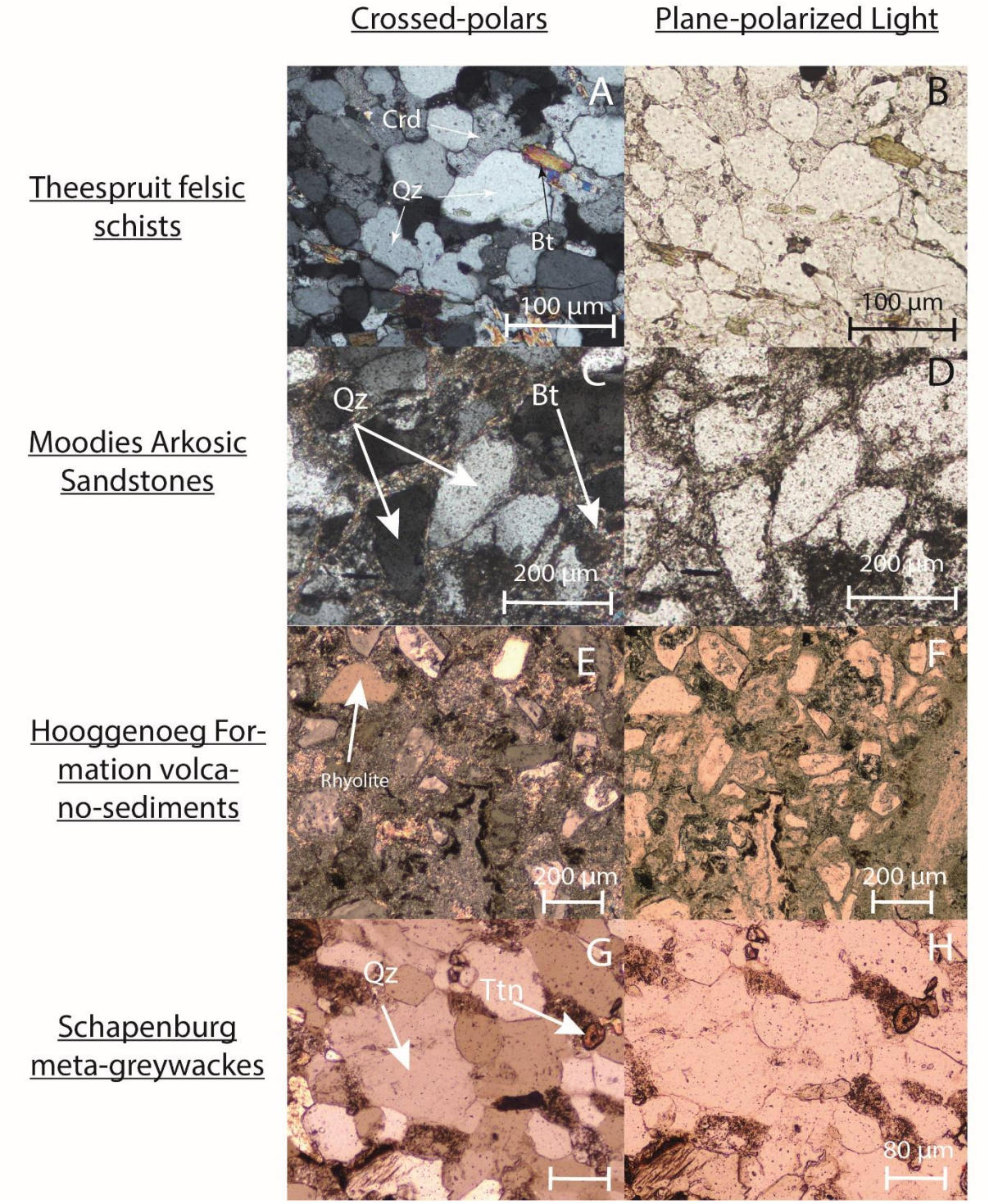

Figure 2-3: Representative thin section photomicrographs (crossed polars on the left, plane-polarized light on the right) of selected samples investigated in this study. A-B) Crd-Qz-Bt bearing felsic schists from the Theespruit Formation (sample TH12). C-D) Moodies arkosic sandstone (sample TH05). E-F) matrix-supported volcano-sediments of the Hooggenoeg Formation (sample H-01). G-H) Meta-greywackes of the Schapenburg Schist Belt (sample SSB-01).

2.3.2. Methods

We have separated zircon from bulk rocks through conventional heavy mineral concentration techniques (hand panning, magnetic and heavy liquid separation) following crushing using the Selfrag

device at the University of Pretoria (South Africa). Zircons were handpicked under a binocular microscope, cast in epoxy resin (together with zircon reference materials Temora-2 and 91500 for SIMS analyses) and polished to a sub-equatorial section. Zircon cathodoluminescence (CL) imaging was performed on scanning electron microscopes (SEM) either at the Central Analytical Facility at Stellenbosch University (South Africa) using a Zeiss Merlin FEG SEM or at Géosciences Environnement Toulouse (France) using a Tescan Vega4 SEM. Zircon O isotopic analyses were performed using the Cameca 1280-HR secondary ion mass spectrometer (SIMS) at the Helmholtz Zentrum Potsdam, operated from the virtual SIMS facility at the University of the Witwatersrand, Johannesburg (South Africa). Simultaneous zircon U-Pb dating and trace element analyses were carried out at the Service ICP-MS of Observatoire Midi-Pyrénées (OMP-UAR831) in Toulouse (France), by laser ablation – inductively coupled plasma – mass spectrometry (LA-ICP-MS) using an Elemental Scientific Instruments NWRfemto solid-state femtosecond laser ablation system set to UV mode (257 nm wavelength) coupled with a ThermoScientific Element XR sector-field ICP-MS. Zircon Lu-Hf isotopic analyses were performed by laser ablation – multi-collection – inductively coupled plasma – mass spectrometry (LA-MC-ICP-MS) using the same laser ablation system as for U-Pb dating and trace elements, coupled to a ThermoScientific Neptune Plus MC-ICP-MS. All LA-(MC-)ICP-MS data were processed using the Iolite v4.0 software. To calculate initial Hf isotopic compositions and $\varepsilon Hf_{(t)}$ values, we have used a decay constant $\lambda^{176}Lu$ of $1.87E^{-11}$ a^{-1} (Bouvier et al., 2008; Scherer et al., 2001; Söderlund et al., 2004) and parameters for today's CHUR reservoir of $^{176}Hf/^{177}Hf = 0.282785$ (see Bouvier et al., 2008; Vervoort & Blichert-Toft, 1999) and $^{176}Lu/^{177}Hf = 0.0336$ (Blichert-Toft & Puchtel, 2010). The Depleted Mantle (DM) curve in all plots corresponds to today's DM values of $^{176}Hf/^{177}Hf = 0.283294$ (Bouvier et al., 2008; Vervoort & Blichert-Toft, 1999) and $^{176}Lu/^{177}Hf = 0.03933$(Blichert-Toft & Puchtel, 2010).

Further details about analytical setups and results on reference materials, together with the entire datasets, are provided in the **Supplementary material to Chapter 2**.

2.4. Results

2.4.1. Filtering of the data

The compositions of ancient zircon are particularly sensitive to the consequences of radiation damage including Pb loss and/or post-magmatic (hydro-)thermal alteration (Bell et al., 2016, 2019; Bolhar et al., 2008, 2021; Hoskin, 2005; Kitajima et al., 2012). Therefore, zircon data were filtered using criteria based on both U-Pb (discordance) and trace elements to only retain analyses that are as representative as possible of pristine (igneous) zircon compositions. We have used the following conventional filters applied in the literature:

1) Zircon concordance (ratio of $^{238}U/^{206}Pb$ to $^{235}U/^{207}Pb$ dates) between 95 and 105%. Outside this range, zircon was considered discordant and thus not considered.
2) LREE contents, which incorporation in zircon is generally a consequence of hydrothermal alteration (Bolhar et al., 2021, Hoskin. 2005) and/or indicates the presence of inclusions. Zircon analyses with La contents above 5 ppm and/or a LREE-Index (Dy/Nd+Dy/Sm) (Bell et al., 2016, 2019) below 20 were considered significantly altered and filtered out.
3) Analyses with Ca contents above 500 ppm were discarded as Ca enrichment may reflect precipitation of zirconolite in amorphous zones (Gieré, 1986; Williams & Gieré, 1996).

In addition to these criteria based on U-Pb and trace element data, further filtering was applied for Lu-Hf data to consider other potential sources of bias (e.g. (Fisher et al., 2014; Vervoort & Kemp, 2016). This is particularly the case of ancient Pb loss events resulting in apparently concordant data, hence calculation of initial Hf isotopic composition at the wrong age. To mitigate this problem, inspired by the method to identify Pb loss in cogenetic populations of igneous zircon (e.g. Gerdes and Zeh, 2009), zircon analyses that plot along sub-horizontal trends in $^{176}Hf/^{177}Hf_{(t)}$ vs $^{207}Pb/^{206}Pb$ date diagrams were discarded. Additionally, data of poor quality, e.g. affected by cracking and/or unstable signal resulting in far too large 2SE propagated uncertainties to be usable for interpretation (i.e. in excess of ±4 εHf-units), were removed.

In summary, the following age distributions and trace elements plots display only zircon data that passed all filtering criteria based on U-Pb and trace elements. Further, all analyses plotted in the $\varepsilon Hf_{(t)}$

vs age plots positively meet the criteria based on Lu-Hf data mentioned above and on U-Pb-trace elements filters. More details on the filtering are provided in **Supplementary material to Chapter 2.**

2.4.3. Zircon dates, trace elements and Hf-O isotopic data

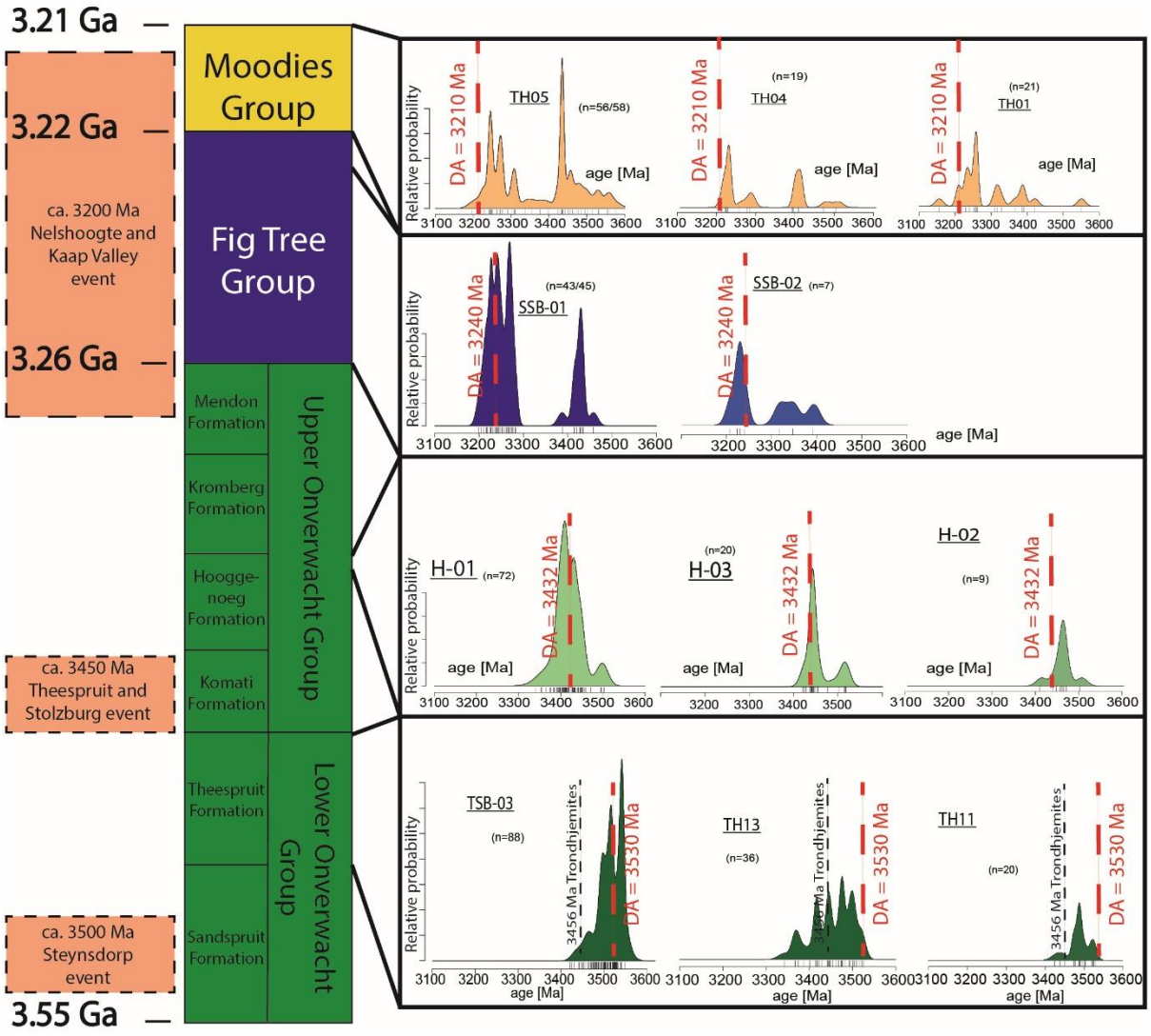

Figure 2-4: Kernel Density Estimates of $^{207}Pb/^{206}Pb$ age distributions for zircon from all samples investigated in this study. Vertical red dashed lines indicate the inferred depositional age (DA) of supracrustal units from literature data (Grosch et al., 2011; Heubeck et al., 2013; Kröner et al., 2016; Stevens et al., 2002) and black dashed lines are dates of intrusive igneous rocks. "3456 Ma trondhjemite depicts the age of intrusion of the Theespruit and Stolzburg trondhjemites ((J. F. A. Diener et al., 2005; Laurent et al., 2020; Moyen et al., 2007) into the stratigraphy of the Lower Onverwacht Theespruit and Sandspruit Formations and provides a minimum age for the deposition of the Theespruit Felsic volcanic rocks.

Zircon date distributions are shown on **Figure 2-4**, CL images of grains with representative $\varepsilon Hf_{(t)}$ and Ti, Th/U and Nb contents on **Figure 2-5** and Hf-O isotopic and trace element data on **Figure 2-6**. The data are further discussed in the following from bottom to top of the Barberton Supergroup stratigraphy. Th/U, Ti, Hf and Nb contents variations in zircons are shown as they produced the strongest differences between populations compared with other trace elements proxies.

2.4.3.1. Theespruit Felsic Volcanic Rocks/Schists of the Tjakastad Schist Belt (TSB)

Zircons from samples of the Tjakastad Schist Belts display the diagnostic oscillatory zoning pattern that is characteristic of magmatic zircons, even though some are darker and more homogeneous (**Figure 2-5**). Zircons from the felsic schist TSB-03 mainly show a range of $^{207}Pb/^{206}Pb$ dates between ca. 3550 and 3480 Ma, with a main peak at ca. 3530 Ma (see **Figure 2-4**). Zircons from this sample show mainly mantle-like $\delta^{18}O$ values (from +5.0 to +5.5‰) and positive $\varepsilon Hf_{(t)}$ (up to +5.0 **Figure 2-6 A-B**) with only 21% having $\varepsilon Hf_{(t)}$ between 0 and -3.2. In contrast, samples TH-13 and TH-11 from the same unit tend to show younger date distributions, generally down to ca. 3450 Ma, and only produced zircons with negative $\varepsilon Hf_{(t)}$ (values between -2.3 and -6.1, **Figure 2-6 B**). In comparison with zircons crystallized in Barberton TTGs plutonic rocks (Laurent et al., 2022; Zeh et al., 2009, 2011) (referred in the following to as "BTTG zircons"), zircons of the TSB samples show more scattered Ti, Nb contents and Th/U ratios, trending to higher Nb (values between 5 to 20 ppm) and Th/U (0.4–1.0) at similar to slightly higher Ti content (2-20 ppm) (**Figure 2-6 C**).

2.4.3.2. Hooggenoeg Formation diamictites

Zircons of the Upper Onverwacht Hooggenoeg Formation are euhedral in shape and all show bright luminescence and the typical oscillatory zoning patterns that one can expect for magmatic zircons (Hoskin & Schaltegger, 2003; Rubatto, 2017) (**Figure 2-5**). Zircons from all samples of the Hooggenoeg Formation display a major, single peak of $^{207}Pb/^{206}Pb$ dates at ca. 3430 Ma (**Figure 2-4**)

and the presence of a minor 3500-3470 Ma population in samples H-03 and H-01 but not in sample H-02, could be related to the lower number of data (n = 9) for the latter.

Hooggenoeg zircons display $\delta^{18}O$ between +5 and +6 ‰ and 88% of radiogenic zircons ($\varepsilon Hf_{(t)}$ values from 0 to +5.2 see **Figure 2-6A-B**) with only few data ranging down to -2.3. In comparison with BTTG zircons (Laurent et al., 2020; Zeh et al., 2009), zircons of the Hooggenoeg Formation show a more scattered $\varepsilon Hf_{(t)}$ vs. age distribution but have similar trace element contents, that is, 2–15 ppm Ti (with few showing up to 25–40 ppm), 1–5 ppm Nb, 7500–10500 ppm Hf and Th/U ratios between 0.2 and 0.6 (**Figure 2-6 C-D**).

2.4.3.3. Fig Tree meta-greywackes of the Schapenburg Schist Belt (SSB)

Fig Tree meta-greywackes of the SSB contain two populations of zircons in terms of morphology and texture (**Figure 2-5**). One is darker in color with faint to no zoning, while the other shows brighter luminescence and diagnostic oscillatory zoning. However, these two groups do not show clear correlations with geochemical data. Two zircon $^{207}Pb/^{206}Pb$ date clusters can be observed in these samples, one dominant population at ca. 3280-3200 Ma and a subordinate, older one, between 3400 and 3350 Ma for SSB-02 and 3500 to 3400 Ma for SSB-01 (**Figure 2-4**).

In terms of O isotopes, the Schapenburg zircons show a dichotomy between the two date groups, with the 3280-3200 Ma zircons showing $\delta^{18}O$ between +6 and +8 ‰ while the older groups (3500-3350 Ma) have more mantle-like values (+5 to +6‰) (**Figure 2-6 A**). This observation fits with the shift towards elevated $\delta^{18}O$ at 3.25 Ga already observed at 3.25 Ga in the Barberton zircon record (Drabon et al. 2022; Wang et al. 2022). The Hf isotopic compositions of the Schapenburg meta-greywackes zircons is mainly supra-chondritic, with ~ 16 % of which with $\varepsilon Hf_{(t)}$ values from 0 to -3.9 and ~ 84% with $\varepsilon Hf_{(t)}$ values from 0 to +6.4 (**Figure 2-6 B**), which overlap well with BTTG zircons. Likewise, trace element contents of these zircons show strong similarity with those of the BTTG and of the Hooggenoeg Formation zircons, with 1–5 ppm Nb, 2–20 ppm Ti, 8000–11000 ppm Hf and Th/U ratios mainly from 0.2 to 0.6 (**Figure 2-6 C-D**).

2.4.3.4. Moodies sandstones

Zircons of the Moodies samples are generally dark in CL images with faint oscillatory zoning patterns, although a few grains show brighter luminescence and more pronounced zoning (**Figure 2-5**). These features resemble the zircons of the Theespruit Formation. Moodies zircons have $^{207}Pb/^{206}Pb$ dates scattering between 3550 and 3200 Ma, which cover the whole magmatic history of the BGB (**Figure 2-4**). The main date peaks, corresponding to the three main magmatic events that affected the BGB (ca. 3550-3480 Ma; ca. 3480-3400 Ma; and ca. 3300-3200 Ma; cf. **Figure 2-4** and Moyen et al. 2007), are represented within each sample. This age distribution is similar to that described by previous studies (Zeh et al., 2013; Drabon et al., 2022, 2024; Wang et al., 2022).

As we could not obtain O isotopic data on the Moodies zircons due to difficulties in the planning of analytical sessions, we have plotted the O isotopes data from Wang et al. (2022) for comparison, which show very similar zircon age distributions as our samples. This, as for the SSB zircons, reveals the mantle-like signature of the oldest age clusters (+5.0 to +6.5‰ at 3550-3400 Ma) and trend towards heavier O isotopic composition between 3300 and 3200 Ma (+5.5 to +8.5‰) (**Figure 2-6 A**). The Hf isotopic composition of the oldest (3580-3480 Ma) cluster is variable with 8 points showing non-radiogenic εHf(t) between 0 to -7.2 and 2 spots plotting above the CHUR line at 0 to +4.0 (**Figure 2-6 B**). The ca. 3480-3360 Ma date cluster shows dominantly subchondritic Hf isotopic compositions, with 27 out of 30 points showing $\varepsilon Hf_{(t)}$ between 0 and -3.6 and the remaining 3 points ranging up to +3.1 (**Figure 2-6 B**). Lastly, among the 48 zircons making up the 3360-3200 Ma cluster, only 3 are radiogenic ($\varepsilon Hf_{(t)}$ values between 0 and +1.6) and the rest have sub-chondritic $\varepsilon Hf_{(t)}$ (down to -8.3; **Figure 2-6 B**). Overall, the three samples of the Moodies arkosic sandstones contain 91% of sub-chondritic zircons, which contrasts with the plutonic zircons from the BTTGs at equivalent dates that show mainly positive $\varepsilon Hf_{(t)}$ (**Figure 2-6 B**). In terms of trace elements, the Moodies zircons largely overlap with the BTTG (and Hooggenoeg Formation and SSB) zircons (2-5 ppm Nb; 2-20 ppm Ti; 8000-12500 ppm Hf), albeit with some data trending towards higher Nb (up to 10 ppm), Ti (up to 40

ppm) contents and Th/U ratios (up to 1.8) (**Figure 2-6 C-D**). Overall, while the age distribution and trace element signatures of our Moodies zircons are similar to those reported by (Drabon et al., 2024; Drabon & Lowe, 2022; Wang et al., 2022) (**Figure 2-6 C**), the Hf isotopic compositions somewhat differ (dominant sub-chondritic in our case) (**Figure 2-6 B-E**).

Theespruit zircons

TH13_56 : $^{207}Pb/^{206}Pb$ age = 3401 +/- 73 Ma
[Ti] = 17.5 ppm
[Nb] = 12.61 ppm
[Hf] = 9139 ppm
Th/U = 0.49
εHf(t) = -4.1 +/- 2.9

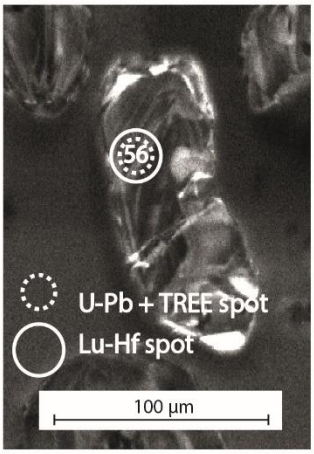

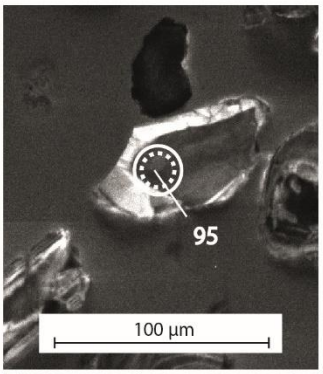

TH13-95 : $^{207}Pb/^{206}Pb$ age = 3492 +/- 45 Ma
[Ti] = 10.53 ppm
[Nb] = 5.21 ppm
[Hf] = 7603 ppm
Th/U = 0.91
εHf(t) = -12.2 +/- **9.9 !!**

TH11-28 : $^{207}Pb/^{206}Pb$ age = 3440 +/- 58 Ma
[Ti] = 14.65 ppm
[Nb] = 9.46 ppm
[Hf] = 7458 ppm
Th/U = 0.92
εHf(t) = -5.2 +/- 2.4

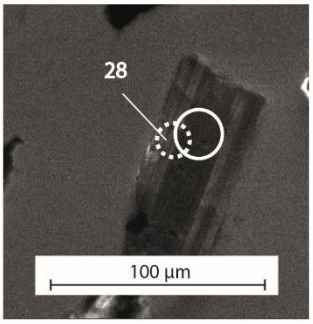

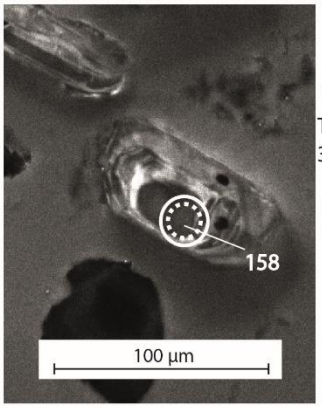

TH13-158 : $^{207}Pb/^{206}Pb$ age = 3417 +/- 46 Ma
[Ti] = 10.77 ppm
[Nb] = 5.86 ppm
[Hf] = 7716 ppm
Th/U = 1.01
εHf(t) = -3.3 +/- 2.6

Hooggenoeg Formation zircons

JB-H-01 : $^{207}Pb/^{206}Pb$ age = 3420 +/- 11 Ma
[Ti] =3.39 ppm
[Nb] = 1.48 ppm
[Hf] = 9650 ppm
Th/U = 0.32
εHf(t) = 2.4 +/- 2.1
$\delta^{18}O$ = 5.41 +/- 1.0

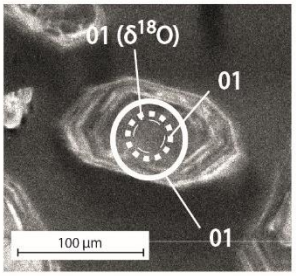

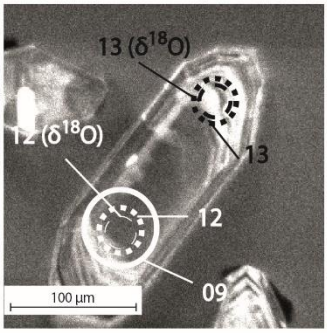

JB-H-01-12 : $^{207}Pb/^{206}Pb$ age = 3399 +/- 13 Ma
[Ti] =3.14 ppm
[Nb] = 2.50 ppm
[Hf] = 10540 ppm
Th/U = 0.36
(09) εHf(t) = 6.9 +/- 2.4
$\delta^{18}O$ = 5.65 +/- 0.12
JB-H-01-13 : concordant spot with [La] = 19.5 ppm et LREE-I >20 => filtered out

JB-H-01-55 : $^{207}Pb/^{206}Pb$ age = 3451 +/- 14.13 Ma
[Ti] =4.66 ppm
[Nb] = 1.24 ppm
[Hf] = 8572 ppm
Th/U = 0.4
(36) εHf(t) = 0.8 +/- 2.4
$\delta^{18}O$ = 5.74 +/- 0.12

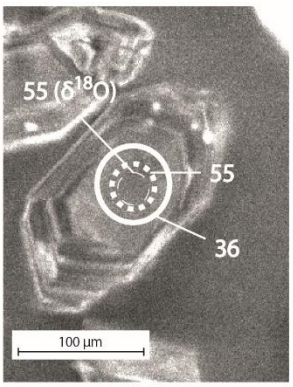

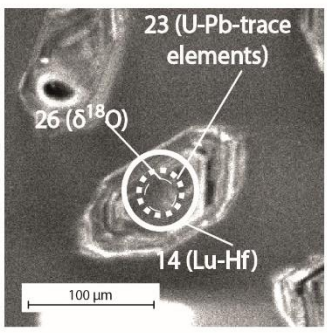

JB-H-01-23 : $^{207}Pb/^{206}Pb$ age = 3391 +/- 17.49 Ma
[Ti] = 3.55 ppm
[Nb] = 2.39 ppm
[Hf] = 10708 ppm
Th/U = 0.42
(14) εHf(t) = 2.6 +/- 2.7
(26) $\delta^{18}O$ = 5.76 +/- 0.08

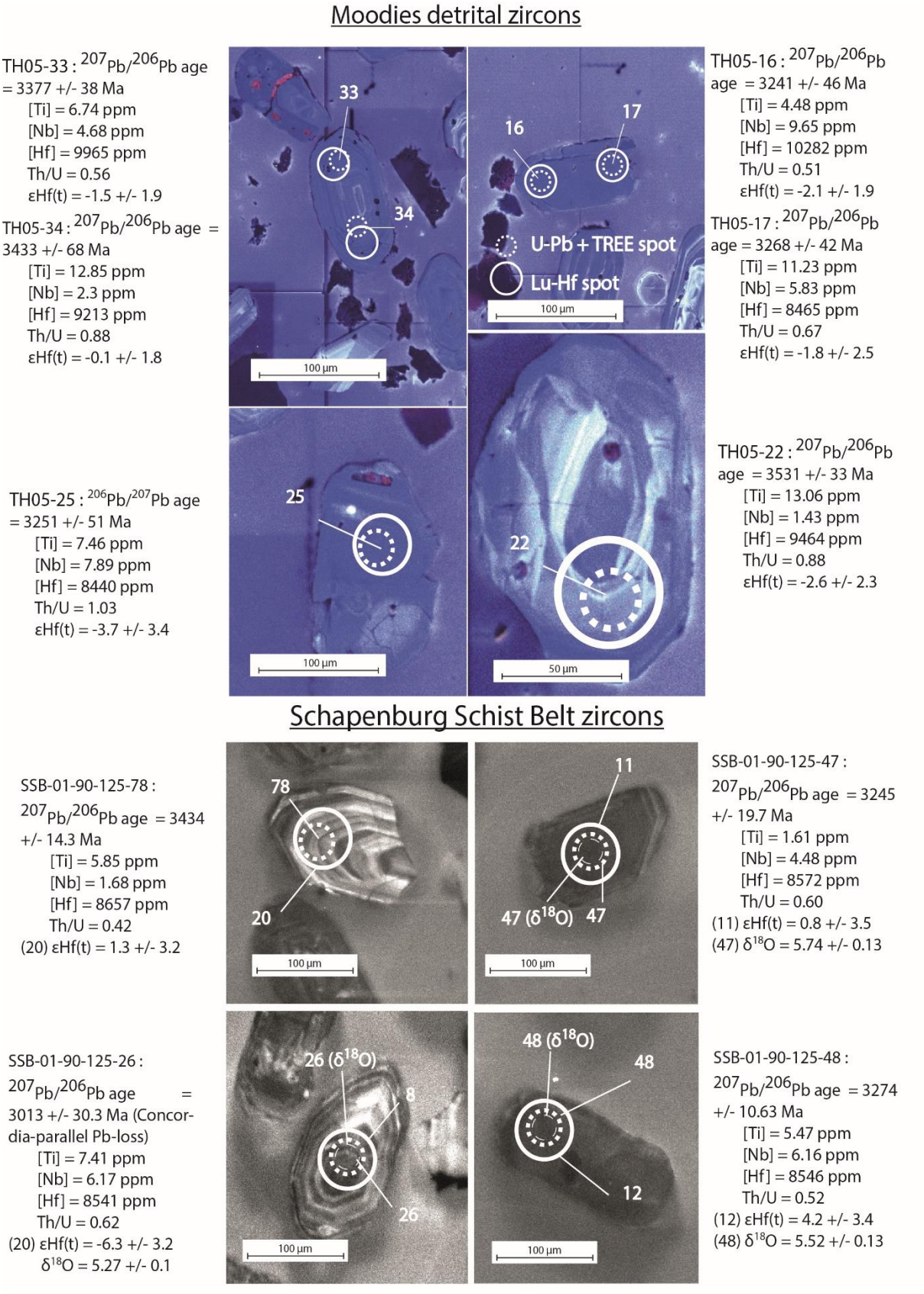

Figure 2-5: Cathodoluminescence images of representative zircons from samples investigated in this study, for each stratigraphic unit. Circles indicate the position of analytical spots. Spot TH13_95 belongs to the "not used" category as it has high 2SE uncertainties on $\varepsilon Hf_{(t)}$. Uncertainties for $^{207}Pb/^{206}Pb$ dates and $\varepsilon Hf_{(t)}$ are given at 95% confidence level (2 SE).

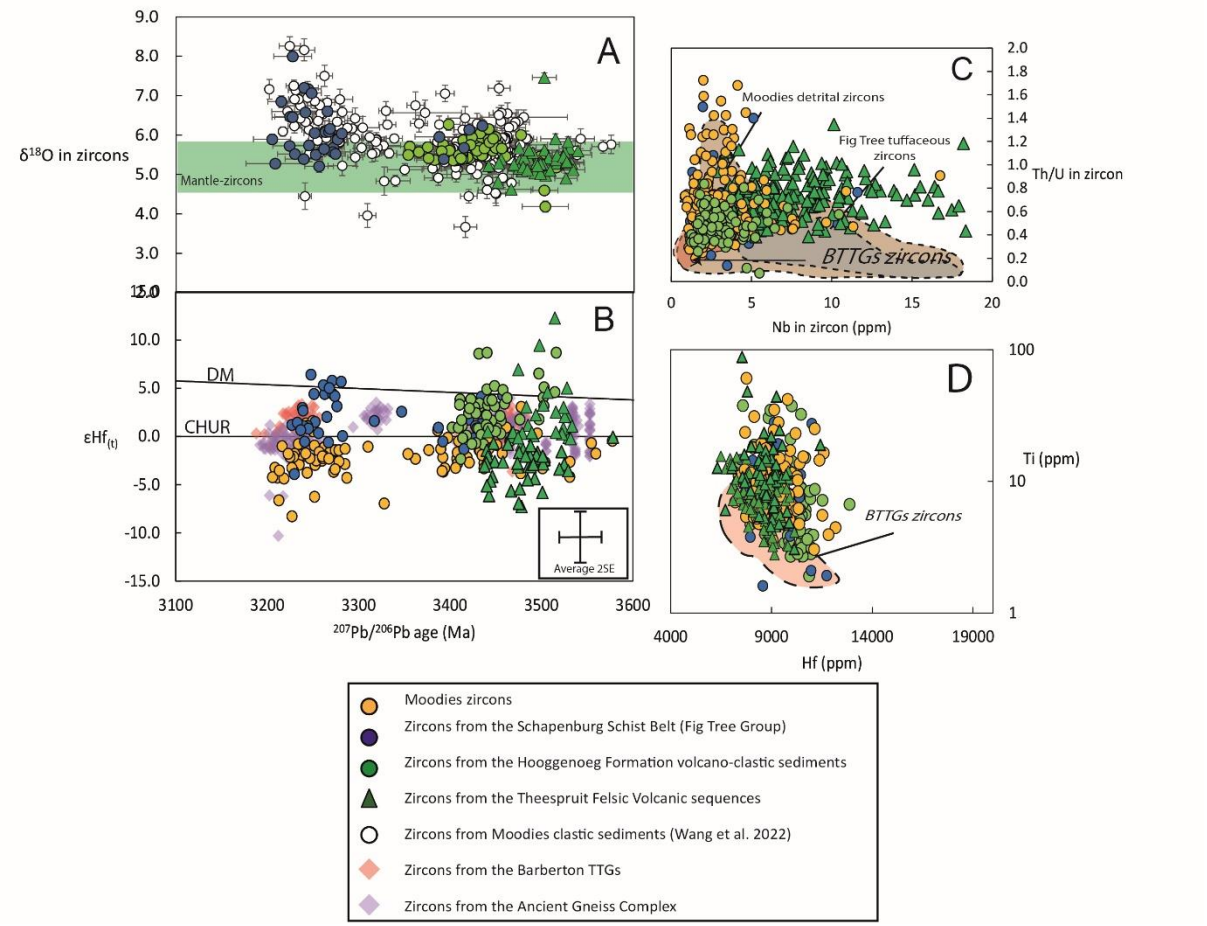

Figure 2-6: Isotopic and chemical data of Barberton supracrustal zircons (this study and literature data). A) $\delta^{18}O$ vs $^{207}Pb/^{206}Pb$ age for zircons of this study and Wang et al. (2022). B) $\varepsilon Hf_{(t)}$ vs $^{207}Pb/^{206}Pb$ age for zircons of this study and Barberton TTG zircons (Laurent et al., 2020; Zeh et al., 2009) and AGC zircons (Hoffmann et al., 2016; Kröner et al., 2014; Zeh et al., 2011). C) Th/U vs Nb and D) Ti vs Hf plots for zircons of this study. In C, Moodies and Fig Tree zircons are from Drabon et al. (2024) and Barberton TTG zircons from Laurent et al. (2022).

2.5. Discussion

2.5.1. Provenance of the studied BGB supracrustal zircons

In this section, we discuss the provenance of zircon populations for each investigated stratigraphic level through comparison with zircon data from putative regional igneous sources. We then discuss the geological implications in terms of sediment sourcing, deposition age and origin/evolution of the BGB volcanic-sedimentary sequences.

2.5.1.1. Tjakastad Schist Belt (TSB)

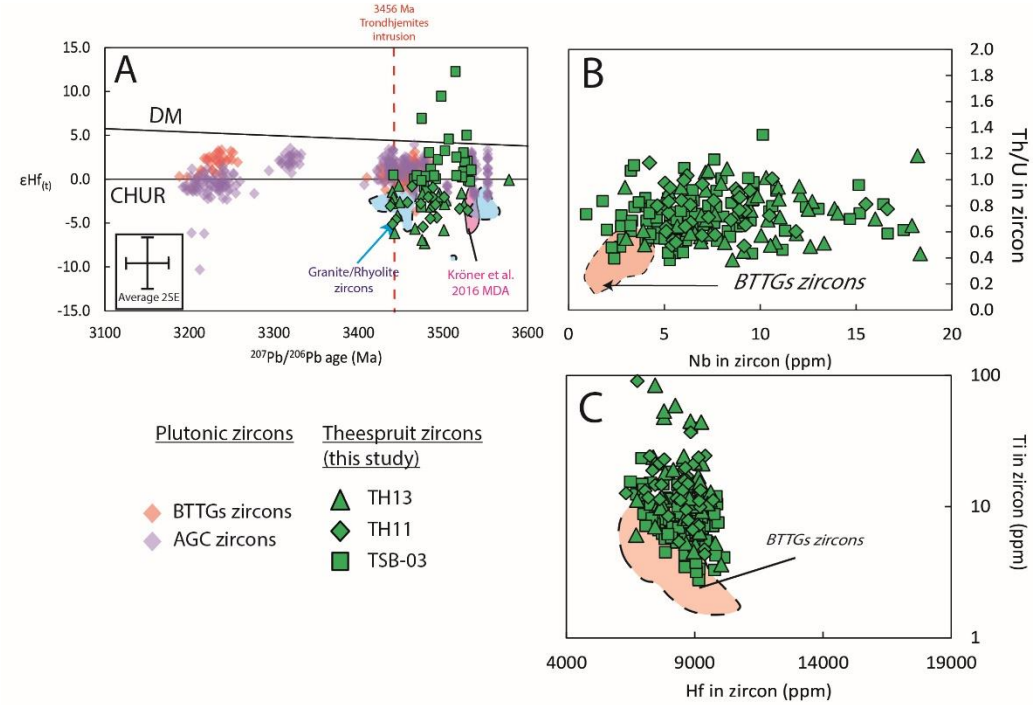

Figure 2-7: Geochemical and isotopic discrimination plots of Theespruit zircons from this study with zircons of the BTTGs (compilation from Laurent et al., 2022, Zeh et al., 2009). A) eHf(t) vs $^{207}Pb/^{206}Pb$ age in zircon compared with BTTG zircon compilation from Laurent et al., 2022, Zeh et al., 2009 and AGC zircon compilation from Hoffman et al., 2016, Kröner et al., 2014 and Zeh et al., 2011 and granitic zircon s from the Moodies Basal Conglomerate from Sanchez-Garrido et al., 2011, 2012. B) Th/U vs Nb contents in zircon). C) Ti vs Hf in zircon. Age of deposition (MDA)in graph A applies to the felsic volcano-clastic rocks sampled by Kröner et al. 2016. In graph B and C, trace elements in BTTG zircons derive from Laurent et al., 2022.

Felsic schists of the TSB, which belongs to the Theespruit Formation (see discussion from Anhaeusser, 1981; De Wit, Armstrong, et al., 1987), yield a relatively large spread of zircon $^{207}Pb/^{206}Pb$ dates (ca. 3540–3440 Ma; **Fig. 2-8A**). This links to debates about the timing of deposition of this supracrustal sequence, proposed to be either 3527 ± 15 Ma (zircon extracted from felsic tuffs and meta-

agglomerates; Kröner et al. 2016, see locality on **Figure 2-1**) or ca. 3453 Ma (zircons extracted from polymictitic diamictite at nearly the same locality; Armstrong et al. 1990). As shown in **Figure 2-7 A**, Theespruit zircons from all three samples investigated here are mostly younger than the maximum deposition age proposed by Kröner et al. (2016). They show dates between ca. 3540 to 3440 Ma, so still older within uncertainty than the age of intrusion of the ca. 3456 Ma-old Theespruit and Stolzburg trondhjemites (Laurent et al., 2020, 2022) that intrude the Theespruit Formation. Thus, they better agree with depositional age initially proposed by (Armstrong et al., 1990). One possibility to explain these dates younger than the depositional age of Kröner et al., 2016 would be that the younger Theespruit zircons suffered ancient Pb loss, or correspond to mixing with metamorphic zircon domains crystallized during the regional, ca. 3230 Ma metamorphic event (Van Kranendonk et al., 2009, Diener et al. 2005, Dziggel et al. 2002, 2006, Lana et al. 2010), as originally argued by Kröner et al., 2016 to discard the ca. 3453 Ma deposition age. However, this possibility is considered unlikely for two reasons. First, our Theespruit zircons passed all the compositional and isotopic filters described in section 2.4.2. and unlikely suffered from ancient Pb loss, as they do not clearly define sub-horizontal trends in graphs of $^{176}Hf/^{177}Hf_{(t)}$ vs $^{207}Pb/^{206}Pb$ date. Second, the U-Pb dates, trace element and Hf isotopic compositions of Theespruit zircons show strong differences from sample to sample, even on a small scale. Sample TSB-03 shows mainly zircons both younger and older than 3500 Ma with $\varepsilon Hf_{(t)}>0$ and relatively low average zircon Ti contents, whereas samples TH13 and TH11, collected few km North of TSB-03 (see **Figure 2-5**), mostly show < 3500 Ma zircons with $\varepsilon Hf_{(t)}<0$ and higher average Ti contents (**Figure 2-7 A-C**). In addition, zircon from sample TSB-03 ($\varepsilon Hf_{(t)}>0$) show lower average zircon Ti content than that from samples TH11 and TH13 (**Figure 2-7 C**).

From the above observations, we argue that the history of the Theespruit Formation is more complex than previously thought. Following Armstrong et al. 1990, we propose that ≤3500 Ma zircons are pristine and date igneous events within or immediately around the Theespruit Formation. Therefore, the maximum depositional age of 3530 Ma proposed by Kröner et al., 2016 may not apply to the entire Formation but only to their investigated samples. Specifically, the contrasting isotopic, chemical and age signatures of zircons from different TSB samples (see **Figure 2-7 A-C**), at distances less than 2 km

from one another, rather indicates that the Theespruit Formation is made of separate volcanic/volcaniclastic sequences, that were likely deposited at different times between 3500 Ma and 3450 Ma and correspond to distinct igneous sources. These interpretations are in line with the documented diversity of Lower Onverwacht silica-rich lithologies, comprising arkosic sandstones (Dziggel et al. 2002), K-feldspar porphyritic dacites (Agangi et al., 2018), felsic agglomerates (Diener et al. 2005) and schistose felsic rocks as documented here. In fact, one of the samples dated by Kröner et al. 2016 was a quartz- and K-feldspar-bearing dacite located near the North-Eastern margin of the Theespruit pluton, different from the samples investigated in the present work both in terms of petrography and location.

In terms of relationships with igneous events, the protoliths of the felsic schists investigated here (volcanic rocks of felsic composition or volcaniclastics, see Diener et al. 2005, Van Kranendonk et al. 2009) must have tapped different magma sources, resulting in different populations of zircons notably in terms of Hf isotopes (juvenile for TSB-03; more crustal for TH11-13, similar to those of Kröner et al. 2013, 2016; **Figure 2-7 A**). The 3580-3450 Ma zircons with positive $\varepsilon Hf_{(t)}$ from sample TSB-03 reasonably match the age and Hf isotopic compositions of nearby TTG gneisses (Steynsdorp) and plutons (Theespruit, Stolzburg) (**Figure 2-7 A**). In contrast, samples TH11 and TH13 produced zircons whose negative $\varepsilon Hf_{(t)}$ overlaps best with zircons crystallized within 3500-3400 Ma granites/rhyolites ($\varepsilon Hf_{(t)}$ mostly between -0.4 and -7.8; see Sanchez-Garrido et al., 2011 and **Figure 2-7 A**) preserved as clasts within the Moodies basal Conglomerate. Combined with our new zircon data, this suggests that the felsic volcanics of the Theespruit Formation might represent volcanic/volcano-sedimentary equivalents to granites/rhyolites of the same age, now found as clasts in the Moodies Basal Conglomerate.

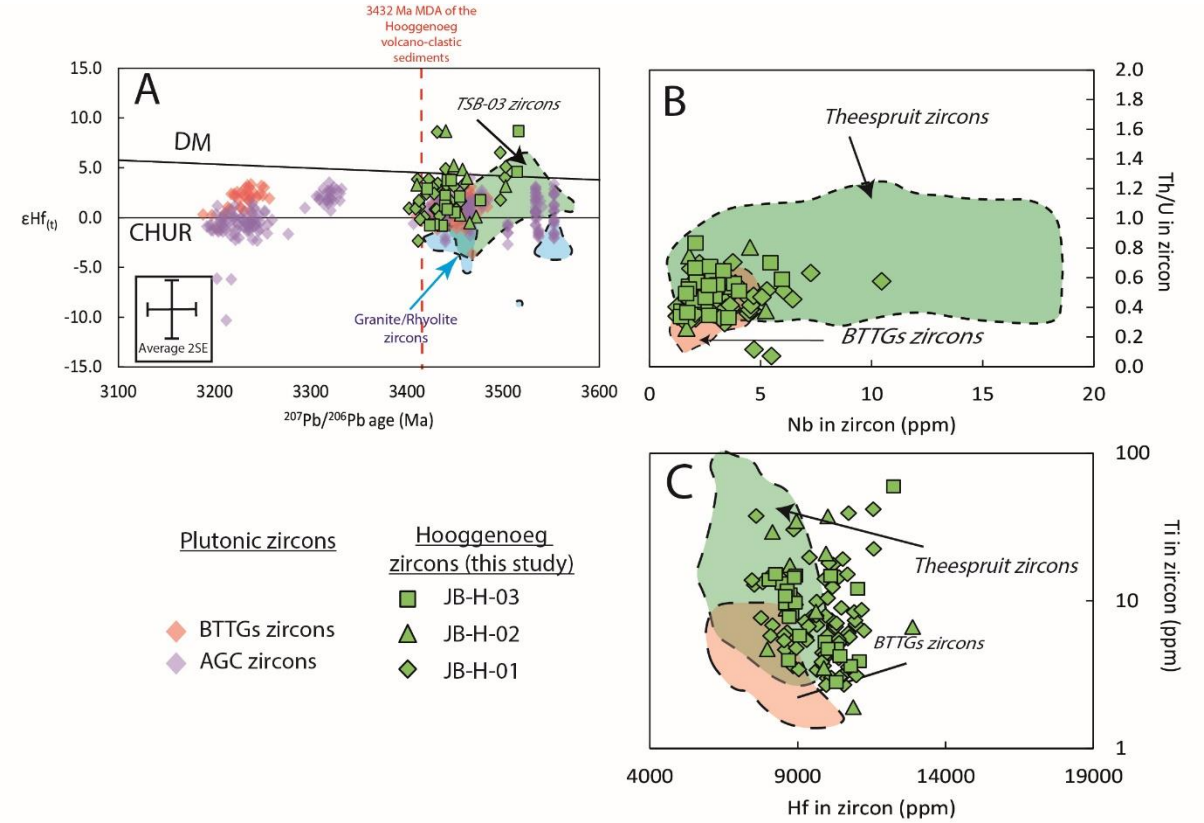

Figure 2-8: Geochemical and Isotopic discrimination plots of Hooggenoeg zircons from this study as compared with zircons of potential granitoid sources (BTTGs, AGC and 3.5-3.4 Ga granitic clasts) and Theespruit zircons. A) eHf(t) vs $^{207}Pb/^{206}Pb$ age in Hooggenoeg zircons compared with BTTG zircon compilation from Laurent et al., 2022, Zeh et al., 2009 and AGC zircon compilation from Hoffman et al., 2016, Kröner et al., 2014 and Zeh et al., 2011 and granitic zircon s from the Moodies Basal Conglomerate from Sanchez-Garrido et al., 2011, 2012. Age of deposition of the Hooggenoeg volcano-sediments of Grosch et al. 2011 is shown as vertical dashed line in graph A. Only TSB-03 zircons from the Theespruit Formation are shown as green area in this plot. B) Th/U vs Nb contents in zircon. C) Ti vs Hf in zircon. In graph B and C, trace elements in BTTG zircons derive from Laurent et al., 2022. Range of composition displayed by Theespruit zircons is also shown on all plots.

2.5.1.2. Hooggenoeg Formation

The youngest zircons from our samples of the Hooggenoeg Formation have $^{207}Pb/^{206}Pb$ dates between 3450 and 3400 Ma (**Figure 2-8 A**), which confirms the maximum deposition age of ca. 3430 Ma proposed by Grosch et al. (2011) for this formation. Zircons mainly show age and (positive) $\varepsilon Hf_{(t)}$ matching those of zircons from the Stolzburg-Theespruit TTGs and Theespruit Formation zircons from sample TSB-03 (see **Figure 2-8 A**). Comparatively, the Hooggenoeg zircons show limited age and isotopic overlap with either the (dominantly negative- $\varepsilon Hf_{(t)}$) zircons of 3500-3400 Ma granitic/rhyolitic rocks represented by the Moodies clasts; or the AGC (notably missing the ca. 3505 to 3553 Ma zircons from that terrane, see **Figure 2-8 A**). In addition to this, the sedimentary facies of the Hooggenoeg

volcano-sediments (coarse, angular, poorly sorted clasts; **Figure 2-2 A, Figure 2-3 E**) implies short sedimentary transport, arguing against a source located in the relatively remote (see **Figure 2-1**) AGC area.

In terms of trace elements, the Hooggenoeg zircon population shows a better match to BTTG zircon compositions (notably in terms of Nb content and Th/U ratios) than the Theespruit zircons (**Figure 2-8 B**). The Hooggenoeg zircons also show somewhat higher Hf contents than BTTGs zircons, and Ti concentrations that are higher than those of BTTG zircons but lower than those of Theespruit zircons (**Figure 2-8 C**). These characteristics suggest that, despite having similar age vs $\varepsilon Hf_{(t)}$ with either Theespruit zircons or BTTG zircons and being relatively close to the Stolzburg terrane in terms of distance, the Hooggenoeg zircons were not sourced from either Theespruit felsic volcanic sequences or ca. 3456 Ma TTGs. This idea is also supported by independent metamorphic studies (Cloete. 1993, 1999, Diener et al. 2005; Van Kranendonk et al. 2009, Cutts et al. 2014) who suggested that rocks of the Theespruit Formation experienced amphibolite-facies metamorphism in P-T conditions of 4 kbar and 600°C, at 3436 ± 10 Ma (Cutts et al. 2014). Although the applicability of this early metamorphic event to the entire (and lithologically composite, see section 5.1.1) Theespruit Formation could be discussed, this suggests that at least parts of the Theespruit Formation, and the underlying ca. 3456 Ma TTGs, were not exposed to surface weathering at the time of deposition of the Hooggenoeg volcano-clastic sediments, and could thus not be part of the eroded area.

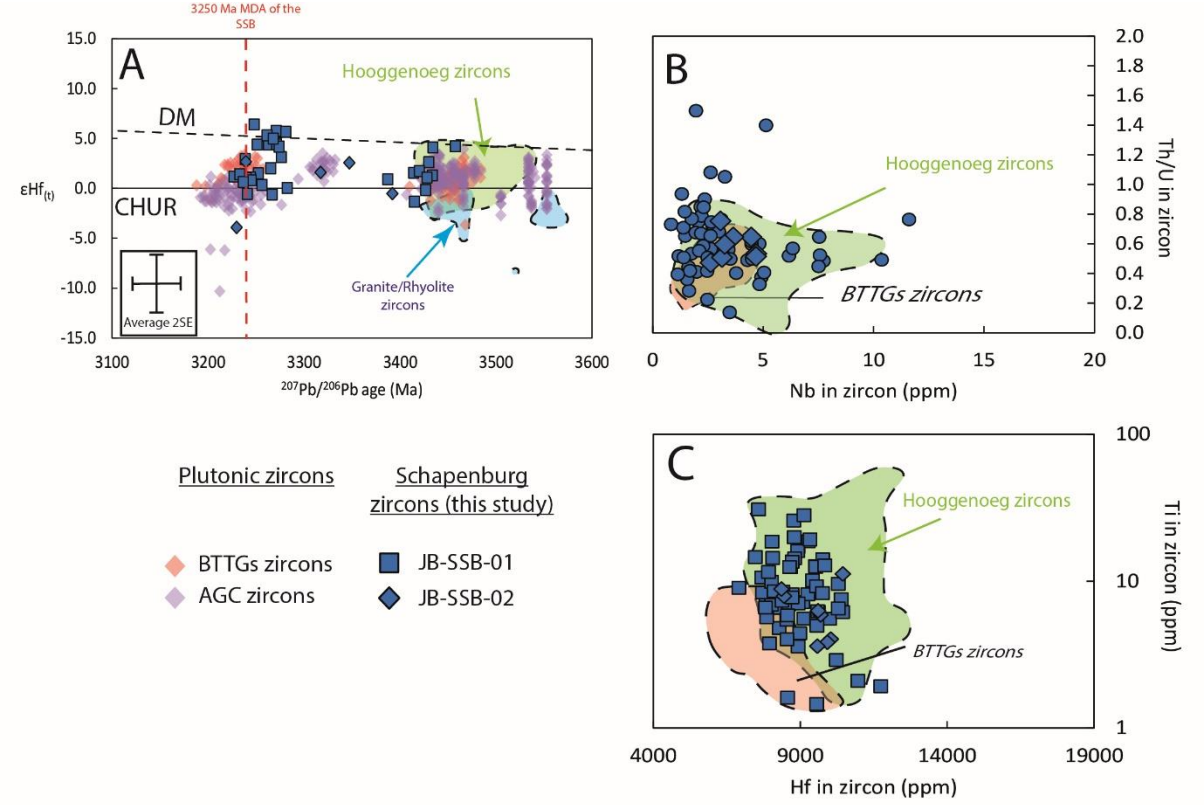

Figure 2-9: Geochemical and Isotopic discrimination plot of Schapenburg zircons from this study as compared with zircons of potential granitoid sources (BTTGs, AGC and 3.5-3.4 Ga granitic clasts) and zircons of the Hooggenoeg volcano-sediments. A) eHf(t) vs $^{207}Pb/^{206}Pb$ age in Schapenburg zircons with BTTG zircon compilation from Laurent et al., 2022, Zeh et al., 2009 , AGC zircon compilation from Hoffmann et al., 2016, Kröner et al., 2014 and Zeh et al., 2011 and granitic zircons from the Moodies Basal Conglomerate from Sanchez-Garrido et al., 2011, 2012. Age of deposition (MDA) in Graph A applies to the clastic sediments of the Schapenburg Schist Belt (SSB) as determined by Stevens et al., 2002 from youngest zircon age cluster. B) Th/U vs Nb contents in zircon. C) Ti vs Hf in zircon. In graph B and C, trace elements in BTTG zircons derive from Laurent et al., 2022. Range of coposition displayed by Hooggenoeg zircons is also shown on all three plots.

2.5.1.3. Fig Tree-aged meta-turbidites of the Schapenburg Schist Belt (SSB)

The SSB samples contain zircons with dominantly supra-chondritic/radiogenic $\varepsilon Hf_{(t)}$ signature, distributed in two age groups, a main cluster at ca. 3280-3240 Ma and one at ca. 3450-3400 Ma. These are present in both zircon samples SSB-01 and SSB-02 (**Figure 2-9 A**). The youngest zircons provide a weighted mean age of 3235±15 Ma, consistent with the maximum depositional age of 3250 Ma already proposed by (Stevens et al., 2002) (**Figure 2-9 A**). The two age clusters overlap well with the known events of TTG emplacement in the BGGT (**Figure 2-6**). For instance, the main, younger cluster of SSB zircons overlaps in age with zircons of the adjacent 3290-3240 Ma Baadplaas Gneiss (Kisters et al., 2010; Moyen et al., 2007) and the older SSB zircons overlap with the field of Stolzburg-

Theespruit TTGs, as well as Hooggenoeg Formation zircons, for Hf(-O) isotopes (**Figure 2-9 A and 2-8 A**). Therefore, one could argue that the SSB zircons were sourced from a variety of plutonic and volcanic/sedimentary rocks located in the BGB and immediate surroundings.

However, a number of regional igneous sources can be discarded for the SSB zircons. This includes the AGC terrane (see **Figure 2-1**), as the SSB zircons strikingly lack two main generations of AGC zircons, namely at ca. 3500-3550 Ma and ca. 3300 Ma (**Figure 2-9 A**). The ca. 3456 Ma Stolzburg and Theespruit TTGs, which represent decent matches in terms of age and $\varepsilon Hf_{(t)}$ for the older SSB zircon population (**Figure 2-9 A**), are unlikely to have been part of the source area either due to mismatching Nb, Ti and Hf contents, notably higher than in BTTG zircons (**Figure 2-9 B-C**). Lastly, zircons of the ca. 3500 to 3200 Ma granites/rhyolites represented by clasts in the Moodies Basal Conglomerate (Sanchez-Garrido, 2012; Sanchez-Garrido et al., 2011) show notably lower $\varepsilon Hf_{(t)}$ than the SSB zircons of similar age (**Figure 2-9 A**), ruling out this possibility as well.

Besides, we have additional reasons to believe that no component located south of the Inyoka Fault has been preserved in the Schapenburg meta-greywackes. The Schapenburg Schist Belt has been proposed to be a part of the Western Domain of the Inyoni Shear Zone/Inyoka Fault (Moyen et al., 2006; Stevens et al., 2002; Stevens & Moyen, 2007), i.e. belong to the Barberton Northern Terrane sensu (Zeh et al., 2009), on the ground that it shares the same apparent geothermal gradient of 30°C/km as the one documented by Dziggel et al. (2006) in the latter. Therefore, we suggest that the meta-greywackes of the SSB were once deposited on the continental shelf of the Northern Terrane and therefore captured a zircon population that represents the corresponding granitoids, including the 3290-3240 Ma Baadplaas Gneiss (A. F. Kisters et al., 2010; A. F. M. Kisters et al., 2003). In this view, the ca. 3450-3400 Ma SSB zircons would derive from plutonic or volcanic rocks with positive $\varepsilon Hf_{(t)}$ and mantle-like $\delta^{18}O$, that have not been preserved, or not yet documented, in the Northern Terrane. This suggests that sediments of the SSB preserve evidence of now missing 3400 Ma felsic plutonic or volcanic components in that terrane. In fact, as the SSB meta-greywackes are fine-grained turbidites (see **Figure 2-2** C and sample description), it is likely that they drained a relatively larger surface

exposure (Bouma. 1964, 2004) than the presently preserved surface area of the Northern Terrane, supporting this possibility.

2.5.1.4. Moodies Group

Zircon dates of the Moodies sandstones cover the full history of the BGB, recording all major igneous events (i.e. 3570-3500 Ma, 3480-3400 Ma and 3300-3200 Ma; **Figure 2-6**). However, our new Hf isotopic data show strong contrasts with the most widespread regional igneous sources, in particular the BTTGs and the AGC. Indeed, the latter produced zircons that are dominantly radiogenic (**Figure 2-10 A**) whereas the Moodies zircons have more diverse isotopic composition, notably extending to non-radiogenic signatures (from -4.2 to -0.4 $\varepsilon Hf_{(t)}$ units for the > 3500 Ma zircons to -8.3 to +3.1 $\varepsilon Hf_{(t)}$ units for <3500 Ma zircons; **Figure 2-10 A**). This negative isotopic pattern of Moodies zircons is present in all published datasets (Drabon et al., 2024; Wang et al., 2022; Zeh et al., 2013), although more abundant in the samples collected in this study (~91 % of data have $\varepsilon Hf_{(t)} < 0$). This negative- $\varepsilon Hf_{(t)}$ population of Moodies zircon is uncommon to completely absent from either the Barberton TTGs or AGC gneiss zircon of similar age (**Figure 2-10 A**). Some AGC zircons show somewhat non-radiogenic Hf isotopic signatures, notably the youngest ca. 3250-3200 Ma population ($\varepsilon Hf_{(t)}$ from -3.2 to +0.8, **Figure 2-10 A**), but the ca. 3300 Ma AGC zircon population showing positive $\varepsilon Hf_{(t)}$ (from 0 to +4.0, see **Figure 2-10 A**) are not observed in the Moodies zircons. In addition, our Moodies zircons have Th/U ratios extending to higher values than zircons of the BTTGs (**Figure 2-10 B**) as well as higher Ti and Hf contents on average (**Figure 2-10 C**).

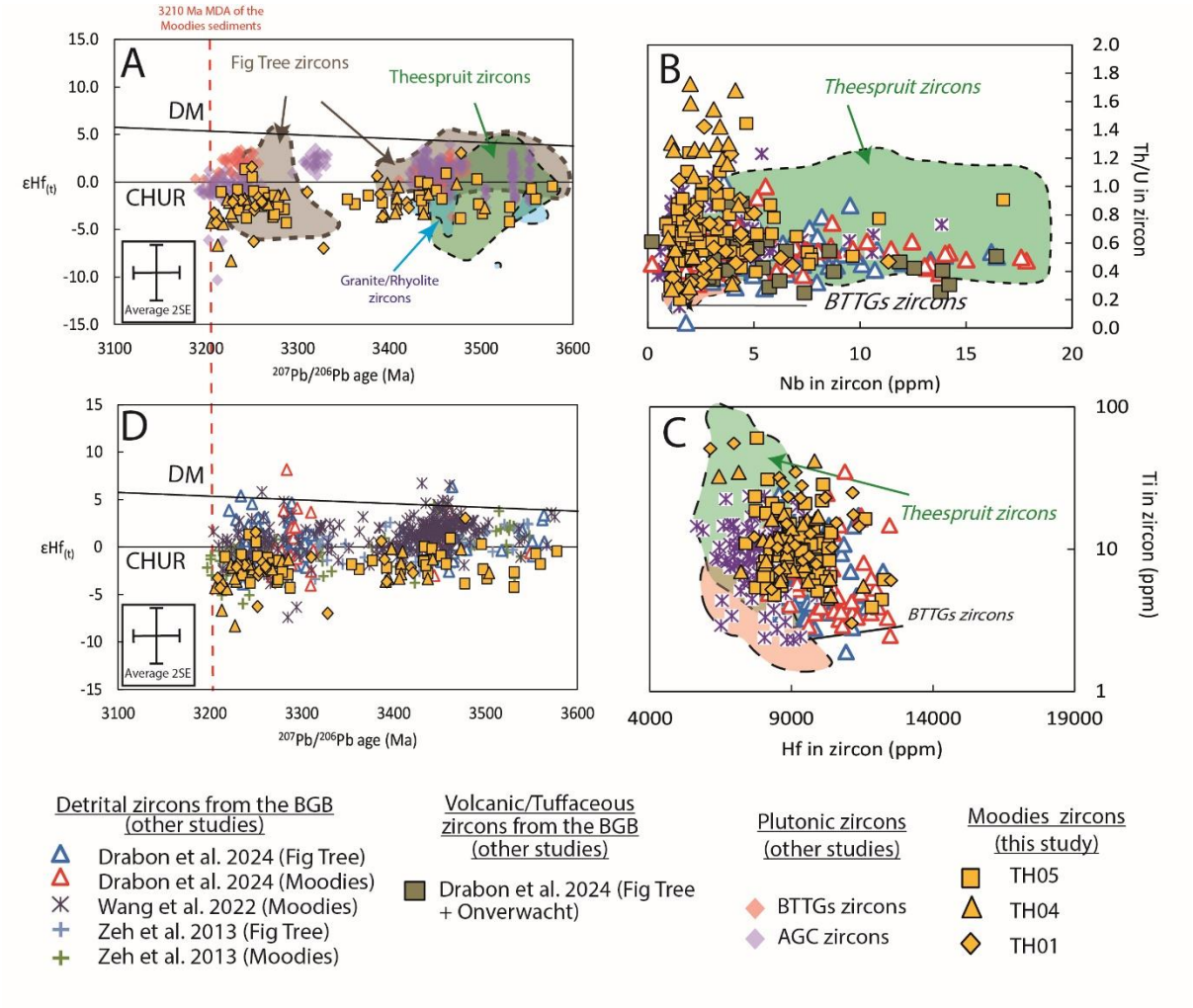

Figure 2-10: Geochemical and Isotopic discrimination plot of Moodies zircons from this study and others as compared with zircons of potential volcanic (Theespruit zircons from this study + Fig Tree tuffaceous zircons), granitoid sources (BTTGs, AGC and 3.5-3.4 Ga granitic clasts) and sedimentary sources (zircons fo the Fig Tree clastic sediments). A) eHf(t) vs $^{207}Pb/^{206}Pb$ age in Moodies zircons as compared with BTTG zircon compilation from Laurent et al., 2022, Zeh et al., 2009 , AGC zircon compilation from Hoffmann et al., 2016, Kröner et al., 2014 and Zeh et al., 2011 and granitic zircon s from the Moodies Basal Conglomerate from Sanchez-Garrido et al., 2011, 2012. Negative eHf(t) of the Theespruit zircons is also shown as green area. MDA in graph A stands for "maximum depositional age" and applies to the supracrustal sequences of the Moodies Group as determined by Heubeck et al., 2013 from youngest zircon age cluster. B) Th/U vs Nb contents in zircons of the Moodies sediments (this study and others). C) Ti vs Hf in zircon. D) eHf(t) vs $^{207}Pb/^{206}Pb$ age in Moodies zircons as compared with BGB detrital zircons from Moodies and Fig Tree groups. In graph B and D, trace elements in BTTG zircons derive from Laurent et al., 2022. Range of composition displayed by Theespruit zircons is also shown on both plots.

Collectively, this suggests that the Moodies zircons analyzed in the present work do not derive from either the presently exposed BTTGs or the AGC, in agreement with conclusions of (Heubeck et al., 2022) who advocated a dominantly intra-BGB origin. Drabon et al. (2024) proposed that part of the Moodies zircons, especially the 3300-3200 Ma population, experienced multiple sedimentary cycles and derived from the stratigraphically underlying Fig Tree strata (tuffaceous and clastic sediments). This conclusion would be apparently supported by the fairly similar Th/U ratios and Nb, Ti and Hf contents between Fig Tree and Moodies zircons (**Figure 2-10 B-C**). However, zircon from Fig tree-age

strata (see **Figure 2-10 A-D**) span a range of $\varepsilon Hf_{(t)}$ values from negative to positive ($\varepsilon Hf_{(t)}$ between -3.5 to + 5.0, see **Figure 2-10 A-C**). The interpretation of (Drabon et al., 2024) applied to our samples would hence imply that only negative- $\varepsilon Hf_{(t)}$ Fig Tree zircons would have been selectively transferred to the Moodies sandstones during erosion and transport, which appears implausible.

Instead, the ca. 3570 Ma to 3400 Ma detrital zircons of the Moodies group with negative $\varepsilon Hf_{(t)}$ overlap well with zircons crystallized in the granitic clasts of the Moodies Basal Conglomerate, but also with isotopically negative Theespruit zircons (see section 5.1.1 above and **Figure 2-10 A**). This is further supported by Moodies and Theespruit zircons with negative $\varepsilon Hf_{(t)}$ (TH11 and TH13) sharing similar Ti contents (average of 12 and 16 ppm respectively), on average higher than zircons from the Barberton TTGs and co-genetic felsic volcanic rocks (average of 5 ppm; data from Laurent et al. 2022). Therefore, following Drabon et al. (2024) and Heubeck et al. (2022), we argue that Moodies zircons derive mainly from intra-BGB sources, including the Fig Tree and Onverwacht detrital, tuffaceous/volcaniclastic sequences (Drabon et al., 2024) and/or granitic/rhyolitic rocks similar to those found as relict clasts in the Moodies Basal Conglomerate but that regional variations over the importance of each of these intra-BGB sources in feeding the Moodies sediments occur as will be explained below.

2.5.2. Detrital zircon patterns at the scale of the BGB and geological implications

Our new and literature data from the BGB zircons highlight distinct age distributions and contrasting isotopic compositions depending on the stratigraphic level, while they preserve as a whole the $^{207}Pb/^{206}Pb$ dates representing the main magmatic events of the BGGT (**Figure 2-6**). From the previous discussion, two salient features can be extracted from our dataset: important local controls on detrital zircon populations; and significant biases in the preservation of the Paleoarchean crustal record, with supracrustal zircon witnessing the former presence of source rocks that are presently under-represented in the exposed crustal record.

2.5.2.1. Local controls on detrital zircon provenance

Local controls on detrital zircon provenance are important factors that dictate the nature of zircon populations in Archean supracrustal sequences, as typically shown by the provenance of detrital zircons from all volcano-sedimentary sequences of the BGB. Different provenance patterns arise for samples collected in similar stratigraphic levels. Typically, discrepancies in zircon provenance between different Moodies samples, as indicated by different distributions of zircon Hf isotopic compositions between our samples and literature data (see section 2.5.1.4 and **Figure 2-10 A**), suggest regional variations in zircon provenance in clastic sediments deposited at the same time. These discrepancies are indeed likely the result of different sampling areas between our work and previous studies (see **Figure 2-1**). For instance, Moodies samples investigated by (Drabon et al., 2024; Wang et al., 2022; Zeh et al., 2013) come from the central part of the BGB, whereas ours derive from the northern BGB (Eureka and Saddleback synclines, see **Figure 2-1**). Therefore, while the former incorporated a significant proportion of zircons from the Fig Tree tuffaceous and sedimentary rocks, the latter collected mainly zircons from a different source showing exclusively negative $\varepsilon Hf_{(t)}$.

Likewise, we document that zircon populations, both in terms of age and isotopic signature, change within volcanic sequences that were described as laterally continuous in the literature (Anhaeusser, 1981; J. F. Diener, 2004; J. F. A. Diener et al., 2005) as in the case of the Theespruit Formation. This illustrates the existence of multiple volcanic events throughout a protracted (~80 Myr) construction history of this supracrustal unit, tapping magma reservoirs with different isotopic signatures.

In general, these local differences in zircon sourcing stress out that the resulting zircon populations may therefore not be representative of the exposed crustal components on a regional scale, which is a well-known bias of detrital zircon studies (e.g., Moecher & Samson, 2006) but somewhat under-considered in the context of the early Earth. This also highlights the importance of sampling, which should be as representative as possible of the stratigraphic complexity and lithological diversity.

2.5.2.2. Biases in preservation of the Paleoarchean crustal record

Previous studies (Drabon et al., 2024; Wang et al., 2022; Zeh et al., 2009, 2013) have used the broadly similar age distribution of BGB detrital zircons and of BTTG magmatic zircons (see **Figure 2-**

6) to argue that detrital zircons were sourced mainly from the surrounding granitoid-gneisses (TTG and AGC). However, our results show that this interpretation is too simplistic. In particular, zircons of the Hooggenoeg volcano-clastic sediments must derive from plutonic or volcanic rocks of similar age and isotopic composition as those of ca. 3550-3450 Ma TTGs from the southern BGGT, but with somewhat different magmatic histories, to explain different zircon trace element compositions (see section 2.5.1.2. and **Figure 2-8 B-C**). Considering the short sedimentary transport required by the sedimentary facies of the Hooggenoeg volcano-clastic sediments, this unpreserved source must have been located close to the depositional setting but is clearly not exposed anymore in the area. In the case of the SSB meta-greywackes, detrital zircons notably record a ca. 3450-3400 Ma magmatic event that is not preserved in the Northern Terrane from which the sediments were presumably sourced (see section 2.5.1.3 and **Figure 2-9 A**). In both cases, there is little constraint on the composition of the source rocks, besides minor trace element differences in zircon, mainly higher average Ti and Hf contents than the BTTG zircons.

Importantly, our work further stresses out here the importance of crustal components showing negative zircon $\varepsilon Hf_{(t)}$ signatures in the BGGT, in strong contrast to the predominantly positive-$\varepsilon Hf_{(t}$ pattern displayed by zircons from exposed granitoids and gneiss lithologies (BTTG and AGC). These negative-$\varepsilon Hf_{(t)}$ components are represented by some ca. 3550-3450 Ma volcanic/volcaniclastic lithologies of the Theespruit Formation, as previously documented by Kröner et al. (2016) and confirmed by our results (see section 2.5.1.1 and **Figure 2-7 A**). More significantly, combining our new results with literature datasets, 40% of all data from Moodies zicons, covering the entire BGGT age range (ca. 3550-3200 Ma), show negative $\varepsilon Hf_{(t)}$ (see section 2.5.1.4, **Figure 2-10 A-B**), with the bulk of $\varepsilon Hf_{(t)}$ values between -5.0 to 0. The negative $\varepsilon Hf_{(t)}$-zircons also show on average higher Ti (and to some extent Nb) contents, and Th/U ratios, than BTTG zircon (**Figures 2-9 B-C and 2-12 B-C**). This implies that the parent magma of the Moodies and Theespruit negative- $\varepsilon Hf_{(t)}$ zircons had different chemical properties than trondhjemites of the TTG suite. In particular, the higher Ti contents may result from possible differences in $aSiO_2$ and $aTiO_2$ upon zircon saturation (Ferry & Watson, 2007; Fonseca Teixeira et al., 2023; Schiller & Finger, 2019) or actual differences in zircon crystallization temperatures

(assuming $aSiO_2$ and $aTiO_2$ = 1, average Ti-in-zircon crystallization temperatures are 750 °C for the Theespruit and Moodies zircons vs. 680 °C for the Barberton TTG zircons).

Altogether, this means that igneous rocks other than the exposed BTTGs may have composed a significant volume of the Paleoarchean felsic upper crust, notably at the time the Moodies sediments were deposited as to source nearly half of their detrital zircons. As mentioned in section 5.1, we propose that this igneous component is now only represented by volcanic/volcaniclastic rocks of the Theespruit Formation hosting negative- $\varepsilon Hf_{(t)}$ zircon; and granitic/rhyolitic clasts now found in the Moodies Basal Conglomerate, both being the only igneous source rocks with clearly negative zircon $\varepsilon Hf_{(t)}$ in the BGGT and surroundings. The Moodies clasts were formed broadly coevally with TTGs, with zircon crystallization dates ranging from as old as ca. 3560 Ma (Kröner et al., 2018) down to ca. 3200 Ma (Sanchez-Garrido, 2012), but in addition to a non-radiogenic $\varepsilon Hf_{(t)}$ signature reflecting the significant contribution of isotopically evolved crust in the petrogenesis of their parent magma, they show a distinctive major and trace element signature. The Moodies clasts indeed bear a primary magmatic K_2O-rich (some >6 wt%, see Kröner et al., 2018; Kröner & Compston, 1988), CaO-poor composition with flat HREE patterns, unlike TTGs (Sanchez-Garrido et al., 2011). Importantly, the felsic schists of the Theespruit Formation share the same high K_2O (as shown by the presence of magmatic K-felsdpar phenocrysts; Agangi et al., 2018), low CaO contents and flat HREE patterns as the Moodies granite/rhyolite clasts (Sanchez-Garrido et al., 2011; Sanchez-Garrido, 2012 PhD thesis). The potential provenance of negative-$\varepsilon Hf_{(t)}$ zircons of the BGB from igneous sources similar to the Moodies granitic/rhyolitic clasts is further supported by modelled trace element compositions of theoretical zircon that would have crystallized from a melt compositionally similar to the latter (**Figure 2-11 A-B**). These modelled zircon compositions show higher Nb/Yb ratio and U/Yb ratio than BTTG zircons at identical Ti content, a pattern similar to that displayed by the Moodies and Theespruit zircons (**Figure 2-11 A-B**).

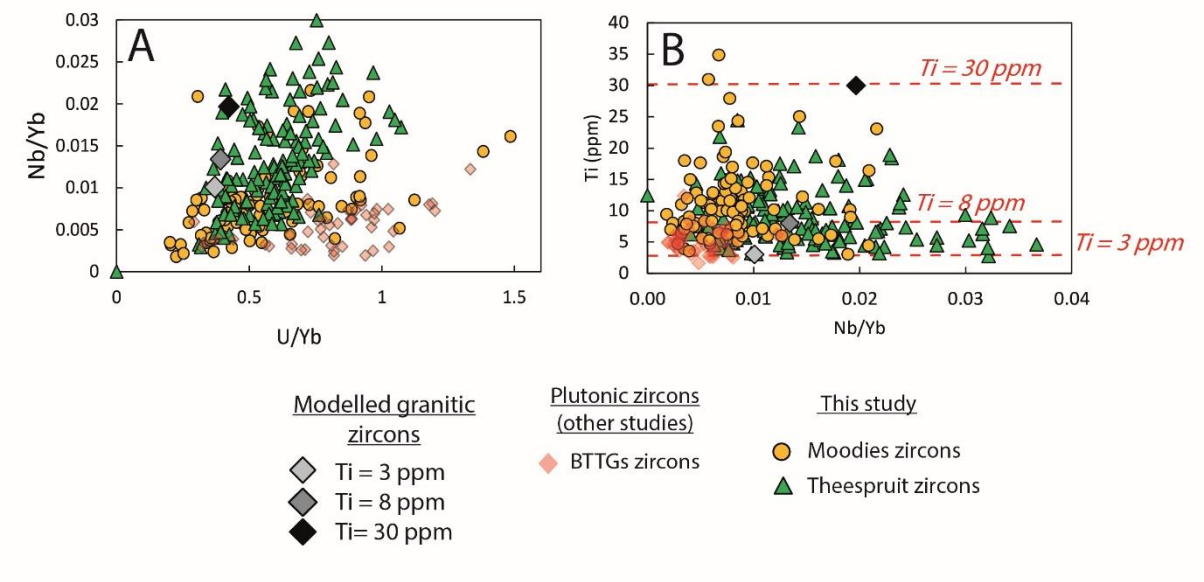

Figure 2-11: Results of chemical modelling. Graph A compares Nb/Yb vs U/Yb for detrital zircons of the Moodies sediments, zircons of the Theespruit volcanics (this study), with modelled granitic zircon and BTTG zircons (Laurent et al., 2022). Graph B shows the evolution of Nb/Yb ratio in modelled granitic zircons with Ti content and compare it with zircons of the Moodies sediment, Theespruit volcanics and BTTGs. Red dashed lines outlines the three input Ti content in the model.

2.5.3. General geological implications

2.5.3.1. Regional Paleoarchean crustal structure and geodynamic evolution

The statistically important population of Moodies detrital zircons having $\varepsilon Hf_{(t)}$ different from that of TTGs but overlapping with that of granitic/rhyolitic clasts of the Moodies Group (this study, Zeh et al. 2013, Wang et al. 2022, Drabon et al. 2017, 2022, 2024) points to the existence of a crustal component that likely formed a significant part of the Archean felsic crust. As discussed above (see section 2.5.2.2), this component was likely represented by K_2O-rich granites/rhyolites. Importantly, the corresponding magmas were formed during the main episodes of crustal development in the BGGT, coevally with TTGs, as shown by similar age distributions between negative- and positive-$\varepsilon Hf_{(t)}$ zircons (**Figure 2-6A, Figure 2-10A-B**). This crustal component is mostly missing out from the exposed rock record in the BGB. Although relicts can be found as 3570- to 3200 Ma-old clasts in the Moodies Basal Conglomerate and ca. 3500-3450 Ma-old felsic schists of the Theespruit Formation, these represent a much smaller surface exposure than what it must have been in Archean times to explain the abundance

of negative- $\varepsilon Hf_{(t)}$ zircons in the Moodies sandstones. Altogether, we propose that this implies a vertically zoned Archean felsic crust, formed by an uppermost, K-rich upper crust (granite/rhyolite sequences) and a Na-rich TTG middle crust (**Figure 2-11**). This vertical structure explains the preferential erosion of the former and preservation of the latter, as other studies have suggested (Clemens et al. 2010, Agangi et al. 2018). This vertical zoning was already acquired as early as ca. 3500 Ma, as shown by the existence of both >3500 Ma TTGs and granitic clasts/zircons.

Explaining this heterogeneous distribution of felsic lithologies in Paleo-Archean continental crust requires to discuss first the nature of the source of the K_2O-rich upper crustal granites/rhyolites, and second, how this source was brought to melting depths. These questions connect with the geodynamic setting of felsic crust production on the Archean Earth, a matter that is still highly debated (Brown et al., 2020; Cawood et al., 2006; Condie & Kröner, 2008; Kusky et al., 2018; Nutman et al., 2020; Palin et al., 2020; Sizova et al., 2014; Smithies, 2000; Stern, 2018; Van Kranendonk, 2011; van Hunen & Moyen, 2012 and references therein). Sanchez-Garrido et al. (2011) proposed a model for the Moodies granitic/rhyolitic clasts, representative of this former uppermost crust (see section 2.5.2.2), whereby a meta-sedimentary (greywacke) source, similar to K_2O-rich volcanic sequences of the Theespruit Formation, buried to >1.5 GPa experienced partial melting (through phengite breakdown) to produce K_2O-rich, CaO-poor granitic melts.

Reaching the high melting pressures required by this model could be achieved either through intraplate melting of the base of an overthickened oceanic plateau (see Palin et al. 2016, 2020), or tectonic burial in a context comparable to modern-day convergent plate margins (Sanchez-Garrido et al. 2011, 2012, Clemens et al. 2010, Agangi et al. 2018). In the former case, sources of either sodic TTGs or potassic granites may occupy different levels of the root zone of an overthickened oceanic plateau and both eventually experience melting at high pressure (triggered by an underlying mantle plume?; Nair & Chacko, 2008; Palin et al., 2016). In this context, the K_2O-rich granites/rhyolites could have been derived from the partial melting of volcano-sedimentary rocks akin to the protoliths of the Theespruit felsic schists and show negative $\varepsilon Hf_{(t)}$ indicative of the involvement of ancient crust. Such supracrustal rocks were likely initially deposited at structurally shallower levels of a composite,

predominantly mafic/ultramafic crust with Enriched tholeiite affinity (Martin et al., 2014). Burial of this composite mafic crust to high-pressure conditions through top-down stacking of basaltic lavas flows (e.g. Kamber, 2015) and/or underplating of mantle-derived mafic magmas, would trigger partial melting of the lower crust. The lowermost, recently emplaced mafic rocks (hence with positive $\varepsilon Hf_{(t)}$) would produce TTG magmas and the structurally shallower levels (made of felsic volcanics/sediments) produce granitic magmas (**Figure 2-12**). Processes such as contrasting depths of melting, possible differences in fluid content in the melt (due to different source composition cf (Sanchez-Garrido et al., 2011) and tectonic drain through the upper crust, might result in the different depths of emplacement of granites vs TTGs-like magmas as suggested in plutonic and volcanic-plumbing systems (Brown, 1994; Cruden & Weinberg, 2018) and explain the proposed stratified structure of the >3.2 Ga felsic crust.

In the case of the youngest, 3300-3200 Ma event of coeval TTGs and K-rich granite production in Barberton, the geodynamic setting can be constrained based on former studies, which proposed a tectonic amalgamation of the Southern and Northern Terranes of the BGGT along the SIFS (see **Figure 2-1**) in a setting comparable to modern convergent plate margins (Clemens et al., 2006; J. F. Diener et al., 2005; Dziggel et al., 2002, 2006b; A. F. Kisters et al., 2010; A. F. M. Kisters et al., 2003; Moyen et al., 2006; Mühlberg et al., 2021; Stevens et al., 2002, Zeh et al. 2009). A convergence margin setting agrees with the documented increase of detrital zircon $\delta^{18}O$ both in the BGB (**Figure 2-6 A**) and from other lines of evidence from the global record (Cawood et al., 2018; Kirkland et al., 2021; Ma et al., 2020; Næraa et al., 2012; Payne et al., 2015; Smithies et al., 2021; Van Kranendonk et al., 2015), which require an increased influx of hydrothermally altered surface sediments to depth at ~3200 Ma, most easily achieved through subduction. In the case of the BGGT, it has been argued that rocks of the Southern Terrane (presently represented by the Stolzburg block) were buried at high pressure below the Northern Terrane through subduction-like processes (e.g. Moyen et al., 2006). The uppermost part of the corresponding crustal package would have been represented by equivalents of the Theespruit felsic volcanic/volcaniclastic rocks, whose chemical composition would be appropriate to represent the source of K_2O-rich, CaO-poor granites/rhyolites (Sanchez-Garrido et al., 2011). These would thus have melted

at lower depth than the mafic, leading edge of the downward going slab (**Figure 2-11 A**), which could have produced the coeval and isotopically juvenile TTGs.

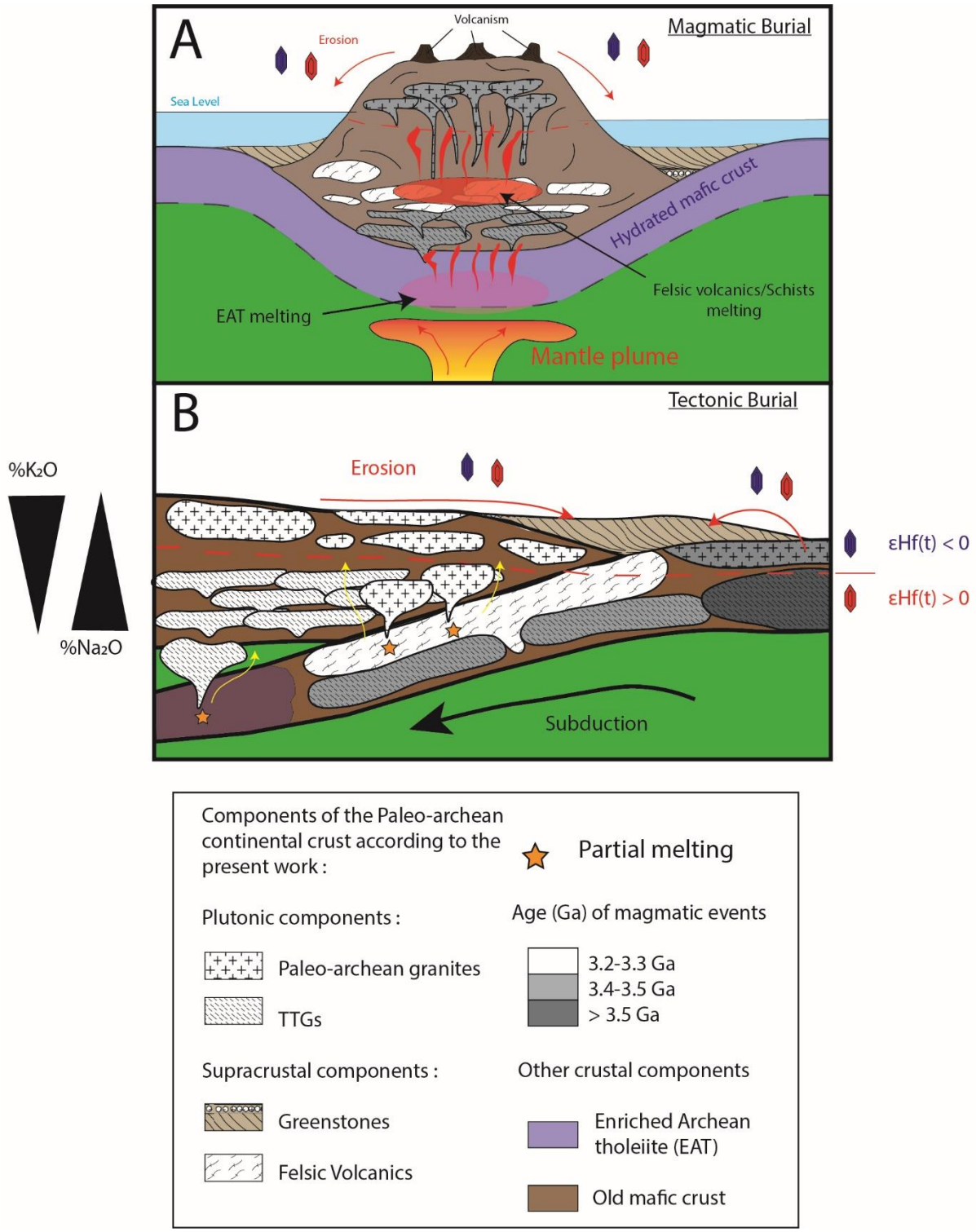

Figure 2-12: Proposed geodynamic scenarios to explain the vertical structure of the Archean crust deduced from our zircon data and known constraints on the geological evolution of the BGGT, for the 3500-3400 (bottom) and 3300-3200 (top) Ma periods (see text for details).

We note that, if some sort of subduction is involved in the petrogenesis of Paleoarchean K_2O-rich granites, it can only apply for sure to the 3300-3200 Ma generation, for which we have field, structural and metamorphic evidence for terrane amalgamation processes akin to horizontal plate tectonics in the BGB (J. F. Diener et al., 2005; Dziggel et al., 2002, 2006a; Moyen et al., 2006). For rocks older than 3400 Ma, we can only be speculative, as there is no such evidence – yet the same vertical zoning of the crust could be explained by different processes, as described above.

2.5.3.2. Global preservation biases in the Archean and limits of detrital zircon studies

Our study stresses out that the Paleoarchean felsic crust of the BGGT must have been compositionally more diverse than suggested by the present, binary juxtaposition of TTGs and greenstones. Previous geochemical and petrological studies shows that this conclusion certainly applies to other Archean terranes. For instance, in the East Pilbara terrane (Australia), (Champion & Smithies, 2007) have documented two granitoid suites, showing similar ranges of emplacement ages (3500-3420 and 3320-3250 Ma) but distinctive petrographic and geochemical features including a high-Al, TTG-like suite; and a low-Al and higher-K_2O suite, notably showing more negative whole-rock $\varepsilon Nd_{(t)}$ values. Reimink et al., 2014, 2016, 2020 investigated the diversity of the Acasta Gneiss Complex in Canada and found out that these are not only made of TTGs, notably comprising some ca. 4020 Ma-old tonalitic gneisses showing major and trace element composition similar to icelandites (enrichment in Fe, very low REE fractionation). Likewise, Neoarchean potassic granites from Eastern Hebei (North China Craton) contain enclaves of trondhjemites and granodiorites, closely associated to ca. 3775 Ma quartz-monzonite and ca. 3786-3640 Ma granites that produced zircons with negative $\varepsilon Hf_{(t)}$ (-6.9 to +0.4) and $\delta^{18}O$ between 5.5 to 7.5 ‰ (Dong et al., 2024). As in the case of the Moodies clasts and Theespruit felsic schists of the BGB, these quartz-monzonites and granites are mostly absent from the exposed geological record besides a few enclaves preserved in more recent granitoids.

Recently, Spencer et al., 2022 examined a global record of detrital and igneous, Hadean to Phanerozoic zircons and identified a decoupling in $\delta^{18}O$, with detrital zircons showing systematically

higher $\delta^{18}O$ than igneous zircons of the preserved, coeval igneous rocks. This observation further supports the idea that detrital zircon grains may record a component of the felsic continental crust that has hardly been preserved in the igneous rock record. On a more local scale, studies of detrital zircon and quartz from sandstones in the vicinity of the Proterozoic Pikes Peak batholith (USA) shows that the detrital grains were dominantly eroded from a no longer exposed volcanic component coeval to the batholith (Fonseca Teixeira et al., 2024)). Overall, these examples show that the proposed vertical zoning of the BGB before ca. 3200 Ma (see section 5.3) is not a local phenomenon but could be applied to other Precambrian terranes. It also highlights the importance of considering preservation biases when dealing with Archean rocks older than 3.2 Ga.

That said, zircon-based studies also suffer from intrinsic biases. Zircon mainly crystallize in intermediate to acidic magmas but very rarely in mafic to ultramafic ones (E. Belousova et al., 2002; Crisp & Berry, 2022; Hoskin & Schaltegger, 2003; Watson & Harrison, 1983), such that if the Archean crust was predominantly mafic until 3.0 Ga as suggested by various lines of evidence (Dhuime et al., 2015; Flament et al., 2013; Ptáček et al., 2020; Rey et al., 2024), detrital zircon would miss most of it. In addition, while zircon $\varepsilon Hf_{(t)}$ can tell apart magma sources with different mantle extraction ages, it is not capable to discriminate between different magma types and petrogenesis (e.g. Couzinié et al., 2016; Payne et al., 2016; Vervoort & Kemp, 2016). Zircon trace element chemistry might help for this purpose, but generally lacks potential to discriminate various granitoid sources due to limited variability (E. Belousova et al., 2002; Bruand et al., 2020). Other accessory minerals are more promising in this respect. In particular, apatite occurs in a broader range of magma composition and shows more sensitive trace element variability to host magma chemistry compared with zircon (Antoine et al., 2020; E. A. Belousova et al., 2001, 2002; Bruand et al., 2020; O'Sullivan et al., 2020). Preliminary recent studies of igneous apatite in the youngest granitoids (ca. 3280-3100 Ma) associated with the BGB already reveal diverse chemical signatures (Miyake et al., 2024; Vezinet et al., 2025), holding promises for a more accurate characterization of the non-preserved Paleoarchean crust using detrital apatite.

2.6. Conclusion

This study has shown the BGB detrital zircons to be of contrasting origins, based on new age, isotopic and chemical data from volcanic/volcaniclastic and sedimentary samples straddling the entire stratigraphy of the belt. Zircon data show the importance of local controls on detrital zircon provenance at different spatial scales (i.e. catchment scale for the Hooggenoeg volcano-clastic sediments and Moodies sandstones, or one specific terrane for the Schapenburg Schist Belt) or magma sources (i.e. the composite nature of the Theespruit Formation). This reveals the importance of investigating supracrustal zircons from a large sample set, representative of the lithological diversity and stratigraphy in a given area.

Additionally, mismatches in trace element composition and/or $\varepsilon Hf_{(t)}$ between supracrustal and igneous/TTG zircon record that some significant components of the Paleoarchean felsic crust are now strongly under-represented or even missing from the preserved, igneous BGGT crust. This is particularly true for the Moodies zircons, nearly half of which may be derived from a formerly widespread, uppermost K_2O-rich crust now only represented by volumetrically minor, ca. 3530-3450 Ma felsic schists/volcaniclastic sediments of the Theespruit Formation; and granitic/rhyolitic clasts found in the ca. 3220 Ma Moodies Basal Conglomerate. Such K_2O-rich igneous rocks formed during three main episodes, coevally with Na_2O-rich TTGs (namely at ca. 3560-3500; 3490-3400 and 3290-3210 Ma), but produced by distinct petrogenetic processes, i.e. partial melting of supracrustal (sedimentary and/or felsic volcanic/volcaniclastic) rocks. While the youngest generation (3290-3210 Ma) is synchronous with regional evidence for HP/LT metamorphism and thus attributed to partial melting of this supracrustal material at high pressure in subduction-like environments, the geodynamic setting of the oldest two generations is less well constrained.

Nonetheless, the existence of this K-rich uppermost crust as early as ca. 3560 Ma and its persistence throughout the following 350 Myr favor that this is a first-order characteristic of felsic crust production in the BGGT; and that the Paleoarchean felsic crust was vertically stratified into shallower K-rich and deeper Na-rich components. These possibilities would require further testing on different Archean cratons.

2.7. Acknowledgements

The PhD project of J.B.C. has been supported by National Research Foundation grant CNRS-129351 (South Africa) as part of the BuCoMO project, the University of Toulouse TREMPLIN grant PRESIZION and by the EUR TESS N°ANR-18-EURE-0018 in the framework of the Programme des Investissements d'Avenir. We thank the Mpumalanga Tourism and Park Agency for giving us access to the Komati Nature Reserve. We thank M. Vinicius Santos Leandro, J.F. Moyen and A. Chauvet for help and guidance during fieldwork and comments on data interpretation. We are grateful to J. Delport and J.P. Nel for help with SELFRAG operation and zircon separation; S. Choy for help with zircon picking and mounting; F. Maubé for help with SEM imaging; A. Marquet and J. Chmeleff for assistance with LA-ICP-MS analyses and M. Grobbelaar-Moolman and R.T. Roussow for whole-rock analysis at the CAF laboratory (Stellenbosch University). We thank the journal editor A.I.S. Kemp, as well as R. Bolhar and two anonymous reviewers, for their very detailed and constructive comments that significantly improved the manuscript.

Declaration of interests

The authors declare that they have no known competing financial interests or personal relationships that could have appeared to influence the work reported in this paper.

2.8. References to Chapter 2

Agangi, A., Hofmann, A., & Elburg, M. A. (2018). A review of Palaeoarchaean felsic volcanism in the eastern Kaapvaal craton : Linking plutonic and volcanic records. *Geoscience Frontiers*, *9*(3), 667-688.

Anhaeusser, C. R. (1980). A geological investigation of the Archaean granite-greenstone terrane south of the Boesmanskop syenite pluton, Barberton Mountain Land. *South African Journal of Geology*, *83*(1), 93-106.

Anhaeusser, C. R. (1981). Geotectonic evolution of the Archaean successions in the Barberton Mountain land, South Africa. In *Developments in Precambrian Geology* (Vol. 4, p. 137-160). Elsevier. https://www.sciencedirect.com/science/article/pii/S0166263508700112

Anhaeusser, C. R. (1983). *The geology of the Schapenburg greenstone remnant and surrounding Archaean granitic terrane south of Badplaas, Eastern Transvaal*. https://pascal-francis.inist.fr/vibad/index.php?action=getRecordDetail&idt=6522482

Anhaeusser, C. R. (2014). Archaean greenstone belts and associated granitic rocks–a review. *Journal of African Earth Sciences*, *100*, 684-732.

Anhaeusser, C. R. (2019). The geology and tectonic evolution of the northwest part of the Barberton Greenstone Belt, South Africa : A review. *South African Journal of Geology*, *122*(4), 421-454. https://doi.org/10.25131/sajg.122.0033

Antoine, C., Bruand, E., Guitreau, M., & Devidal, J. -L. (2020). Understanding Preservation of Primary Signatures in Apatite by Comparing Matrix and Zircon-Hosted Crystals From the Eoarchean Acasta Gneiss Complex (Canada). *Geochemistry, Geophysics, Geosystems*, *21*(7), e2020GC008923. https://doi.org/10.1029/2020GC008923

Armstrong, R. A., Compston, W., De Wit, M. J., & Williams, I. S. (1990). The stratigraphy of the 3.5-3.2 Ga Barberton Greenstone Belt revisited : A single zircon ion microprobe study. *Earth and Planetary Science Letters*, *101*(1), 90-106.

Barker, F., & Arth, J. G. (1976). Generation of trondhjemitic-tonalitic liquids and Archean bimodal trondhjemite-basalt suites. *Geology*, *4*(10), 596-600.

Bédard, J. H. (2006). A catalytic delamination-driven model for coupled genesis of Archaean crust and sub-continental lithospheric mantle. *Geochimica et Cosmochimica Acta*, *70*(5), 1188-1214. https://doi.org/10.1016/j.gca.2005.11.008

Bell, E. A., Boehnke, P., Barboni, M., & Harrison, T. M. (2019). Tracking chemical alteration in magmatic zircon using rare earth element abundances. *Chemical Geology*, *510*, 56-71.

Bell, E. A., Boehnke, P., & Harrison, T. M. (2016). Recovering the primary geochemistry of Jack Hills zircons through quantitative estimates of chemical alteration. *Geochimica et Cosmochimica Acta*, *191*, 187-202.

Belousova, E. A., Griffin, W. L., O'Reilly, S. Y., & Fisher, N. I. (2002). Apatite as an indicator mineral for mineral exploration : Trace-element compositions and their relationship to host rock type. *Journal of Geochemical Exploration*, *76*(1), 45-69.

Belousova, E. A., Walters, S., Griffin, W. L., & O'Reilly, S. Y. (2001). Trace-element signatures of apatites in granitoids from the Mt Isa Inlier, northwestern Queensland. *Australian Journal of Earth Sciences*, *48*(4), 603-619. https://doi.org/10.1046/j.1440-0952.2001.00879.x

Belousova, E., Griffin, W., O'Reilly, S. Y., & Fisher, N. (2002). Igneous zircon : Trace element composition as an indicator of source rock type. *Contributions to Mineralogy and Petrology*, *143*(5), 602-622. https://doi.org/10.1007/s00410-002-0364-7

Bickle, M. J., Nisbet, E. G., & Martin, A. (1994). Archean Greenstone Belts Are Not Oceanic Crust. *The Journal of Geology*, *102*(2), 121-137. https://doi.org/10.1086/629658

Bleeker, W. (2003). The late Archean record : A puzzle in ca. 35 pieces. *Lithos*, *71*(2-4), 99-134.

Blichert-Toft, J., & Puchtel, I. S. (2010). Depleted mantle sources through time : Evidence from Lu–Hf and Sm–Nd isotope systematics of Archean komatiites. *Earth and Planetary Science Letters*, *297*(3), 598-606. https://doi.org/10.1016/j.epsl.2010.07.012

Bolhar, R., Hofmann, A., Allen, C. M., & Maas, R. (2021). A LA-ICPMS zircon record of magmatic crystallization and compositional alteration in meta-igneous rocks of the eastern Kaapvaal Craton. *South African Journal of Geology*, *124*(3), 761-782. https://doi.org/10.25131/sajg.124.0042

Bolhar, R., Weaver, S. D., Whitehouse, M. J., Palin, J. M., Woodhead, J. D., & Cole, J. W. (2008). Sources and evolution of arc magmas inferred from coupled O and Hf isotope systematics of plutonic zircons from the Cretaceous Separation Point Suite (New Zealand). *Earth and Planetary Science Letters*, *268*(3-4), 312-324.

Bouvier, A., Vervoort, J. D., & Patchett, P. J. (2008). The Lu–Hf and Sm–Nd isotopic composition of CHUR : Constraints from unequilibrated chondrites and implications for the bulk composition of terrestrial planets. *Earth and Planetary Science Letters*, *273*(1-2), 48-57.

Brown, M. (1994). The generation, segregation, ascent and emplacement of granite magma : The migmatite-to-crustally-derived granite connection in thickened orogens. *Earth-Science Reviews*, *36*(1), 83-130. https://doi.org/10.1016/0012-8252(94)90009-4

Brown, M., Johnson, T., & Gardiner, N. J. (2020). Plate Tectonics and the Archean Earth. *Annual Review of Earth and Planetary Sciences*, *48*(1), 291-320. https://doi.org/10.1146/annurev-earth-081619-052705

Bruand, E., Fowler, M., Storey, C., Laurent, O., Antoine, C., Guitreau, M., Heilimo, E., & Nebel, O. (2020). Accessory mineral constraints on crustal evolution : Elemental fingerprints for magma discrimination. *Geochemical Perspectives Letters*, *13*, 7-12.

Byerly, G. R., Kröner, A., Lowe, D. R., Todt, W., & Walsh, M. M. (1996). Prolonged magmatism and time constraints for sediment deposition in the early Archean Barberton greenstone belt : Evidence from the Upper Onverwacht and Fig Tree groups. *Precambrian Research*, *78*(1-3), 125-138.

Cawood, P. A., Hawkesworth, C. J., Pisarevsky, S. A., Dhuime, B., Capitanio, F. A., & Nebel, O. (2018). Geological archive of the onset of plate tectonics. *Philosophical Transactions of the Royal Society A: Mathematical, Physical and Engineering Sciences*, *376*(2132), 20170405. https://doi.org/10.1098/rsta.2017.0405

Cawood, P. A., Kroner, A., & Pisarevsky, S. (2006). Precambrian plate tectonics : Criteria and evidence. *GSA today*, *16*(7), 4.

Champion, D. C., & Smithies, R. H. (2007). Chapter 4.3 Geochemistry of Paleoarchean Granites of the East Pilbara Terrane, Pilbara Craton, Western Australia : Implications for Early Archean

Crustal Growth. In M. J. van Kranendonk, R. H. Smithies, & V. C. Bennett (Éds.), *Developments in Precambrian Geology* (Vol. 15, p. 369-409). Elsevier. https://doi.org/10.1016/S0166-2635(07)15043-X

Clemens, J. D., Yearron, L. M., & Stevens, G. (2006). Barberton (South Africa) TTG magmas : Geochemical and experimental constraints on source-rock petrology, pressure of formation and tectonic setting. *Precambrian Research*, *151*(1-2), 53-78.

Cloete, D. (1993). *Processing Remotely Sensed Data for Geological Content Over a Part of the Barberton Greenstone Belt, Republic of South Africa* [Master's Thesis, University of the Witwatersrand, Johannesburg (South Africa)]. https://search.proquest.com/openview/5cfcd55e3605de82a0efba46f3e2c020/1?pq-origsite=gscholar&cbl=2026366&diss=y

Cloete, M. (1999). *Aspects of volcanism and metamorphism of the Onverwacht group lavas in the South-Western portion of the Barberton greenstone belt.* [PhD Thesis]. https://wiredspace.wits.ac.za/items/cd520741-8d50-41a3-851e-bbc95bf82b2b

Condie, K. C. (1976). Trace-element geochemistry of Archean greenstone belts. *Earth-Science Reviews*, *12*(4), 393-417.

Condie, K. C. (1981). *Archean greenstone belts* (Vol. 3). Elsevier. https://books.google.com/books?hl=fr&lr=&id=6LkEpT_nlOAC&oi=fnd&pg=PP1&dq=Condie.+1981+greenstone&ots=hree9KwIBD&sig=7UDlC2znn7-ELP9jVJhBV46josw

Condie, K. C., & Kröner, A. (2008). *When did plate tectonics begin? Evidence from the geologic record*. https://pubs.geoscienceworld.org/gsa/books/edited-volume/594/chapter-abstract/3804524

Condie, K. C., Macke, J. E., & Reimer, T. O. (1970). Petrology and geochemistry of early Precambrian graywackes from the Fig Tree Group, South Africa. *Geological Society of America Bulletin*, *81*(9), 2759-2776.

Couzinié, S., Laurent, O., Moyen, J.-F., Zeh, A., Bouilhol, P., & Villaros, A. (2016). Post-collisional magmatism : Crustal growth not identified by zircon Hf–O isotopes. *Earth and Planetary Science Letters*, *456*, 182-195. https://doi.org/10.1016/j.epsl.2016.09.033

Crisp, L. J., & Berry, A. J. (2022). A new model for zircon saturation in silicate melts. *Contributions to Mineralogy and Petrology*, *177*(7), 71. https://doi.org/10.1007/s00410-022-01925-6

Cruden, A. R., & Weinberg, R. F. (2018). Chapter 2—Mechanisms of Magma Transport and Storage in the Lower and Middle Crust—Magma Segregation, Ascent and Emplacement. In S. Burchardt (Éd.), *Volcanic and Igneous Plumbing Systems* (p. 13-53). Elsevier. https://doi.org/10.1016/B978-0-12-809749-6.00002-9

De Ronde, C. E. J., & De Wit, M. J. (1994). Tectonic history of the Barberton greenstone belt, South Africa : 490 million years of Archean crustal evolution. *Tectonics*, *13*(4), 983-1005. https://doi.org/10.1029/94TC00353

De Wit, M. J., Armstrong, R., Hart, R. J., & Wilson, A. H. (1987). Felsic igneous rocks within the 3.3- to 3.5-Ga Barberton Greenstone Belt : High crustal level equivalents of the surrounding Tonalite-Trondhjemite Terrain, emplaced during thrusting. *Tectonics*, *6*(5), 529-549. https://doi.org/10.1029/TC006i005p00529

De Wit, M. J., & Furnes, H. (2016). 3.5-Ga hydrothermal fields and diamictites in the Barberton Greenstone Belt—Paleoarchean crust in cold environments. *Science Advances*, *2*(2), e1500368. https://doi.org/10.1126/sciadv.1500368

De Wit, M. J., Hart, R. A., & Hart, R. J. (1987). The Jamestown Ophiolite Complex, Barberton mountain belt : A section through 3.5 Ga oceanic crust. *Journal of African Earth Sciences (1983)*, *6*(5), 681-730.

Decker, N. B., Byerly, G. R., Stiegler, M. T., Lowe, D. R., & Stefurak, E. (2015). High resolution tephra and U/Pb chronology of the 3.33–3.26 Ga Mendon Formation, Barberton Greenstone Belt, South Africa. *Precambrian Research*, *261*, 54-74.

de Wit, M. J. (1982). Gliding and overthrust nappe tectonics in the Barberton Greenstone Belt. *Journal of Structural Geology*, *4*(2), 117-136.

de Wit, M. J., Furnes, H., & Robins, B. (2011). Geology and tectonostratigraphy of the Onverwacht Suite, Barberton greenstone belt, South Africa. *Precambrian Research*, *186*(1-4), 1-27.

Dhuime, B., Wuestefeld, A., & Hawkesworth, C. J. (2015). Emergence of modern continental crust about 3 billion years ago. *Nature Geoscience*, *8*(7), 552-555. https://doi.org/10.1038/ngeo2466

Diener, J. F. (2004). *The tectono-metamorphic evolution of the Theespruit Formation in the Tjakastad schist belt and surrounding areas of the Barberton Greenstone Belt, South Africa* [PhD Thesis, Stellenbosch: University of Stellenbosch]. https://scholar.sun.ac.za/handle/10019.1/16309

Diener, J. F. A., Stevens, G., Kisters, A. F. M., & Poujol, M. (2005). Metamorphism and exhumation of the basal parts of the Barberton greenstone belt, South Africa : Constraining the rates of Mesoarchaean tectonism. *Precambrian Research*, *143*(1), 87-112. https://doi.org/10.1016/j.precamres.2005.10.001

Diener, J. F., Stevens, G., Kisters, A. F., & Poujol, M. (2005). Metamorphism and exhumation of the basal parts of the Barberton greenstone belt, South Africa : Constraining the rates of Mesoarchaean tectonism. *Precambrian Research*, *143*(1-4), 87-112.

Dong, C., Liu, S., Nutman, A. P., Li, P., Xie, H., Li, Y., Liu, D., & Wan, Y. (2024). New discovery of 3.84–3.64 Ga diverse granitoids in eastern Hebei, North China Craton : Petrogenesis and significance. *Geological Society of America Bulletin*, *136*(11-12), 5249-5261.

Drabon, N., Byerly, B. L., Byerly, G. R., Wooden, J. L., Wiedenbeck, M., Valley, J. W., Kitajima, K., Bauer, A. M., & Lowe, D. R. (2022). Destabilization of Long-Lived Hadean Protocrust and the Onset of Pervasive Hydrous Melting at 3.8 Ga. *AGU Advances*, *3*(2), e2021AV000520. https://doi.org/10.1029/2021AV000520

Drabon, N., Galić, A., Mason, P. R., & Lowe, D. R. (2019). Provenance and tectonic implications of the 3.28–3.23 Ga Fig Tree Group, central Barberton greenstone belt, South Africa. *Precambrian Research*, *325*, 1-19.

Drabon, N., Kirkpatrick, H. M., Byerly, G. R., & Wooden, J. L. (2024). Trace elements in zircon record changing magmatic processes and the multi-stage build-up of Archean proto-continental crust. *Geochimica et Cosmochimica Acta*, *373*, 136-150.

Drabon, N., & Lowe, D. R. (2022). Progressive accretion recorded in sedimentary rocks of the 3.28–3.23 Ga Fig Tree Group, Barberton Greenstone Belt. *GSA Bulletin*, *134*(5-6), 1258-1276.

Dziggel, A., Stevens, G., Poujol, M., Anhaeusser, C. R., & Armstrong, R. A. (2002). Metamorphism of the granite–greenstone terrane south of the Barberton greenstone belt, South Africa : An insight into the tectono-thermal evolution of the 'lower' portions of the Onverwacht Group. *Precambrian Research*, *114*(3), 221-247. https://doi.org/10.1016/S0301-9268(01)00225-X

Dziggel, A., Stevens, G., Poujol, M., & Armstrong, R. A. (2006a). *Contrasting source components of clastic metasedimentary rocks in the lowermost formations of the Barberton greenstone belt*.

Dziggel, A., Stevens, G., Poujol, M., & Armstrong, R. A. (2006b). *Contrasting source components of clastic metasedimentary rocks in the lowermost formations of the Barberton greenstone belt*.

Eglington, B. M., & Armstrong, R. A. (2004). The Kaapvaal Craton and adjacent orogens, southern Africa : A geochronological database and overview of the geological development of the craton. *South African Journal of Geology*, *107*(1-2), 13-32.

Eriksson, K. A., Krapez, B., & Fralick, P. W. (1994). Sedimentology of Archean greenstone belts : Signatures of tectonic evolution. *Earth-Science Reviews*, *37*(1-2), 1-88.

Ferrero, S., Nicoli, G., & Gresky, K. (2022). Mesoarchean nanogranitoids and fluid inclusions in garnet from migmatites of the Kangerlussuaq basement, Southeast Greenland. *EGU General Assembly Conference Abstracts*, EGU22-4099. https://ui.adsabs.harvard.edu/abs/2022EGUGA..24.4099F/abstract

Ferry, J. M., & Watson, E. B. (2007). New thermodynamic models and revised calibrations for the Ti-in-zircon and Zr-in-rutile thermometers. *Contributions to Mineralogy and Petrology*, *154*(4), 429-437. https://doi.org/10.1007/s00410-007-0201-0

Fisher, C. M., Hanchar, J. M., Samson, S. D., Dhuime, B., Blichert-Toft, J., Vervoort, J. D., & Lam, R. (2011). Synthetic zircon doped with hafnium and rare earth elements : A reference material for in situ hafnium isotope analysis. *Chemical Geology*, *286*(1-2), 32-47.

Fisher, C. M., Vervoort, J. D., & Hanchar, J. M. (2014). Guidelines for reporting zircon Hf isotopic data by LA-MC-ICPMS and potential pitfalls in the interpretation of these data. *Chemical geology*, *363*, 125-133.

Flament, N., Coltice, N., & Rey, P. F. (2013). The evolution of the 87Sr/86Sr of marine carbonates does not constrain continental growth. *Precambrian Research*, *229*, 177-188. https://doi.org/10.1016/j.precamres.2011.10.009

Foley, S. (2008). *A trace element perspective on Archean crust formation and on the presence or absence of Archean subduction*. https://pubs.geoscienceworld.org/gsa/books/edited-volume/594/chapter-abstract/3804352

Fonseca Teixeira, L. M., Laurent, O., Troch, J., Siddoway, C. S., Tavazzani, L., Deering, C., & Bachmann, O. (2024). Tracking quartz and zircon provenance in sedimentary rocks using Ti distributions : Unlocking the volcanic-plutonic connection in old igneous systems. *Earth and Planetary Science Letters*, *643*, 118906. https://doi.org/10.1016/j.epsl.2024.118906

Fonseca Teixeira, L. M., Troch, J., & Bachmann, O. (2023). The dynamic nature of aTiO2 : Implications for Ti-based thermometers in magmatic systems. *Geology*, *52*(1), 92-96. https://doi.org/10.1130/G51587.1

Gerya, T. (2014). Precambrian geodynamics : Concepts and models. *Gondwana Research*, *25*(2), 442-463.

Gier□, R. (1986). Zirconolite, allanite and hoegbomite in a marble skarn from the Bergell contact aureole : Implications for mobility of Ti, Zr and REE. *Contributions to Mineralogy and Petrology*, *93*(4), 459-470. https://doi.org/10.1007/BF00371716

Gorman, B. E., Pearce, T. H., & Birkett, T. C. (1978). On the structure of Archean greenstone belts. *Precambrian Research*, *6*(1), 23-41.

Grimes, C. B., John, B. E., Kelemen, P. B., Mazdab, F. K., Wooden, J. L., Cheadle, M. J., Hanghøj, K., & Schwartz, J. J. (2007). Trace element chemistry of zircons from oceanic crust : A method for distinguishing detrital zircon provenance. *Geology*, *35*(7), 643-646.

Grimes, C. B., Wooden, J. L., Cheadle, M. J., & John, B. E. (2015). "Fingerprinting" tectono-magmatic provenance using trace elements in igneous zircon. *Contributions to Mineralogy and Petrology*, *170*(5-6), 46. https://doi.org/10.1007/s00410-015-1199-3

Grosch, E. G. (2019). Metamorphic processes preserved in early Archean supracrustal rocks of the Barberton Greenstone Belt, South Africa. *Geological Society, London, Special Publications*, *478*(1), 315-334. https://doi.org/10.1144/SP478.15

Grosch, E. G., Kosler, J., McLoughlin, N., Drost, K., Slama, J., & Pedersen, R. B. (2011). Paleoarchean detrital zircon ages from the earliest tectonic basin in the Barberton Greenstone Belt, Kaapvaal craton, South Africa. *Precambrian Research*, *191*(1-2), 85-99.

Grosch, E. G., Vidal, O., Abu-Alam, T., & McLoughlin, N. (2012). P–T constraints on the metamorphic evolution of the Paleoarchean Kromberg type-section, Barberton Greenstone Belt, South Africa. *Journal of Petrology*, *53*(3), 513-545.

Harrison, T. M., Bell, E. A., & Boehnke, P. (2017). Hadean zircon petrochronology. *Reviews in Mineralogy and Geochemistry*, *83*(1), 329-363.

Hawkesworth, C., Cawood, P. A., Dhuime, B., & Kemp, T. (2024). Tectonic processes and the evolution of the continental crust. *Journal of the Geological Society*, *181*(4), jgs2024-027. https://doi.org/10.1144/jgs2024-027

Hawkesworth, C., Cawood, P., Kemp, T., Storey, C., & Dhuime, B. (2009). A Matter of Preservation. *Science*, *323*(5910), 49-50. https://doi.org/10.1126/science.1168549

Hawkesworth, C. J., Cawood, P. A., & Dhuime, B. (2020). The evolution of the continental crust and the onset of plate tectonics. *Frontiers in earth science*, *8*, 326.

Hawkesworth, C. J., Cawood, P. A., Dhuime, B., & Kemp, T. I. S. (2017). Earth's Continental Lithosphere Through Time. *Annual Review of Earth and Planetary Sciences*, *45*(1), 169-198. https://doi.org/10.1146/annurev-earth-063016-020525

Hawkesworth, C. J., & Kemp, A. I. S. (2006). Using hafnium and oxygen isotopes in zircons to unravel the record of crustal evolution. *Chemical Geology*, *226*(3-4), 144-162.

Heubeck, C. (2019). The Moodies Group—A High-Resolution Archive of Archaean Surface Processes and Basin-Forming Mechanisms. In A. Kröner & A. Hofmann (Éds.), *The Archaean Geology of the Kaapvaal Craton, Southern Africa* (p. 133-169). Springer International Publishing. https://doi.org/10.1007/978-3-319-78652-0_6

Heubeck, C., Drabon, N., Byerly, G., Leisgang, I., Linnemann, U., Lowe, D., Mertz-Kraus, R., Gonzalez-Pinzon, A., Thomsen, T. B., & Zeh, A. (2022). Detrital zircon provenance of the Archean Moodies Group, Barberton Greenstone Belt, South Africa and Eswatini. *American Journal of Science*, *322*(2), 65-107.

Heubeck, C., Engelhardt, J., Byerly, G. R., Zeh, A., Sell, B., Luber, T., & Lowe, D. R. (2013). Timing of deposition and deformation of the Moodies Group (Barberton Greenstone Belt, South Africa) : Very-high-resolution of Archaean surface processes. *Precambrian Research*, *231*, 236-262.

Heubeck, C., & Lowe, D. R. (1994). Late syndepositional deformation and detachment tectonics in the Barberton Greenstone Belt, South Africa. *Tectonics*, *13*(6), 1514-1536. https://doi.org/10.1029/94TC01809

Hoffmann, J. E., Kröner, A., Hegner, E., Viehmann, S., Xie, H., Iaccheri, L. M., Schneider, K. P., Hofmann, A., Wong, J., & Geng, H. (2016). Source composition, fractional crystallization and magma mixing processes in the 3.48–3.43 Ga Tsawela tonalite suite (Ancient Gneiss Complex, Swaziland)–Implications for Palaeoarchaean geodynamics. *Precambrian Research*, *276*, 43-66.

Hofmann, A. (2005). The geochemistry of sedimentary rocks from the Fig Tree Group, Barberton greenstone belt : Implications for tectonic, hydrothermal and surface processes during mid-Archaean times. *Precambrian Research*, *143*(1), 23-49. https://doi.org/10.1016/j.precamres.2005.09.005

Hofmann, A., Bolhar, R., Orberger, B., & Foucher, F. (2013). Cherts of the Barberton Greenstone Belt, South Africa : Petrology and trace-element geochemistry of 3.5 to 3.3 Ga old silicified volcaniclastic sediments. *South African Journal of Geology*, *116*(2), 297-322.

Hoskin, P. W. (2005). Trace-element composition of hydrothermal zircon and the alteration of Hadean zircon from the Jack Hills, Australia. *Geochimica et cosmochimica acta*, *69*(3), 637-648.

Hoskin, P. W., & Schaltegger, U. (2003). The composition of zircon and igneous and metamorphic petrogenesis. *Reviews in mineralogy and geochemistry*, *53*(1), 27-62.

Jahn, B.-M., Glikson, A. Y., Peucat, J. J., & Hickman, A. H. (1981). REE geochemistry and isotopic data of Archean silicic volcanics and granitoids from the Pilbara Block, Western Australia : Implications for the early crustal evolution. *Geochimica et Cosmochimica Acta*, *45*(9), 1633-1652. https://doi.org/10.1016/S0016-7037(81)80002-6

Johnson, T. E., Brown, M., Gardiner, N. J., Kirkland, C. L., & Smithies, R. H. (2017). Earth's first stable continents did not form by subduction. *Nature*, *543*(7644), 239-242.

Johnson, T. E., Kirkland, C. L., Gardiner, N. J., Brown, M., Smithies, R. H., & Santosh, M. (2019). Secular change in TTG compositions : Implications for the evolution of Archaean geodynamics. *Earth and Planetary Science Letters*, *505*, 65-75.

Kamber, B. S. (2015). The evolving nature of terrestrial crust from the Hadean, through the Archaean, into the Proterozoic. *Precambrian Research*, *258*, 48-82.

Kamo, S. L., & Davis, D. W. (1994). Reassessment of Archean crustal development in the Barberton Mountain Land, South Africa, based on U-Pb dating. *Tectonics*, *13*(1), 167-192. https://doi.org/10.1029/93TC02254

Kirkland, C. L., Hartnady, M. I. H., Barham, M., Olierook, H. K. H., Steenfelt, A., & Hollis, J. A. (2021). Widespread reworking of Hadean-to-Eoarchean continents during Earth's thermal peak. *Nature Communications*, *12*(1), 331. https://doi.org/10.1038/s41467-020-20514-4

Kisters, A. F., Belcher, R. W., Poujol, M., & Dziggel, A. (2010). Continental growth and convergence-related arc plutonism in the Mesoarchaean : Evidence from the Barberton granitoid-greenstone terrain, South Africa. *Precambrian Research*, *178*(1-4), 15-26.

Kisters, A. F. M., Stevens, G., Dziggel, A., & Armstrong, R. A. (2003). Extensional detachment faulting and core-complex formation in the southern Barberton granite–greenstone terrain, South Africa : Evidence for a 3.2 Ga orogenic collapse. *Precambrian Research*, *127*(4), 355-378. https://doi.org/10.1016/j.precamres.2003.08.002

Kitajima, K., Ushikubo, T., Kita, N. T., Maruyama, S., & Valley, J. W. (2012). Relative retention of trace element and oxygen isotope ratios in zircon from Archean rhyolite, Panorama Formation, North Pole Dome, Pilbara Craton, Western Australia. *Chemical Geology*, *332*, 102-115.

Kohler, E. A., & Anhaeusser, C. R. (2002). Geology and geodynamic setting of Archaean silicic metavolcaniclastic rocks of the Bien Venue Formation, Fig Tree Group, northeast Barberton greenstone belt, South Africa. *Precambrian Research*, *116*(3-4), 199-235.

Korenaga, J. (2012). Plate tectonics and planetary habitability : Current status and future challenges. *Annals of the New York Academy of Sciences*, *1260*(1), 87-94. https://doi.org/10.1111/j.1749-6632.2011.06276.x

Korenaga, J. (2018). Crustal evolution and mantle dynamics through Earth history. *Philosophical Transactions of the Royal Society A: Mathematical, Physical and Engineering Sciences*, *376*(2132), 20170408.

Kröner, A., Anhaeusser, C. R., Hoffmann, J. E., Wong, J., Geng, H., Hegner, E., Xie, H., Yang, J., & Liu, D. (2016). Chronology of the oldest supracrustal sequences in the Palaeoarchaean Barberton Greenstone Belt, South Africa and Swaziland. *Precambrian Research*, *279*, 123-143.

Kröner, A., & Compston, W. (1988). Ion microprobe ages of zircons from early Archaean granite pebbles and greywacke, Barberton greenstone belt, southern Africa. *Precambrian Research*, *38*(4), 367-380.

Kröner, A., Hegner, E., Wendt, J. I., & Byerly, G. R. (1996). The oldest part of the Barberton granitoid-greenstone terrain, South Africa : Evidence for crust formation between 3.5 and 3.7 Ga. *Precambrian Research*, *78*(1-3), 105-124.

Kröner, A., Hoffmann, J. E., Xie, H., Münker, C., Hegner, E., Wan, Y., Hofmann, A., Liu, D., & Yang, J. (2014). Generation of early Archaean grey gneisses through melting of older crust in the eastern Kaapvaal craton, southern Africa. *Precambrian Research*, *255*, 823-846.

Kröner, A., Hoffmann, J. E., Xie, H., Wu, F., Münker, C., Hegner, E., Wong, J., Wan, Y., & Liu, D. (2013). Generation of early Archaean felsic greenstone volcanic rocks through crustal melting in the Kaapvaal, craton, southern Africa. *Earth and Planetary Science Letters*, *381*, 188-197.

Kröner, A., Wong, J., & Xie, H. (2018). The oldest granite clast in the Moodies conglomerate, Barberton greenstone belt, South Africa, and its likely origin. *South African Journal of Geology*, *121*(1), 43-50.

Kusky, T. M., Windley, B. F., & Polat, A. (2018). Geological evidence for the operation of plate tectonics throughout the Archean : Records from Archean paleo-plate boundaries. *Journal of Earth Science*, *29*(6), 1291-1303.

Large, R. R., Mukherjee, I., Zhukova, I., Corkrey, R., Stepanov, A., & Danyushevsky, L. V. (2018). Role of upper-most crustal composition in the evolution of the Precambrian ocean–atmosphere system. *Earth and Planetary Science Letters*, *487*, 44-53.

Laurent, O., Björnsen, J., Wotzlaw, J.-F., Bretscher, S., Pimenta Silva, M., Moyen, J.-F., Ulmer, P., & Bachmann, O. (2020). Earth's earliest granitoids are crystal-rich magma reservoirs tapped by silicic eruptions. *Nature Geoscience*, *13*(2), 163-169.

Laurent, O., Guitreau, M., Bruand, E., & Moyen, J.-F. (2024). At the dawn of continents : Archean tonalite-trondhjemite-granodiorite suites. *Elements*, *20*(3), 174-179.

Laurent, O., Martin, H., Moyen, J.-F., & Doucelance, R. (2014). The diversity and evolution of late-Archean granitoids : Evidence for the onset of "modern-style" plate tectonics between 3.0 and 2.5 Ga. *Lithos*, *205*, 208-235.

Laurent, O., Moyen, J.-F., Wotzlaw, J.-F., Björnsen, J., & Bachmann, O. (2022). Early Earth zircons formed in residual granitic melts produced by tonalite differentiation. *Geology*, *50*(4), 437-441.

Lowe, D. R. (1999). *Geologic evolution of the Barberton Greenstone Belt and vicinity*. https://pubs.geoscienceworld.org/gsa/books/edited-volume/486/chapter-pdf/967261/i0-8137-2329-9-329-0-287.pdf

Lowe, D. R., & Byerly, G. R. (2007). An overview of the geology of the Barberton Greenstone Belt and vicinity : Implications for early crustal development. *Developments in Precambrian geology*, *15*, 481-526.

Lowe, D. R., & Byerly, G. R. (2020). The non-glacial and non-cratonic origin of an early Archean felsic volcaniclastic unit, Barberton Greenstone Belt, South Africa. *Precambrian Research*, *341*, 105647.

Ma, Q., Xu, Y.-G., Huang, X.-L., Zheng, J.-P., Ping, X., & Xia, X.-P. (2020). Eoarchean to Paleoproterozoic crustal evolution in the North China Craton : Evidence from U-Pb and Hf-O isotopes of zircons from deep-crustal xenoliths. *Geochimica et Cosmochimica Acta*, *278*, 94-109. https://doi.org/10.1016/j.gca.2019.09.009

Martin, H. (1986). Effect of steeper Archean geothermal gradient on geochemistry of subduction-zone magmas. *Geology*, *14*(9), 753-756.

Martin, H., Moyen, J.-F., Guitreau, M., Blichert-Toft, J., & Le Pennec, J.-L. (2014). Why Archaean TTG cannot be generated by MORB melting in subduction zones. *Lithos*, *198*, 1-13.

Matsumura, R. (2014). *The petrogenesis of the Nelshoogte pluton : The youngest and most compositionally variable TTG pluton in the Barberton Granite-Greenstone Terrain* [PhD Thesis, Stellenbosch: Stellenbosch University]. https://scholar.sun.ac.za/handle/10019.1/86589

Miyake, S., Aoki, K., Komiya, T., Aoki, S., Fukuyama, M., & Ogasawara, M. (2024). Geochemical Signatures of Igneous Zircon and Apatite : Generation of Archean TTGs in the Barberton Granitoid-Greenstone Terrain, South Africa. *Island Arc*, *33*(1). https://doi.org/10.1111/iar.12536

Moecher, D. P., & Samson, S. D. (2006). Differential zircon fertility of source terranes and natural bias in the detrital zircon record : Implications for sedimentary provenance analysis. *Earth and Planetary Science Letters*, *247*(3-4), 252-266.

Moyen, J.-F. (2011). The composite Archaean grey gneisses : Petrological significance, and evidence for a non-unique tectonic setting for Archaean crustal growth. *Lithos*, *123*(1-4), 21-36.

Moyen, J.-F., & Martin, H. (2012). Forty years of TTG research. *Lithos*, *148*, 312-336.

Moyen, J.-F., Stevens, G., & Kisters, A. (2006). Record of mid-Archaean subduction from metamorphism in the Barberton terrain, South Africa. *Nature*, *442*(7102), 559-562.

Moyen, J.-F., Stevens, G., Kisters, A. F., & Belcher, R. W. (2007). TTG plutons of the Barberton granitoid-greenstone terrain, South Africa. *Developments in Precambrian Geology*, *15*, 607-667.

Mühlberg, M., Stevens, G., Moyen, J.-F., Kisters, A. F., & Lana, C. (2021). Thermal evolution of the Stolzburg Block, Barberton granitoid-greenstone terrain, South Africa : Implications for Paleoarchean tectonic processes. *Precambrian Research*, *359*, 106082.

Næraa, T., Scherstén, A., Rosing, M. T., Kemp, A. I. S., Hoffmann, J. E., Kokfelt, T. F., & Whitehouse, M. J. (2012). Hafnium isotope evidence for a transition in the dynamics of continental growth 3.2 Gyr ago. *Nature*, *485*(7400), 627-630. https://doi.org/10.1038/nature11140

Nocita, B. W., & Lowe, D. R. (1990). Fan-delta sequence in the Archean Fig Tree Group, Barberton Greenstone Belt, South Africa. *Precambrian Research*, *48*(4), 375-393.

Nutman, A. P., Bennett, V. C., Friend, C. R., & Yi, K. (2020). Eoarchean contrasting ultra-high-pressure to low-pressure metamorphisms (< 250 to> 1000° C/GPa) explained by tectonic plate convergence in deep time. *Precambrian Research*, *344*, 105770.

Nutman, A. P., & Hiess, J. (2009). A granitic inclusion suite within igneous zircons from a 3.81 Ga tonalite (W. Greenland) : Restrictions for Hadean crustal evolution studies using detrital zircons. *Chemical Geology*, *261*(1-2), 77-82.

O'Sullivan, G., Chew, D., Kenny, G., Henrichs, I., & Mulligan, D. (2020). The trace element composition of apatite and its application to detrital provenance studies. *Earth-Science Reviews*, *201*, 103044.

Palin, R. M., Santosh, M., Cao, W., Li, S.-S., Hernández-Uribe, D., & Parsons, A. (2020). Secular change and the onset of plate tectonics on Earth. *Earth-Science Reviews*, *207*, 103172.

Palin, R. M., White, R. W., & Green, E. C. (2016). Partial melting of metabasic rocks and the generation of tonalitic–trondhjemitic–granodioritic (TTG) crust in the Archaean : Constraints from phase equilibrium modelling. *Precambrian Research*, *287*, 73-90.

Payne, J. L., Hand, M., Pearson, N. J., Barovich, K. M., & McInerney, D. J. (2015). Crustal thickening and clay : Controls on O isotope variation in global magmatism and siliciclastic sedimentary rocks. *Earth and Planetary Science Letters*, *412*, 70-76. https://doi.org/10.1016/j.epsl.2014.12.037

Payne, J. L., McInerney, D. J., Barovich, K. M., Kirkland, C. L., Pearson, N. J., & Hand, M. (2016). Strengths and limitations of zircon Lu-Hf and O isotopes in modelling crustal growth. *Lithos*, *248-251*, 175-192. https://doi.org/10.1016/j.lithos.2015.12.015

Polat, A. (2012). Growth of Archean continental crust in oceanic island arcs. *Geology*, *40*(4), 383.

Pourteau, A., Doucet, L. S., Blereau, E. R., Volante, S., Johnson, T. E., Collins, W. J., Li, Z.-X., & Champion, D. C. (2020). TTG generation by fluid-fluxed crustal melting : Direct evidence from the Proterozoic Georgetown Inlier, NE Australia. *Earth and Planetary Science Letters*, *550*, 116548.

Ptáček, M. P., Dauphas, N., & Greber, N. D. (2020). Chemical evolution of the continental crust from a data-driven inversion of terrigenous sediment compositions. *Earth and Planetary Science Letters*, *539*, 116090.

Reimer, T. O., Condie, K. C., Schneider, G., & Georgi, A. (1985). Petrography and geochemistry of granitoid and metamorphite pebbles from the early Archaean Moodies Group, Barberton Mountainland/South Africa. *Precambrian Research*, *29*(4), 383-404.

Reimink, J. R., Chacko, T., Stern, R. A., & Heaman, L. M. (2014). Earth's earliest evolved crust generated in an Iceland-like setting. *Nature Geoscience*, *7*(7), 529-533.

Reimink, J. R., Davies, J., Chacko, T., Stern, R. A., Heaman, L. M., Sarkar, C., Schaltegger, U., Creaser, R. A., & Pearson, D. G. (2016). No evidence for Hadean continental crust within Earth's oldest evolved rock unit. *Nature Geoscience*, *9*(10), 777-780.

Reimink, J. R., Davies, J. H., Bauer, A. M., & Chacko, T. (2020). A comparison between zircons from the Acasta Gneiss Complex and the Jack Hills region. *Earth and Planetary Science Letters*, *531*, 115975.

Rey, P. F., Coltice, N., & Flament, N. (2024). Archean geodynamics underneath weak, flat, and flooded continents. *Elements*, *20*(3), 180-186.

Rollinson, H. R. (1996). Tonalite-trondhjemite-granodiorite magmatism and the genesis of Lewisian crust during the Archaean. *Geological Society, London, Special Publications*, *112*(1), 25-42. https://doi.org/10.1144/GSL.SP.1996.112.01.02

Rubatto, D. (2017). Zircon : The metamorphic mineral. *Reviews in mineralogy and geochemistry*, *83*(1), 261-295.

Sanchez-Garrido, C. J. (2012). *The petrogenesis of the older (> 3.0 Ga) potassic granitoids of eastern Mpumalanga (South Africa) and Swaziland : An investigation of crustal formation processes in the early Earth* [PhD Thesis, Stellenbosch: Stellenbosch University]. https://scholar.sun.ac.za/handle/10019.1/20044

Sanchez-Garrido, C. J., Stevens, G., Armstrong, R. A., Moyen, J.-F., Martin, H., & Doucelance, R. (2011). Diversity in Earth's early felsic crust : Paleoarchean peraluminous granites of the Barberton Greenstone Belt. *Geology*, *39*(10), 963-966.

Scherer, E., Münker, C., & Mezger, K. (2001). Calibration of the Lutetium-Hafnium Clock. *Science*, *293*(5530), 683-687. https://doi.org/10.1126/science.1061372

Schiller, D., & Finger, F. (2019). Application of Ti-in-zircon thermometry to granite studies : Problems and possible solutions. *Contributions to Mineralogy and Petrology*, *174*(6), 51. https://doi.org/10.1007/s00410-019-1585-3

Schoene, B., De Wit, M. J., & Bowring, S. A. (2008). Mesoarchean assembly and stabilization of the eastern Kaapvaal craton : A structural-thermochronological perspective. *Tectonics*, *27*(5), 2008TC002267. https://doi.org/10.1029/2008TC002267

Sizova, E., Gerya, T., & Brown, M. (2014). Contrasting styles of Phanerozoic and Precambrian continental collision. *Gondwana Research*, *25*(2), 522-545.

Smit, M. A., & Mezger, K. (2017). Earth's early O2 cycle suppressed by primitive continents. *Nature Geoscience*, *10*(10), 788-792.

Smithies, R. H. (2000). The Archaean tonalite–trondhjemite–granodiorite (TTG) series is not an analogue of Cenozoic adakite. *Earth and Planetary Science Letters*, *182*(1), 115-125.

Smithies, R. H., Lu, Y., Kirkland, C. L., Johnson, T. E., Mole, D. R., Champion, D. C., Martin, L., Jeon, H., Wingate, M. T. D., & Johnson, S. P. (2021). Oxygen isotopes trace the origins of Earth's earliest continental crust. *Nature*, *592*(7852), 70-75. https://doi.org/10.1038/s41586-021-03337-1

Söderlund, U., Patchett, P. J., Vervoort, J. D., & Isachsen, C. E. (2004). The 176Lu decay constant determined by Lu–Hf and U–Pb isotope systematics of Precambrian mafic intrusions. *Earth and Planetary Science Letters*, *219*(3-4), 311-324.

Spencer, C. J., Cavosie, A. J., Morrell, T. R., Lu, G. M., Liebmann, J., & Roberts, N. M. W. (2022). Disparities in oxygen isotopes of detrital and igneous zircon identify erosional bias in crustal rock record. *Earth and Planetary Science Letters*, *577*, 117248. https://doi.org/10.1016/j.epsl.2021.117248

Spencer, C. J., Kirkland, C. L., Roberts, N. M. W., Evans, N. J., & Liebmann, J. (2020). Strategies towards robust interpretations of in situ zircon Lu–Hf isotope analyses. *Geoscience Frontiers*, *11*(3), 843-853.

Spohn, T., & Breuer, D. (2016). Plate tectonics, habitability and life. *EGU General Assembly Conference Abstracts*, EPSC2016-18377. https://ui.adsabs.harvard.edu/abs/2016EGUGA..1818377S/abstract

Stern, R. J. (2018). The evolution of plate tectonics. *Philosophical Transactions of the Royal Society A: Mathematical, Physical and Engineering Sciences*, *376*(2132), 20170406. https://doi.org/10.1098/rsta.2017.0406

Stevens, G., Droop, G. T. R., Armstrong, R. A., & Anhaeusser, C. R. (2002). Amphibolite facies metamorphism in the Schapenburg schist belt : A record of the mid-crustal response to∼ 3.23 Ga terrane accretion in the Barberton greenstone belt. *South African Journal of Geology*, *105*(3), 271-284.

Stevens, G., & Moyen, J.-F. (2007). Metamorphism in the Barberton Granite Greenstone Terrain : A record of Paleoarchean accretion. *Developments in precambrian geology*, *15*, 669-698.

Sun, W. (2018). The formation of the continental crust. *Solid Earth Sciences*, *3*(2), 31-32.

Tang, M., Chen, K., & Rudnick, R. L. (2016). Archean upper crust transition from mafic to felsic marks the onset of plate tectonics. *Science*, *351*(6271), 372-375. https://doi.org/10.1126/science.aad5513

Trower, E. J., & Lowe, D. R. (2016). Sedimentology of the 3.3 Ga upper Mendon Formation, Barberton Greenstone Belt, South Africa. *Precambrian Research*, *281*, 473-494.

Valley, J. W., Lackey, J. S., Cavosie, A. J., Clechenko, C. C., Spicuzza, M. J., Basei, M. A. S., Bindeman, I. N., Ferreira, V. P., Sial, A. N., & King, E. M. (2005). 4.4 billion years of crustal maturation : Oxygen isotope ratios of magmatic zircon. *Contributions to Mineralogy and Petrology*, *150*, 561-580.

Van Kranendonk, M. J. (2011). Cool greenstone drips and the role of partial convective overturn in Barberton greenstone belt evolution. *Journal of African Earth Sciences*, *60*(5), 346-352.

Van Kranendonk, M. J., Kirkland, C. L., & Cliff, J. (2015). Oxygen isotopes in Pilbara Craton zircons support a global increase in crustal recycling at 3.2 Ga. *Lithos*, *228-229*, 90-98. https://doi.org/10.1016/j.lithos.2015.04.011

Van Kranendonk, M. J., Kröner, A., Hegner, E., & Connelly, J. (2009). Age, lithology and structural evolution of the c. 3.53 Ga Theespruit Formation in the Tjakastad area, southwestern Barberton Greenstone Belt, South Africa, with implications for Archaean tectonics. *Chemical Geology*, *261*(1-2), 115-139.

van Hunen, J., & Moyen, J.-F. (2012). Archean Subduction : Fact or Fiction? *Annual Review of Earth and Planetary Sciences*, *40*(1), 195-219. https://doi.org/10.1146/annurev-earth-042711-105255

Vervoort, J. D., & Blichert-Toft, J. (1999). Evolution of the depleted mantle : Hf isotope evidence from juvenile rocks through time. *Geochimica et Cosmochimica Acta*, *63*(3), 533-556. https://doi.org/10.1016/S0016-7037(98)00274-9

Vervoort, J. D., & Kemp, A. I. (2016). Clarifying the zircon Hf isotope record of crust–mantle evolution. *Chemical Geology*, *425*, 65-75.

Vezinet, A., Flores-Rojas, J., Sobolev, A. V., Léger, J., Chugunov, A. V., Batanova, V. G., Elburg, M. A., Hofmann, A., Balvay, M., & Paradis, N. (2025). Igneous apatite geochemistry indicates early cratonization of continents. *Precambrian Research*, *430*, 107927. https://doi.org/10.1016/j.precamres.2025.107927

Vezinet, A., Moyen, J.-F., Stevens, G., Nicoli, G., Laurent, O., Couzinié, S., & Frei, D. (2018). A record of 0.5 Ga of evolution of the continental crust along the northern edge of the Kaapvaal Craton, South Africa : Consequences for the understanding of Archean geodynamic processes. *Precambrian Research*, *305*, 310-326.

Wang, H., Yang, J.-H., Zhu, Y.-S., Huang, C., Xu, L., Wu, S.-T., & Liu, Y. (2022). Archean crustal growth and reworking revealed by combined U-Pb-Hf-O isotope and trace element data of detrital zircons from ancient and modern river sediments of the eastern Kaapvaal Craton. *Geochimica et Cosmochimica Acta*, *320*, 79-104.

Watson, E. B., & Harrison, T. M. (1983). Zircon saturation revisited : Temperature and composition effects in a variety of crustal magma types. *earth and planetary science letters*, *64*(2), 295-304.

Williams, C. T., & Gieré, R. (1996). Zirconolite : A review of localities worldwide, and a compilation of its chemical compositions. *BULLETIN-NATURAL HISTORY MUSEUM GEOLOGY SERIES*, *52*, 1-24.

Yearron, L., Clemens, J., Stevens, G., & Anhaeusser, C. (2003). Geochemistry and petrogenesis of the granitoids of the Barberton Mountain Land, South Africa. *EGS-AGU-EUG Joint Assembly*, 2639. https://ui.adsabs.harvard.edu/abs/2003EAEJA.....2639Y/abstract

Zeh, A., Gerdes, A., & Barton Jr, J. M. (2009). Archean accretion and crustal evolution of the Kalahari Craton—The zircon age and Hf isotope record of granitic rocks from Barberton/Swaziland to the Francistown Arc. *Journal of Petrology*, *50*(5), 933-966.

Zeh, A., Gerdes, A., & Heubeck, C. (2013). U–Pb and Hf isotope data of detrital zircons from the Barberton Greenstone Belt : Constraints on provenance and Archaean crustal evolution. *Journal of the Geological Society*, *170*(1), 215-223.

Zeh, A., Gerdes, A., & Millonig, L. (2011). Hafnium isotope record of the Ancient Gneiss Complex, Swaziland, southern Africa : Evidence for Archaean crust–mantle formation and crust reworking between 3.66 and 2.73 Ga. *Journal of the Geological Society*, *168*(4), 953-964. https://doi.org/10.1144/0016-76492010-117

3. Chapter 3: presentation of research paper 2 - Geochemistry of igneous and detrital apatites from the Barberton Granitoid-Greenstone Terrane (South Africa) reveals granitoid diversity in the Paleoarchean felsic crust.

This manuscript, first authored by Jean-Baptiste Combaz is under final revision by co-authors and will be submitted early in January 2026 to *Geochemica and Cosmochemica Acta*. Supplementary materials are available as an electronic link provided in Chapter 6.

Jean-Baptiste Combaz: Conceptualization, Methodology, Validation, Formal analysis, Investigation, Resources, Data Curation, Writing (original draft), Writing, Review and Editing, Visualization, Project administration, Funding acquisition **Oscar Laurent**: Conceptualization, Methodology, Validation, Resources, Writing-Review and Editing, Visualization, Project administration, Supervision, Funding acquisition **Gary Stevens**: Conceptualization, Validation, Writing-Review and Editing, Project administration, Supervision, Funding acquisition **Emilie Bruand**: Validation, Formal analysis, Resources, Writing-Review and Editing **Philippe de Parseval**: Resources, Data Curation, Writing-Review and Editing.

Geochemistry of igneous and detrital apatites from the Barberton Granitoid-Greenstone Terrane (South Africa) reveals granitoid diversity in the Paleoarchean felsic crust.

Combaz Jean-Baptiste[*,a,b], Laurent Oscar[b], Stevens Gary[a], Bruand Emilie[c], de Parseval Philippe[d]

[a]Department of Geology, University of Stellenbosch, Private Bag X1, Matieland 7602, South Africa
[b]Université de Toulouse, CNRS, Géosciences Environnement Toulouse, Toulouse, France
[c]Laboratoire Geo-Ocean, CNRS, Université de Bretagne Occidentale, France
[d]Centre de Microcaractérisation Raimond Castaing, Université de Toulouse, Toulouse, France

*Corresponding author: jean-baptiste.combaz@orange.fr; https://orcid.org/0009-0007-1021-4052

Abstract

Apatite halogen and trace elements contents have increasingly been calibrated to constrain parent magma identity in cases where the original context has been lost, such as detrital studies. We use these new calibrations to constrain the parent magma signatures of detrital apatites collected from Paleoarchean metasediments in the Barberton Greenstone Belt (BGB). In addition, we compare halogen and trace element compositions analyzed via EPMA and LA-ICP-MS in detrital apatites with magmatic apatites of the surrounding granitoid-gneisses of the TTG series to assess the temporal variation of sediment provenance in Archean time. Detrital apatites from the Hooggenoeg volcano-clastic sediments (DA of ~3.43 Ga, Upper Onverwacht Group) and Schapenburg meta-turbidites (DA of 3.25 Ga, Fig Tree Group) show halogen and trace element characteristics quite distinct from one another. Both retained a clear magmatic chemistry as they show strong fractionation of their REE spectra (La_N/Lu_N = 29.4 and 5.43 respectively) and a low Eu/Eu* (~ 0.5 and 0.8 respectively) but they share different provenance as their contrasted chemistry suggests. The Hooggenoeg apatites have strong REE fractionation (La_N/Lu_N ~30), have high amount of Sr (from 600 up to 1200ppm), are enriched in F (~2.2 wt%) and have high amounts of Cl (~ 0.4 wt%) while the Schapenburg apatites have lower fractionation of their REE spectra, have fairly uniform and low Sr content (~ 200 ppm), are much more enriched in F (~ 3.2 wt%), have lower amounts of Cl (~ 0.01 wt%). However, some of these characteristics do not match with apatites of the Barberton TTGs but rather overlap well with apatites crystallized in Mg-rich sanukitoids of the Neoarchean-Proterozoic transition and suggests that these were already present (and exposed to surface alteration) in the Paleoarchean felsic crust at the time the metasediments were deposited. The apatite proxies utilized in the present work strongly suggest that a more compositionally diverse felsic crust already existed in the environs of the BGB as early as 3.4 Ga, and that the onset of observed granitoid diversity in the Neoarchean is an artifact related to preservation bias. Reasons for the non-preservation of Paleoarchean sanukitoids in the rock record could be related to their emplacement at upper crustal level, making them more exposed to surface weathering than underlying, mid-crustal TTGs. Additionally, their formation during an epoch when there was intense crustal recycling in transient subduction zones and little to no continent-continent collisions (little "shielding") might have reduced their preservation potential. The appearance of compositionally diverse granitoids in the geological record at 3.0 Ga clearly coincides with the amalgamation and stabilization of the Kaapvaal Cratonic Lithosphere from different continental blocks which provided the necessary "shielding" that these compositionally diverse felsic rocks required to survive to our time.

3.1. Introduction

Accessing the Paleoarchean rock record is challenging due to generally poor preservation of the Earth's earliest felsic crust. For this reason, most of the geological inferences and interpretations about periods of the Earth's history for which little to no magmatic rock has survived derive from data obtained on a single detrital accessory mineral, zircon (Bell et al., 2015; Blichert-Toft & Albarède,

2008; Compston & Pidgeon, 1986; Drabon et al., 2022; Harrison, 2009; Kröner & Compston, 1988; Nutman & Hiess, 2009; Valley et al., 2005, 2015; Wilde et al., 2001; Zeh et al., 2013). Zircon is powerful in its capacity to retain reliable crystallization U-Pb ages and constrain the mantle extraction age and degree of hydration of its parent magma source, respectively through Lu-Hf isotopes (Fisher et al., 2011, 2014; Spencer et al., 2020) and O isotopes (Valley et al., 2005). However, zircon chemistry, in particular trace element composition, does not give the full picture on the nature of its parent rock. For example, although several studies acknowledged the peculiar trace element composition of early Earth zircons relative to those formed in most post-Archean settings (Carley et al., 2014; Laurent et al., 2022; Reimink et al., 2020), this signature fails to capture the actual compositional diversity of the different felsic magmas from which it crystallized (Roberts et al., 2024; Combaz et al., 2025). In addition to this, zircon mainly crystallizes in rocks of intermediate to acidic compositions (Hoskin & Schaltegger, 2003) and its REE composition is not so variable with changing parent magma composition (Grimes et al., 2007, 2015), so its ability to precisely track the existence of potentially more mafic rocks in the source area of clastic sediments is limited.

To circumvent those issues, an increasing number of studies have changed the focus towards other accessory minerals like apatite (Antoine et al., 2020; Belousova et al., 2002; Bruand et al., 2016, 2017, 2020; Chew & Spikings, 2021; Chu et al., 2009; Gillespie et al., 2018; Henrichs et al., 2019; Kieffer et al., 2023, 2024; Kirkland et al., 2017, 2018; Miyake et al., 2024; Nutman, 2007; G. O'Sullivan et al., 2020; Zeh, 2004). Apatite is indeed a much better candidate for constraining the composition of the source. Its halogen contents and trace element (including REE) patterns are much more sensitive to changes in magma composition than zircon's and vary systematically with parameters such as alumina saturation index (ASI) and silica content of the parent magma (Bruand et al., 2017; Chu et al., 2009; Loferski & Ayuso, 1995; London, 1997; Montel, 1986; P. Piccoli & Candela, 1994; P. M. Piccoli & Candela, 2002; Pichavant et al., 1992; Wolf & London, 1994, 1995). Furthermore, apatite is also a more ubiquitous mineral, i.e. it crystallizes in a compositionally more diverse set of rock, from ultramafic to acidic (Chakhmouradian et al., 2017; Chu et al., 2009; G. O'Sullivan et al., 2020; G. J. O'Sullivan et al., 2018). For these reasons, apatite chemistry has been the focus of a series of recent studies (Antoine

et al., 2020; Bruand et al., 2016, 2017, 2020; Combaz et al., 2025; Henrichs et al., 2019; Kieffer et al., 2023, 2024; G. O'Sullivan et al., 2020; G. J. O'Sullivan et al., 2018; Vezinet et al., 2025) which have established a series of discrimination diagrams based on halogen, trace and REE data that aim at identifying the sources and provenance of detrital apatite.

These geochemical proxies can become powerful tools in the case of Archean detrital apatites, for which relatively little has been published in terms of halogen, trace and REE data. It is generally assumed that Archean clastic meta-sediments are the products of weathering and erosion of the exposed greenstone sequences and surrounding TTG (Tonalite-Trondhjemite-Granodiorite) plutons (Anhaeusser, 1980, 1981; De Ronde & De Wit, 1994; Drabon et al., 2024), which compose around 80% of the Archean continental crust preserved today (Bleeker, 2003; Laurent et al., 2020, 2024; J.-F. Moyen & Martin, 2012; Polat, 2012). However, a growing number of studies show that this might have been different in the Archean, as remnants of non-TTG felsic crustal components, which might have been originally present but not preserved to the present day, are found as detrital zircon, clasts or volcanic units in the Archean supracrustal record (Sanchez-Garrido et al., 2011; Agangi et al., 2018; Drabon et al., 2024; Combaz et al., 2025…). In this context, apatite can fill some of the gaps and provide some chemical constraints on the sources of Archean meta-sediments and cross-check hypothesis derived from the zircon studies. (Bruand et al., 2020) have shown that TTG-hosted apatite has a specific trace element composition, which discriminates it from apatite from sanukitoids, a generally late-Archean suite of rocks considered to mark the transition towards modern-style plate tectonics (e.g., Laurent et al., 2014). Nevertheless, this first-order distinction is based on a limited set of samples and the data from Bruand et al. (2020) already suggest a potential diversity in apatite trace element compositions from TTG themselves, following the known diversity of bulk-rock trace element signatures of this rock series (Moyen, 2011). Therefore, the above-mentioned issues show that it is necessary to (1) better characterize the potential chemical diversity of apatite from Archean TTGs; and (2) obtain detrital apatite data from Archean supracrustal rocks to complement and evaluate the findings based on detrital zircon.

The Barberton Greenstone Belt (BGB) in South Africa and Eswatini, provides the right framework for this purpose, for three reasons. (1) It is a well-documented Archean terrane for which extensive work has been published on the geochemical, petrological, age and isotopic characteristics of the main rock components (greenstone and TTG granitoids-gneisses) and the associated stratigraphic and tectonic evolution (e.g. Anhaeusser, 1980, 1981; Anhaeusser & Kisters, 1995; De Ronde & De Wit, 1994; De Wit et al., 1987; Heubeck et al., 2022; Heubeck & Lowe, 1994; A. F. Kisters et al., 2010; A. F. M. Kisters et al., 2003; Kröner et al., 1996; Lana et al., 2010; Lowe, 1999; Lowe & Byerly, 2007; J.-F. Moyen et al., 2006, 2007a; Yearron et al., 2003). (2) The greenstone belt preserves voluminous sequences of clastic metasediments, of already well-constrained provenance and age of deposition from detrital zircon studies (Combaz et al., 2025; Drabon et al., 2022, 2024; H. Wang et al., 2022; Zeh et al., 2013), thus making these good targets for a detrital apatite study. (3) Some of these studies have shown that substantial preservation bias occurs in the BGB (Drabon et al., 2021, 2022, 2024; Sanchez-Garrido et al., 2011) and a significant fraction of the former Paleoarchean uppermost felsic crust might be missing from the exposed rock record because of erosion (Combaz et al. s. d.). That this must be so is also obvious from the ubiquitous regional metamorphic overprint, which demonstrate that the lowest grade rocks exposed represent material buried to depths equating with at least 3 kbars pressure at ca 3.2 Ga – a minimum of some 10km of Paleoarchean upper crust have been lost.

Following up on these studies, which have so far only investigated zircon, we have obtained here new halogen and trace element data of detrital apatite from samples of clastic sediments from different stratigraphic levels of the BGB; and igneous apatite from TTG granitoid-gneisses representative of the three main magmatic and felsic crust-forming events of this area (ca. 3.55-3.52, 3.47-3.42 and 3.29-3.21 Ga; e.g. Moyen et al., 2007). The comparison between the two detrital and igneous apatite datasets allows us to assess the relative importance between TTGs and potential other magmatic sources in the Archean Crust at the time of deposition of the meta-sediments. The results confirm, first, the strong sensitivity of apatite trace element composition on host rock/melt chemistry and its potential as a source rock indicator; and second, that the Paleoarchean felsic crust was composed of a more diverse range of granitoids than previously thought.

Naming convention

Throughout this manuscript, plutonic apatites from the Barberton TTGs will be referred to by the name of their host rock (i.e. apatites from the Kaap Valley tonalite will be called "Kaap Valley apatites", apatites from the Steyndorp "Steynsdorp apatites, etc…). Detrital apatites of the Hooggenoeg volcano-clastic sediments will be called "Hooggenoeg apatites" and those from the Fig Tree-aged Schapenburg Schist Belt will be called "Schapenburg apatites".

3.2. Geological Setting

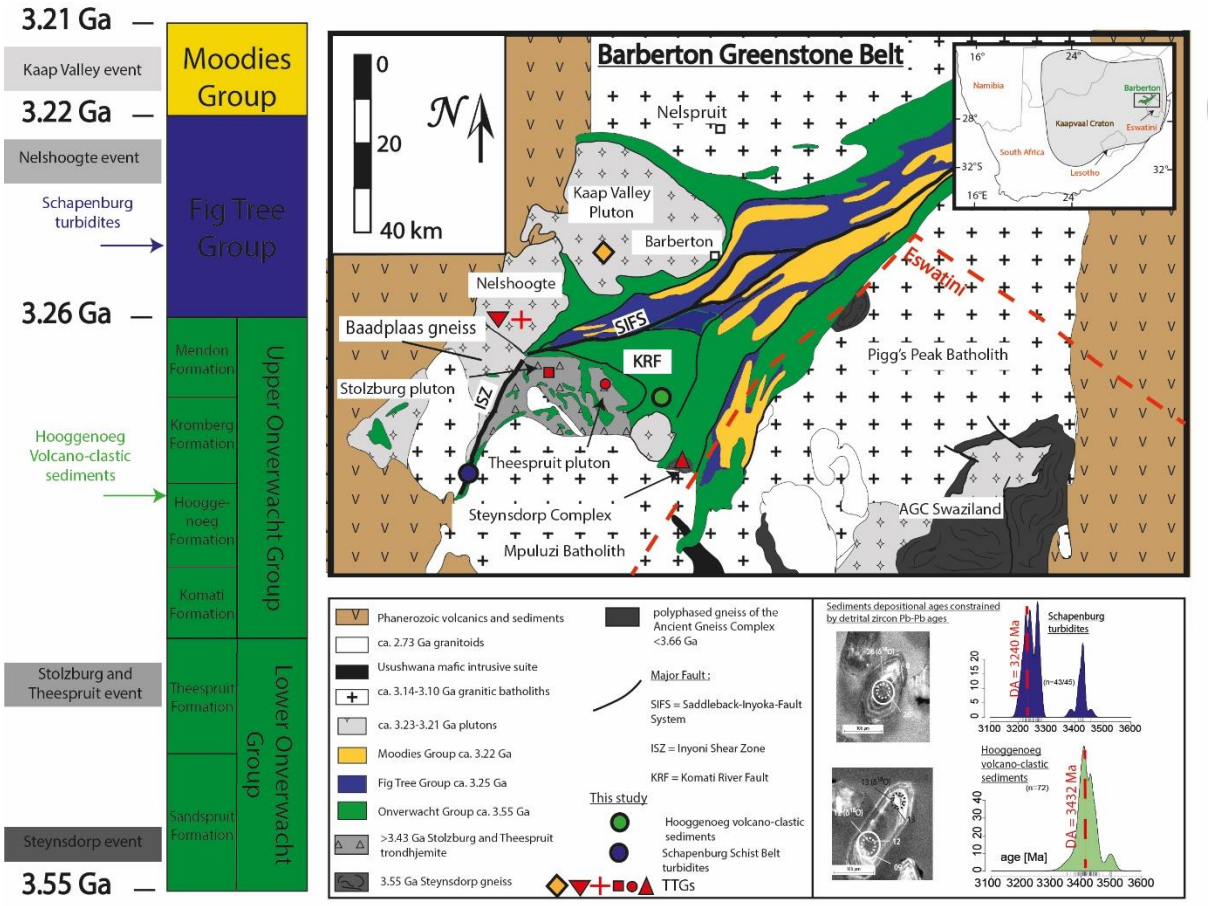

Figure 3-1 : Geological map and synthetic stratigraphic log of the Barberton Greenstone Belt, from Combaz et al. (2025) after Anhaeusser (1980, 1981) and Schoene et al. (2008). Sample localities are indicated as colored symbols.

The Barberton Greenstone Belt (BGB) is located at the suture zone between the Witwatersrand Block and Swaziland Block in the eastern Kaapvaal Craton, South Africa (Eglington & Armstrong, 2004). The Greenstone sequence is composed of three main stratigraphic groups with, from bottom to top : the Onverwacht Group which was deposited from 3.55 to 3.26 Ga (Viljoen and Viljoen., 1969, Anhaeusser, 1980, 1981; De Ronde & De Wit, 1994; De Wit et al., 1987; Kamo & Davis, 1994; Lowe, 1999; Lowe & Byerly, 2007) and mostly comprises rocks of mafic to ultramafic composition, with minor felsic volcanics and sediments (Diener et al., 2005; Dziggel et al., 2002, 2006; Kröner et al., 1996, 2016). The Onverwacht Group is then capped by the Fig Tree Group which contains a greater number of rocks of siliciclastic or felsic composition, commonly showing up as dacites or rhyo-dacites. This group was deposited from 3.26 to 3.23 Ga (Byerly et al., 1996; Decker et al., 2015; Drabon et al., 2019) and is overlain by the predominantly volcano-sedimentary group of the Moodies Group. This last supracrustal sequence was deposited from 3.22 to 3.21 Ga and largely corresponds to clastic sediments

of conglomerates and sandstones with intercalated volcanic tuffs (Heubeck et al., 2013; Heubeck, 2019; Heubeck et al., 2022; Heubeck & Lowe, 1994; van Rensburg et al., 2021). The BGB presumably marks the suture between two litho-tectonic blocks (referred to as Barberton Northern Terrane and Southern Terrane after (Zeh et al., 2009, 2013), corresponding to separate microcontinents or arcs that were accreted to the proto-Kaapvaal Craton at ca. 3.2 Ga during a main collision event (Lowe & Byerly, 2007; J.-F. Moyen et al., 2007; Stevens & Moyen, 2007). Remnants of this event are now preserved along the Saddleback-Inyoka-Fault-System(Dziggel et al., 2002; A. F. M. Kisters et al., 2003; J.-F. Moyen et al., 2006; Stevens & Moyen, 2007) (SIFS see **Figure 3-1**).

The terranes surrounding the BGB are largely made up of granitoid-gneisses of dominant TTG affinity, altogether forming the Barberton-Granitoids-Greenstone-Terrane (BGGT). The TTG granitoid-gneisses emplaced in three successive magmatic episodes that are briefly outlined below (see Moyen et al., 2007a for thorough review):

1) At 3.55-3.52 Ga, shallow melting of an enriched basaltic crust (Martin et al., 2014, Moyen et al., 2007a) produced the magmas which formed the Steynsdorp pluton, the oldest TTG gneiss of the BGB. This pluton mainly show a tonalitic/trondhjemitic composition and is often cross-cut by leucocratic dykes (Anhaeusser & Kisters, 1995; Guitreau et al., 2012; Lana et al., 2010).
2) At 3.47-3.42 Ga, the greenstone sequences of the Barberton Southern Terrane were intruded by leucocratic, high-Sr trondhjemites of the Stolzburg and Theespruit Plutons (Anhaeusser, 1980, 1981; Kröner et al., 1996, 2016; Laurent et al., 2020; Van Kranendonk et al., 2009).
3) At 3.29-3.21 Ga, during convergence and collision of the two terranes, the Barberton Northern Terrane was intruded by the composite Baadplaas gneiss (tonalite to trondhjemite in composition; A. F. Kisters et al., 2010; J.-F. Moyen et al., 2007a) and Nelshoogte trondhjemite (Matsumura, 2014) formed through the partial melting at deep levels of subducted enriched mafic crust (possibly the leading edge of a downgoing slab of the Southern Terrane). The end of TTG magmatism is marked by the emplacement at ca. 3.22 Ga of the least evolved Kaap Valley Tonalite (Robb et al., 1986), likely formed through high degrees of partial melting of a mafic protolith, and the Dalmein pluton (Kamo & Davis, 1994; J.-F. Moyen et al., 2007).

From 3.1 Ga, the BGGT is affected by potassic magmatism in the form of voluminous K_2O-rich Granodiorite-monzogranite-syenite granitoids (GMS suite) which emplace as sheet-like laccolith and terminates the stabilization of the eastern Kaapvaal Craton (Clemens et al., 2010; J. F. Moyen et al., 2021; Santos Leandro et al., s. d.).

3.3. Sampling and methods

3.3.1. Sampling strategy and sample description

We have investigated detrital apatite chemistry from two samples of clastic sediments already studied for detrital zircon U-Pb ages, trace elements Lu-Hf isotopes (Combaz et al. 2025). These are therefore already well-characterized in terms of depositional and source ages, and potential provenance. Moreover, the two samples were collected in distinct stratigraphic layers of the BGB. The first sample (H-01) was collected in the diamictites/volcano-clastic sediments of the Upper Onverwacht Group (H6 layer of the Hooggenoeg Formation; **Figure 3-1**). The second sample was collected in the Schapenburg Schist Belt, which is part of the Fig Tree Group (**Figure 3-1**), and corresponds to the meta-turbidite-greywackes (Anhaeusser, 1983; Stevens et al., 2002). More details about the sampling localities and petrography of the sedimentary samples are reported in Combaz et al. (2025).

To compare the detrital apatite record with the magmatic/plutonic record, we have investigated igneous apatite chemistry from TTG granitoid-gneiss samples of the BGGT. These were chosen as to be representative of the three main magmatic events identified on a regional scale, and include the ca. 3.55-3.52 Ga Steynsdorp tonalitic gneiss; the ca. 3.47-3.42 Ga Stolzburg and Theespruit trondhjemites; the ca. 3.25 Ga Nelshoogte trondhjemitic gneiss and the ca. 3.21 Ga Kaap Valley tonalite (**Figure 3-1**). The chosen samples were previously investigated by different authors for general petrographic, geochemical and/or geochronological studies, as summarized in **Table 3-1**. While apatite from most TTG samples were investigated directly in situ on thin sections available from these previous studies,

the Kaap Valley tonalite was sampled on our own and apatites were separated following the same procedure as for the detrital populations.

Sample name	Stratigraphic position	Location	Lithology	Latitude	Longitude	Detrital vs plutonic	Age (Ma)	Authors
H-01	Onverwacht Group, H6 layer	Eastern limb of the Onverwacht Anticline	Polymictitic diamictite	-26.024619	30.988467	Detrital	3430±16[a]; 3432±5[b]	This study
SSB-02	Fig Tree Group	Schapenburg Schist Belt	Amphibolitized, cross-bedded turbidites	-26.18109	30.54041	Detrital	3233±17[a];3240±5[c]	This study
KVT-1	plutonic rock	North-West of Barberton town	Bt-bearing tonalite	-25.712016	31.16085	Plutonic	3211±94[d]; 3229±5[e]; 3223±4[f]; 3226±5[f]; 3226±14[g]	This study
NLS	plutonic rock	East of Emanzana	Trondhjemite	-25.867417	30.659683	Plutonic	3236±1[h]; 3212±2[i]; 3215±15[j]	Sanchez-Garrido. 2012 (PhD thesis)
JB-17-C6	plutonic rock	East of Emahlalehni	Trondhjemite	-26.00833	30.73317	Plutonic	3445±3[l]: 3431±11[m]; 3460±5[n]; 3456±10[o]	Laurent et al. 2020
JB-17-C1	plutonic rock	East of Emahlalehni	Trondhjemite	-26.05583	30.85083	Plutonic	3443±4[n]; 3440±5[l]; 3437±6[l]; 3460±8[o]	Laurent et al. 2020
STEY1.5-8	plutonic rock	Border between SA and Swaziland	Tonalitic-trondhjemitic gneiss	-26.15425	30.9611667	Plutonic	>3540±3[k]; 3553±4[k]	Sanchez-Garrido. 2012 (PhD thesis)
STEY1.7-8	plutonic rock	Border between SA and Swaziland	Tonalitic-trondhjemitic gneiss	-26.152967	30.9687167	Plutonic	>3540±3[k]; 3553±4[k]	Sanchez-Garrido. 2012 (PhD thesis)

[a] = U-Pb on zircon through LA-ICP-MS (Combaz et al., s.d.)
[b] = U-Pb on zircon through LA-ICP-MS (Grosch et al., 2011)
[c] = U-Th-Pb on zircon through SHRIMP (Stevens et al. 2002)
[d] = Whole-rock U-Pb dating (Robb et al. 1986)
[e] = U-Pb in zircon through SHRIMP (Tegtmeyer and Kröner. 1987)
[f] = U-Pb in zircon through TIMS (Kamo and Davies. 1994)
[g] = U-Pb in zircon through SIMS (Armstrong et al. 1990)
[h] = U-Pb in zircon through TIMs (de Ronde and Kamo. 2000)
[i] = U-Pb in zircon (York et al. 1989)
[j] = U-Pb in zircon through TIMS (Matsumura. 2014)
[k] = U-Pb in zircons through SHRIMP-I (Kröner et al. 1996)
[l] = U-Pb in zircons through SHRIMP-I (Kröner et al. 1991)
[m] = U-Pb in zircon through conventional dating (Dziggel et al. 2002)
[n] = U-Pb in zircon through TIMS (Kamo and Davies. 1994)
[o] = U-Pb in zircon through LA-ICP-MS (Laurent et al. 2020)

Table 3-1 : Summary of samples collected, stratigraphic position, location, lithology, GPS coordinates, and relevant geochronological data.

3.3.2. Mineral separation and concentration

For the two sedimentary samples and the Kaap Valley tonalite, apatites were extracted from crushed samples using conventional mineral separation techniques, handpicked, set in 1-inch epoxy mounts and polished. More details of the mineral separation techniques used are provided in Combaz et al. 2025. Other apatites were investigated directly on thin sections.

3.3.3. Scanning electron microscopy (SEM)

The internal structures of the apatite grains were characterized by cathodoluminescence (CL), using the Vega4 (Tescan) scanning electron microscope (SEM) equipped with a multispectral CL detector at Géosciences Environnement Toulouse, France. Instrumental conditions were an acceleration voltage of 10 kV and beam current of 3 nA. Image resolution was set to 768 × 768 pixels with a sweep time of ca. 2 min, corresponding to ca. 0.2 ms per pixel.

3.3.4. Electron Probe Micro-analysis (EPMA)

Analysis of major and minor elements in apatite, including halogens (F, Cl) and S, were performed using an electron microprobe at the Centre de Microcaractérisation Raimond Castaing (Université Paul Sabatier – Toulouse III) with a Cameca SXFive. Operating conditions were 15kV beam conditions with 20 nA beam current and sample volume is less than 5 μm^3. Samples were carbon coated (~50nm) using a Leica EM ACE600 coater. Details on the detectors, used standards, data validation techniques and quality controls are provided in **Supplementary material to Chapter 3**.

3.3.5. LA-ICP-MS

Apatite minor and trace (including REE) analyses were conducted by laser ablation – inductively coupled plasma – mass spectrometry (LA-ICP-MS) at the Service ICP-MS of Observatoire Midi-Pyrénées (OMP-UAR831) in Toulouse, France. The analyses were carried using a NWRfemto (Elemental Scientific Instruments) solid-state femtosecond laser ablation system set to UV mode (257 nm wavelength) coupled with an Element XR (ThermoScientific) sector-field ICP-MS. The laser was operated with a spot diameter of 35 µm, a repetition rate of 4 to 6 Hz and an energy density of ca. 2 J cm^{-2}. The ablated aerosol was transported to the ICP-MS by He carrier gas (ca. 0.7 L/min) to which was admixed Ar make-up gas (ca. 0.8 L/min) downstream of the ablation cell. A typical run consisted of 15 seconds of background signal acquisition, followed by 25 seconds of ablation and 10 seconds of

washout. The list of acquired masses, corresponding dwell times, details about the instrument optimization and data acquisition procedures are provided in the **Supplementary material to Chapter 3**. The data were processed offline with the Iolite v4 software. Trace elements were quantified using the NIST SRM610 glass reference material (Jochum et al., 2011) as external standard, using conventional standard-sample bracketing for instrumental drift correction. Apatite stoichiometric Ca content (39 wt.%) was used as internal standard for relative sensitivity correction. Accuracy and reproducibility were evaluated through repeated analysis of natural apatite reference materials Madagascar and Durango (using reference values from GeoReM website). The results show that the total external reproducibility of the method is in the order of 10 to 20% relative for all elements and that the data are accurate within this range. Data from unknowns and reference materials are reported in **Supplementary material to Chapter 3**.

3.4. Results

3.4.1. Apatite petrography in TTGs

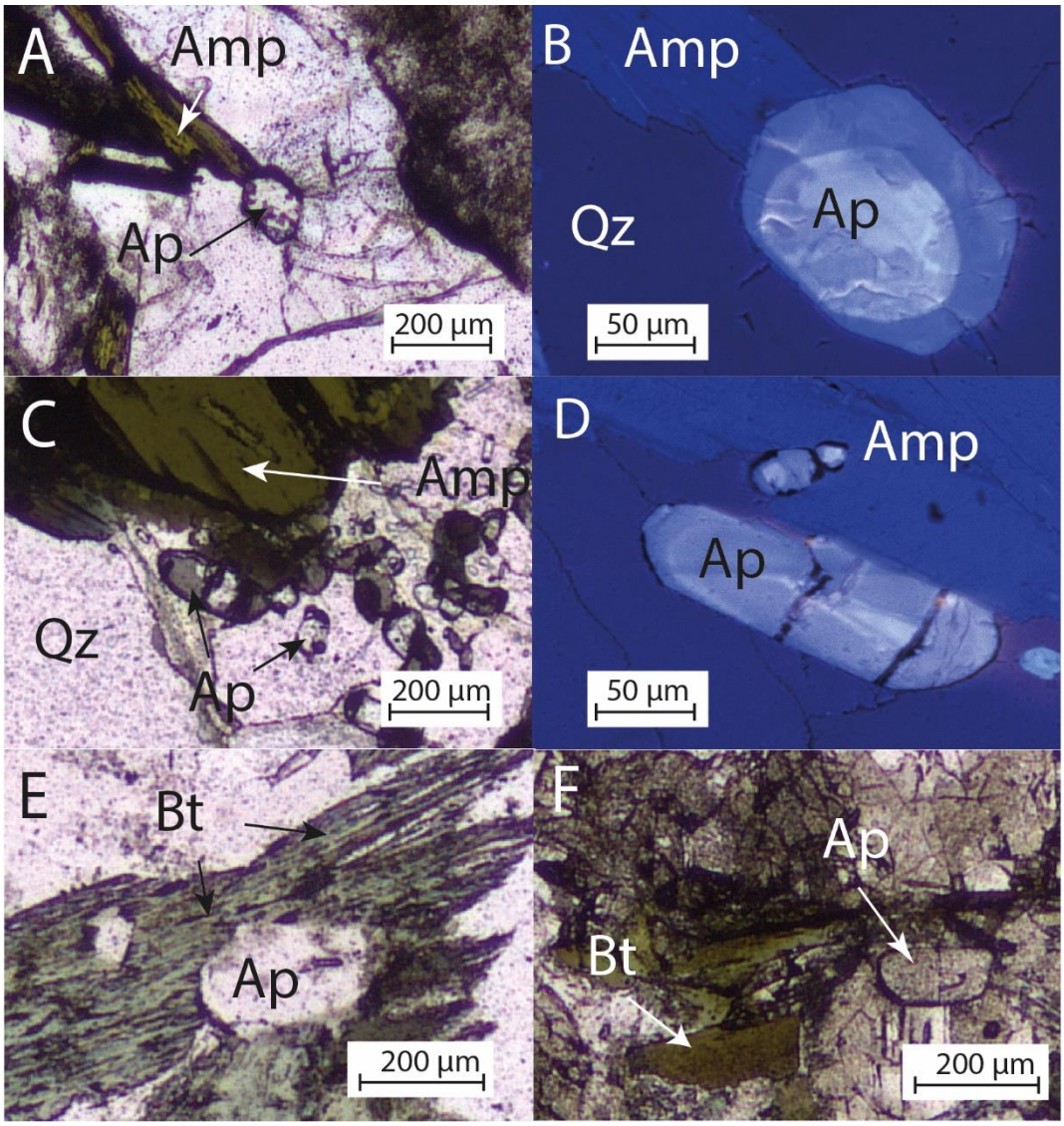

Figure 3-2 : Petrography of Barberton TTG apatites in plane-polarized photomicrographs. Image A corresponds to Theespruit pluton. Image B to Stolzburg pluton. Image C to Nelshoogte pluton. Image D to Steynsdorp pluton.

Apatites in TTGs are closely associated with biotite and /or amphiboles in thin sections of all Barberton trondhjemites collected in this study (see **Figure 3-2**). They show up as interstitial phases between plagioclase and quartz and are subhedral to euhedral in shape and commonly range in size from 50 to 150 µm (see **Figure 3-2**). Under CL images, they display the characteristic oscillatory zoning and little to no inclusions of secondary phases like xenotime or monazite.

3.4.2. Apatite internal structures

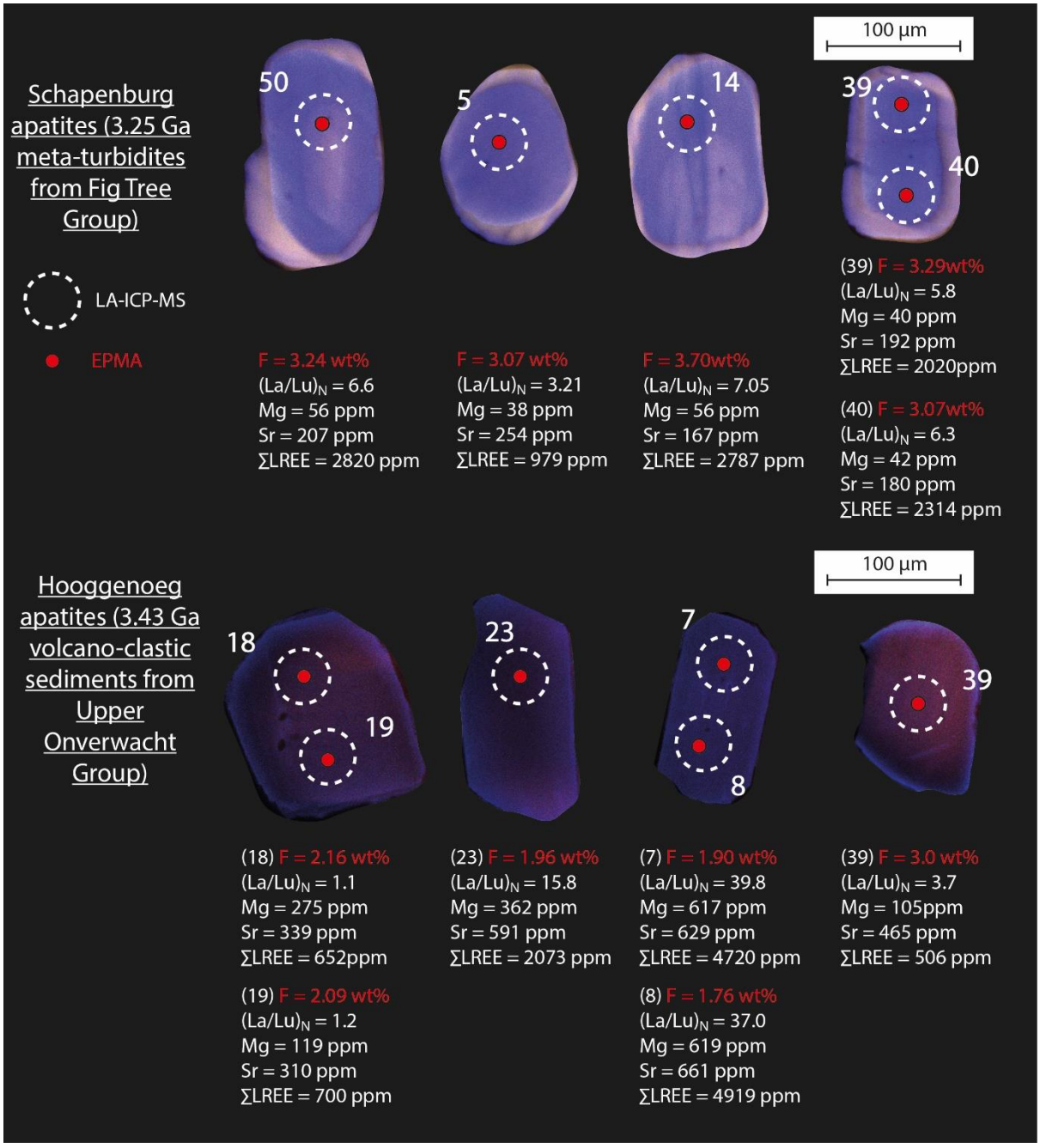

Figure 3-3 : Representative Cathodoluminescence images of apatites from the investigated samples showing the position of EPMA and LA-ICP-MS spots and relevant geochemical data (part1).

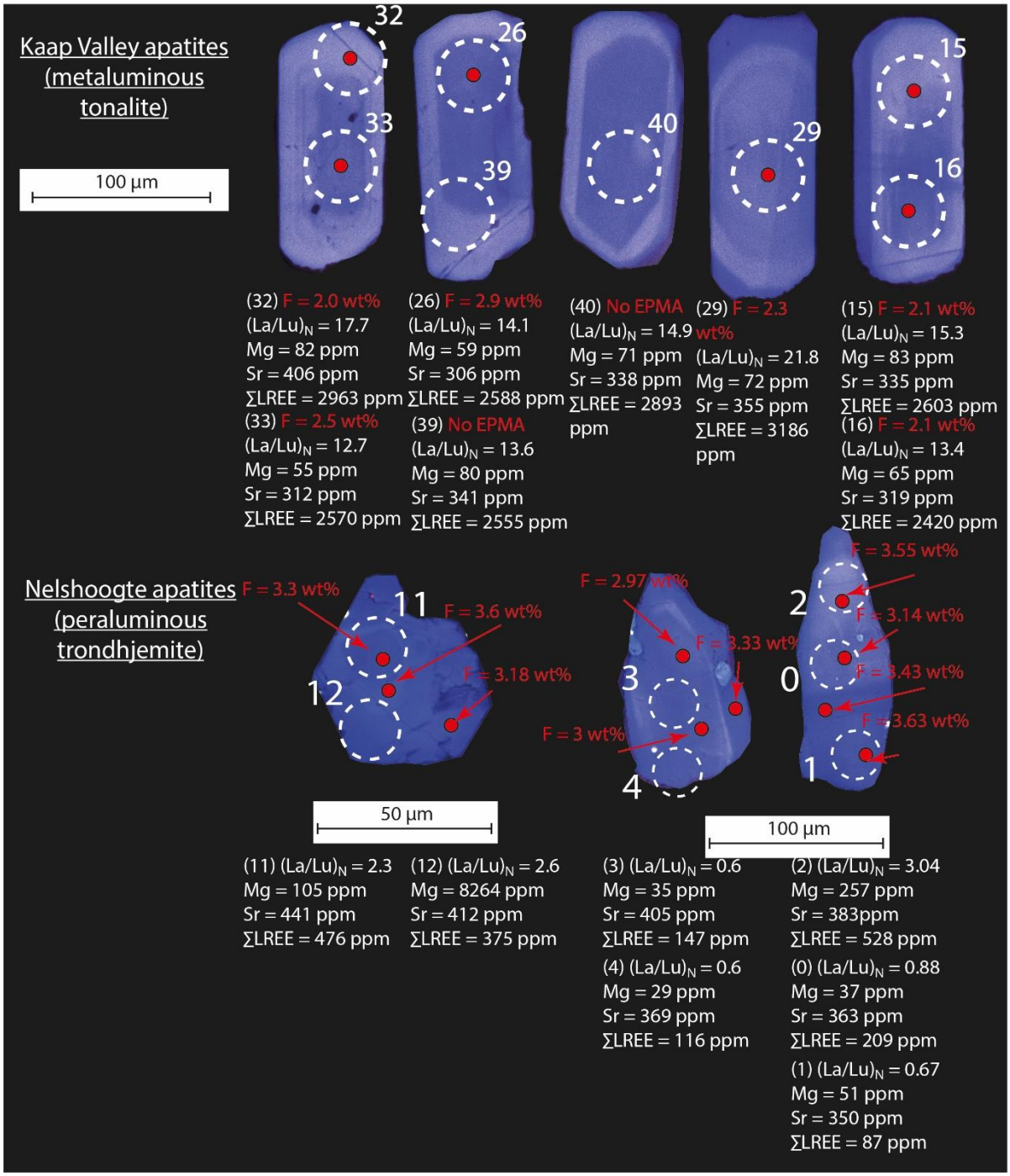
Kaap Valley apatites (metaluminous tonalite)
100 µm
32
33
26
39
40
29
15
16
(32) F = 2.0 wt%
(La/Lu)N = 17.7
Mg = 82 ppm
Sr = 406 ppm
∑LREE = 2963 ppm
(33) F = 2.5 wt%
(La/Lu)N = 12.7
Mg = 55 ppm
Sr = 312 ppm
∑LREE = 2570 ppm
(26) F = 2.9 wt%
(La/Lu)N = 14.1
Mg = 59 ppm
Sr = 306 ppm
∑LREE = 2588 ppm
(39) No EPMA
(La/Lu)N = 13.6
Mg = 80 ppm
Sr = 341 ppm
∑LREE = 2555 ppm
(40) No EPMA
(La/Lu)N = 14.9
Mg = 71 ppm
Sr = 338 ppm
∑LREE = 2893 ppm
(29) F = 2.3 wt%
(La/Lu)N = 21.8
Mg = 72 ppm
Sr = 355 ppm
∑LREE = 3186 ppm
(15) F = 2.1 wt%
(La/Lu)N = 15.3
Mg = 83 ppm
Sr = 335 ppm
∑LREE = 2603 ppm
(16) F = 2.1 wt%
(La/Lu)N = 13.4
Mg = 65 ppm
Sr = 319 ppm
∑LREE = 2420 ppm
Nelshoogte apatites (peraluminous trondhjemite)
F = 3.3 wt%
11
F = 3.6 wt%
12
F = 3.18 wt%
50 µm
F = 2.97 wt%
F = 3.33 wt%
3
F = 3 wt%
4
2
F = 3.55 wt%
F = 3.14 wt%
0
F = 3.43 wt%
F = 3.63 wt%
1
100 µm
(11) (La/Lu)N = 2.3
Mg = 105 ppm
Sr = 441 ppm
∑LREE = 476 ppm
(12) (La/Lu)N = 2.6
Mg = 8264 ppm
Sr = 412 ppm
∑LREE = 375 ppm
(3) (La/Lu)N = 0.6
Mg = 35 ppm
Sr = 405 ppm
∑LREE = 147 ppm
(4) (La/Lu)N = 0.6
Mg = 29 ppm
Sr = 369 ppm
∑LREE = 116 ppm
(2) (La/Lu)N = 3.04
Mg = 257 ppm
Sr = 383ppm
∑LREE = 528 ppm
(0) (La/Lu)N = 0.88
Mg = 37 ppm
Sr = 363 ppm
∑LREE = 209 ppm
(1) (La/Lu)N = 0.67
Mg = 51 ppm
Sr = 350 ppm
∑LREE = 87 ppm

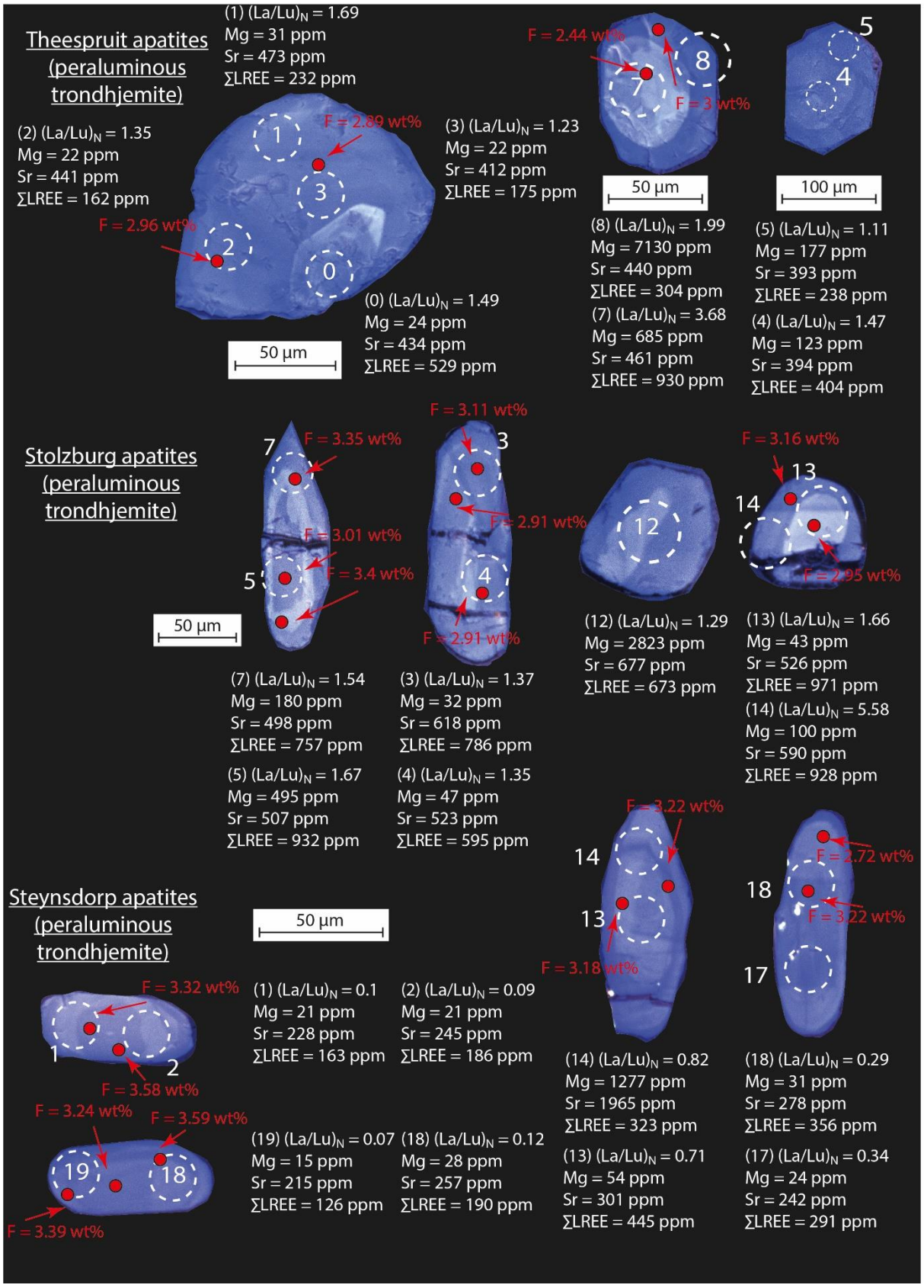

Hooggenoeg detrital apatites do not show any chemical zoning under CL images and appear to be quite homogeneous and dark (**Figure 3-3**). Many show the diagnostic hexagonal shape. Schapenburg

detrital apatites on the other hand, show clear chemical zoning in CL images and generally exhibit higher luminescence than Hooggenoeg apatites. Their crystal terminations are rounded but the diagnostic hexagonal shape is still visible. The BTTG apatites are also quite luminescent and display the diagnostic core vs rim zoning under CL images (**Figure 3-3**). Many grains preserved a clear hexagonal shape, particularly visible in the Kaap Valley apatites (**Figure 3-3**). Apatites of the Stolzburg trondhjemite and the Nelshoogte trondhjemite are also a little more fractured compared to apatites of the other plutons but laser spots were placed away from cracks in every case. Lastly, the Steynsdorp apatites are also quite zoned but display smaller sizes relative to the other plutons. The Theespruit pluton produced apatites that are generally small (~ 50 µm see **Figure 3-3**) except for one grain (spots 0-1-2-3 see Figure 3) which shows a diameter of around 150 µm and a beautiful core-to-rim zoning. At first glance, apatites showing the highest core vs rim brightness contrast seem to be often associated with hydrous minerals like amphibole or biotite except for this big apatites of the Theespruit pluton which is surrounded by quartz and Feldspar (see **Figure 3-3**) so there seem to be little correlation between these two observations.

3.4.3. Halogen chemistry

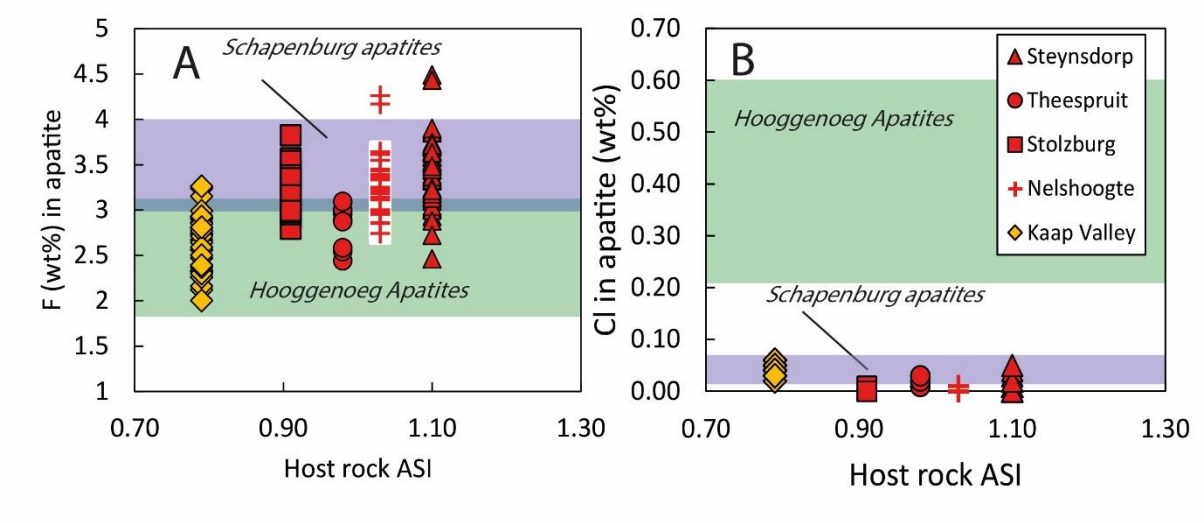

Figure 3-4 : F and Cl content in apatites of the BTTGs as a function of Aluminum Saturation Index (ASI). ASI of the BTTGs has been taken from data from Moyen and Stevens., 2007 and Yearron., 2003. Range of Cl and F of Hooggenoeg and Schapenburg apatites is indicated as colored rectangles for comparison.

3.4.3.1. Detrital apatite

Average F and Cl content in the Hooggenoeg apatites are 2.93 wt% and 0.38 wt% respectively (see **Figure 3-4 A-B**). In the Schapenburg apatites, the F content is higher with mean F ~3.25 wt% but the Cl content is lower with mean Cl~ 0.01 wt%, close to that of the BTTG apatites (see section below). Little intra-grain chemical variation is observed in either populations as F content remains remarkably constant. For example, spots 18 and 19 of the same grain in the Hooggenoeg population changes from 2.09 to 2.16 wt% (see **Figure 3-3**). The same is observed in the Schapenburg apatites where, for example F changes from 3.07 to 3.29 wt % within the same growth zone targeted with EPMA (spots 18 and 19, **Figure 3-3**). Sulfur in apatite occurs in exceedingly low amounts, quite below the detection limit of the EPMA even though the content changes a lot depending on the apatite investigated. The Hooggenoeg apatites have mean SO_3 content of 0.032 wt% while the Schapenburg apatites have mean SO_3 content of 0.016 so two times lower than Hooggenoeg's.

3.4.3.2. Igneous apatite

In the BTTGs, the apatite halogen content is more contrasted. The Kaap Valley apatites show mean F and Cl content of 2.63 and 0.04 quite close to values exhibited by the Theespruit apatites (mean F ~ 2.79 wt% and mean Cl ~ 0.02 wt%). The Steynsdorp apatites on the other hand, have F and Cl content of 3.44 wt% and 0.007 wt% respectively, similar within uncertainty to apatites of the Nelshoogte (mean F ~ 3.3 wt% and mean Cl ~ 0.002 wt%) and Stolzburg trondhjemites (mean F ~ 3.21 wt% and mean Cl ~ 0.003 wt%). Changes in F content within the same grain seem to be more acute than the detrital apatites. There seems to be an increase in F content towards toward the rim of the apatites for all samples of the BTTGs (in Theespruit apatites, F increases from 2.5 to 3 wt% from core to rim while in Stolzburg it changes from 3.01 to 3.35 wt% see grains in **Figure 3-3**). In the case of the Barberton TTG apatites, we notice the same contrast between the different plutons. The Kaap Valley apatites have a mean SO_3 of 0.121 wt% close to the mean values displayed by the Stolzburg apatites (0.097 wt%). However, the Steynsdorp and Theespruit apatites have similar mean SO_3 content of 0.02 wt%. Lastly, the Nelshoogte apatites exhibit mean SO_3 content of 0.072 wt%.

3.4.4. Trace element chemistry

Trace element analysis were acquired through LA-ICP-MS as explained in previous section. Concerning the detrital populations of Hooggenoeg Formation and Schapenburg Schist Belt, we targeted one spot per grains when these were small and two when the apatites were bigger (a few examples of these are shown on **Figure 3-3**). In the case of the BTTG apatites, the Steynsdorp, Stolzburg, Theespruit and Nelshoogte apatites were analyzed from thin sections studied during PhD thesis of (Sanchez-Garrido, 2012). This limited the number of grains of a size sufficient to accommodate two or three spots (see **Figure 3-3**). Also, another difficulty lies in the small thickness of the thin section, leading to many grains being drilled through and yielding aberrant data. These spots have been removed from the graphs shown in this study but are provided in **Supplementary material to Chapter 3.** Only

apatites from the Kaap Valley tonalite were separated following the same procedure as for the Hooggenoeg and Schapenburg apatites as explained in "Samples and method" section.

3.4.4.1. Igneous apatite

Apatites of the Barberton TTGs were analyzed at several locations as outlined in **Figure 3-3**. Clear core-to-rim zoning could be observed under CL images so we ensured to extract trace element data from both core and rims whenever the grain size allowed it. However, due to the low number of apatites cropping out of the thin sections of the Nelshoogte trondhjemite, and the fact that many were drilled through during laser ablation, we were unable to produce reliable data from core and rim of the same grain for this sample. Therefore, the Nelshoogte apatites only produced three reliable spots belonging to different grains (shown in **Figure 3-3**).

The Kaap Valley apatites are, without doubt, the one that gave out the highest rate of success for assessing the core-to-rim variations of chemical information. As outlined in **Figure 3-3**, the core-to-rim zoning observed under CL images correlates with changing trace element chemistry. We observed an increase in Mg concentrations from core to rim where core concentration is around 50 ppm and rim concentration is more around 80-90 ppm (see spots **KVT-33(core)** vs **KVT-32(rim)** and KVT-16(core) vs KVT-15(rim) in **Figure 3-3** and **supplementary material 6.2**). The same pattern is observed in apatites of the Stolzburg trondhjemite (see spots **JB-17-C6-13 (core)** vs **JB-17-C6-14 (rim)** in Figure 3) and in the Steynsdorp (see spots **STEY-1.7-17 (core)** vs **STEY-1.7-18 (rim)** in **Figure 3-3**). However, Sr concentration and LREE seem to remain quite uniform (around 300 to 400 ppm and 2500 ppm respectively) throughout a single grain (see **Figure 3-3**) suggesting that the chemical variations limit itself to Mg.

Y, for example, seems to be quite uniform from core to rim as little chemical changes were observed across single apatite grains for all the samples. Y is notably more enriched in apatites of the Steynsdorp (mean Y ~ 1600 ppm) and in the Stolzburg (mean Y ~ 500 ppm) compared with apatites of the Nelshoogte, Theespruit and Kaap Valley (mean Y ~ 200 ppm). Eu/Eu* is constrained to values between 0.5 (Kaap Valley tonalite) to 0.95 (Theespruit trondhjemite) (see **Figure 3-5 B**). The Kaap

Valley apatites have a strongly fractionated REE pattern with mean $(La/Lu)_N$ of 16.8 (see **Figure 3-6**) translating into LREE content that is significantly higher than of apatites of the more evolved trondhjemites of Stolzburg, Theespruit, Nelshoogte and Steynsdorp plutons. Indeed, apatites from these plutons have low amounts of LREE compared with HREE ($(La/Lu)_N$ goes from 0.42 in Steynsdorp apatites to 2.27 in Stolzburg apatites) and also have lower amounts of Nd (below 500 ppm see **Figure 3-5 B**).

Finally, there is some cross-sample variability in Sr content recorded by apatites of the BTTGs at similar values of Pb+Th+U. For example, while the Kaap Valley, Nelshoogte, Theespruit and Steynsdorp samples produced apatites with Sr content around 300 ppm (see **Figure 3-5 C**), the Stolzburg trondhjemites produced apatites containing Sr at much higher amounts (~ 600 ppm see Figure 6B) overlapping with apatites of the Hooggenoeg volcano-clastic sediments.

3.4.4.2. Detrital apatite

The Hooggenoeg apatites display strong fractionation of their REE pattern (see **Figure 3-6 A**) with average $(La/Lu)_N$ of 29.4. 83% have Eu/Eu* below 0.5 and 17% have it weak or close to 1. They have high La/Sm ratio (see **Figure 3-5 A**) and Th/U which overlap well with apatites of the Schapenburg schist belt. The latter on the other hand, have a weaker REE fractionation (mean La/Lu_N of 5.43 and see **Figure 3-6 B**) and show lower Nd content than the Hooggenoeg apatites (below 800 ppm vs above 800 ppm respectively, see **Figure 3-5 B**). The Schapenburg apatites have an Eu/Eu* between 0.5 to 1.5 but with the bulk of the data between 0.5 and 1. Finally, both detrital populations of apatite show contrasting Sr content at similar Pb+Th+U. In fact, as outlined in **Figure 3-5 C**, the Hooggenoeg apatites have Sr content mainly from 500 to 900 ppm with one subgroup going up to 1200 ppm, a pattern that we do not see in the Schapenburg apatites where most grains are consistently around 200 ppm. Little intra-grain chemical variations were observed in either population as illustrated on **Figure 3-3**. As an example, spots H-01-7 and H-01-8 (see position of the spots in **Figure 3-3** and data in the **supplementary material to chapter 3**) which were analyzed from the same grain, gave similar F content (1.9 vs 1.76 wt%), $(La/Lu)_N$ (39.8 vs 37), Mg content (617 vs 619 ppm), Sr content (629 vs 661 ppm) and sum of

LREE (4720 vs 4919 ppm). The same can be said of the Schapenburg apatites where, for example, spots SSB-02-39 and SSB-02-40, analyzed from the same grain, gave similar F content (3.29 vs 3.07 wt%), $(La/Lu)_N$ (5.8 vs 6.3), Mg content (40 vs 42 ppm), Sr content (192 vs 180 ppm) and sum of LREE (2020 vs 2314 ppm). Therefore, both samples seem to contain apatites with strong intra-grain homogeneity.

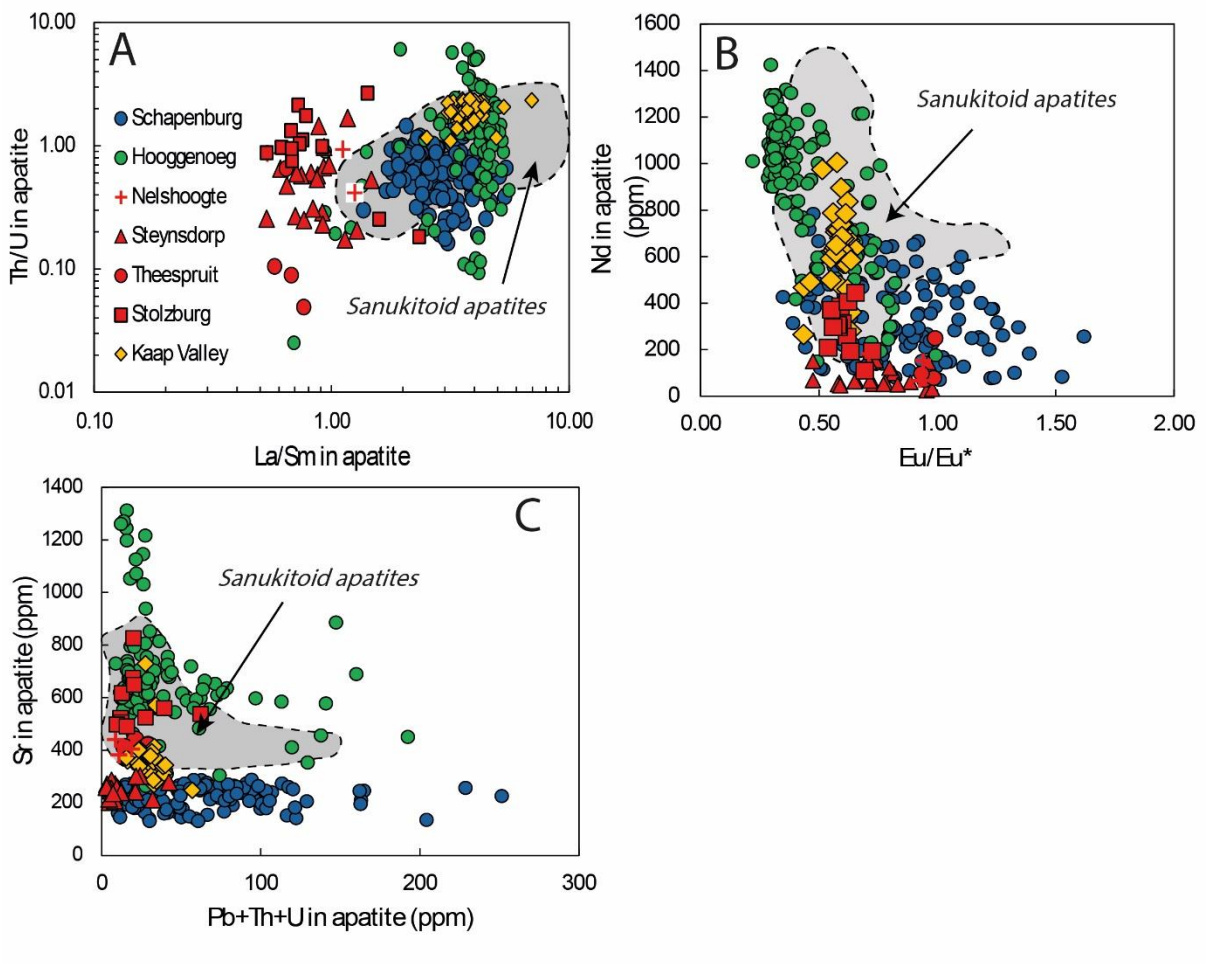

Figure 3-5 : Trace element chemistry of apatites from the Barberton Greenstone Belt. Grey field in the background corresponds to apatite data from sanukitoids from Bruand et al. 2020.

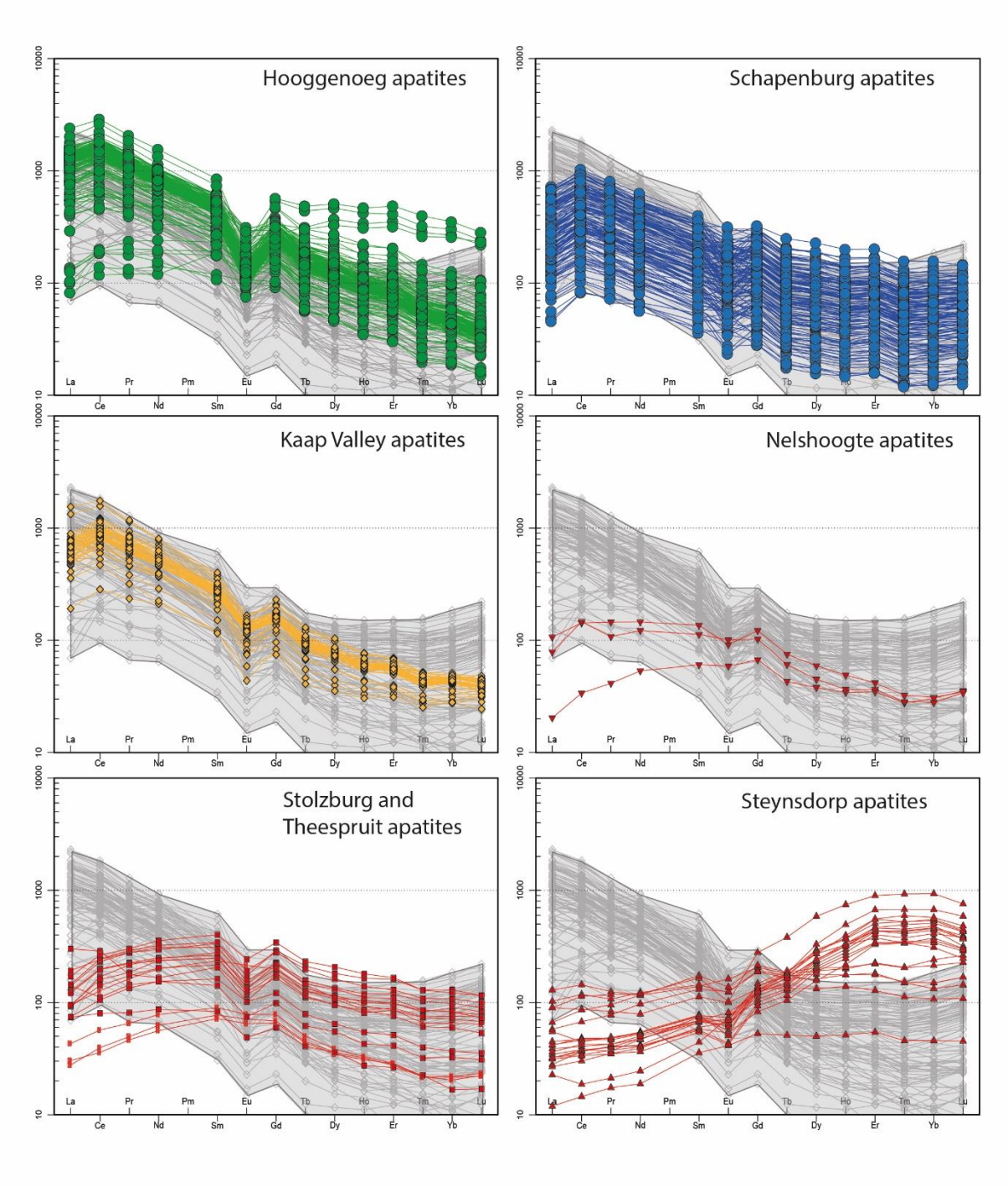

Figure 3-6: REE diagrams normalized to Primitive Mantle Composition of Sun and McDonough. 1995 for all apatites investigated in this study. Grey field and data plotted in the background correspond to apatite REE data from sanukitoïds of Bruand et al. 2020.

3.5. Discussion

3.5.1. Preservation of magmatic compositions in apatite

A beam of arguments points towards Hooggenoeg and Schapenburg apatites to be of magmatic origin. First, they display high F content (>2.2 wt% for the Hooggenoeg and >3.2 wt% for the Schapenburg apatites see **Figure 3-4**), low Cl content (~0.38 wt % for the Hooggenoeg and ~0.01 wt% for the Schapenburg apatites) and do not contain any secondary inclusions of monazite or xenotime visible under CL images, all suggesting that there has been little alteration of their halogen chemistry (Harlov, 2015; Harlov et al., 2005). Both apatite populations show a strongly fractionated REE spectra which, again, is a strong sign of their magmatic origin (Henrichs et al., 2019; G. O'Sullivan et al., 2020; G. J. O'Sullivan et al., 2018). Hooggenoeg and Schapenburg apatites also show systematically low Eu/Eu* (see **Figure 3-5 B**), a parameter that would be much more variable in case these apatites had suffered from fluid-aided dissolution-reprecipitation (Antoine et al., 2020; Bruand et al., 2016, 2017; Harlov, 2015; G. O'Sullivan et al., 2020). Also, low-grade metamorphic and metasomatic apatites generally show really high amounts of Sr (>1500 ppm for low-grade metapelites, see database of Henrichs et al., 2019) a pattern that we do not see in either detrital populations for Hooggenoeg apatites have Sr content lower than 1200 ppm and Schapenburg apatites have Sr content consistently around 200 ppm (**Figure 3-5 C**).

Also we argue that these grains are not from metamorphic origin since their enrichment in LREE and high Th/U ratio also suggests that they crystallized in the absence of any other REE-bearing phase such as monazite (Nutman, 2007). All these arguments suggest that Hooggenoeg and Schapenburg detrital apatites preserved their magmatic chemistry and that little to no fluid alteration or high-grade metamorphism has affected these grains.

While their occurrence within a magmatic fabric is a strong sign of their igneous origin, BTTG apatites could have been affected by various post-crystallization processes. Indeed, the Steynsdorp apatites for example, have remarkably low LREE content (**Figure 3-8 B**), plotting in the "Low-grade metamorphic and metasomatic field" of (G. O'Sullivan et al., 2020) so one could argue that they must have been affected by various forms of fluid-aided dissolution-reprecipitation processes. However, their

high F and low Cl content (>2.5 wt% and < 0.01wt% respectively) combined with their strongly fractionated REE spectra (**Figure 3-6**) and a remarkably low Sr content (mostly below 600 ppm for all the BTTGs) strongly suggests that they retained a magmatic chemical signature through the ages. In addition to this, most show strong negative Eu anomaly (see **Figure 3-6** and **3-5 B**), a feature that would be much more variable in case these samples had been affected by fluid-aided dissolution-reprecipitation (Kieffer et al., 2024; G. O'Sullivan et al., 2020). Finally, the diagnostic zoning observed in every TTG apatite investigated in this study suggests retention of magmatic signature.

3.5.2. Igneous apatite: meaning of the TTG apatite signature

The trace element chemistry of igneous apatite is greatly influenced by whole-rock parameters such as the SiO_2 content, the ASI, the oxygen fugacity and total alkalis as demonstrated by previous work (Belousova et al., 2001, 2002; Bruand et al., 2016, 2017; Chu et al., 2009; Henrichs et al., 2019; Kieffer et al., 2023, 2024; Montel, 1986; G. O'Sullivan et al., 2020; P. Piccoli & Candela, 1994; P. M. Piccoli & Candela, 2002; Pichavant et al., 1992; Wolf & London, 1994, 1995). Study of (Bruand et al., 2016) has documented the negative correlation between Sr in apatite and the degree of melt evolution (i.e. SiO_2 content) for various granitoids. At high degrees of differentiation, most of the Sr in the melt would be partitioned into plagioclase, leaving little available to late-crystallizing apatite. Following this relationship, a highly evolved felsic rock having 75% of SiO_2 should produce apatites with less than 100 ppm of Sr. This is not observed in our dataset (**Figure 3-7, A-B**) where apatites crystallized in the Stolzburg pluton (trondhjemite with 73.41 wt% of SiO_2, see whole-rock data from Laurent et al., 2020; J.-F. Moyen et al., 2007; Yearron et al., 2003) show Sr content between 500 to 700 ppm (with one outlier at 827 ppm!). This could be explained by the exceptionally Sr-rich nature of the Stolzburg trondhjemite (Sr content of 586 ppm, see J.-F. Moyen et al., 2007) allowing for both plagioclase and apatite to inherit a Sr-rich composition. However, we discard this possibility since many granite and granodiorite samples compiled by (Bruand et al., 2016) also have whole-rock Sr content above 500 ppm (some going up to 1000 ppm) and yet the correlation Sr-in apatite vs Sr whole-rock still holds. Another possibility would be that apatite crystallized earlier than plagioclase in the magmatic history of the pluton and therefore recorded a Sr-rich composition. Since apatite is an accessory phase in TTGs, its

early crystallization would not greatly affect the whole-rock Sr content, leaving still plenty for plagioclase afterwards. However, in this case, the negative Eu anomaly that one observes in the apatite REE spectrum (see section above, **Figure 3-6**) would not be the product of plagioclase fractionation sucking up most Eu^{2+} but would rather reflect some reduction process turning Eu^{3+} into Eu^{2+} (Yakymchuk et al., 2023) and becoming incompatible with apatite crystal lattice. However, this does not fit the interstitial nature of the BTTG apatites. Indeed, as explained above (**Figure 3-2**) apatites are closely associated with biotites or amphiboles in all Barberton trondhjemites and commonly occur as interstitial phases around plagioclase and quartz, suggesting that they crystallized late in the magmatic history (and notably later than plagioclase). Therefore, it is likely that another process must control the Sr-enrichment of apatite in felsic melts but this is beyond the scope of this work to resolve. Suffice it to say that Sr content in BTTG apatite does not record the degree of differentiation of the host granitoids (as shown by the case of the Stolzburg apatites).

Belousova et al., 2001, 2002 have highlighted the positive correlation of La/Ce ratio in apatite with the alkaline content of the parent melt. For melts with 5.5 wt% of Na_2O, the La/Ce of apatite would be between 0.4 and 0.8. This correlation is hardly observed in our dataset (**Figure 3-7 C**) where at Na_2O of 5.5 wt% the corresponding La/Ce in apatite is around 0.3 (Theespruit trondhjemite, see **Figure 3-7 C**). Therefore, in the case of the BTTGs, the La/Ce ratio in apatite is rather a weak proxy of the alkalinity of the host granitoid and, thus, cannot be relied upon. The same observation occurs for the oxygen fugacity of the granitoids since the Eu/Eu* recorded by TTG apatite is likely to be influenced by fractionation of co-existing phases like plagioclase rather than by the sole oxidation state of the magma (Belousova et al., 2001, 2002). Both alkalinity and oxygen fugacity of the host TTG are therefore poorly reflected in their apatite trace element chemistry.

The REE chemistry of igneous apatite is strongly controlled by the timing of crystallization which is in turn, dictated by the Aluminum Saturation Index of the parent magma (Bruand et al., 2020; Montel, 1986; Pichavant et al., 1992; Wolf & London, 1995). Indeed, in a metaluminous (ASI<0.9) magma, apatite would crystallize before monazite or other REE-bearing accessory phases and suck up the LREE budget of the melt whereas in a peraluminous (ASI>0.9) magma, monazite and epidote would

crystallize first, capturing most LREE and leaving a residual liquid that is depleted in LREE. Thus, when apatite crystallizes, it will record a LREE-depleted signature. This phenomenon is verified when one looks at the REE spectra of the BTTG apatites (cf **Figure 3-6**) where the only pluton that produced LREE-enriched apatites is the Kaap Valley tonalite (ASI = 0.79 <0.9 see Robb et al., 1986) whereas all the other plutons investigated here produced apatite with a LREE depleted signature, consistent with their peraluminous nature (ASI>1.0, see Laurent et al., 2020; J.-F. Moyen et al., 2007; Yearron et al., 2003). This observation enables us to reassess previous ternary discrimination plot of (Bruand et al., 2020). Indeed, the different granitoid composition fields labeled on the 10Sr vs LREE vs 10Y ternary plot of (Bruand et al., 2020) were calibrated from a limited apatite dataset that did not include apatites crystallized in metaluminous tonalitic magmas at the time of publication. From the above observations we can fairly say that the ternary plot of (Bruand et al., 2020) mainly separates apatites from TTGs having different degrees of evolution and ASI but does not necessarily discriminate TTG vs non-TTG apatites as the least evolved tonalitic magma of the BTTG series (the Kaap Valley tonalite) can produce LREE-enriched apatites plotting outside the "TTG" field while still being part of the TTG series. This confirms previous claim from (J.-F. Moyen et al., 2024; Vezinet et al., 2025) about the intermediate nature of the Kaap Valley tonalite, in-between that of TTGs and sanukitoids . Therefore, in our BTTG dataset, it is fair to associate LREE-enriched apatite with less evolved metaluminous granitoids and LREE-depleted apatite with highly evolved peraluminous granitoids.

To conclude we can say that while reconstructing the SiO_2 content, alkalinity and oxidation state of the host granitoids (as demonstrated from the Stolzburg pluton) from the trace element chemistry of apatite can be difficult, there is a good correlation between the degree of evolution and ASI of the melt and the REE composition of the produced apatites. Notably the LREE turned out to be a strong proxy to discriminate less evolved metaluminous from highly differentiated peraluminous parental melts.

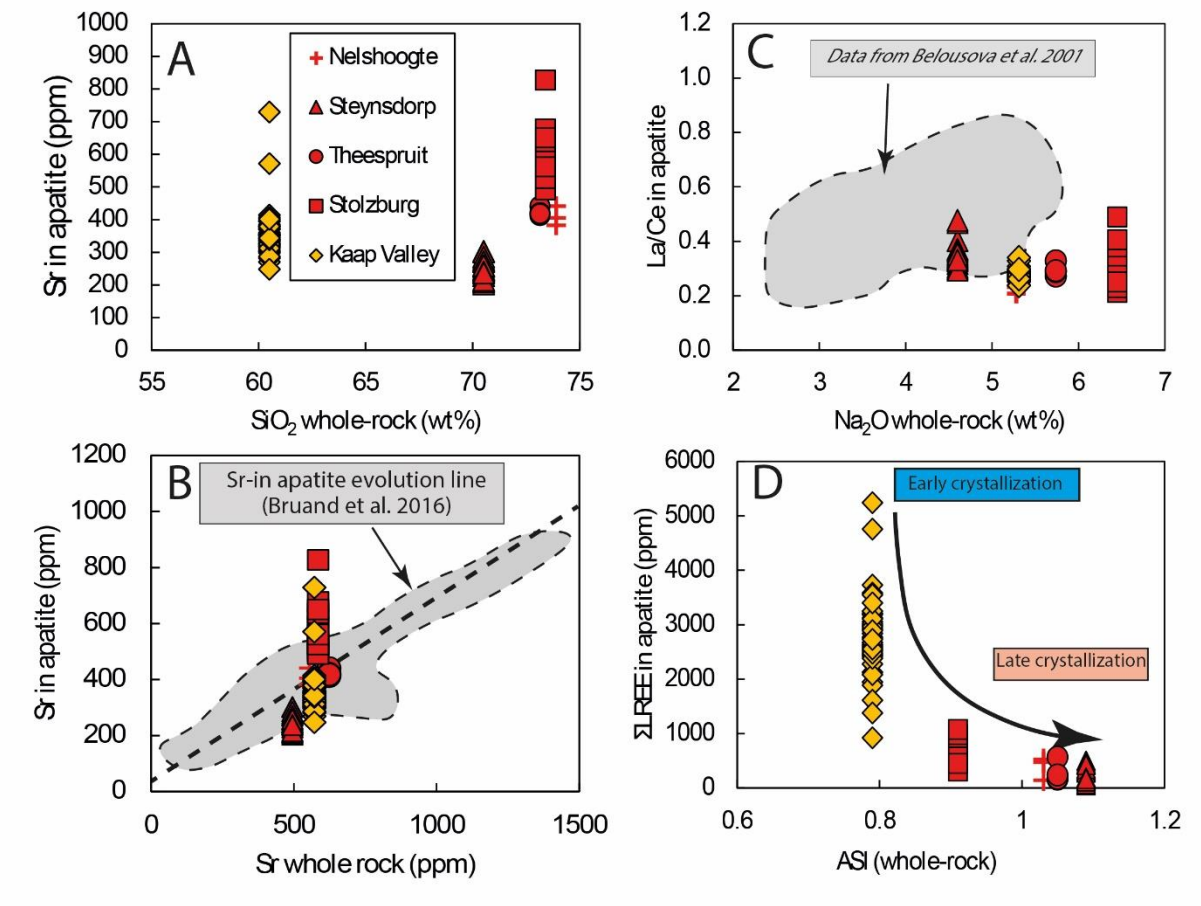

Figure 3-7 : Trace element characteristics of BTTG apatites compared with granitoid apatite data from the literature (Belousova et al., 2001; Bruand et al., 2016). See explanations in the main text.

3.5.3. Detrital apatite: provenance and source rocks

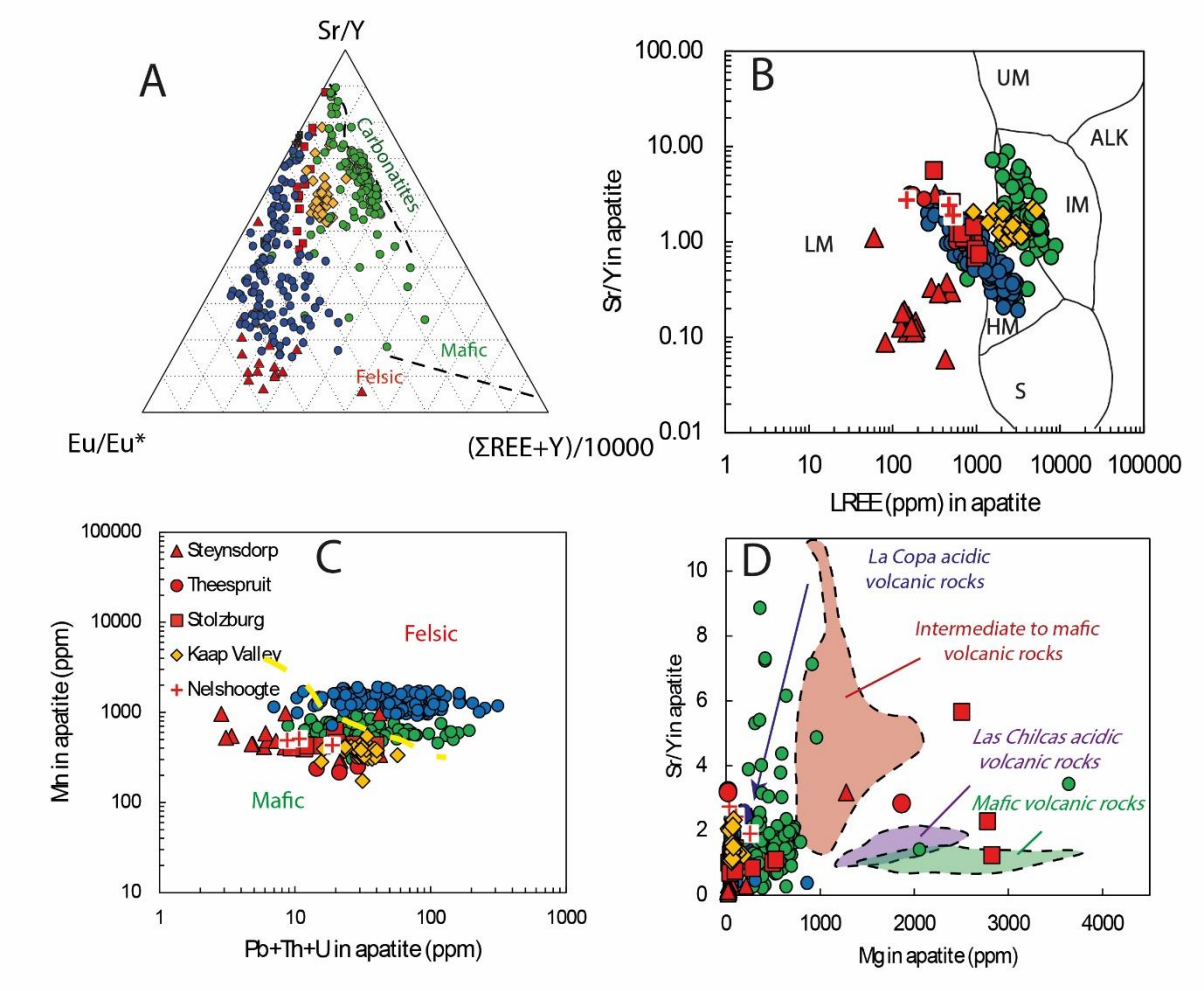

Figure 3-8: Trace element characterization of Barberton apatites. Graph A is from (Kieffer et al., 2024). Graph B is from (O'Sullivan et al., 2020). Graph C is from (Kieffer et al., 2024). Graph D compares maficity of Barberton apatites with apatites from a series of compositionally different volcanic rocks from (Nathwani et al., 2020) . See explanations in the main text.

To assess the provenance of the detrital apatites, we rely on a series of geochemical proxies that enable scientists to filter apatites from different lithologies (Belousova et al., 2001; Chakhmouradian et al., 2017; Henrichs et al., 2019; Kieffer et al., 2023, 2024; O'Reilly & Griffin, 2000; G. O'Sullivan et al., 2020). Kieffer et al., 2023 published a new ternary Sr/Y vs ΣREE+Y/10000 vs Eu/Eu* plot to distinguish apatites from mafic vs felsic vs ultramafic/carbonatitic sources which we use on **Figure 3-8 A**. Apatite crystallizing in carbonatitic melts or in mantle metasomatized melts usually incorporates larger amount of Sr (from 2500 ppm up to 22 000 ppm when apatite is associated with metasomatized mantle peridotite, see O'Reilly & Griffin, 2000) translating into extremely high Sr/Y ratio (see Sr/Y vs LREE plot of (G. O'Sullivan et al., 2020) in **Figure 3-8 B**). Following this, we notice that none of the detrital or BTTG apatites from this work fall in the carbonatitic field of (Kieffer et al., 2024). In addition

to this, Chakhmouradian et al., 2017; O'Sullivan et al., 2020 discussed the systematic absence of Eu anomaly in apatite crystallizing from ultramafic rocks such as carbonatites, a clear difference with our dataset documented in here (see **Figure 3-6**). Therefore, it is fair to assume that none of the detrital apatites investigated in this study is sourced from ultramafic lithologies.

Excluding ultramafic lithologies as potential sources for detrital apatites, there is the possibility that these apatites do not derive from felsic but rather from mafic lithologies. Chu et al., 2009; Kieffer et al., 2024; Stokes et al., 2019 discussed the reliability of Mn in apatite as a proxy of the degree of differentiation of the parental melt. With increasing degree of crystal fractionation (magma becoming more felsic and polymerized), Mn content in the residual melt increases, translating into felsic apatite recording very high amounts of Mn (> 300 ppm see Figure 7A from Kieffer et al., 2024) compared with apatites crystallized in mafic melts. With that said, the BTTG apatites, which crystallized in melts with >65% SiO_2, should display very high amounts of Mn. This trend is not observed in the current dataset as the Theespruit apatites (SiO_{2WR} = 73.15% see J.-F. Moyen et al., 2007; Yearron et al., 2003) exhibit Mn content systematically lower than 350 ppm (**Figure 3-8 C**) so well below the boundary between mafic and felsic fields defined by (Kieffer et al., 2024). Therefore, we argue that apatite Mn content is not a robust proxy of the degree of differentiation of the parental melt in the present dataset. Instead, to get a better constraint on the degree of evolution of the source rock, one can rely on the apatite Mg content as recommended by (Nathwani et al., 2020). Their Sr/Y vs Mg diagram proves to be a more robust discriminator of apatites populations since the felsic BTTG apatites (whole rock >65% SiO_2 see studies above) plot at Mg values lower than 500 ppm (excluding a few outliers, see **Figure 3-8 D**), which corresponds to the field of acidic volcanic formations of La Copa (Nathwani et al., 2020). Seeing that the Schapenburg apatites have Mg content lower than 150 ppm (see **Figure 3-8 D**) we can then argue that they must derive from a highly acidic source. The Hooggenoeg apatites on the other hand, have Mg content between 200 to 800 ppm so they must derive from a less acidic source than the Schapenburg apatites.

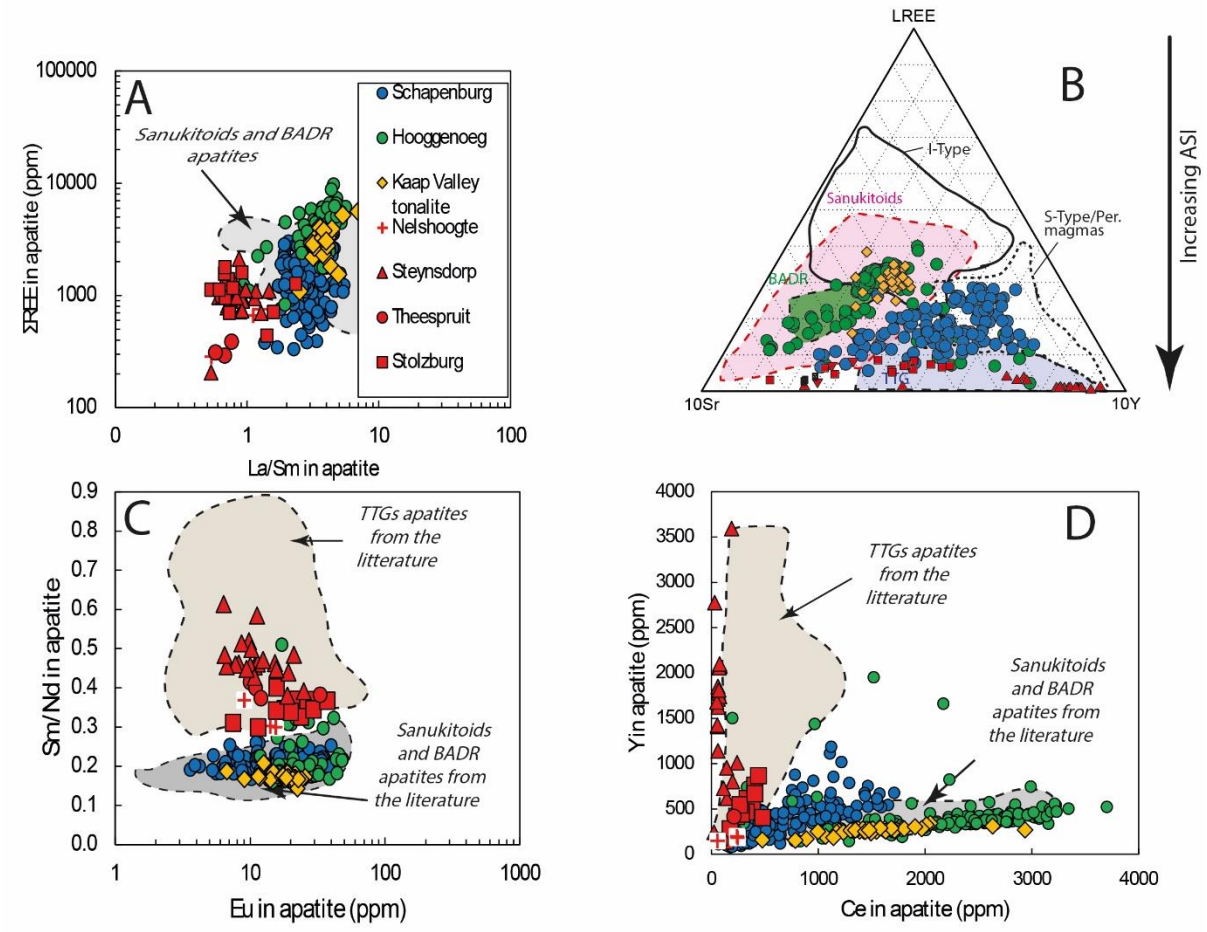

Figure 3-9: Trace element comparison between Barberton detrital apatites, BTTG apatites, and sanukitoids/BADR apatites from the literature (Bruand et al., 2020). See explanations in the main text.

A question remains as to the exact nature of the rocks that produced the Hooggenoeg and Schapenburg apatites. From the above observations it is clear that the Hooggenoeg apatites have trace element composition that separate them from the BTTG apatites, at least from the most differentiated plutons. However, as discussed in previous section, they exhibit similar LREE-enrichment and F content as apatites of the Kaap Valley tonalite (see **Figure 3-4 A, 3-5, 3-6, 3-9 B**) which could, at first glance, suggest that they crystallized in a compositionally similar magma that was present in the source area of the Hooggenoeg volcano-clastic sediments at 3.43 Ga. This magma must have been metaluminous and with silica content close to that of the Kaap Valley tonalite. The existence of tonalitic magma in surface exposures at 3.43 Ga is supported by geochemical study from Laurent et al., 2020 who suggested that rocks of the TTG series might derive from variable degrees of evolution of a single initial tonalitic magma. This tonalitic magma experienced crystal-liquid segregation and subsequent interstitial liquid loss to volcanic eruptions. 3.45 Ga Trondhjemites of Stolzburg and Theespruit plutons

would thus represent "fossil crystal-rich magma reservoir left behind by the eruption of silicic volcanic rocks" (see Laurent et al., 2020). Therefore, it is likely that magmas of tonalitic composition were exposed and participated in the input of detrital grains to volcano-clastic sediments at 3.43 Ga. However, despite some obvious resemblances, some chemical differences also occur between the KVT apatites and the Hooggenoeg apatites, namely the Sr content. While Sr content has proven itself to be a weak discriminator for the degree of evolution of apatite parental melt (see discussion above), one cannot obviate the fact that the Hooggenoeg detrital apatites have much higher Sr content (600 to 1200 ppm, see **Figure 3-5 C**) than the KVT apatites (350-400 ppm). This can suggest either that the parent magma had a higher bulk Sr content than Kaap Valley tonalite or that at similar Sr content, it crystallized apatite earlier than competing plagioclase, enabling it to record a more Sr-rich composition. However, as the Hooggenoeg apatites have a strong negative Eu anomaly, it is likely that plagioclase had already formed in significant amounts and sucked up most of the Eu budget by the time apatite started to crystallize. The contrasting Sr contents of the two populations is therefore ascribed to the different bulk-rock Sr content of their parent magma. In fact, trace element characteristics of Hooggenoeg apatites overlap quite well with apatite formed in late-Archean Sanukitoids (see **Figure 3-9**). Both populations have similar La/Sm ratio, LREE content, Sm/Nd ratio and Y vs Ce content (**Figure 3-9**) in addition to sharing similar Sr content (**Figure 3-5**). This strongly suggests that magmas of sanukitoid affinity were part of the source area of the Hooggenoeg volcano-clastic sediments. In the case of the Schapenburg apatites, the combination of low Mg (see **Figure 3-8 D**) and Sm/Nd ratio (**Figure 3-9 C**) with high LREE (**Figure 3-6**) and La/Sm ratio (**Figure 3-9 A**) points towards an evolved acidic parent melt of non-TTG affinity. Indeed, at similar Mg content, evolved BTTGs produced LREE-depleted apatites compared with Schapenburg detrital grains where apatites are LREE-enriched. Sanukitoids apatites also show a good overlap with Schapenburg apatites in terms of La/Sm ratio, Y vs Ce and Sm/Nd content (**Figure 3-9**), outlining their potential source-to-sink relationship.

Therefore, detrital apatites of the Barberton Greenstone sequence seem to have a different provenance than the exposed BTTGs. In fact, their trace element chemistry suggests that they must have been crystallized in granitoids that were more metaluminous and less evolved than the preserved

Barberton TTGs, potentially similar to late-Archean sanukitoids. This observation highlights the compositional diversity of the Paleo-archean felsic crust and its poor reflection in the preserved geological record. This supports claims made by (Combaz et al., 2025) who identified detrital zircons in the volcano-sediments of the Hooggenoeg Formation that have different trace element patterns than zircons of the exposed BTTGs, suggesting different provenance. The same was argued for zircons of the SSB which produced an age component that does not have any whole-rock equivalent in the terrane where these zircons were deposited and from which they were presumably sourced (Combaz et al., in press). In addition to this, if detrital apatites and zircons found within the same sedimentary rock sample can be assumed to derive from the same source (this is, we agree, not sure as clasts and detrital grains can have multiple sources while being deposited within the same sedimentary succession), then this source carried a population of zircons that is clearly chondritic to supra-chondritic in nature as Hooggenoeg Clastic Sediments and Schapenburg Schist Belt produced zircons predominantly with a positive Hf isotopic signature (Combaz et al., 2025).

3.5.4. Geological and geodynamic implications

The existence of Paleo-Archean sanukitoids in the source area of Hooggenoeg and Schapenburg apatites strongly challenges the accepted two-stage model of granitoid magmatism in the Archean and documented in every terrane across the world (Bédard, 1996; Davis & Hegner, 1992; de Oliveira et al., 2009, 2010, 2011; Jayananda et al., 2018, 2020; Jiang et al., 2016; Laurent et al., 2011; Li et al., 2024; Ma et al., 2014; Martin et al., 2009; J.-F. Moyen et al., 2003; Shirey & Hanson, 1984; Smithies & Champion, 2000; Stevenson et al., 1999; Sun et al., 2020; Sutcliffe et al., 1990; W. Wang et al., 2024; Zhai et al., 2006). In this model, a TTG-dominated >3.0 Ga Archean continental crust is ultimately followed by a <3.0 Ga more diverse set of plutonic felsic rocks being emplaced in the Archean crust, reflecting increasing involvement of crustal-derived material and mantle-metasomatized peridotite in the petrogenesis of Neo-Archean-Proterozoic granitoids (TTGs, sanukitoids, two-mica granites and hybrid granitoids, see Laurent et al., 2014) as a result of the increasing depth at which buried mafic material start melting and the secular cooling of the Earth. In fact the earliest documented sanukitoid occurs at 2.95 Ga with the High-Mg diorite suite of the Mallina Basin in the Pilbara Craton (Smithies

& Champion, 2000). In the KaapVaal Craton, the earliest occurrence of sanukitoids comes from granitoids of the Pietersburg Block and Limpopo Southern Marginal Zone (2.68-2.71 Ga, see Laurent et al., 2014, 2019) and the later Bulai Pluton of the Limpopo Belt (2.65 Ga, see Laurent et al., 2011). Again, Schapenburg clastic sediments were deposited at 3.25 Ga (Anhaeusser, 1983; Stevens et al., 2002; Combaz et al., 2025) and the Hooggenoeg volcano-clastic sediments at 3.43 Ga (Grosch et al., 2011; Combaz et al., 2025) based on strong detrital zircon age constraints from independent studies. The existence of non-TTG felsic rock in the source area of Barberton clastic sediments deposited ~300 to 500 Ma before the earliest documented sanukitoïd, strongly suggests that the observed higher diversity of granitoids at the Neo-Archean to Proterozoic transition is an artifact related to preservation bias. This confirms previous observations of Combaz et al., 2025 who, from a detrital zircon perspective, demonstrated the existence of now-missing Paleo-Archean K_2O-rich granites that were only preserved as clasts or isotopically negative zircons deposited in the Moodies sedimentary successions.

The existence of rocks of sanukitoid affinity as early as 3.43 Ga suggests that some form of subduction operated by that time as well as incipient cratonization and SCLM-crust coupling as suggested by (Vezinet et al., 2025), at least in the region of the Eastern Kaapvaal Craton. Indeed Sanukitoids are considered to mark the onset of plate-tectonics on Earth and their petrogenesis involve burial of LILE-rich material (TTGs and/or sediments) to deep pressures and their mixing with metasomatized mantle peridotite, a process that is more easily achieved through subduction than sagduction (Fowler & Rollinson, 2012; Laurent et al., 2014; Nebel et al., 2018, 2024; Vezinet et al., 2018; W. Wang et al., 2024). This confirms previous conclusions of Combaz et al., 2025 who has shown the necessity to tectonically bury felsic volcanic material to produce the youngest, 3.2 Ga generation of Paleo-Archean granitic clasts of the Moodies Basal Conglomerate. While there were multiple ways to produce generations of granites at 3.4 and 3.5 Ga other than through classical subduction, the existence of >3.43 Ga sanukitoids in the source area of Barberton clastic sediments strongly advocates for the early operation of subduction at least in the Barberton area.

The non-preservation of the whole range of Paleo-Archean granitoid diversity might be related to their emplacement into the shallower levels of the Archean crust, making them more exposed to surface weathering and recycling while their Neo-Archean to Proterozoic counterparts were progressively emplaced at deeper levels (as proposed by Agangi et al., 2018 and Combaz et al., 2025) following the secular cooling of the Earth. A possible reason why rocks of the TTG series had survived better than other granitoids is that they were probably emplaced at middle-crustal level and were thus less exposed to surface weathering and erosion (Agangi et al., 2018). However, this might also be related to their formation in an ephemeral subduction setting. Studies of Cawood et al., 2012; Hawkesworth et al., 2009 have documented the variation of preservation potential of igneous rocks with the tectonic setting in which they were formed. Igneous rocks formed during continent-continent collisions (mostly granites) are shielded inside a stable and strong continental lithosphere and thus are not recycled easily within the mantle (high preservation potential). In contrast, rocks formed during convergent/subduction (Scholl & Von Huene, 2009, 2010; Scholl & von Huene, 2007; Von Huene & Scholl, 1991, 1993) or extensional settings are easily recycled through tectonic erosion and thus their preservation potential is quite low. Therefore, a possible explanation for the non-preservation of old sanukitoids and granites could be that they were formed in a time when global geodynamics were dominated by transient subduction processes involving micro-plates and only few continent-continent collisions and thus, were easily recycled back into the mantle through tectonic erosion or lost to surface weathering. While the stabilization of the Kaapvaal craton that happened after ca. 3.0 Ga (James et al., 2003; Laurent et al., 2011, 2014, 2019; Luskin et al., 2019; Schoene et al., 2008, 2009; Vezinet et al., 2018) and the building of a stronger and colder continental lithosphere (C. J. Hawkesworth et al., 2017, 2020) might indeed help to increase the preservation potential of diverse granitoids, we would see little reason to explain why pre-3.0 Ga sanukitoïds would have been tectonically recycled whereas TTGs emplaced broadly at the same time (e.g. the ca. 3.45 Ga Theespruit and Stolzburg trondhjemites) would not. This for us suggests that the non-preservation of sanukitoïds before 3.0 Ga is an effect of surface weathering affecting upper crustal rocks and less, so rocks emplaced at deeper levels (i.e. TTGs).

3.6. Conclusion

Detrital apatites of the Barberton Greenstone Belt reveal more heterogeneous and diversified Paleoarchean felsic crust than can be discerned from the exposed rock record. Rocks of sanukitoïd and granitic composition already existed in Paleoarchean time, at least 500 Ma before their earliest documented onset. This observation highlights the importance of considering preservation biases, a factor that is often considered for old Hadean zircons of the Jack Hills but somewhat under-considered when dealing with younger (but still old!!) Eo and Paleoarchean terranes. Paleo-archean sanukitoids likely formed during transient subduction processes but did not survive these as they were likely recycled back into the Mantle or lost to surface weathering. In contrast, their occurrence in the geological record after 3.0 Ga likely reflects the stabilization of the craton and their shielding inside rigid and rheologically strong continental lithosphere. This study emphasizes the powerful role of detrital apatite as a record of missing segments of the Earth's earliest crust.

3.7. Acknowledgments

The PhD project of J.B.C. has been supported by National Research Foundation grant CNRS-129351 (South Africa) as part of the BuCoMO project, the University of Toulouse TREMPLIN grant PRESIZION and by the EUR TESS N°ANR-18-EURE-0018 in the framework of the Programme des Investissements d'Avenir. We thank the Mpumalanga Tourism and Park Agency for giving us access to the Komati Nature Reserve. We thank M. Vinicius Santos Leandro, J.F. Moyen and A. Chauvet for help and guidance during fieldwork and comments on data interpretation. We are grateful to J. Delport and J.P. Nel for help with SELFRAG operation and apatite separation; S. Choy for help with apatite picking and mounting; F. Maubé for help with SEM imaging; A. Marquet and J. Chmeleff for assistance with LA-ICP-MS analyses and M. Grobbelaar-Moolman and R.T. Roussow for whole-rock analysis at the CAF laboratory (Stellenbosch University).

3.8. References

Agangi, A., Hofmann, A., & Elburg, M. A. (2018). A review of Palaeoarchaean felsic volcanism in the eastern Kaapvaal craton : Linking plutonic and volcanic records. *Geoscience Frontiers*, *9*(3), 667-688.

Anhaeusser, C. R. (1980). A geological investigation of the Archaean granite-greenstone terrane south of the Boesmanskop syenite pluton, Barberton Mountain Land. *South African Journal of Geology*, *83*(1), 93-106.

Anhaeusser, C. R. (1981). Geotectonic evolution of the Archaean successions in the Barberton Mountain land, South Africa. In *Developments in Precambrian Geology* (Vol. 4, p. 137-160). Elsevier. https://www.sciencedirect.com/science/article/pii/S0166263508700112

Anhaeusser, C. R. (1983). *The geology of the Schapenburg greenstone remnant and surrounding Archaean granitic terrane south of Badplaas, Eastern Transvaal*. https://pascal-francis.inist.fr/vibad/index.php?action=getRecordDetail&idt=6522482

Anhaeusser, C. R., & Kisters, A. F. M. (1995). The structural significance of the Steynsdorp pluton and anticline within the tectonomagmatic framework of the Barberton Mountain Land. *South African Journal of Geology*, *98*(1), 43-51.

Antoine, C., Bruand, E., Guitreau, M., & Devidal, J. -L. (2020). Understanding Preservation of Primary Signatures in Apatite by Comparing Matrix and Zircon-Hosted Crystals From the Eoarchean Acasta Gneiss Complex (Canada). *Geochemistry, Geophysics, Geosystems*, *21*(7), e2020GC008923. https://doi.org/10.1029/2020GC008923

Bédard, L. P. (1996). Archean high-Mg quartz-monzodiorite suite : A re-evaluation of the parental magma and differentiation. *The Journal of Geology*, *104*(6), 713-728.

Bell, E. A., Boehnke, P., Hopkins-Wielicki, M. D., & Harrison, T. M. (2015). Distinguishing primary and secondary inclusion assemblages in Jack Hills zircons. *Lithos*, *234*, 15-26.

Belousova, E. A., Griffin, W. L., O'Reilly, S. Y., & Fisher, N. I. (2002). Apatite as an indicator mineral for mineral exploration : Trace-element compositions and their relationship to host rock type. *Journal of Geochemical Exploration*, *76*(1), 45-69.

Belousova, E. A., Walters, S., Griffin, W. L., & O'Reilly, S. Y. (2001). Trace-element signatures of apatites in granitoids from the Mt Isa Inlier, northwestern Queensland. *Australian Journal of Earth Sciences*, *48*(4), 603-619. https://doi.org/10.1046/j.1440-0952.2001.00879.x

Bleeker, W. (2003). The late Archean record : A puzzle in ca. 35 pieces. *Lithos*, *71*(2-4), 99-134.

Blichert-Toft, J., & Albarède, F. (2008). Hafnium isotopes in Jack Hills zircons and the formation of the Hadean crust. *Earth and Planetary Science Letters*, *265*(3-4), 686-702.

Bruand, E., Fowler, M., Storey, C., & Darling, J. (2017). Apatite trace element and isotope applications to petrogenesis and provenance. *American Mineralogist*, *102*(1), 75-84. https://doi.org/10.2138/am-2017-5744

Bruand, E., Fowler, M., Storey, C., Laurent, O., Antoine, C., Guitreau, M., Heilimo, E., & Nebel, O. (2020). Accessory mineral constraints on crustal evolution : Elemental fingerprints for magma discrimination. *Geochemical Perspectives Letters*, *13*, 7-12.

Bruand, E., Storey, C., & Fowler, M. (2016). An apatite for progress : Inclusions in zircon and titanite constrain petrogenesis and provenance. *Geology*, *44*(2), 91-94.

Byerly, G. R., Kröner, A., Lowe, D. R., Todt, W., & Walsh, M. M. (1996). Prolonged magmatism and time constraints for sediment deposition in the early Archean Barberton greenstone belt : Evidence from the Upper Onverwacht and Fig Tree groups. *Precambrian Research*, *78*(1-3), 125-138.

Carley, T. L., Miller, C. F., Wooden, J. L., Padilla, A. J., Schmitt, A. K., Economos, R. C., Bindeman, I. N., & Jordan, B. T. (2014). Iceland is not a magmatic analog for the Hadean : Evidence from the zircon record. *Earth and Planetary Science Letters*, *405*, 85-97.

Cawood, P. A., Hawkesworth, C. J., & Dhuime, B. (2012). Detrital zircon record and tectonic setting. *Geology*, *40*(10), 875-878.

Chakhmouradian, A. R., Reguir, E. P., Zaitsev, A. N., Couëslan, C., Xu, C., Kynickỳ, J., Mumin, A. H., & Yang, P. (2017). Apatite in carbonatitic rocks : Compositional variation, zoning, element partitioning and petrogenetic significance. *Lithos*, *274*, 188-213.

Chew, D. M., & Spikings, R. A. (2021). Apatite U-Pb Thermochronology : A Review. *Minerals*, *11*(10), Article 10. https://doi.org/10.3390/min11101095

Chu, M.-F., Wang, K.-L., Griffin, W. L., Chung, S.-L., O'Reilly, S. Y., Pearson, N. J., & Iizuka, Y. (2009). Apatite composition : Tracing petrogenetic processes in Transhimalayan granitoids. *Journal of Petrology*, *50*(10), 1829-1855.

Clemens, J. D., Belcher, R. W., & Kisters, A. F. (2010). The Heerenveen batholith, Barberton Mountain Land, South Africa : Mesoarchaean, potassic, felsic magmas formed by melting of an ancient subduction complex. *Journal of Petrology*, *51*(5), 1099-1120.

Combaz, J.-B., Stevens, G., & Laurent, O. (2025). A zircon and apatite perspective on the nature of the Paleoarchean continental crust. *Goldschmidt 2025 Conference*. https://conf.goldschmidt.info/goldschmidt/2025/meetingapp.cgi/Paper/28381

Compston, W., & Pidgeon, R. T. (1986). Jack Hills, evidence of more very old detrital zircons in Western Australia. *Nature*, *321*(6072), 766-769.

Davis, W. J., & Hegner, E. (1992). Neodymium isotopic evidence for the tectonic assembly of Late Archean crust in the Slave Province, northwest Canada. *Contributions to Mineralogy and Petrology*, *111*(4), 493-504.

De Ronde, C. E. J., & De Wit, M. J. (1994). Tectonic history of the Barberton greenstone belt, South Africa : 490 million years of Archean crustal evolution. *Tectonics*, *13*(4), 983-1005. https://doi.org/10.1029/94TC00353

De Wit, M. J., Armstrong, R., Hart, R. J., & Wilson, A. H. (1987). Felsic igneous rocks within the 3.3- to 3.5-Ga Barberton Greenstone Belt : High crustal level equivalents of the surrounding Tonalite-Trondhjemite Terrain, emplaced during thrusting. *Tectonics*, *6*(5), 529-549. https://doi.org/10.1029/TC006i005p00529

Decker, N. B., Byerly, G. R., Stiegler, M. T., Lowe, D. R., & Stefurak, E. (2015). High resolution tephra and U/Pb chronology of the 3.33–3.26 Ga Mendon Formation, Barberton Greenstone Belt, South Africa. *Precambrian Research*, *261*, 54-74.

de Oliveira, M. A., Dall'Agnol, R., Althoff, F. J., & da Silva Leite, A. A. (2009). Mesoarchean sanukitoid rocks of the Rio Maria granite-greenstone terrane, Amazonian craton, Brazil. *Journal of South American Earth Sciences*, *27*(2-3), 146-160.

de Oliveira, M. A., Dall'Agnol, R., & de Almeida, J. de A. C. (2011). Petrology of the Mesoarchean Rio Maria suite and the discrimination of sanukitoid series. *Lithos*, *127*(1-2), 192-209.

de Oliveira, M. A., Dall'Agnol, R., & Scaillet, B. (2010). Petrological constraints on crystallization conditions of Mesoarchean sanukitoid rocks, southeastern Amazonian craton, Brazil. *Journal of Petrology*, *51*(10), 2121-2148.

Diener, J. F., Stevens, G., Kisters, A. F., & Poujol, M. (2005). Metamorphism and exhumation of the basal parts of the Barberton greenstone belt, South Africa : Constraining the rates of Mesoarchaean tectonism. *Precambrian Research*, *143*(1-4), 87-112.

Drabon, N., Byerly, B. L., Byerly, G. R., Wooden, J. L., Keller, C. B., & Lowe, D. R. (2021). Heterogeneous Hadean crust with ambient mantle affinity recorded in detrital zircons of the Green Sandstone Bed, South Africa. *Proceedings of the National Academy of Sciences*, *118*(8), e2004370118.

Drabon, N., Byerly, B. L., Byerly, G. R., Wooden, J. L., Wiedenbeck, M., Valley, J. W., Kitajima, K., Bauer, A. M., & Lowe, D. R. (2022). Destabilization of Long-Lived Hadean Protocrust and the Onset of Pervasive Hydrous Melting at 3.8 Ga. *AGU Advances*, *3*(2), e2021AV000520. https://doi.org/10.1029/2021AV000520

Drabon, N., Galić, A., Mason, P. R., & Lowe, D. R. (2019). Provenance and tectonic implications of the 3.28–3.23 Ga Fig Tree Group, central Barberton greenstone belt, South Africa. *Precambrian Research*, *325*, 1-19.

Drabon, N., Kirkpatrick, H. M., Byerly, G. R., & Wooden, J. L. (2024). Trace elements in zircon record changing magmatic processes and the multi-stage build-up of Archean proto-continental crust. *Geochimica et Cosmochimica Acta*, *373*, 136-150.

Dziggel, A., Stevens, G., Poujol, M., Anhaeusser, C. R., & Armstrong, R. A. (2002). Metamorphism of the granite–greenstone terrane south of the Barberton greenstone belt, South Africa : An insight into the tectono-thermal evolution of the 'lower'portions of the Onverwacht Group. *Precambrian Research*, *114*(3-4), 221-247.

Dziggel, A., Stevens, G., Poujol, M., & Armstrong, R. A. (2006). *Contrasting source components of clastic metasedimentary rocks in the lowermost formations of the Barberton greenstone belt*.

Eglington, B. M., & Armstrong, R. A. (2004). The Kaapvaal Craton and adjacent orogens, southern Africa : A geochronological database and overview of the geological development of the craton. *South African Journal of Geology*, *107*(1-2), 13-32.

Fisher, C. M., Hanchar, J. M., Samson, S. D., Dhuime, B., Blichert-Toft, J., Vervoort, J. D., & Lam, R. (2011). Synthetic zircon doped with hafnium and rare earth elements : A reference material for in situ hafnium isotope analysis. *Chemical Geology*, *286*(1-2), 32-47.

Fisher, C. M., Vervoort, J. D., & Hanchar, J. M. (2014). Guidelines for reporting zircon Hf isotopic data by LA-MC-ICPMS and potential pitfalls in the interpretation of these data. *Chemical geology*, *363*, 125-133.

Fowler, M., & Rollinson, H. (2012). Phanerozoic sanukitoids from Caledonian Scotland : Implications for Archean subduction. *Geology*, *40*(12), 1079-1082.

Fralick, P. W., & Kronberg, B. I. (1997). Geochemical discrimination of clastic sedimentary rock sources. *Sedimentary Geology*, *113*(1), 111-124. https://doi.org/10.1016/S0037-0738(97)00049-3

Gillespie, J., Glorie, S., Khudoley, A., & Collins, A. S. (2018). Detrital apatite U-Pb and trace element analysis as a provenance tool : Insights from the Yenisey Ridge (Siberia). *Lithos*, *314*, 140-155.
Grimes, C. B., John, B. E., Kelemen, P. B., Mazdab, F. K., Wooden, J. L., Cheadle, M. J., Hanghøj, K., & Schwartz, J. J. (2007). Trace element chemistry of zircons from oceanic crust : A method for distinguishing detrital zircon provenance. *Geology*, *35*(7), 643-646.
Grimes, C. B., Wooden, J. L., Cheadle, M. J., & John, B. E. (2015). "Fingerprinting" tectono-magmatic provenance using trace elements in igneous zircon. *Contributions to Mineralogy and Petrology*, *170*(5-6), 46. https://doi.org/10.1007/s00410-015-1199-3
Grosch, E. G., Kosler, J., McLoughlin, N., Drost, K., Slama, J., & Pedersen, R. B. (2011). Paleoarchean detrital zircon ages from the earliest tectonic basin in the Barberton Greenstone Belt, Kaapvaal craton, South Africa. *Precambrian Research*, *191*(1-2), 85-99.
Guitreau, M., Blichert-Toft, J., Martin, H., Mojzsis, S. J., & Albarède, F. (2012). Hafnium isotope evidence from Archean granitic rocks for deep-mantle origin of continental crust. *Earth and Planetary Science Letters*, *337*, 211-223.
Harlov, D. E. (2015). Apatite : A fingerprint for metasomatic processes. *Elements*, *11*(3), 171-176.
Harlov, D. E., Wirth, R., & Förster, H.-J. (2005). An experimental study of dissolution–reprecipitation in fluorapatite : Fluid infiltration and the formation of monazite. *Contributions to Mineralogy and Petrology*, *150*(3), 268-286. https://doi.org/10.1007/s00410-005-0017-8
Harrison, T. M. (2009). The Hadean Crust : Evidence from >4 Ga Zircons. *Annual Review of Earth and Planetary Sciences*, *37*(1), 479-505. https://doi.org/10.1146/annurev.earth.031208.100151
Hawkesworth, C., Cawood, P., Kemp, T., Storey, C., & Dhuime, B. (2009). A Matter of Preservation. *Science*, *323*(5910), 49-50. https://doi.org/10.1126/science.1168549
Hawkesworth, C. J., Cawood, P. A., & Dhuime, B. (2020). The evolution of the continental crust and the onset of plate tectonics. *Frontiers in earth science*, *8*, 326.
Hawkesworth, C. J., Cawood, P. A., Dhuime, B., & Kemp, T. I. S. (2017). Earth's Continental Lithosphere Through Time. *Annual Review of Earth and Planetary Sciences*, *45*(1), 169-198. https://doi.org/10.1146/annurev-earth-063016-020525
Henrichs, I. A., Chew, D. M., O'Sullivan, G. J., Mark, C., McKenna, C., & Guyett, P. (2019). Trace Element (Mn-Sr-Y-Th-REE) and U-Pb Isotope Systematics of Metapelitic Apatite During Progressive Greenschist- to Amphibolite-Facies Barrovian Metamorphism. *Geochemistry, Geophysics, Geosystems*, *20*(8), 4103-4129. https://doi.org/10.1029/2019GC008359
Heubeck, C. (2019). The Moodies Group—A High-Resolution Archive of Archaean Surface Processes and Basin-Forming Mechanisms. In A. Kröner & A. Hofmann (Éds.), *The Archaean Geology of the Kaapvaal Craton, Southern Africa* (p. 133-169). Springer International Publishing. https://doi.org/10.1007/978-3-319-78652-0_6
Heubeck, C., Drabon, N., Byerly, G., Leisgang, I., Linnemann, U., Lowe, D., Mertz-Kraus, R., Gonzalez-Pinzon, A., Thomsen, T. B., & Zeh, A. (2022). Detrital zircon provenance of the Archean Moodies Group, Barberton Greenstone Belt, South Africa and Eswatini. *American Journal of Science*, *322*(2), 65-107.
Heubeck, C., Engelhardt, J., Byerly, G. R., Zeh, A., Sell, B., Luber, T., & Lowe, D. R. (2013). Timing of deposition and deformation of the Moodies Group (Barberton Greenstone Belt, South Africa) : Very-high-resolution of Archaean surface processes. *Precambrian Research*, *231*, 236-262.
Heubeck, C., & Lowe, D. R. (1994). Late syndepositional deformation and detachment tectonics in the Barberton Greenstone Belt, South Africa. *Tectonics*, *13*(6), 1514-1536. https://doi.org/10.1029/94TC01809
Hoskin, P. W., & Schaltegger, U. (2003). The composition of zircon and igneous and metamorphic petrogenesis. *Reviews in mineralogy and geochemistry*, *53*(1), 27-62.
James, D. E., Niu, F., & Rokosky, J. (2003). Crustal structure of the Kaapvaal craton and its significance for early crustal evolution. *Lithos*, *71*(2-4), 413-429.
Jayananda, M., Aadhiseshan, K. R., Kusiak, M. A., Wilde, S. A., Sekhamo, K., Guitreau, M., Santosh, M., & Gireesh, R. V. (2020). Multi-stage crustal growth and Neoarchean geodynamics in the Eastern Dharwar Craton, southern India. *Gondwana Research*, *78*, 228-260.
Jayananda, M., Santosh, M., & Aadhiseshan, K. R. (2018). Formation of Archean (3600–2500 Ma) continental crust in the Dharwar Craton, southern India. *Earth-Science Reviews*, *181*, 12-42.

Jiang, N., Guo, J., Fan, W., Hu, J., Zong, K., & Zhang, S. (2016). Archean TTGs and sanukitoids from the Jiaobei terrain, North China craton : Insights into crustal growth and mantle metasomatism. *Precambrian Research*, *281*, 656-672.

Kamo, S. L., & Davis, D. W. (1994). Reassessment of Archean crustal development in the Barberton Mountain Land, South Africa, based on U-Pb dating. *Tectonics*, *13*(1), 167-192. https://doi.org/10.1029/93TC02254

Kieffer, M. A., Dare, S. A., & Gendron, M. (2024). Trace element discrimination diagrams to identify igneous apatite from I-, S-and A-type granites and mafic intrusions : Implications for provenance studies and mineral exploration. *Chemical Geology*, *649*, 121965.

Kieffer, M. A., Dare, S. A., & Namur, O. (2023). The use of trace elements in apatite to trace differentiation of a ferrobasaltic melt in the Sept-Iles Intrusive Suite, Quebec, Canada : Implications for provenance discrimination. *Geochimica et Cosmochimica Acta*, *342*, 169-197.

Kirkland, C. L., Hollis, J., Danišík, M., Petersen, J., Evans, N. J., & McDonald, B. J. (2017). Apatite and titanite from the Karrat Group, Greenland; implications for charting the thermal evolution of crust from the U-Pb geochronology of common Pb bearing phases. *Precambrian Research*, *300*, 107-120.

Kirkland, C. L., Yakymchuk, C., Szilas, K., Evans, N., Hollis, J., McDonald, B., & Gardiner, N. J. (2018). Apatite : A U-Pb thermochronometer or geochronometer? *Lithos*, *318*, 143-157.

Kisters, A. F., Belcher, R. W., Poujol, M., & Dziggel, A. (2010). Continental growth and convergence-related arc plutonism in the Mesoarchaean : Evidence from the Barberton granitoid-greenstone terrain, South Africa. *Precambrian Research*, *178*(1-4), 15-26.

Kisters, A. F. M., Stevens, G., Dziggel, A., & Armstrong, R. A. (2003). Extensional detachment faulting and core-complex formation in the southern Barberton granite–greenstone terrain, South Africa : Evidence for a 3.2 Ga orogenic collapse. *Precambrian Research*, *127*(4), 355-378. https://doi.org/10.1016/j.precamres.2003.08.002

Kröner, A., Anhaeusser, C. R., Hoffmann, J. E., Wong, J., Geng, H., Hegner, E., Xie, H., Yang, J., & Liu, D. (2016). Chronology of the oldest supracrustal sequences in the Palaeoarchaean Barberton Greenstone Belt, South Africa and Swaziland. *Precambrian Research*, *279*, 123-143.

Kröner, A., & Compston, W. (1988). Ion microprobe ages of zircons from early Archaean granite pebbles and greywacke, Barberton greenstone belt, southern Africa. *Precambrian Research*, *38*(4), 367-380.

Kröner, A., Hegner, E., Wendt, J. I., & Byerly, G. R. (1996). The oldest part of the Barberton granitoid-greenstone terrain, South Africa : Evidence for crust formation between 3.5 and 3.7 Ga. *Precambrian Research*, *78*(1-3), 105-124.

Lana, C., Kisters, A., & Stevens, G. (2010). Exhumation of Mesoarchean TTG gneisses from the middle crust : Insights from the Steynsdorp core complex, Barberton granitoid-greenstone terrain, South Africa. *Bulletin*, *122*(1-2), 183-197.

Laurent, O., Björnsen, J., Wotzlaw, J.-F., Bretscher, S., Pimenta Silva, M., Moyen, J.-F., Ulmer, P., & Bachmann, O. (2020). Earth's earliest granitoids are crystal-rich magma reservoirs tapped by silicic eruptions. *Nature Geoscience*, *13*(2), 163-169.

Laurent, O., Guitreau, M., Bruand, E., & Moyen, J.-F. (2024). At the dawn of continents : Archean tonalite-trondhjemite-granodiorite suites. *Elements*, *20*(3), 174-179.

Laurent, O., Martin, H., Doucelance, R., Moyen, J.-F., & Paquette, J.-L. (2011). Geochemistry and petrogenesis of high-K "sanukitoids" from the Bulai pluton, Central Limpopo Belt, South Africa : Implications for geodynamic changes at the Archaean–Proterozoic boundary. *Lithos*, *123*(1-4), 73-91.

Laurent, O., Martin, H., Moyen, J.-F., & Doucelance, R. (2014). The diversity and evolution of late-Archean granitoids : Evidence for the onset of "modern-style" plate tectonics between 3.0 and 2.5 Ga. *Lithos*, *205*, 208-235.

Laurent, O., Zeh, A., Brandl, G., Vezinet, A., & Wilson, A. (2019). Granitoids and Greenstone Belts of the Pietersburg Block—Witnesses of an Archaean Accretionary Orogen Along the Northern Edge of the Kaapvaal Craton. In A. Kröner & A. Hofmann (Éds.), *The Archaean Geology of the Kaapvaal Craton, Southern Africa* (p. 83-107). Springer International Publishing. https://doi.org/10.1007/978-3-319-78652-0_4

Li, J., Liu, S.-A., Ma, H., Wu, C., Zhu, D.-C., & Liu, J. (2024). Pervasive Neoarchean melting of subducted sediments generating sanukitoid and associated magmatism in the North China Craton, with implications for the operation of plate tectonics. *Geological Society of America Bulletin*, *136*(7-8), 3121-3136.

Loferski, P. J., & Ayuso, R. A. (1995). Petrography and mineral chemistry of the composite Deboullie pluton, northern Maine, USA : Implications for the genesis of Cu Mo mineralization. *Chemical Geology*, *123*(1-4), 89-105.

London, D. (1997). Estimating abundances of volatile and other mobile components in evolved silicic melts through mineral–melt equilibria. *Journal of Petrology*, *38*(12), 1691-1706.

Lowe, D. R. (1999). *Geologic evolution of the Barberton Greenstone Belt and vicinity*. https://pubs.geoscienceworld.org/gsa/books/edited-volume/486/chapter-pdf/967261/i0-8137-2329-9-329-0-287.pdf

Lowe, D. R., & Byerly, G. R. (2007). An overview of the geology of the Barberton Greenstone Belt and vicinity : Implications for early crustal development. *Developments in Precambrian geology*, *15*, 481-526.

Luskin, C., Wilson, A., Gold, D., & Hofmann, A. (2019). The Pongola Supergroup : Mesoarchaean Deposition Following Kaapvaal Craton Stabilization. In A. Kröner & A. Hofmann (Éds.), *The Archaean Geology of the Kaapvaal Craton, Southern Africa* (p. 225-254). Springer International Publishing. https://doi.org/10.1007/978-3-319-78652-0_9

Ma, X., Fan, H.-R., Santosh, M., Liu, X., & Guo, J.-H. (2014). Origin of sanukitoid and hornblendite enclaves in the Dajitu pluton from the Yinshan Block, North China Craton : Product of Neoarchaean ridge subduction? *International Geology Review*, *56*(10), 1197-1212.

Martin, H., Moyen, J.-F., Guitreau, M., Blichert-Toft, J., & Le Pennec, J.-L. (2014). Why Archaean TTG cannot be generated by MORB melting in subduction zones. *Lithos*, *198*, 1-13.

Martin, H., Moyen, J.-F., & Rapp, R. (2009). The sanukitoid series : Magmatism at the Archaean–Proterozoic transition. *Earth and Environmental Science Transactions of the Royal Society of Edinburgh*, *100*(1-2), 15-33.

Matsumura, R. (2014). *The petrogenesis of the Nelshoogte pluton : The youngest and most compositionally variable TTG pluton in the Barberton Granite-Greenstone Terrain* [PhD Thesis, Stellenbosch: Stellenbosch University]. https://scholar.sun.ac.za/handle/10019.1/86589

Miyake, S., Aoki, K., Komiya, T., Aoki, S., Fukuyama, M., & Ogasawara, M. (2024). Geochemical Signatures of Igneous Zircon and Apatite : Generation of Archean TTGs in the Barberton Granitoid-Greenstone Terrain, South Africa. *Island Arc*, *33*(1). https://doi.org/10.1111/iar.12536

Montel, J.-M. (1986). Experimental determination of the solubility of Ce-monazite in SiO2-Al2O3-K2O-Na2O melts at 800 C, 2 kbar, under H2O-saturated conditions. *Geology*, *14*(8), 659-662.

Moyen, J. F., Zeh, A., Cuney, M., Dziggel, A., & Carrouée, S. (2021). The multiple ways of recycling Archaean crust : A case study from the ca. 3.1 Ga granitoids from the Barberton Greenstone Belt, South Africa. *Precambrian Research*, *353*, 105998.

Moyen, J.-F., & Martin, H. (2012). Forty years of TTG research. *Lithos*, *148*, 312-336.

Moyen, J.-F., Martin, H., Jayananda, M., & Auvray, B. (2003). Late Archaean granites : A typology based on the Dharwar Craton (India). *Precambrian Research*, *127*(1-3), 103-123.

Moyen, J.-F., Stevens, G., & Kisters, A. (2006). Record of mid-Archaean subduction from metamorphism in the Barberton terrain, South Africa. *Nature*, *442*(7102), 559-562.

Moyen, J.-F., Stevens, G., Kisters, A. F., & Belcher, R. W. (2007). TTG plutons of the Barberton granitoid-greenstone terrain, South Africa. *Developments in Precambrian geology*, *15*, 607-667.

Moyen, J.-F., Vezinet, A., Guitreau, M., Chauvet, A., Paquette, J.-L., Stevens, G., & Bruand, E. (2024, septembre). Long term melt-generation in the Archaean crust : A case study from the Northern Kaapvaal craton, South Africa. *Granulites & Granulites 2024*. https://hal.science/hal-04714679

Nathwani, C. L., Loader, M. A., Wilkinson, J. J., Buret, Y., Sievwright, R. H., & Hollings, P. (2020). Multi-stage arc magma evolution recorded by apatite in volcanic rocks. *Geology*, *48*(4), 323-327.

Nebel, O., Capitanio, F. A., Moyen, J.-F., Weinberg, R. F., Clos, F., Nebel-Jacobsen, Y. J., & Cawood, P. A. (2018). When crust comes of age : On the chemical evolution of Archaean, felsic continental crust by crustal drip tectonics. *Philosophical Transactions of the Royal Society A: Mathematical, Physical and Engineering Sciences*, *376*(2132), 20180103. https://doi.org/10.1098/rsta.2018.0103

Nebel, O., Vandenburg, E. D., Capitanio, F. A., Smithies, R. H., Mulder, J., & Cawood, P. A. (2024). Early Earth "subduction" : Short-lived, off-craton, shuffle tectonics, and no plate boundaries. *Precambrian Research*, *408*, 107431.

Nutman, A. P. (2007). Apatite recrystallisation during prograde metamorphism, Cooma, southeast Australia : Implications for using an apatite – graphite association as a biotracer in ancient metasedimentary rocks. *Australian Journal of Earth Sciences*, *54*(8), 1023-1032. https://doi.org/10.1080/08120090701488321

Nutman, A. P., & Hiess, J. (2009). A granitic inclusion suite within igneous zircons from a 3.81 Ga tonalite (W. Greenland) : Restrictions for Hadean crustal evolution studies using detrital zircons. *Chemical Geology*, *261*(1-2), 77-82.

O'Reilly, S. Y., & Griffin, W. L. (2000). Apatite in the mantle : Implications for metasomatic processes and high heat production in Phanerozoic mantle. *Lithos*, *53*(3-4), 217-232.

O'Sullivan, G., Chew, D., Kenny, G., Henrichs, I., & Mulligan, D. (2020). The trace element composition of apatite and its application to detrital provenance studies. *Earth-Science Reviews*, *201*, 103044.

O'Sullivan, G. J., Chew, D. M., Morton, A. C., Mark, C., & Henrichs, I. A. (2018). An Integrated Apatite Geochronology and Geochemistry Tool for Sedimentary Provenance Analysis. *Geochemistry, Geophysics, Geosystems*, *19*(4), 1309-1326. https://doi.org/10.1002/2017GC007343

Piccoli, P., & Candela, P. (1994). Apatite in felsic rocks; a model for the estimation of initial halogen concentrations in the Bishop Tuff (Long Valley) and Tuolumne Intrusive Suite (Sierra Nevada Batholith) magmas. *American Journal of Science*, *294*(1), 92-135.

Piccoli, P. M., & Candela, P. A. (2002). Apatite in igneous systems. *Reviews in Mineralogy and Geochemistry*, *48*(1), 255-292.

Pichavant, M., Montel, J.-M., & Richard, L. R. (1992). Apatite solubility in peraluminous liquids : Experimental data and an extension of the Harrison-Watson model. *Geochimica et Cosmochimica Acta*, *56*(10), 3855-3861.

Polat, A. (2012). Growth of Archean continental crust in oceanic island arcs. *Geology*, *40*(4), 383.

Robb, L. J., Barton Jr, J. M., Kable, E. J. D., & Wallace, R. C. (1986). Geology, geochemistry and isotopic characteristics of the Archaean Kaap Valley pluton, Barberton mountain land, South Africa. *Precambrian Research*, *31*(1), 1-36.

Roberts, N. M., Yakymchuk, C., Spencer, C. J., Keller, C. B., & Tapster, S. R. (2024). Revisiting the discrimination and distribution of S-type granites from zircon trace element composition. *Earth and Planetary Science Letters*, *633*, 118638.

Sanchez-Garrido, C. J. (2012). *The petrogenesis of the older (> 3.0 Ga) potassic granitoids of eastern Mpumalanga (South Africa) and Swaziland : An investigation of crustal formation processes in the early Earth* [PhD Thesis, Stellenbosch: Stellenbosch University]. https://scholar.sun.ac.za/handle/10019.1/20044

Sanchez-Garrido, C. J., Stevens, G., Armstrong, R. A., Moyen, J.-F., Martin, H., & Doucelance, R. (2011). Diversity in Earth's early felsic crust : Paleoarchean peraluminous granites of the Barberton Greenstone Belt. *Geology*, *39*(10), 963-966.

Santos Leandro, M. V., Stevens, G., Moyen, J.-F., Kisters, A., & Ferreira, A. (s. d.). Archean Syenites by Intracrustal Processes : The Boesmanskop Alkaline Complex, Eastern Kaapvaal Craton. *Eastern Kaapvaal Craton*. Consulté 16 mai 2025, à l'adresse https://papers.ssrn.com/sol3/papers.cfm?abstract_id=4972697

Schoene, B., De Wit, M. J., & Bowring, S. A. (2008). Mesoarchean assembly and stabilization of the eastern Kaapvaal craton : A structural-thermochronological perspective. *Tectonics*, *27*(5), 2008TC002267. https://doi.org/10.1029/2008TC002267

Schoene, B., Dudas, F. O. L., Bowring, S. A., & De Wit, M. (2009). Sm–Nd isotopic mapping of lithospheric growth and stabilization in the eastern Kaapvaal craton. *Terra Nova*, *21*(3), 219-228. https://doi.org/10.1111/j.1365-3121.2009.00877.x

Scholl, D. W., & Von Huene, R. (2009). *Implications of estimated magmatic additions and recycling losses at the subduction zones of accretionary (non-collisional) and collisional (suturing) orogens*. https://pubs.geoscienceworld.org/books/edited-volume/1682/chapter/107516057

Scholl, D. W., & Von Huene, R. (2010). Subduction zone recycling processes and the rock record of crustal suture zonesThis article is one of a series of papers published in this Special Issue on the theme *Lithoprobe—Parameters, processes, and the evolution of a continent* . *Canadian Journal of Earth Sciences*, *47*(5), 633-654. https://doi.org/10.1139/E09-061

Scholl, D. W., & von Huene, R. (2007). *Crustal recycling at modern subduction zones applied to the past—Issues of growth and preservation of continental basement crust, mantle geochemistry, and supercontinent reconstruction*. https://pubs.geoscienceworld.org/books/edited-volume/443/chapter/3799072

Shirey, S. B., & Hanson, G. N. (1984). Mantle-derived Archaean monozodiorites and trachyandesites. *Nature*, *310*(5974), 222-224.

Smithies, R. H., & Champion, D. C. (2000). The Archaean high-Mg diorite suite : Links to tonalite–trondhjemite–granodiorite magmatism and implications for early Archaean crustal growth. *Journal of Petrology*, *41*(12), 1653-1671.

Spencer, C. J., Kirkland, C. L., Roberts, N. M. W., Evans, N. J., & Liebmann, J. (2020). Strategies towards robust interpretations of in situ zircon Lu–Hf isotope analyses. *Geoscience Frontiers*, *11*(3), 843-853.

Stevens, G., Droop, G. T. R., Armstrong, R. A., & Anhaeusser, C. R. (2002). Amphibolite facies metamorphism in the Schapenburg schist belt : A record of the mid-crustal response to∼ 3.23 Ga terrane accretion in the Barberton greenstone belt. *South African Journal of Geology*, *105*(3), 271-284.

Stevens, G., & Moyen, J.-F. (2007). Metamorphism in the Barberton Granite Greenstone Terrain : A record of Paleoarchean accretion. *Developments in precambrian geology*, *15*, 669-698.

Stevenson, R., Henry, P., & Gariépy, C. (1999). Assimilation–fractional crystallization origin of Archean sanukitoid suites : Western Superior Province, Canada. *Precambrian Research*, *96*(1-2), 83-99.

Stokes, T. N., Bromiley, G. D., Potts, N. J., Saunders, K. E., & Miles, A. J. (2019). The effect of melt composition and oxygen fugacity on manganese partitioning between apatite and silicate melt. *Chemical Geology*, *506*, 162-174. https://doi.org/10.1016/j.chemgeo.2018.12.015

Sun, G., Liu, S., Wang, M., Bao, H., & Teng, G. (2020). Complex Neoarchean mantle metasomatism : Evidence from sanukitoid diorites-monzodiorites-granodiorites in the northeastern North China Craton. *Precambrian Research*, *342*, 105692.

Sutcliffe, R. H., Smith, A. R., Doherty, W., & Barnett, R. L. (1990). Mantle derivation of Archean amphibole-bearing granitoid and associated mafic rocks : Evidence from the southern Superior Province, Canada. *Contributions to Mineralogy and Petrology*, *105*, 255-274.

Valley, J. W., Lackey, J. S., Cavosie, A. J., Clechenko, C. C., Spicuzza, M. J., Basei, M. A. S., Bindeman, I. N., Ferreira, V. P., Sial, A. N., & King, E. M. (2005). 4.4 billion years of crustal maturation : Oxygen isotope ratios of magmatic zircon. *Contributions to Mineralogy and Petrology*, *150*, 561-580.

Valley, J. W., Reinhard, D. A., Cavosie, A. J., Ushikubo, T., Lawrence, D. F., Larson, D. J., Kelly, T. F., Snoeyenbos, D. R., & Strickland, A. (2015). Nano-and micro-geochronology in Hadean and Archean zircons by atom-probe tomography and SIMS : New tools for old minerals. *American Mineralogist*, *100*(7), 1355-1377.

Van Kranendonk, M. J., Kröner, A., Hegner, E., & Connelly, J. (2009). Age, lithology and structural evolution of the c. 3.53 Ga Theespruit Formation in the Tjakastad area, southwestern Barberton Greenstone Belt, South Africa, with implications for Archaean tectonics. *Chemical Geology*, *261*(1-2), 115-139.

van Rensburg, D. J., Heubeck, C. E., & Reimann, S. (2021). Volcanoes in the estuaries : Insights into Earth's oldest (3.22 Ga) terrestrial microbial habitats, Moodies Group, Barberton Greenstone Belt. *Precambrian Research*, *365*, 106325.

Vezinet, A., Flores-Rojas, J., Sobolev, A. V., Léger, J., Chugunov, A. V., Batanova, V. G., Elburg, M. A., Hofmann, A., Balvay, M., & Paradis, N. (2025). Igneous apatite geochemistry indicates early cratonization of continents. *Precambrian Research*, *430*, 107927. https://doi.org/10.1016/j.precamres.2025.107927

Vezinet, A., Moyen, J.-F., Stevens, G., Nicoli, G., Laurent, O., Couzinié, S., & Frei, D. (2018). A record of 0.5 Ga of evolution of the continental crust along the northern edge of the Kaapvaal Craton, South Africa : Consequences for the understanding of Archean geodynamic processes. *Precambrian Research*, *305*, 310-326.

Von Huene, R., & Scholl, D. W. (1991). Observations at convergent margins concerning sediment subduction, subduction erosion, and the growth of continental crust. *Reviews of Geophysics*, *29*(3), 279-316. https://doi.org/10.1029/91RG00969

Von Huene, R., & Scholl, D. W. (1993). The return of sialic material to the mantle indicated by terrigeneous material subducted at convergent margins. *Tectonophysics*, *219*(1-3), 163-175.

Wang, H., Yang, J.-H., Zhu, Y.-S., Huang, C., Xu, L., Wu, S.-T., & Liu, Y. (2022). Archean crustal growth and reworking revealed by combined U-Pb-Hf-O isotope and trace element data of detrital zircons from ancient and modern river sediments of the eastern Kaapvaal Craton. *Geochimica et Cosmochimica Acta*, *320*, 79-104.

Wang, W., Lu, Y., Gao, L., Sun, G., Zhou, X., Yao, J., Yang, W., & Liang, X. (2024). Late Archean K-rich intermediate magmatism driven by deep supracrustal recycling. *Chemical Geology*, *662*, 122215.

Weltje, G. J., & von Eynatten, H. (2004). Quantitative provenance analysis of sediments : Review and outlook. *Sedimentary Geology*, *171*(1), 1-11. https://doi.org/10.1016/j.sedgeo.2004.05.007

Wilde, S. A., Valley, J. W., Peck, W. H., & Graham, C. M. (2001). Evidence from detrital zircons for the existence of continental crust and oceans on the Earth 4.4 Gyr ago. *Nature*, *409*(6817), 175-178.

Wolf, M. B., & London, D. (1994). Apatite dissolution into peraluminous haplogranitic melts : An experimental study of solubilities and mechanisms. *Geochimica et cosmochimica acta*, *58*(19), 4127-4145.

Wolf, M. B., & London, D. (1995). Incongruent dissolution of REE-and Sr-rich apatite in peraluminous granitic liquids : Differential apatite, monazite, and xenotime solubilities during anatexis. *American Mineralogist*, *80*(7-8), 765-775.

Yakymchuk, C., Holder, R. M., Kendrick, J., & Moyen, J.-F. (2023). Europium anomalies in zircon : A signal of crustal depth? *Earth and Planetary Science Letters*, *622*, 118405. https://doi.org/10.1016/j.epsl.2023.118405

Yearron, L., Clemens, J., Stevens, G., & Anhaeusser, C. (2003). Geochemistry and petrogenesis of the granitoids of the Barberton Mountain Land, South Africa. *EGS-AGU-EUG Joint Assembly*, 2639. https://ui.adsabs.harvard.edu/abs/2003EAEJA.....2639Y/abstract

Zeh, A. (2004). Crystal size distribution (CSD) and textural evolution of accessory apatite, titanite and allanite during four stages of metamorphism : An example from the Moine Supergroup, Scotland. *Journal of Petrology*, *45*(10), 2101-2132.

Zeh, A., Gerdes, A., & Barton Jr, J. M. (2009). Archean accretion and crustal evolution of the Kalahari Craton—The zircon age and Hf isotope record of granitic rocks from Barberton/Swaziland to the Francistown Arc. *Journal of Petrology*, *50*(5), 933-966.

Zeh, A., Gerdes, A., & Heubeck, C. (2013). U–Pb and Hf isotope data of detrital zircons from the Barberton Greenstone Belt : Constraints on provenance and Archaean crustal evolution. *Journal of the Geological Society*, *170*(1), 215-223.

Zhai, M., Kampunzu, A. B., Modisi, M. P., & Bagai, Z. (2006). Sr and Nd isotope systematics of Francistown plutonic rocks, Botswana : Implications for Neoarchaean crustal evolution of the Zimbabwe craton. *International Journal of Earth Sciences*, *95*, 355-369.

4. Chapter 4: Presentation of research paper 3 - New U-Pb and trace element data on Paleo-to-Mesoarchean rutiles of the Barberton Greenstone Belt, South Africa, document tectonic unroofing of lower-crustal units in a post-orogenic context.

This manuscript, first authored by Jean-Baptiste Combaz is under revision by co-authors and will be submitted early in January 2026 to *Lithos*. Supplementary materials to this chapter are available as an electronic link provided in Chapter 6.

Jean-Baptiste Combaz: Conceptualization, Methodology, Validation, Formal analysis, Investigation, Resources, Data Curation, Writing (original draft), Writing, Review and Editing, Visualization, Project administration, Funding acquisition **Oscar Laurent**: Conceptualization, Methodology, Validation, Resources, Writing-Review and Editing, Visualization, Project administration, Supervision, Funding acquisition **Gary Stevens**: Conceptualization, Validation, Writing-Review and Editing, Project administration, Supervision, Funding acquisition.

New U-Pb and trace element data on Paleo- to Mesoarchean rutile grains of the Barberton Greenstone Belt, South Africa, document tectonic unroofing of lower-crustal units in a post-orogenic context.

Combaz Jean-Baptiste[*,a,b], Laurent Oscar[b], Stevens Gary[a]

[a]Department of Geology, University of Stellenbosch, Private Bag X1, Matieland 7602, South Africa
[b]Université de Toulouse, CNRS, Géosciences Environnement Toulouse, Toulouse, France

*Corresponding author: jean-baptiste.combaz@orange.fr; https://orcid.org/0009-0007-1021-4052

Abstract:

We present new LA-ICP-MS U-Pb and trace element data from supracrustal rutiles preserved in >3.45 Ga felsic volcano-sediments of the Barberton Greenstone Belt, South Africa. These felsic volcano-sediments have experienced upper amphibolite facies conditions at ca. 3230 Ma during the main regional tectono-metamorphic event. Rutiles were collected at two different locations, corresponding to two different protoliths of the same supracrustal sequence. They show homogeneous U-Pb ages and trace element concentrations at the sample scale but contrasting patterns between the two samples. A felsic meta-volcani(clasti)c rock contains rutile with a weighted mean $^{207}Pb/^{206}Pb$ age of 3474 ± 70 Ma (MSWD = 1.3, n = 34) and mean Zr-in rutile temperature of 846 °C, with high amounts of Nb (4000 ppm) and Ta (ca. 500 ppm) and low amounts of W (< 50 ppm). In contrast, an aluminous meta-sedimentary rock (sampled 3 km to the South) produced rutiles with a weighted mean age of 3180 ± 64 Ma (MSWD = 1.5, n = 150) and mean Zr-in rutile Temperature of 601°C, low amounts of Nb (<2000 ppm) and Ta (ca. 90 ppm) and high amounts of W (ca.1000 ppm). Despite inter-sample differences, trace element signatures are interpreted to reflect a metamorphic origin of the grains for both populations, indicating crystallization during two regionally well-documented metamorphic episodes at ca.3.45 Ga and ca.3.20 Ga. The petrographic context and a Zr-in rutile temperature lower than that of peak metamorphism (i.e. 660°C) favor that the ca. 3.20 Ga rutiles were initially crystallized during the retrograde path of the amphibolitized host rocks and record cooling after significant exhumation. In contrast, rutile from the other sample underwent only very minor resetting of the U-Pb clock after crystallization as to retain a ca. 3.45 Ga age, although it experienced the same peak metamorphic conditions at ca. 3.20 Ga. This non-resetting of the U-Pb clock, together with literature geochronological and metamorphic constraints, collectively entail a minimum cooling rate of the Southern BGGT between 22 and 60°C/Ma during exhumation. Such high cooling rates were so far not documented for Paleo- to Mesoarchean tectono-metamorphic events and underpin the likely existence of conditions similar to those prevailing in modern “cold” orogens at that time.

4.1. Introduction

Rutile (TiO_2), an accessory mineral that crystallizes at P-T conditions above that of amphibolite facies (Angiboust & Harlov, 2017; Zack & Kooijman, 2017), has emerged as a robust tracer of the thermal evolution of high-grade metamorphic rocks (Bonnet et al., 2022; J. A. Cutts et al., 2019; Ewing et al., 2015; Kohn et al., 2016; Mezger et al., 1989; Tual et al., 2018; Zeh et al., 2018). Its exceptional utility in constraining cooling rates arises from its retention of U-Pb ages below a closure temperature (ca. 500-600°C, see Cherniak, 2000) that mimic those encountered in the middle crust. In addition to

this, rutile possesses a strong affinity for high-field strength elements such as Zr, U, Hf, W, Nb and Ta, the proportions of which enable geologists to discriminate metamorphic vs hydrothermal vs magmatic vs authigenic rutiles and, to a lesser extent, the lithological nature of their former host rock (Luvizotto et al., 2009; Meinhold et al., 2008; Pereira et al., 2019; Pereira & Storey, 2023; Schirra & Laurent, 2021; Sciuba & Beaudoin, 2021; Triebold et al., 2007, 2012; Zack, von Eynatten, et al., 2004). This, together with its resistance to chemical weathering and sedimentary cycles, make rutile a foremost accessory mineral for who wants to investigate the nature of sediment sources that are long eroded away. Lastly, the Zr concentration in rutile provides estimate of the temperature of crystallization (Ferry & Watson, 2007; Zack, Moraes, et al., 2004) such that it may record the metamorphic history of its host rock. In particular, a global compilation of Zr-in-rutile temperatures has been recently used to trace the onset of HP/LT, subduction-like metamorphic processes in the global rock-record (Pereira et al., 2021).

Whereas rutile have been widely used as a thermo-chronometer for characterizing the cooling rates at which Proterozoic-Phanerozoic orogens were cooled (Angiboust & Harlov, 2017; Bonnet et al., 2022; Ewing et al., 2015; Pereira & Storey, 2023; Smye & Stockli, 2014; Zack et al., 2007), similar studies for Archean high-grade metamorphic rocks are few, and mainly confined to the Neo-Archean granulitic domains which typically produced slow cooling rates that range between 2.2 to 0.4 °C/Ma (data from the Pikwitonei Granulite domain; Kooijman et al., 2010). Seldom has the Paleo-Mesoarchean rock record (more dominated by greenschist to amphibolite facies rocks, e.g. Anhaeusser, 2014; Percival, 1994) been investigated for such a purpose. Yet, the thermal history and cooling rate of high-grade metamorphic rocks bears important implications on the controlling tectonic processes and associated uplift rates, which for this period of the Earth's history are still debated. Following the categorization of (Jamieson & Beaumont, 2013) of Phanerozoic orogens, "Small Cold Orogens" (SCO) are characterized by cooling rates above 5°C/Ma and generally associated with tectonic exhumation of lower crustal units through low-angle detachment systems (Brown & Dallmeyer, 1996; Byrne et al., 2024a; Huet et al., 2011; Labrousse et al., 2016; Ring et al., 1999; Vanderhaeghe et al., 2003). In contrast, "Large Hot Orogens" (LHO) are characterized by cooling rates lower than 5°C/Ma, due to higher radiogenic heat buildup due to the orogen's larger size and/or higher mantle heat transfer, which results in the development of a hot

(partially-molten) middle-lower crust and lateral rather than vertical crustal flow, entailing slower cooling of the lower crustal units (Ashwal et al., 1999; Cagnard et al., s. d.; Chardon et al., 2009; Collins, 2002; Kelsey & Hand, 2015; Korhonen et al., 2013; Vanderhaeghe & Teyssier, 2001; Willigers et al., 2002).

Therefore, characterizing the cooling rate of > 3.2 Ga high-grade metamorphic rocks might shed light on the exhumation mechanisms that drove these rocks back to the surface after reaching their peak metamorphic conditions and enable to constrain the local tectonic setting of orogenic events at that time. A common assumption in articles investigating the thermal evolution of Archean metamorphic rocks is that these must have cooled at inherently slow rates, i.e. lower than 5°C/Ma, as a result of the higher radiogenic heat production happening within the > 3.0 Ga Mantle (Brown et al., 2022; Brown & Johnson, 2018; Herzberg et al., 2010; Korenaga, 2018; Scibiorski et al., 2015). Indeed, as stated by (Scibiorski et al., 2015) from their global compilation of cooling rates from Proterozoic to Phanerozoic orogens, the increase of cooling rates observed in high-grade metamorphic rocks with decreasing ages is interpreted to result from secular cooling of the Continental Crust and underlying Mantle. Nevertheless, modern plate tectonics are characterized by the coexistence of orogenic belts that experience contrasting thermal histories, such that characterizing the complexity of metamorphic cooling rates at any given time of the Earth's history appears just as essential as investigating their secular evolution.

The ca. 3.55 -3.21 Ga Barberton-Granitoid-Greenstone-Terrane (BGGT) in South Africa provides the right framework to investigate the cooling rates of Paleoarchean metamorphic rocks since extensive petrological, stratigraphic, structural and sedimentological studies going back to the 1960s have well documented the tectonic-magmatic-metamorphic processes that presided to its formation (Anhaeusser et al., 1969; Anhaeusser, 1980, 1981; Condie et al., 1970; De Wit et al., 1987; de Wit, 1982; J. F. Diener et al., 2005; J. F. A. Diener & Dziggel, 2021; Dziggel et al., 2002, 2005, 2006, 2006; Hofmann, 2005; Kamo & Davis, 1994; A. F. M. Kisters et al., 2003; Lowe, 1999; Lowe & Byerly, 2007; J. F. Moyen et al., 2021; J.-F. Moyen et al., 2006, 2007; Mühlberg et al., 2021; Nédélec et al., 2012; Schoene et al., 2008, 2009; Stevens et al., 2002). The BGGT present structural architecture of the

BGGT features the archetypal volcanic-sedimentary ("greenstone") rock association together with tonalite-trondhjemite-granodiorite (TTG) domes. It has been proposed that the entire terrane got assembled at ca. 3.2 Ga by the amalgamation of two separate microcontinents along the NE-SW tending Inyoni-Inyoka-Fault System (Zeh et al., 2009, **Figure 4-1A**). This episode led to burial of the granitoid-greenstone block South of the Komati-River Fault down to amphibolite facies conditions (J. F. Diener et al., 2005; Dziggel et al., 2002, 2005, 2006). However, while the tectonic setting is now better constrained, the exact duration of the main episode of (collision-related) metamorphism remains debated with some studies arguing for a 50 Myr-long regional metamorphism (K. A. Cutts et al., 2014; Kamo & Davis, 1994; Peng et al., 2019) and others, involving geochronological work, arguing for a <30 Myr-long event (J. F. Diener et al., 2005; Lana et al., 2010). A key question that remains unsolved is the rate at which these high-grade amphibolitized units were subsequently cooled from peak temperature of 600-700°C (J. F. A. Diener & Dziggel, 2021). Rutile grains found in amphibolitized felsic schists, interpreted to be deformed ca. 3.45 Ga meta-volcano-sediments, and identified by (J. F. Diener, 2004) and Combaz et al., (in revision) have potential to shed light on the likely cooling rate experienced by the Southern BGGT at 3.2 Ga. The objectives of the present work are therefore to (i) characterize these rutiles, which occur in >3.45 Ga volcano-sediments metamorphosed to P-T conditions of ca. 8-9 kbar-660°C, using LA-ICP-MS U-Pb and trace element analyses; and (ii) use the results to reconstruct the cooling rate experienced by rocks of the Southern BGGT.

4.2. Geological setting of the BGGT

The Barberton Greenstone Belt (BGB) is located in the Eastern Kaapvaal Craton, South Africa. The BGB is part of the Witwatersrand Block of (Eglington & Armstrong, 2004) and forms one of the best preserved Paleo-to- Mesoarchean supracrustal rock sequence in the world. It encompasses supracrustal lithologies emplaced from >3.55 Ga to ca. 3.21 Ga and the stratigraphic relationships with respect to surrounding granitoid-gneisses have been described since the late 1980s (Anhaeusser, 1976, 1980, 1981) and better emphasized in later studies (De Wit et al., 1987; de Wit, 1982; de Wit et al., 2011;

Heubeck & Lowe, 1994; Lowe, 1999; Lowe & Byerly, 1999, 2007). The greenstone lithologies are separated into three main lithostratigraphic groups:

- The Onverwacht Group (ca. >3.55 to ca.3.26 Ga) which is mostly made of mafic and ultramafic volcanic rocks (komatiites, basalt, Parman et al., 1997), felsic volcanic and volcano-clastic sequences (such as present in the Theespruit Formation, De Wit et al., 1987) and minor clastic sediments (Dziggel et al., 2002, 2006). The deposition of this group is diachronous across the belt with units of the Northern Terrane (**Figure 4-1**) deposited at a later time than units of the Southern Terrane (Lowe & Byerly, 2007).
- The Fig Tree Group (ca. 3.26 to 3.23 Ga) represent extrusive sequences of more evolved magmas, the latter commonly producing dacites, rhyodacites as well as chemical sediments of the BIF series (Byerly et al., 1996; Condie et al., 1970; Hofmann, 2005; Kohler & Anhaeusser, 2002).
- The Moodies Group (ca. 3.22 to 3.21 Ga) which is the final term of the Barberton sedimentary history and is mostly made of clastic sediments (sandstones, conglomerates) and minor volcanic tuff layers (Heubeck, 2019; Heubeck et al., 2022).

The greenstone belt is surrounded by voluminous granitoids-gneisses of different chemical affinities which can be lumped together into two different families, emplaced at different times. The Tonalite-Trondhjemite-Granodiorite (TTG) series is the earliest family and represents Na-rich granitoids that were emplaced at ca. 3550 Ma (Steynsdorp gneiss, e.g. Kröner et al., 1996, **Figure 4-1**), ca. 3456 Ma (Stolzburg and Theespruit plutons; Armstrong et al., 1990; Kamo & Davis, 1994; Laurent et al., 2020 **Figure 4-1B**) and ca. 3290-3210 Ma (Nelshoogte, Badplaas gneisses, Anhaeusser, 1983; A. F. Kisters et al., 2010; Matsumura, 2014; and Kaap Valley tonalite, Robb et al., 1986; **Figure 4-1**). Together with the BGB, these granitoids-gneisses form the Barberton-Granitoid-Greenstone Terrane (BGGT). The BGGT has been intruded at ca. 3100 Ma by a second family of granitoids, represented by voluminous K-rich alkaline granitoid laccoliths belonging to the Granite-Monzonite-Syenite suite (GMS, Clemens et al., 2010; Kamo & Davis, 1994; Santos Leandro et al., s. d.).

The BGGT experienced several deformation events from ca. 3.55 to 3.20 Ga, of which the main one occurred from ca. 3230 Ma to 3203 Ma (the D2 event, see references below). This event was associated with upper amphibolite facies metamorphic conditions, with maximum P/T conditions reaching ca.10 kbar and ca.650-700 °C as recorded by rock units of the Stolzburg Terrane (**Figure 4-1B**) (K. A. Cutts et al., 2014, 2021; J. F. Diener et al., 2005; J. F. A. Diener & Dziggel, 2021; Dziggel et al., 2002; Kato et al., 2018, 2018; J.-F. Moyen et al., 2006; Nédélec et al., 2012; Peng et al., 2019; Wang et al., 2019). This event correspond to the burial of the Stolzburg Terrane to garnet-amphibolite facies conditions in a classical thickening event of the crust, resembling that of Phanerozoic orogenic systems. The preservation of > 3.23 Ga U-Pb ages in igneous apatites of the Stolzburg and Theespruit Plutons identified by (Mühlberg et al., 2021) show that little partial melting of the 3.45 Ga trondhjemite has occurred during the 3.2 Ga collision event, thereby ruling out scenario of partial convective overturn of the crust proposed in earlier studies (Peng et al., 2019; Van Kranendonk et al., 2014; Wang et al., 2019). The Stolzburg Terrane thus behaved as a coherent, solid-state and cold tectono-metamorphic units and represent the footwall of the Komati River Normal Fault (**Figure 4-1B**) as described by (A. F. M. Kisters et al., 2003).

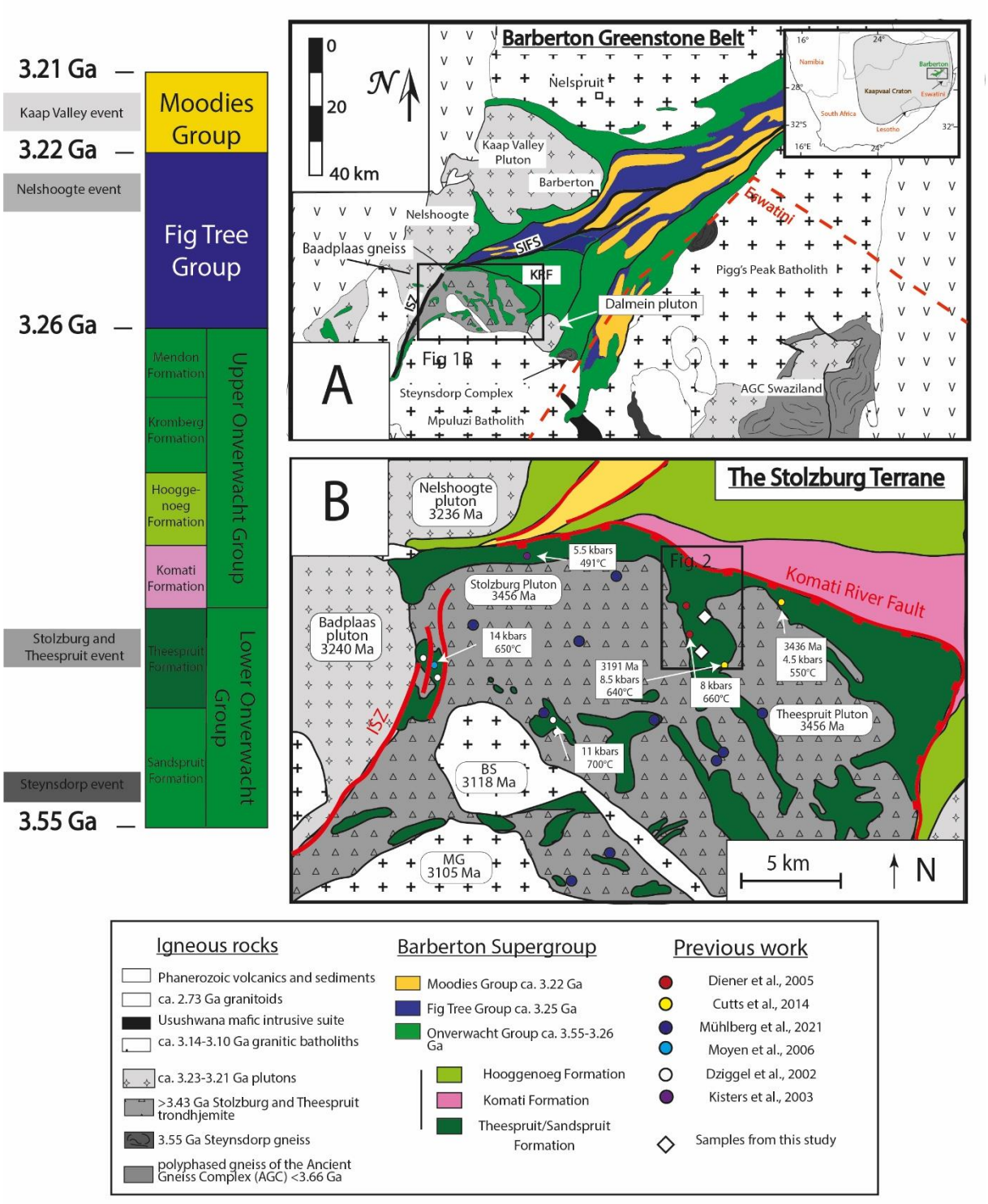

Figure 4-1 : Sketch geological maps of A) the Barberton Greenstone Belt (modified after Schoene et al., 2008, 2009 and Combaz et al., in revision) and regional map of the Stolzburg Terrane (modified after (Mühlberg et al., 2021) showing the position of outcrops sampled in this work and previous studies with associated P/T conditions (references in the legend). Igneous ages for the various granitoid gneisses are from (Laurent et al., 2020) for Stolzburg and Theespruit trondhjemitic plutons, (A. F. Kisters et al., 2010) for the Badplaas pluton, (Schoene et al., 2008) for the Nelshoogte pluton, (Kamo & Davis, 1994) for the Boesmanskop Syenite and the Mpuluzi Granite. SIFS = Saddleback-Inyoka Fault System, ISZ = Inyoni Shear zone, KRF = Komati River Fault, BS = Boesmanskop Syenite and MG = Mpuluzi Granite.

4.2.1. The Tjakastad Schist Belt

The samples investigated in this study were collected in the Tjakastad Schist Belt (TSB), which is part of the Theespruit Formation in the lower Onverwacht Group (**Figure 4-1B**). The TSB encompasses metamorphosed supracrustal rocks sequences of various felsic/silicic lithologies described as "felsic volcanics" or "volcano-clastic sediments" since the early 1980s (De Wit et al., 1987; de Wit, 1982). Protoliths of these metapelitic rocks in the TSB are difficult to ascertain given the substantial modification of the original fabric and mineral assemblages by metamorphic and alteration processes. Nevertheless, felsic schists from the North (muscovite-schists) are closer in mineralogy and composition to volcanic rocks, whereas schists from the South (garnet-staurolite-kyanite-schists) are much more likely to represent deformed Al-rich clastic sediments of pelitic composition (J. F. Diener, 2004). In the North, the age of deposition of the felsic volcano-clastic sequences is constrained through zircon U-Pb dating at ca. 3470-3480 Ma for two samples of felsic schists (TH11 and TH13 respectively), which are lithologically similar, and sampled in the immediate vicinity of TH12 (**Figure 4-2A**) Combaz et al., in revision). South of the Theespruit river, the youngest detrital zircons in a meta-sedimentary rock (TSB-03, see **Figure 4-2A**), arguably comparable to TSB-04, have a weighted mean age of 3507 ± 1.6 Ma (Combaz et al., in revision). The felsic lithologies of the TSB are intruded by the ca. 3456 Ma trondhjemitic plutons: the Stolzburg plutons in the West and the Theespruit pluton in the East (see **Figure 4-2**).

Together with the surrounding ca. 3456 Ma plutons, the TSB is part of the Stolzburg Terrane, a high-grade block of the BGGT that experienced 2 episodes of metamorphism from 3450 to 3200 Ma (**Figure 4-1B&4-2**):

1) An older, local event of contact metamorphism dated at 3436 ± 18 Ma (U-Pb in monazite of felsic schists; Cutts et al., 2014 – see outcrop position in **Figure 1B**) attributed to the intrusion of the Stolzburg and Theespruit plutons that heated up the intruded supracrustal sequences of the TSB. The peak P-T conditions for this early metamorphic event have been constrained to

4.5 kbars and 550°C through garnet compositions and phase diagram modelling (K. A. Cutts et al., 2014).

2) A younger metamorphic event of regional importance that reached amphibolite facies conditions up to the stability field of garnet (J. F. Diener et al., 2005; Dziggel et al., 2002, 2006; Lana et al., 2010; J.-F. Moyen et al., 2006) at ca. 3230 Ma. This event is documented by geothermobarometric studies conducted at different locations of the Stolzburg Terrane, showing that peak metamorphic conditions increase from the Komati River Fault to the greenstone remnants located in the center of the Stolzburg Pluton (**Figure 4-1B**). Peak P/T conditions of the amphibolite schists located close to the Komati river fault were constrained to 5.5 kbars-490°C (A. F. M. Kisters et al., 2003), to 6.1 kbars-570°C at locality 61406 (see **Figure 4-2A**, J. F. Diener et al., 2005), to ca. 10 kbars-610°C at locality Tj10 (**Figure 4-2A**, J. F. A. Diener & Dziggel, 2021) in the TSB, to 8 kbars-660°C at locality 62107 (**Figure 4-2A**, J. F. A. Diener & Dziggel, 2021) in the TSB and to ca. 11 kbars-700°C in the Sandspruit-age amphibolite clastic sediments of the central Stolzburg Domain (**Figure 4-1B**, J. F. A. Diener & Dziggel, 2021), the farthest from the Komati River Fault. We have represented the maximum metamorphic temperature recorded at different localities as isotherms in **Figure 4-2A**.

In the TSB, peak P-T conditions during the second, regional episode were attained at 3229 ± 5 Ma (U-Pb titanite dating by Dziggel et al., 2005) during the exhumation of the TSB felsic schists, as the peak mineral assemblage is present in the S-C schistosity planes that define the exhumation fabric of the rocks (J. F. Diener et al., 2005). This episode of burial is related to the main terrane accretion event (see above; Moyen et al., 2007; Stevens & Moyen, 2007) that juxtaposed the Southern and Northern Terranes of the BGB (sensu Zeh et al., 2009) along the Saddleback-Inyoka-Fault-System (SIFS). The collision at 3230 Ma was ultimately followed by exhumation of the Stolzburg Terrane along the Komati River Fault (**Figure 4-1B** and A. F. M. Kisters et al., 2003) in settings similar to metamorphic core complex formation. The entire metamorphic cycle reached an end before 3203 ± 7 Ma, which is the age of emplacement of the Dalmein pluton, a shallow intrusion truncating the high-grade greenstone stratigraphy and containing angular xenoliths of amphibolite-facies supracrustal rocks (Lana et al.,

2010). Cooling ages of ca. 3190 ± 19 Ma were obtained from hornblende Ar-Ar dating in ISZ amphibolites (Peng et al., 2019) and crystallization, U-Pb ages of monazite at 3191 ± 9 Ma in felsic schists on the eastern side of the Theespruit pluton (**Figure 4-1B**, K. A. Cutts et al., 2014). The monazite age is interpreted to reflect the age of retrograde metamorphism of the TSB, whereas the ages of hornblende in the ISZ are interpreted to reflect the cooling of the Stolzburg Terrane below closure temperature for Ar diffusion (ca. 500°C, Chew & Spikings, 2015).

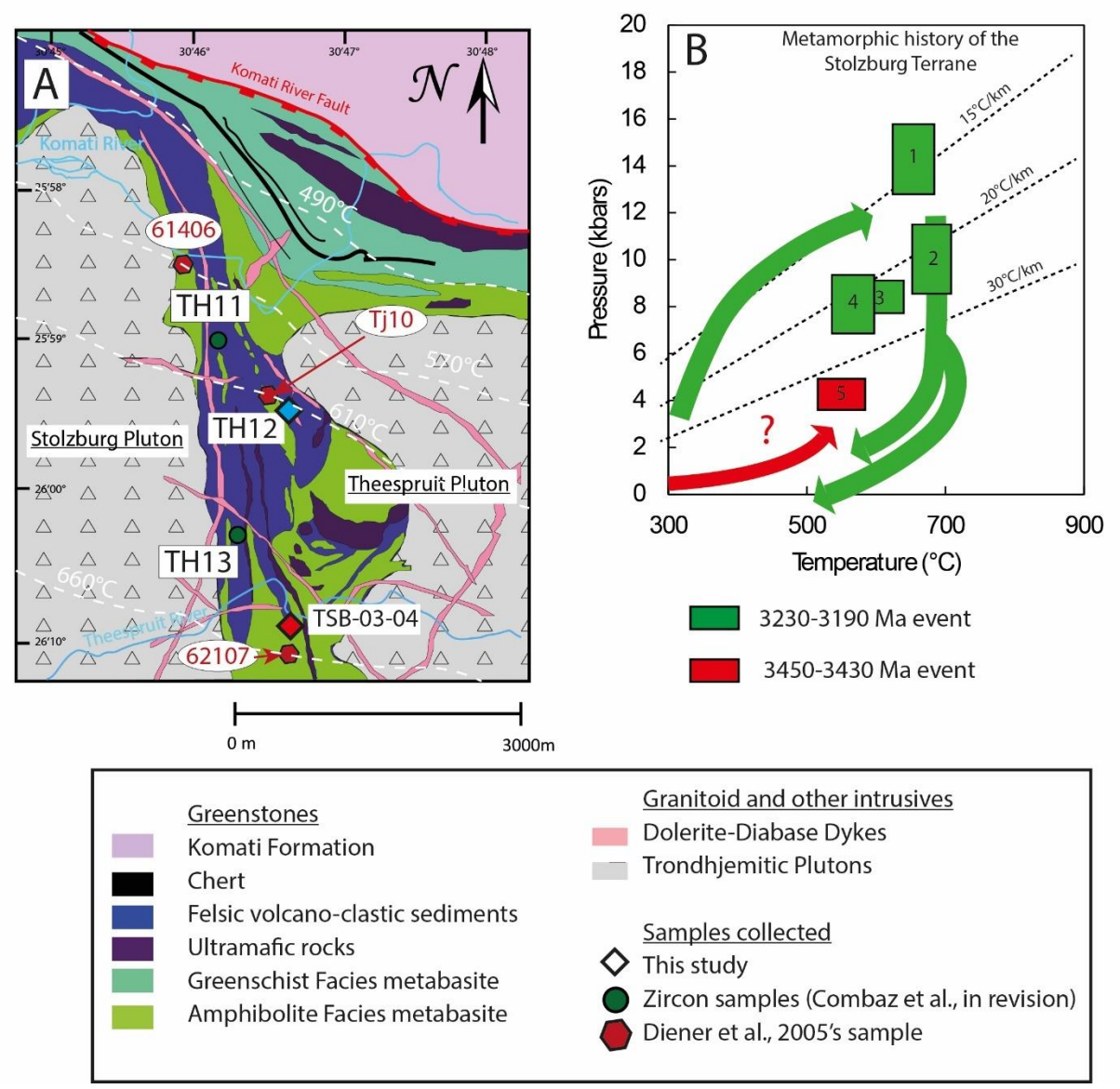

Figure 4-2: Local geologic context of samples investigated in this study. (A) Sketch geological map of the Tjakastad Schist Belt (after Diener et al., 2005) showing the location of samples investigated for zircon dating (Combaz et al., in revision) as well as sample Tj10, 61406 and 62107 of Diener et al., 2005. The white dashed lines represent isotherms of maximum metamorphic temperature from (Kisters et al., 2003, Dziggel et al., 2002, Diener et al., 2005 and Diener and Dziggel., 2021. (B) P-T diagram summarizing the metamorphic history of the Stolzburg Terrane with the conditions corresponding to the two metamorphic events (ca. 3450-3430 Ma and 3230-3190 Ma) shown as green and red boxes respectively. Note that the exact geometry of the prograde P-T path for 3436 Ma monazites from Cutts et al. 2014 is still not fully constrained (contact

metamorphism - question mark). Data from Moyen et al., 2006 (1), Dziggel et al., 2002 (2), Stevens et al., 2002 (3), Diener et al., (2005) (4) and Cutts et al., (2014) (5).

4.3. Materials and methods

4.3.1. Samples

Two samples of felsic schists belonging to the Theespruit formation were collected in the TSB (**Table 1**). More details on the petrography are provided below. Rutiles were extracted from crushed samples using conventional heavy mineral separation techniques (Wilfley table, hand panning, Frantz magnetic separator), handpicked, set in 1-inch epoxy mounts and polished. More details of the mineral separation techniques used are provided in Combaz et al. 2025.

Sample	Stratigraphic position	Location	Lithology	Latitude	Longitude
TH12	Theespruit Formation, Lower Onverwacht Group	Tjakastad Schist Belt	Qz-Ms-felsic schist	-25.049722	30.873333
TSB-04	Theespruit Formation, Lower Onverwacht Group	Tjakastad Schist Belt	Grt-St-Ky-Ms felsic schist	-26.013972	30.783972

Table 4-1 : Geographic, Lithological and Stratigraphic information about the samples investigated in this study.

4.3.2. SEM

The internal structures of the rutile grains were characterized by back-scattered electron images (BSE), using the Vega4 (Tescan) scanning electron microscope (SEM) equipped with a BSE detector at Géosciences Environnement Toulouse, France. Instrumental conditions were an acceleration voltage of 15 keV and beam current of 3 nAImage resolution was set to 1024 × 1024 pixels with a sweep time of ca. 34 s per image, corresponding to a dwell time of ca. 31 ms per pixel.

4.3.3. LA-ICP-MS

Simultaneous analyses of U-Pb isotopes and trace elements in rutiles were conducted by laser ablation – inductively coupled plasma – mass spectrometry (LA-ICP-MS) at the Service ICP-MS of Observatoire Midi-Pyrénées (OMP-UAR831), Toulouse, France. The analyses were carried using a NWRfemto (Elemental Scientific Instruments) solid-state femtosecond laser ablation system set to UV

mode (257 nm wavelength) coupled with an Element XR (ThermoScientific) sector-field ICP-MS. Measurements were performed with a laser spot diameter of 40 µm, a repetition rate of 8 Hz for TH12 and 5 Hz for TSB-04 and an energy density of ca. 3.5 J/cm^2. Ablation was performed in the built-in, dual-volume, fast-washout ablation cell (<1 cm^3 effective volume) flushed with He carrier gas (ca. 0.6 L/min) to which was admixed Ar make-up gas (ca. 0.85 L/min) downstream of the ablation cell before introduction in the plasma. A typical run consisted of three pre-ablation pulses (for surface cleaning) followed by 7 seconds washout; 15 seconds of background signal acquisition; and 20 seconds of ablation. The list of acquired masses, corresponding dwell times, details about the instrument optimization and data acquisition procedures are provided in the **Supplementary material to Chapter 4**.

The resulting intensities were processed offline with the Iolite v4.0 software, using the U-Pb geochronology data reduction scheme with VizualAge add-in (after Petrus & Kamber, 2012). The R10 rutile reference material (using isotope ratios from Luvizotto et al., 2009) was used as primary standard for correction of instrumental drift, mass bias and laser-induced U/Pb fractionation through conventional standard-sample bracketing following the procedure of (Zack et al., 2011). Secondary rutile standards R13 (Schmitt & Zack, 2012a) and WODB (Schirra & Laurent, 2021) were analyzed as unknowns to confirm the accuracy of the results. The obtained U-Pb ages for all secondary standards (see **Supplementary material to Chapter 4**) are accurate within the total bulk reproducibility of the method, estimated at ca. 2% relative [2σ] (see below). The data from unknowns and reference materials are provided in **Supplementary material to Chapter 4**. Concordia diagrams and age distributions were constructed using the IsoplotR online package (Vermeesch, 2018). Systematic uncertainties were propagated in the uncertainties of pooled ages (i.e. calculated from the average of several individual data points) as recommended by (Horstwood et al., 2016) and employing a long-term excess scatter of 2% relative on both $^{206}Pb/^{238}U$ and $^{207}Pb/^{206}Pb$ ages, based on results of multiple sessions during which the R13 reference material has been analyzed at OMP over a period of about 4 years.

Trace element concentrations were calibrated against the NIST SRM610 glass reference material (Jochum et al., 2011). The same signal integration intervals as defined for U-Pb dating were used for

trace element quantification, ensuring that both are obtained on the same rutile volume. The stoichiometric Ti content of rutile (60 wt.%) was used as internal standard for relative sensitivity correction. Natural rutile reference material R10 was employed to check for any remaining matrix effect due to the high Ti concentration difference between NIST SRM610 and rutile, and a further correction factor (typically in the order of 15–20% relative) was applied to rutile element concentrations as to get HFSE (Zr, Hf, Nb, Ta) and W contents in R10 matching those analyzed by ID-MC-ICP-MS by Luvizotto et al. (2009). The results show that trace element quantification is accurate within the analytical reproducibility of the method (between 5% and 20% relative depending on the element and concentration **Supplementary material to Chapter 4**). More details about the analytical conditions can be found in **Supplementary material to Chapter 4**; the data from unknowns and reference materials are provided in **Supplementary material to Chapter 4**.

4.4. Results

4.4.1. Sample petrography and rutile morphology

Samples collected in this study present different mineralogical compositions and textures. TH12 (collected in the North, 1km away from the Theespruit pluton, see **Figure 4-2**) is quartz-muscovite-rich schist (**Figure 4-3A&B**) of probable volcano-clastic origin, whereas TSB-04 is a garnet-kyanite-staurolite-phengite bearing schist (**Figure 4-3C&4-3D**) resembling those described by (J. F. Diener et al., 2005) and more typically corresponds to a schistose, clastic meta-sediment. Garnet, kyanite and staurolite occur as early porphyroclasts partially disaggregated and replaced by phengite and quartz (**Figure 4-3C&4-3D**). In both samples, rutile occurs as an accessory phase included within muscovite (or phengite) and/or quartz, which define the main schistosity of the rock. TSB-04 produced much larger crystals than in TH12 (mean diameter is estimated to be 80 µm in TH12 and 200 µm in TSB-04, **Figure 4-3E&4-3F**). Under BSE images, TH12 rutiles contain inclusions of quartz, albite and chlorite, whereas TSB-04 rutiles are mostly inclusion-free, besides a few that contain quartz. In both samples, rutile shows little to no chemical zoning in BSE images (**Figure 4-4**). TH12 rutile crystals,

while being smaller, also have more rounded edges than those of TSB-04 (**Figure 4-4A and 4-4C**). Additionally, no evidence of exsolution lamellae of zircon and/or baddeleyite was observed in either sample. The different rutile grain size fractions investigated separately in sample TSB-04 (75-90 µm; 90-125 µm; 125-250µm, see supplementary table S3) did not reveal any systematic difference in terms of crystal morphologies and proportion/diversity of inclusions.

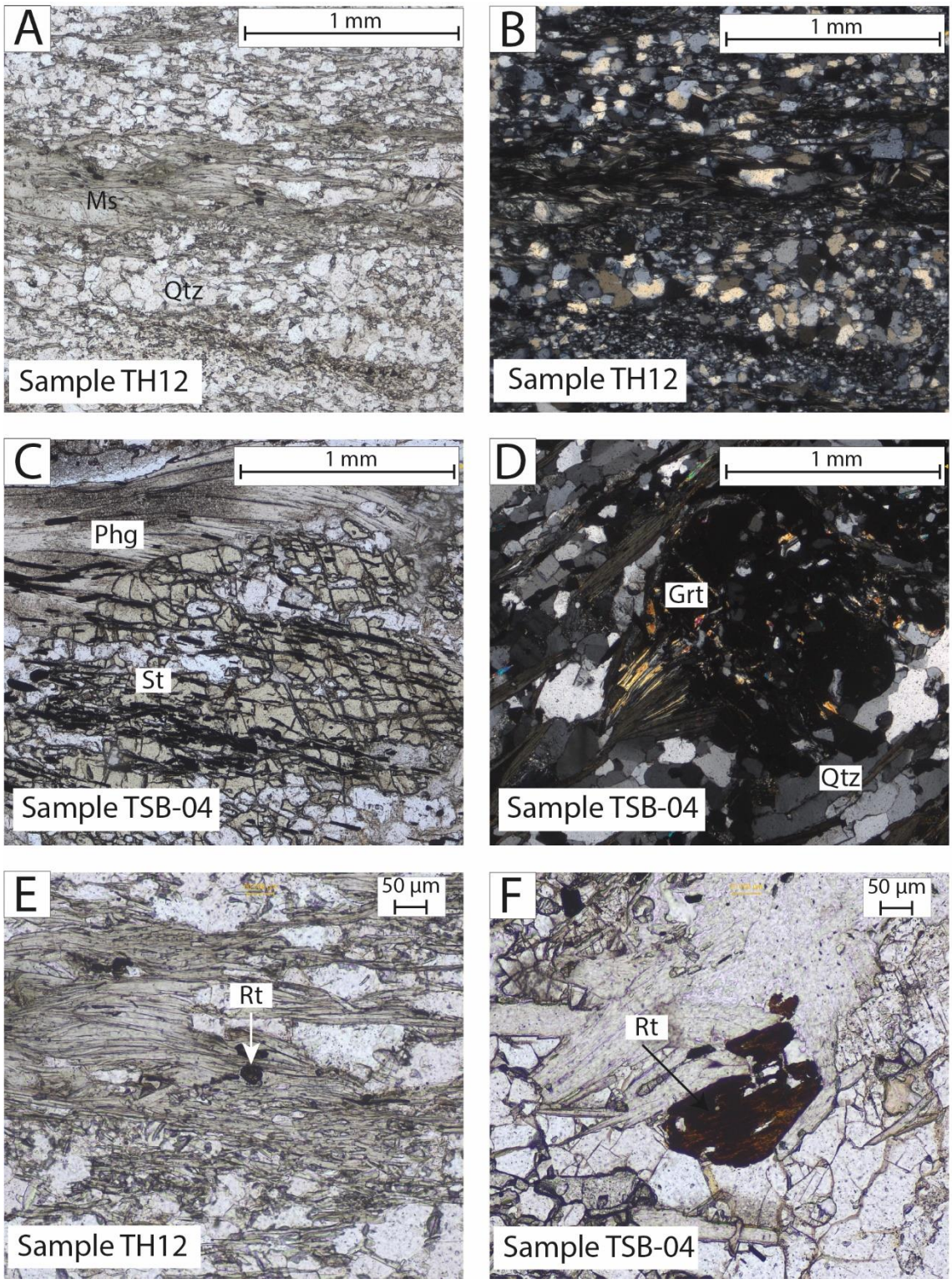

Figure 4-3 : Representative thin section photomicrographs of samples investigated in this study. (A) plan-polarized light (PPL) and (B) crossed-polarized light (CPL) images of sample TH12 (schistose felsic meta-volcani(clasti)c rock); (C) PPL and (D) XPL images of sample TSB-04 (schistose clastic meta-sediment). Representative PPL images of rutile crystal morphologies in TH12 (E) and TSB-04 (F) are also shown. Ms = muscovite; Grt = garnert; Qtz = quartz; Rt = rutile; Phg = phengite.

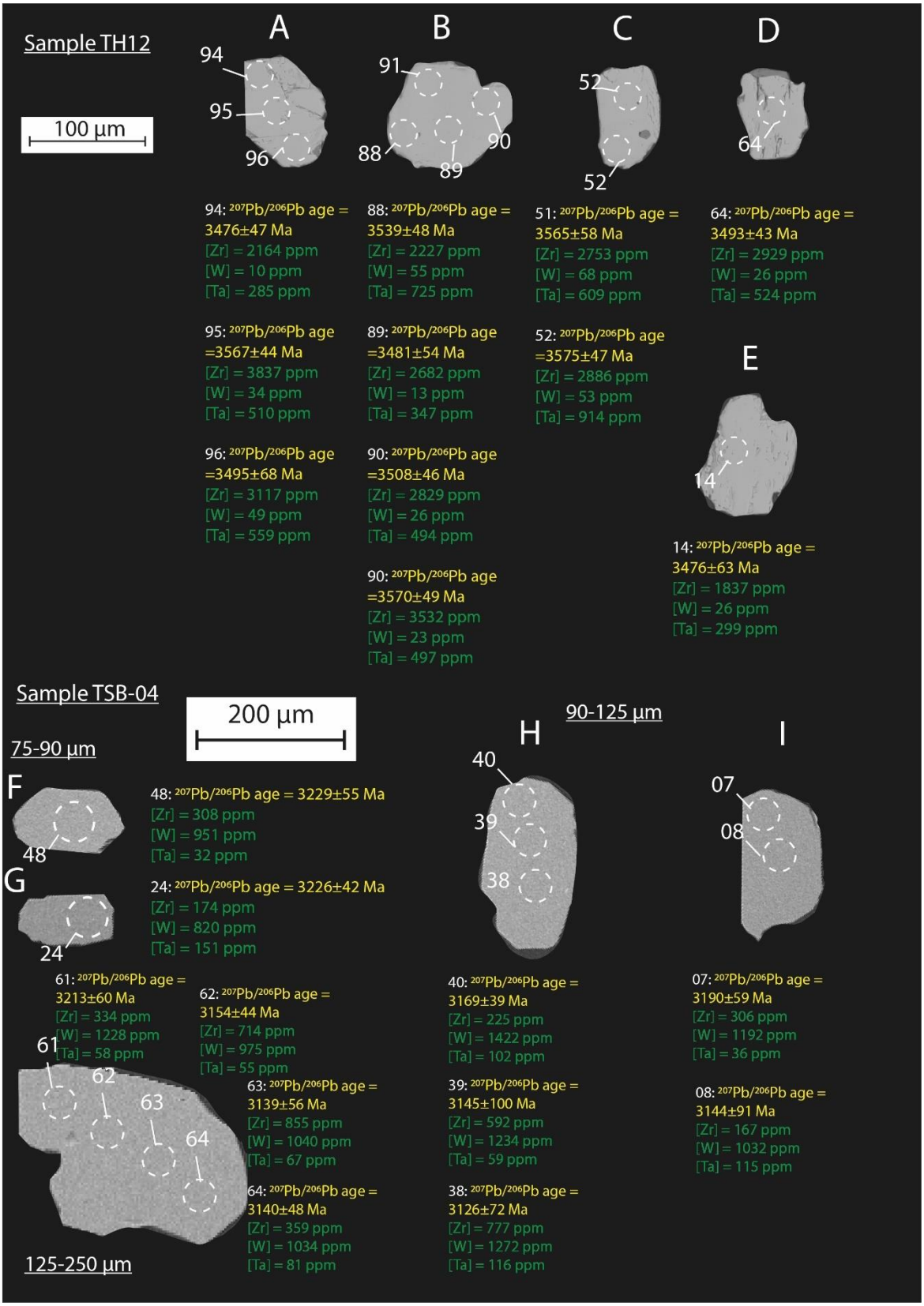

Figure 4-4: Representative back-scattered electron images of rutiles of the Tjakastad Schist Belt with geochronological (yellow) and geochemical (green) information associated with LA-ICP-MS spots (dashed circles).

4.4.2. Rutile U-Pb dating

Due to the small size of TH12 rutiles (mean diameter ca. 80µm), only 6 grains could be analyzed at different locations. Three examples are shown in **Figure 4-4** (grains A, B and C). In the case of TSB-04, rutiles belonging to the three size fractions (75-90 µm, 90-125 µm and 125-250 µm, see **Supplementary material to Chapter 4** and **Figure 4-4**) were analyzed separately to assess the potential influence of grain size on retention of chemical and chronological properties (Cherniak, 2000; Kohn, 2016, 2020; Zack & Kooijman, 2017). In total, 143 simultaneous U-Pb and trace-element analyses were carried out in TH12 rutiles and 311 in TSB-04 rutiles (including 67 in the 75-90 µm; 100 in 90-125 µm; 144 in 125-250 µm, see **Supplementary material to Chapter 4**).

In both samples, a significant range of $^{207}Pb/^{206}Pb$ dates is observed, with an increase of $^{207}Pb/^{206}Pb$ dates with increasing ^{204}Pb content (**Figure 4-5A**). Therefore, we interpret the observed spread of $^{207}Pb/^{206}Pb$ dates as reflecting the presence of common Pb (Pb_c), which is a common feature in rutile (Bracciali et al., 2013; Schmitt & Zack, 2012b; Zack et al., 2007, 2011; Zack & Kooijman, 2017). We have decided to exclude rutile analyses for which ^{204}Pb contents are above 1.5 ppm (open diamonds in **Figure 4-5A&B**), which corresponds to the average limit of detection (see **Supplementary material to Chapter 4**– analyses not considered in the interpretation were labelled "not used" in these tables). Even after filtering for analyses containing significant Pb_c, rutile data for both samples show significant scatter in Tera-Wasserburg diagrams (**Figure 4-6A&B**). Most analyses are indeed sub-concordant but spread along the Concordia between ca. 3650 and 3300 Ma for TH12 (**Figure 4-6A**) and between ca. 3400 and 3100 Ma for TSB-04 (**Figure 4-6B**). Nonetheless, concordant data from both rutile populations have statistically different distributions of $^{207}Pb/^{206}Pb$ dates. TH12 rutiles show a near-normal distribution with a clear mode at ca. 3510 Ma (**Figure 4-6C**) whereas for TSB-04, the distribution is asymmetrical, with a peak at ca. 3180 Ma and a tail towards older dates up to ca. 3600 Ma (**Figure 4-6D**).

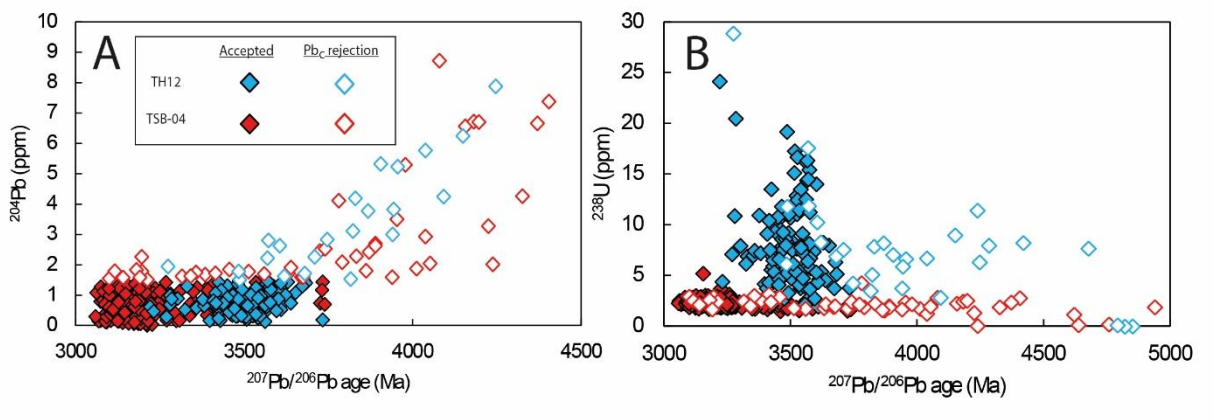

Figure 4-5: Plots of ^{204}Pb (A) and ^{238}U (B) concentration in analyzed rutiles as a function of $^{207}Pb/^{206}Pb$ dates. The open symbols correspond to analyses with >1.5 ppm ^{204}Pb considered as too rich in common Pb (Pb_c) to yield meaningful U-Pb dates.

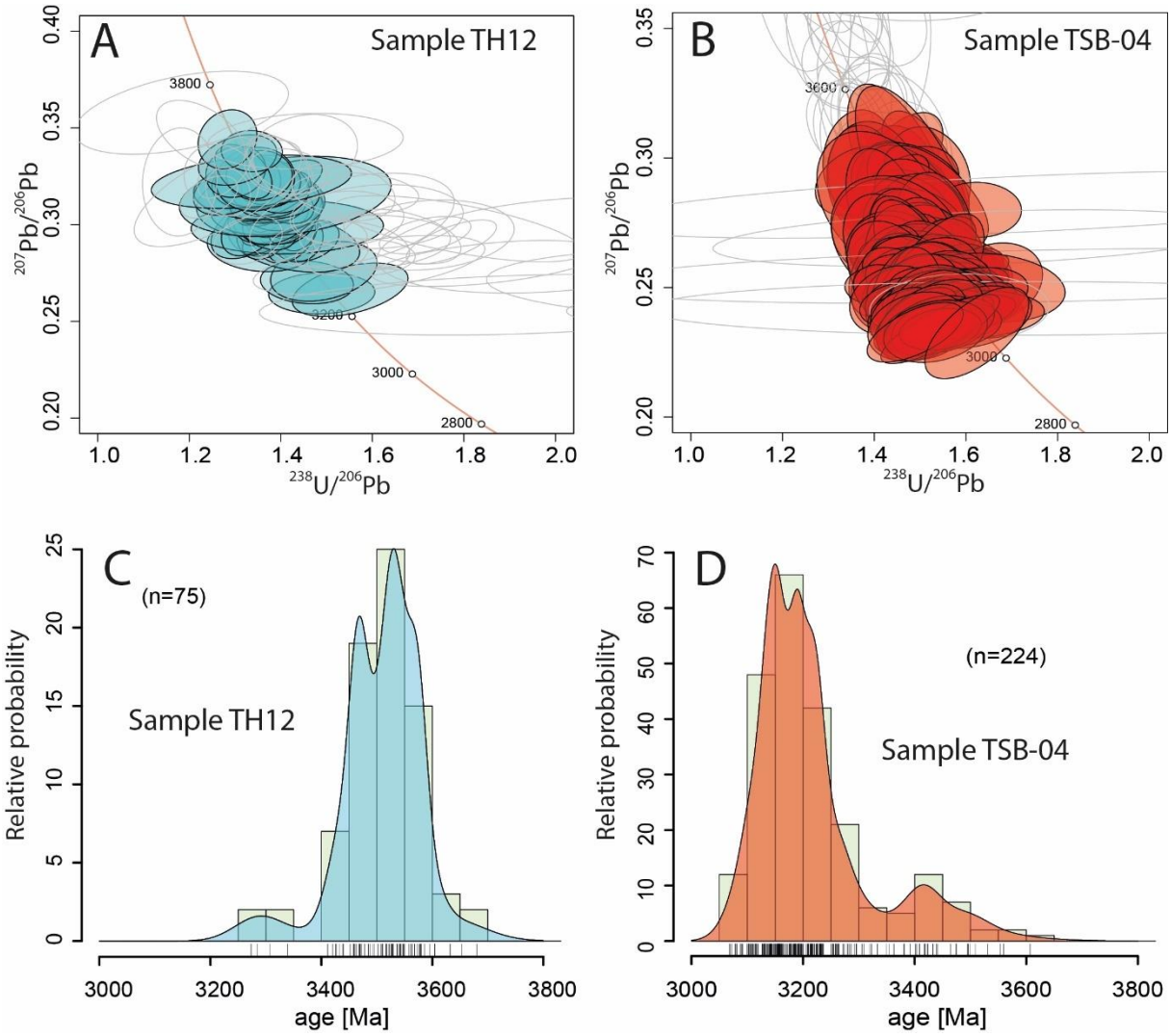

Figure 4-6: Geochronological data for rutiles of the Tjakastad Schist Belt. Graph A and B are Tera-Wasserburg plots for rutile samples TH12 (A) and TSB-04 (B). Colored ellipses represent spots that are concordant and with [Pb_c] below limit of detection (LOD) whereas grey ellipses show discordant and common Pb-rich spots. Graphs C and D show histograms and Kernel Density Estimates of $^{207}Pb/^{206}Pb$ dates of both rutile samples, only showing concordant data with [Pb_c] < LOD.

In details, there is no systematic correlation between $^{207}Pb/^{206}Pb$ date and grain size and/or the position of the analytical spot in a given rutile crystal. In sample TSB-04, 55 grains were analyzed at multiple spot locations, with selected core-to-rim date profiles illustrated in **Figure 4-7A&4-7-E**. While rare grains show systematic variations, notably rims apparently older than the cores (**Figure 4-7A)** or the opposite (**Figure 4-7C**), most analyzed crystals show homogenous intra-grain patterns of $^{207}Pb/^{206}Pb$ dates (**Figure 4-7B&E&F**), with rare outliers (**Figure 4-7C&D**). In fact, at the scale of one grain, outlying $^{207}Pb/^{206}Pb$ dates are commonly grouped in the same area of the crystal (see e.g. points #2 in **Figure 4-7C** and#5 in **Figure 4-7D**) such that in general, the observed intra-grain variations likely

reflect minor disturbance of the U-Pb system, in particular Pb_c incorporation. TH12 rutiles analyzed multiple times show the same homogeneous pattern (**Figure 4-7F** and **Figure 4-4**).

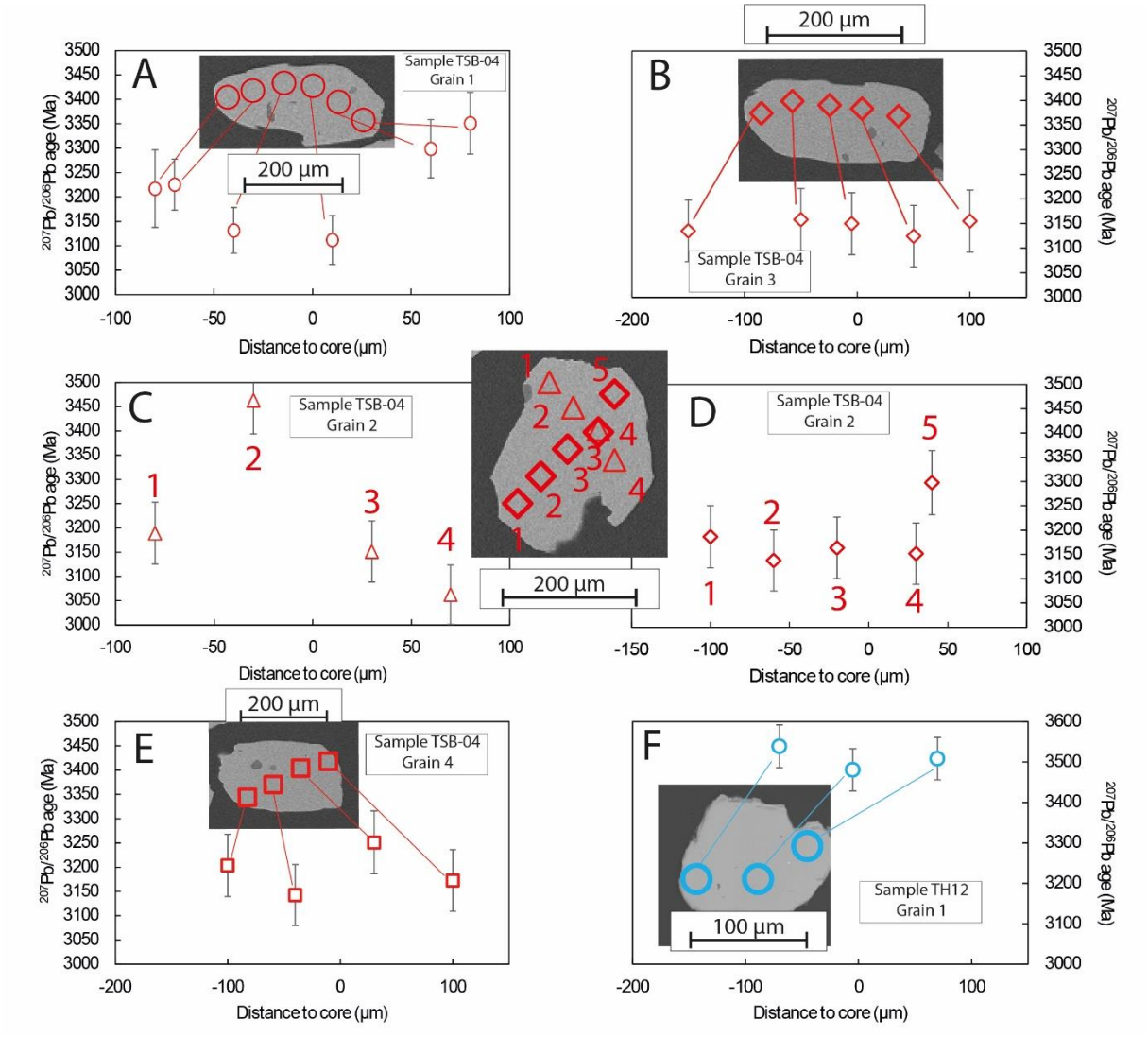

Figure 4-7: Results of selected age profiles performed in rutile grains from the TSB samples, including BSE image with position of analytical spots and corresponding $^{207}Pb/^{206}Pb$ dates arranged as a function to the distance to the geometric core of the grain.

4.4.3. Rutile trace element data

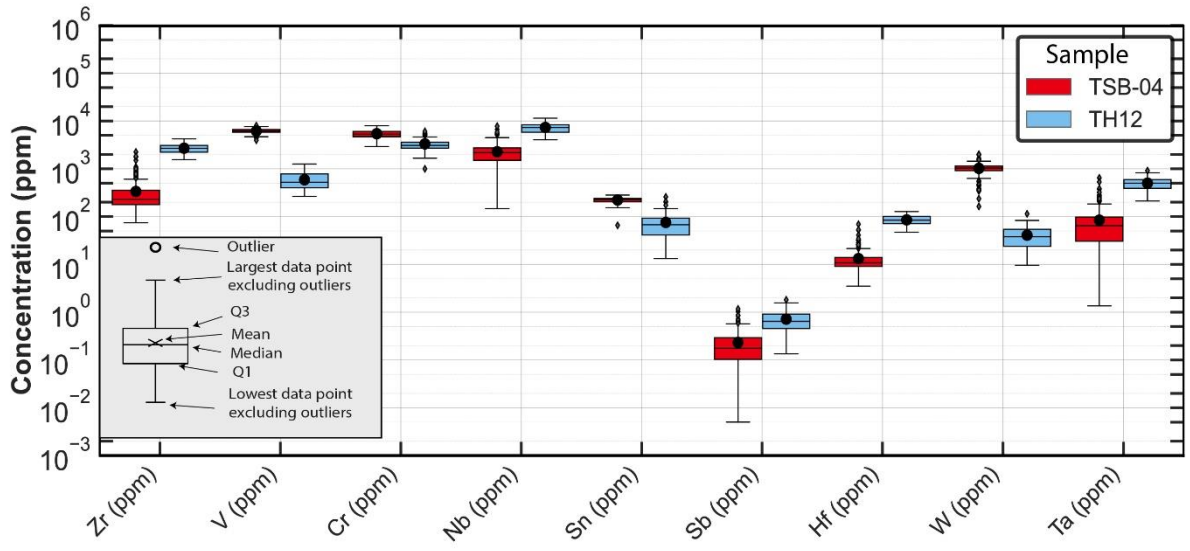

Figure 4-8 : Boxplots showing the distribution of selected trace element concentrations in rutiles from the two studied TSB samples.

The rutiles analyzed in this study show limited to no variability (within uncertainties) of trace element compositions at the scale of individual grains or even within a given sample. However, they show contrasting chemical compositions between the two samples investigated (**Figure 4-8**). Notably, TH12 rutiles display much higher Zr (mean ca. 2700 ppm), Nb (mean ca. 7300 ppm) and Ta (mean ca. 500 ppm) contents than TSB-04 (mean Zr ca. 300 ppm, mean Nb ca. 2300 ppm and mean Ta ca. 80 ppm) (**Figure 4-8**). On the other hand, TH12 rutiles have notably lower W and Cr contents (mean ca. 40 and 3300 ppm respectively) than TSB-04 rutiles (mean ca. 1000 and 5400 ppm respectively). Although both populations show very low amounts of Sb, Sn and Hf, differences between the two samples persist for these elements (for TH12 and TSB-04, mean contents are 0.88 vs. 0.23 ppm for Sb; 82 vs. 228 ppm for Sn and 83 vs. 13 ppm for Hf) (**Figure 4-8**).

4.5. Discussion

4.5.1. Thermometry and chemistry of rutiles from the TSB

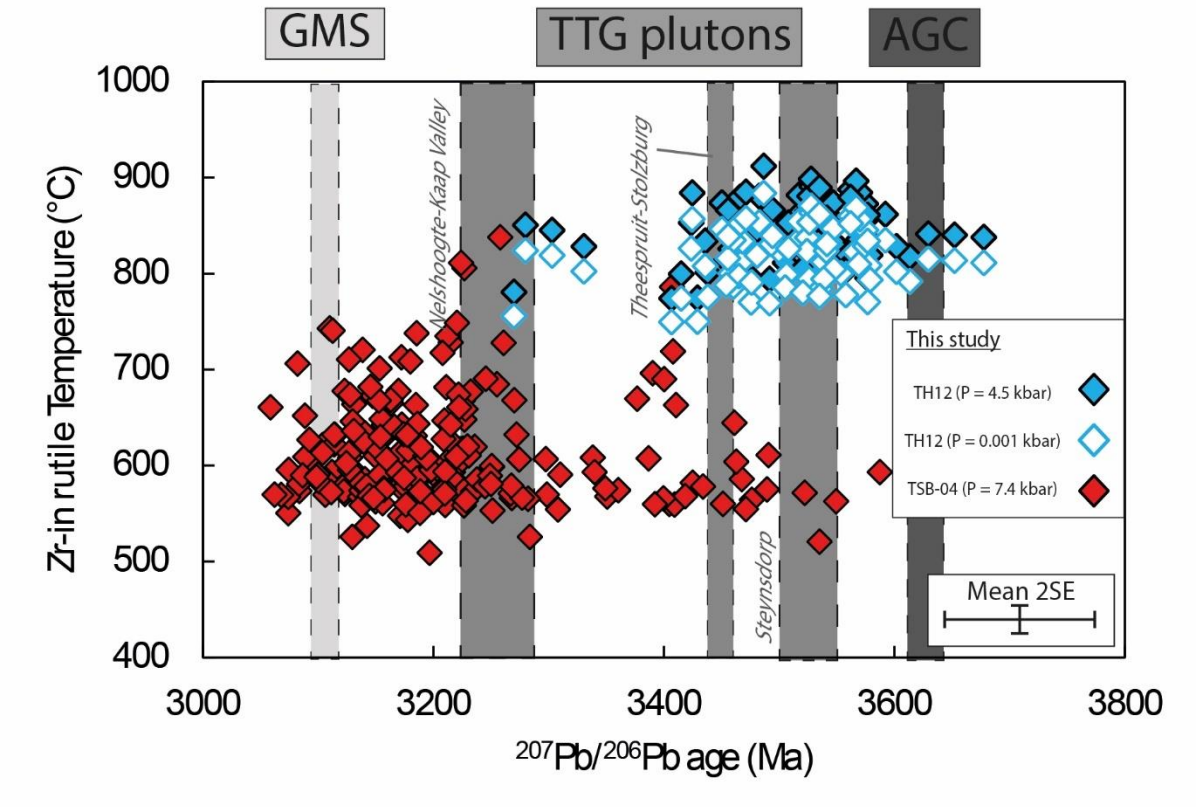

Figure 4-9: Plot of calculated Zr-in-rutile temperatures (after Kohn, 2020) for the TSB rutiles, assuming pressures of 5 kbar for both samples). Temperatures were also calculated at 1 bar for TH12 to test the pressure dependence of the calculated temperatures (see text for details). Uncertainties correspond to the 2SE analytical uncertainties for the Pb-Pb ages and ±15°C for the temperature (Kohn, 2020). The shaded grey vertical bars correspond to documented felsic igneous events in the BGGT (ages after Compston & Kröner, 1988; Kröner et al., 2013 for the AGC; Laurent et al., 2020; Moyen et al., 2007 for the TTGs; and Santos Leandro et al., s. d. for the GMS)

The contrasting Zr content of both rutile samples (**Figure 4-8**) translates into different crystallization temperatures. We have utilized the combined model of (Kohn, 2020) to calculate the Zr-in-rutile temperatures (**Figure 4-9**), assuming that quartz and zircon were both present and in equilibrium at the time rutile crystallized. This is a reasonable assumption given the fact that zircons were found in lithologically similar (volcano-sediments or clastic sediments assimilable to pelites, see result section above) and nearby samples TH11, TH13 and sample TSB-03 (Combaz et al., in revision) and that quartz is present in the rock and as inclusions in rutile for both samples (cf **Figure 4-3** and **4-**

4). Pressure does not significantly impact the calculation of Zr-in rutile temperature as calculation conducted at 5 kbar on one hand and 0.001 kbar on the other hand produced temperatures that differ by ca. 3.5% relative only so we used a minimum P estimate of 5 kbar for both samples to allow comparison. Since metapelitic rutile generally crystallizes at pressure conditions higher than that of amphibolite facies metamorphism (Force, 1980; Pereira et al., 2021; Triebold et al., 2012; Zack, Moraes, et al., 2004), 5 kbar is a conservative but reasonable assumption. The results show that the higher Zr contents of TH12 rutiles (cf. **Figure 4-8**) translates to significantly higher temperatures than the Zr-poorer TSB-04 rutiles, with mean values of 846 °C vs. 601°C (± ca. 40°C) respectively (**Figure 4-9**).

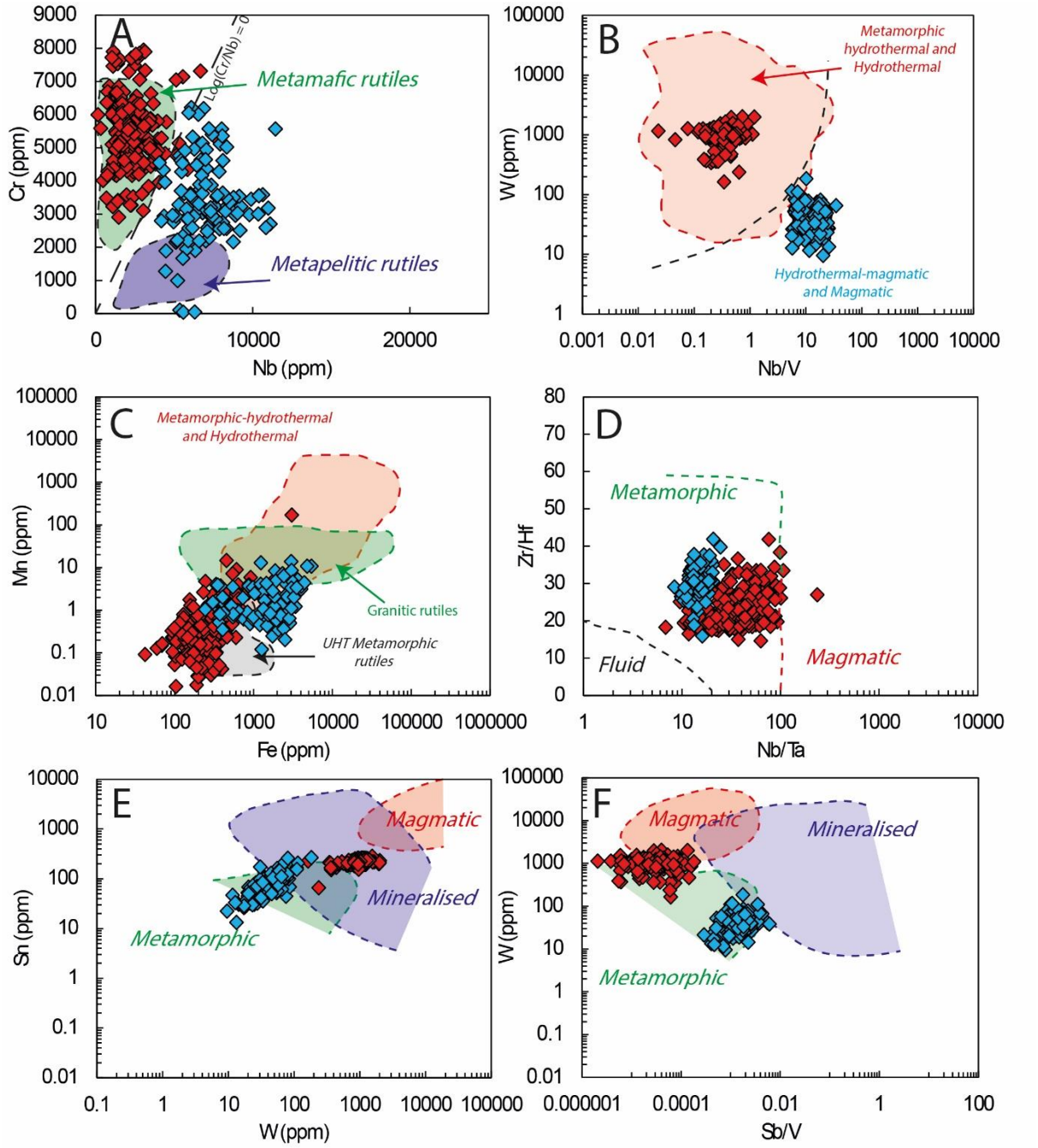

Figure 4-10: Trace element composition of the TSB rutiles plotted in proposed binary discrimination diagrams for rutile from different rock types: (A) Cr vs Nb plot from Meinhold et al., 2008; Pereira et al., 2021; Triebold et al., 2012; Zack, von Eynatten, et al., 2004; (B) W vs Nb/V and (C) Mn vs Fe plots from Sciuba and Beaudoin (2021); (D) Zr/Hf vs Nb/Ta, (E) Sn vs W and (F) W vs Sb/V from Pereira et al (2021).

We have plotted the trace element compositions of both rutile populations in diagrams proposed to discriminate rutile from different rock types. It turns out that TH12 rutiles have high Cr vs Nb contents overlapping with that of metapelitic rutiles **(**Figure 4-10A, Pereira et al., s. d.; Triebold et al., 2007, 2012), an observation that is consistent with their petrographic context (metamorphosed silica-

rich felsic volcanic rocks, see section above) and their notably higher U content (**Figure 4-5B**) which overlap with most rutiles derived from pelitic sources (Zack & Kooijman, 2017). On the other hand, TSB-04 rutiles have a Cr vs Nb pattern (and U contents) that show strong similarity with rutiles of meta-igneous mafic sources (**Figure 4-10A**). However, such high Cr contents are commonly observed in Archean sediments (Maslov, 2007; Taylor & McLennan, 1983), so that this feature of TSB-04 rutiles might just reflect a relatively mafic, Cr-rich composition of the sedimentary protolith. Furthermore, the reliability of the Cr vs Nb graph to discriminate metapelitic vs metamafic rutiles has been recently cautioned: Zack & Kooijman (2017) showed that rutile data from both mafic and pelitic rocks formed a single cluster overlapping the metamafic vs metapelitic dividing line.

In fact, in all other trace element plots, rutiles from each sample define a relatively well-constrained compositional cluster, suggesting that they represent single populations with a common origin for all the grains. In the Mn vs Fe, Zr/Hf vs Nb/Ta, Sn vs W and W vs Sb/V diagrams, the chemistry of the TSB rutiles from both samples overlap to a large extent with that described for metamorphic rutiles (**Figure 4-10C–F**), which supports a metamorphic origin. This is particularly true for TSB-04 rutiles. For these, a metamorphic origin is further backed by the petrographic context of these grains, occurring in textural association with the retrograde phengitic muscovite + quartz assemblage replacing the peak mineral assemblage of garnet + staurolite (see **Figure 4-3**), and their dominant population of $^{207}Pb/^{206}Pb$ dates at ~3150-3250 Ma (**Figure 4-6D&9**) matching the age of the main regional metamorphic event ((J. F. Diener et al., 2005; Dziggel et al., 2002, 2006; J.-F. Moyen et al., 2006), as further discussed below. In the case of TH12 rutiles, their high Nb/V ratio overlaps with that of hydrothermal–magmatic rutiles (**Figure 4-10B**), which may suggest the participation of some magmatic-derived fluids in their crystallization (possibly related to the intrusion of the Theespruit pluton at 3456 Ma, Laurent et al., 2020). Also, TSB-04 rutiles show notably high W content (**Figure 4-8D&10E**), which is a typical feature of hydrothermal rutile (Schirra & Laurent, 2021) and thus suggests the involvement of a fluid in their crystallization. Additionally, both populations show different Sn vs W and W vs Sb/V patterns from one another but both plot outside the range described for magmatic rutiles (**Figure 4-10E&F**).

Collectively, this suggests that TH12 and TSB-04 rutiles are most likely of metamorphic origin, with the possible involvement of fluids in their crystallization. Their different trace element clustering is herein interpreted as a signature of their different protolith composition (meta-volcano-clastic for TH12, vs metamorphosed clastic sediments for TSB-04) and/or of the composition of the hydrothermal fluid, which results in distinct co-existing mineral assemblages.

4.5.2. Age of rutiles in the Tjakastad Schist Belt

From the above section, it is clear that both rutile samples differ in their trace element chemistry (while being all metamorphic in origin) and Zr-in rutile temperature with TH12 showing high-temperature (ca. 850°C) and TSB-04 showing low temperature of crystallization (ca. 600°C). They also differ in terms of age distribution with dominant populations at ca. 3400-3550 Ma and 3150-3250 Ma respectively (**Figure 4-6**), suggesting that they record two metamorphic events of very different ages. However, in both cases, we observe a notable scatter of $^{207}Pb/^{206}Pb$ dates that deserves discussion as this scatter covers, or even exceeds, the entire documented range of ages for tectono-metamorphic events of the BGGT (**Figures 4-5, 4-6** and **4-9**).

4.5.2.1. TH12 rutile

Rutile in TH12 shows ca. 30% of grains apparently older than 3550 Ma (up to 3670 Ma, **Figure 4-9**), i.e. older than the crystallization age of a felsic volcanic rock of the Steynsdorp anticline at 3510.0 ± 2 Ma (Kröner et al., 1996b), representing the oldest identified igneous event in the BGGT. This could mean, at first glance, that TH12 represent detrital grains derived from an older, and somewhat distal high-grade metamorphic rocks, like the up-to-3.66 Ga-old Ancient Gneiss Complex in Eswatini and/or some unpreserved equivalent. In that case, these >3550 Ma rutiles would be expected to show more variable trace element patterns, consistent with a detrital origin (Pereira & Storey, 2023). However, this does not match with the intra-sample chemical homogeneity of TH12 rutiles, that show little variations between the >3550 Ma and the 3400-3550 Ma populations, as discussed in the previous section (see

Figure 4-8 and **Figure 4-10**). In this regard, rutiles with ages >3550 Ma most likely represents grains with minor Pb_c incorporation, which affected the $^{207}Pb/^{206}Pb$ dates but not ^{204}Pb to the point that it could be measured at the (relatively high) state-of-the-art detection limits of LA-ICP-MS (**Figure 4-5A**) (see also section 4.4.2). Further, 4 concordant data points show a range of $^{207}Pb/^{206}Pb$ dates younger than the main population, i.e. between 3270 and 3400 Ma (**Figure 4-6**), and presumably correspond to partially reset rutile crystals during the regional, ca. 3200 Ma metamorphic event (**Figure 4-11**).

A number of studies both from field work (D. Cloete, 1993; M. Cloete, 1999; Van Kranendonk et al., 2009) and accessory minerals geochronology (K. A. Cutts et al., 2014) have suggested that the Lower Onverwacht strata (including the TSB) must have experienced an early episode of contact metamorphism at the time of intrusion of the Theespruit and Stolzburg plutons at ca. 3456 Ma (see recent U-Pb dating from Laurent et al., 2020). Cutts et al., 2014 have dated metamorphic monazite at 3436 ± 18 Ma in a andalusite-kyanite-rich felsic schist recording P-T conditions of 4.5 kbar and 550°C. Rutiles investigated here show a main range of $^{207}Pb/^{206}Pb$ dates between ca. 3410 and 3550 Ma (**Figure 4-6**), which combined with the similar proximity to the Theespruit pluton, apparently supports the idea of TH12 rutiles crystallizing in similar contact metamorphic conditions. The youngest weighted mean date that can be obtained from the main population of sample TH12, i.e. excluding >3550 Ma and <3400 Ma analyses and keeping only the younger end of the dominant age population as to get a statistically meaningful, single population (MSWD of ca.1), is 3474 ± 8 Ma | 70 Ma (excluding | including propagation of systematic uncertainties; MSWD = 1.3; n = 34) (**Figure 4-11**). Considering the systematic uncertainty of ± 70 Ma (**Figure 4-11**), the similar distance between the Theespruit pluton and both our sample TH12 and that hosting ca. 3436 Ma monazites (Cutts et al., 2014) (**Figure 4-1B**) supports a crystallization of both minerals during the intrusion of the Theespruit pluton at ca. 3456 Ma. With that said, the high Zr-in rutile temperature calculated above requires that TH12 rutiles crystallized during the early, high-temperature stages of intrusion of the Theespruit pluton, in which case the monazite would have crystallized later, after significant cooling has occurred (down to temperatures of ca. 550°C, Cutts et al., 2014). In this case, considering a minimum cooling rate of granitic plutons of ca. 10°C/Ma in Phanerozoic settings (Floess & Baumgartner, 2015), cooling from ca. 850°C to 550°C

would require a maximum time of 30 Myr. This is within the range of the total uncertainties reported on both rutile and monazite ages.

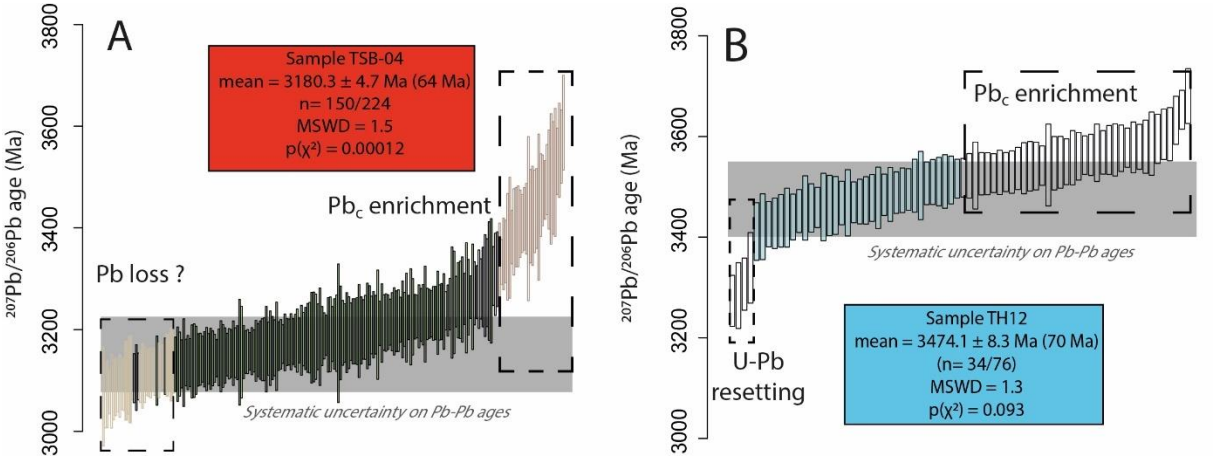

Figure 4-11: Weighted mean ages of TSB-04 (A) and TH12 (B) rutiles with rejected measurements (and reasons specified). Uncertainties including the propagated 2% systematic uncertainties are indicated between brackets in the colored box and as a grey bar on the plots.

4.5.2.2. TSB-04 rutile

Although a number of TSB-04 rutiles show $^{207}Pb/^{206}Pb$ dates >3240 Ma, these are texturally and chemically undistinguishable from the dominant and younger population (**Figure 4-10**), such that similar to TH12, these are interpreted as grains containing minor Pb_c (not identified based only on ^{204}Pb signals) (**Figure 4-11**). In addition, a number of analyses show significantly younger ages (<3120 Ma) than the youngest recorded magmatic event in the area, i.e. the intrusion of the GMS suite at ca. 3120-3100 Ma (Kamo and Davis, 1994; Zeh et al., 2009) and must therefore reflect some extent of Pb loss during this younger event. Excluding both the oldest and youngest analyses accordingly and keeping as many analyses as possible as to get a statistically meaningful population, the calculated weighted mean age is 3180 ± 6 Ma | 64 Ma (excluding | including propagation of systematic uncertainties; MSWD = 1.5; n = 150). This age well overlaps, within the propagated systematic uncertainties of ± 64 Ma (**Figure 4-11**), with the age of the main metamorphic event at ca. 3230-3203 Ma documented by (K. A. Cutts et al., 2014; J. F. Diener et al., 2005; Dziggel et al., 2005; Lana et al., 2010) and support cooling of TSB-04 rutiles under their closure temperature for Pb diffusion during that time.

The retrograde crystallization of rutile in TSB-04 is supported by the calculated mean Zr-in-rutile temperature of 601°C, i.e. lower than peak temperature conditions experienced by the Stolzburg Terrane at ca. 3230 Ma (ca. 600-700°C, J. F. Diener et al., 2005; J. F. A. Diener & Dziggel, 2021; Dziggel et al., 2002; A. F. M. Kisters et al., 2003; J.-F. Moyen et al., 2006) and by the microtextural context of the rutiles (**Figure 4-3**), occurring within the retrograde assemblage of quartz and muscovite replacing garnet and staurolite. Exactly how soon after crystallization were the TSB-04 cooled under the closure temperature for Pb diffusion will be discussed in the next section.

4.5.3. Implications for the thermal history of the Stolzburg terrane

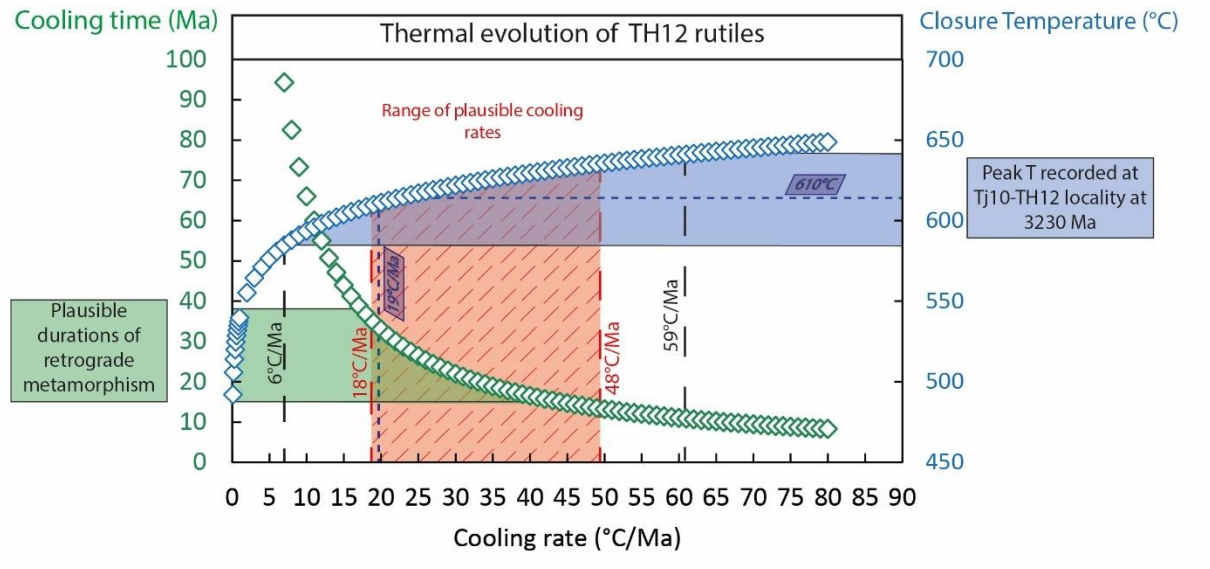

Figure 4-12: Evolution of closure temperature (blue diamonds) and cooling time (green diamonds) as function of the cooling rate of TH12 rutile grains. The blue area represents the Temperature recorded by sample Tj10 (Diener et al., 2005) including ±30°C of uncertainties. This brackets the cooling rates of TH12 rutile grains between 6 and 59°C/Ma. The utilization of

minimum and maximum duration of retrograde metamorphism allowed by data from Lana et al., 2010 (green area) helps to narrow down this range to between 18 to 48°C/Ma (red dashed area in the center.

While the systematic uncertainties on the measured rutile ages are high and, thus, do not allow for a precise assignment of the crystallization of the two rutile samples to a specific time in the geologic history of the Stolzburg Terrane, both rutile populations still preserve statistically different U-Pb ages (**Figure 4-6&9&11**), beyond analytical uncertainties. A trivial conclusion from the above discussion is that TH12 rutiles, despite their small sizes, went through the ca. 3230-3203 Ma metamorphic event (and later GMS-derived heating at ca. 3120-3100 Ma) without being significantly reset to younger ages. Considering the maximum metamorphic temperatures recorded in the Stolzburg Terrane of 500-700°C (increasing from ca. 490°C in schists close to the Komati River Fault to ca. 700°C in amphibolite greenstone remnants in the South, see J. F. Diener et al., 2005; J. F. A. Diener & Dziggel, 2021; Dziggel et al., 2002; A. F. M. Kisters et al., 2003 and **Figure 4-2A**), arguably covering the range of closure temperatures for Pb diffusion in rutile (Cherniak, 2000), this requires that both the heating and subsequent cooling of TH12 rutiles were geologically fast.

Using the local maximum metamorphic temperature of 610 ± 30 °C recorded by sample Tj10 (J. F. A. Diener & Dziggel, 2021), arguably the closest in distance to our sample TH12 (**Figure 4-2A**), we have calculated the minimum cooling rate a hypothetical spherical rutile 80 µm in diameter (typical size of TH12 grains) could undergo without having its U-Pb clock being reset, based on the T_c calculation of (Dodson, 1973; Kohn, 2016). The details of the calculation are provided in the **supplementary material to chapter 4**. The minimum cooling rates obtained range between 6°C/Ma for the lower-end estimate of peak temperature, to 59C/Ma for the upper-end estimate, with a median value of 22C/Ma at 610°C (**Figure 4-12**). Using this range of cooling rates, the TSB-04 locality, which was heated up to ca. 660°C (see J. F. A. Diener & Dziggel, 2021), would reach the Zr-in rutile temperature of 601°C in less than 1 to less than 10 Myr, with a median value of ca. 3 Myr. Additionally, reaching a mean Archean surface temperature of ca. 20°C (Catling & Zahnle, 2020) from peak

temperature in the TSB of 660°C would necessitate 11 to 110 Myr with a median time of 33 Myr (see **Figure 4-12**).

Angular xenoliths of amphibolite-facies supracrustal rocks of the Theespruit Formation in the Dalmein granodiorite, indicating little mixing between both lithologies, suggests that cooling of the Stolzburg Block was largely terminated by the time the Dalmein pluton intruded the stratigraphy at 3203 ± 7 Ma (Lana et al., 2010). Considering the peak metamorphic age of 32290 ± 5 Ma (Dziggel et al., 2005), this places an upper limit on the duration of retrograde metamorphism to 14 to 38 Myr (considering uncertainties) and, therefore, refines the possible cooling rates of the TSB to ca. 15 to 50°C/Ma. Considering all geochronological and metamorphic constraints from (Lana et al., 2010) and (J. F. A. Diener & Dziggel, 2021), this is interpreted as the likely minimum cooling rate experienced by TH12 rutiles.

While it would be a foregone conclusion to apply this cooling rate to the entire Stolzburg Terrane without further thermochronological work, we note that such high cooling rates are consistent with claims made by (J. F. Diener et al., 2005) who suggested fast exhumation of felsic schists in the TSB in less than 30 Myr at tectonic rates of 2-5 mm/a to allow for preservation of peak mineral assemblages. Moreover, a recent study by (Mühlberg et al., 2021) has demonstrated the preservation of ca. 3450 Ma U-Pb ages within the cores of igneous apatites of the Stolzburg trondhjemite throughout the ca. 3230 Ma metamorphic event and this, on a regional scale (see position of samples from Mühlberg et al., 2021 in **Figure 4-1B**). This observation also requires a sufficiently fast cooling of the Stolzburg trondhjemite after peak conditions to avoid resetting of the U-Pb system in apatite, in which T_c are even lower than in rutile (Chew et al., 2011; Chew & Spikings, 2015, 2021). This confirms that the cooling rates calculated from TH12 rutiles are minimum values and may be apply regionally. In turn, the Stolzburg Block must have behaved as a coherent solid and cold block during burial and exhumation at ca. 3230-3200 Ma. The preservation of ages significantly older than ca. 3.1 Ga for both rutile populations excludes any major influence of heat dissipation from the Mpuluzi batholith and other GMS granitoids onto the Stolzburg Terrane at 3.1 Ga as previously suggested by (Kamo & Davis, 1994; Schoene et al., 2008) as this would have likely reset both rutile samples more uniformly to ca. 3.1 Ga

ages, even more so when considering the small size of TH12 rutiles (ca. 80 µm Cherniak, 2000). Neither rutile samples seem to have been affected by the alleged heating of the BGGT at 3.1 Ga.

4.5.4. Tectonic exhumation of a Mesoarchean cold orogenic core

The range of cooling rates calculated in the present work overlap with that described in Phanerozoic orogenic systems (Abbott et al., 1997; Brown et al., 2022; Brown & Dallmeyer, 1996; Vanderhaeghe et al., 2003; Willigers et al., 2002; Zou et al., 2020) but are so far not documented for Archean metamorphic rocks (Scibiorski et al., 2015) which are, instead, expected to cool at rates lower than 5°C/Ma as a result of the presumably higher heat budget of the Archean continental crust and underlying mantle (Herzberg et al., 2010; Korenaga, 2018, 2021). Cooling rates above 22°C/Ma are commonly observed during the final stages of extension in modern post-orogenic contexts (Ring et al., 1999) where deep-seated rock units experience tectonic-mediated exhumation (Byrne et al., 2024b; England & Thompson, 1986, 1984; Giuntoli et al., 2024; Jamieson & Beaumont, 2013; Scibiorski et al., 2015) and supports the idea of the Stolzburg Terrane representing a metamorphic core complex as proposed by (A. F. M. Kisters et al., 2003). Indeed, metamorphic core complexes in Phanerozoic settings cool at inherently high rates, up to c.a. >50°C/Ma (Gardien et al., 2022; Huet et al., 2011; Labrousse et al., 2016; Virgo et al., 2018) and their exhumation can be tectonically accommodated through low-angle shear zone/faults as footwall blocks as shown in the Neoproterozoic Eastern Adirondack Highlands by (M. S. Wong et al., 2012). The Komati River Fault (**Figure 4-1B**) would be the tectonic break that drives exhumation of the Stolzburg Terrane (A. F. M. Kisters et al., 2003). Therefore, the present discovery enables further categorization of the >3.2 Ga Stolzburg Terrane into the "small, cold orogen" (SCO) of (Jamieson & Beaumont, 2013) because these are the orogenic belts that produce fast cooling rates of their lower crustal roots due to low radiogenic heat buildup and limited thickening (<50 km). This is opposed to Large Hot Orogens (LHO) where the thermal insulation of the middle-to-lower crust (often leading to partial melting thereof) makes cooling of the lower crustal units inherently slow (below 5°C/Ma, see Ashwal et al., 1999; Rivers, 2008; Schulmann et al., 2008), as documented e.g. in the Himalayas (Hacker et al., 2014; Nelson et al., 1996) or the Variscan belt (Laurent et al., 2023). While the data derived from the TSB rutile cannot be globally applied to other Archean

terranes without further investigation of metamorphic rutiles in other cratons, the present work still has significance to nuance the assumption of Archean orogens being uniformly hot, as argued by (Scibiorski et al., 2015).

4.6. Conclusion

The present work has described two samples of metamorphic rutiles preserved in ca. 3.47-3.51 Ga felsic volcanic rocks and clastic sediments of the Tjakastad Schist Belt. Both samples show contrasting U-Pb ages (3474 ± 70 Ma vs. 3180 ± 64 Ma) as well as remarkable differences in trace element chemistry and Zr-in rutile temperature (850°C vs. 601 °C, respectively), yet both interpreted as reflecting metamorphic rutile crystallization (during contact metamorphism and retrograde exhumation following the peak of regional metamorphism, respectively). The absence of resetting of the U-Pb system of ca. 3474 Ma rutiles during the main tectono-metamorphic event at ca. 3230-3200 Ma, together with geochronological and metamorphic constraints from the literature, enabled us to determine a cooling rate of 22 (+37/-16) °C/Myr corresponding to the exhumation of the Stolzburg Terrane after reaching peak metamorphic conditions. Such fast cooling rates are not presently documented in Archean high-grade metamorphic rocks but they bracket cooling rates observed in core complexes during the final stages of post-orogenic extension in Phanerozoic time. The cooling of the Stolzburg felsic crust at rates of ca. 22°C/Ma confirms the role of tectonic faults in the tectonic denudation of an Archean small, cold, orogenic core and calls for a reappraisal of the diversity in thermal regimes of Archean tectonic-metamorphic events.

4.7. Acknowledgements

The PhD project of J.B.C. has been supported by National Research Foundation grant CNRS-129351 (South Africa) as part of the BuCoMO project, the University of Toulouse TREMPLIN grant PRESIZION and by the EUR TESS N°ANR-18-EURE-0018 in the framework of the Programme des Investissements d'Avenir. We thank the Mpumalanga Tourism and Park Agency for giving us access to the Komati Nature Reserve. We thank M. Vinicius Santos Leandro, J.F. Moyen and A. Chauvet for help and guidance during fieldwork and comments on data interpretation. We are grateful to J. Delport and J.P. Nel for help with SELFRAG operation and rutile separation; S. Choy for help with rutile picking and mounting; F. Maubé for help with SEM imaging; A. Marquet and J. Chmeleff for assistance with LA-ICP-MS analyses.

4.7. References to chapter 4

Abbott, L. D., Silver, E. A., Anderson, R. S., Smith, R., Ingle, J. C., Kling, S. A., Haig, D., Small, E., Galewsky, J., & Sliter, W. S. (1997). Measurement of tectonic surface uplift rate in a young collisional mountain belt. *Nature*, *385*(6616), 501-507. https://doi.org/10.1038/385501a0

Angiboust, S., & Harlov, D. (2017). Ilmenite breakdown and rutile-titanite stability in metagranitoids : Natural observations and experimental results. *American Mineralogist: Journal of Earth and Planetary Materials*, *102*(8), 1696-1708.

Anhaeusser, C. R. (1976). Archean metallogeny in southern Africa. *Economic Geology*, *71*(1), 16-43.

Anhaeusser, C. R. (1980). A geological investigation of the Archaean granite-greenstone terrane south of the Boesmanskop syenite pluton, Barberton Mountain Land. *South African Journal of Geology*, *83*(1), 93-106.

Anhaeusser, C. R. (1981). Geotectonic evolution of the Archaean successions in the Barberton Mountain land, South Africa. In *Developments in Precambrian Geology* (Vol. 4, p. 137-160). Elsevier. https://www.sciencedirect.com/science/article/pii/S0166263508700112

Anhaeusser, C. R. (1983). *The geology of the Schapenburg greenstone remnant and surrounding Archaean granitic terrane south of Badplaas, Eastern Transvaal*. https://pascal-francis.inist.fr/vibad/index.php?action=getRecordDetail&idt=6522482

Anhaeusser, C. R. (2014). Archaean greenstone belts and associated granitic rocks–a review. *Journal of African Earth Sciences*, *100*, 684-732.

Anhaeusser, C. R., Mason, R., Viljoen, M. J., & Viljoen, R. P. (1969). A reappraisal of some aspects of Precambrian shield geology. *Geological Society of America Bulletin*, *80*(11), 2175-2200.

Armstrong, R. A., Compston, W., De Wit, M. J., & Williams, I. S. (1990). The stratigraphy of the 3.5-3.2 Ga Barberton Greenstone Belt revisited : A single zircon ion microprobe study. *Earth and Planetary Science Letters*, *101*(1), 90-106.

Ashwal, L. D., Tucker, R. D., & Zinner, E. K. (1999). Slow cooling of deep crustal granulites and Pb-loss in zircon. *Geochimica et Cosmochimica Acta*, *63*(18), 2839-2851. https://doi.org/10.1016/S0016-7037(99)00166-0

Bonnet, G., Chopin, C., Locatelli, M., Kylander-Clark, A. R. C., & Hacker, B. R. (2022). Protracted Subduction of the European Hyperextended Margin Revealed by Rutile U-Pb Geochronology Across the Dora-Maira Massif (Western Alps). *Tectonics*, *41*(4), e2021TC007170. https://doi.org/10.1029/2021TC007170

Bracciali, L., Parrish, R. R., Horstwood, M. S., Condon, D. J., & Najman, Y. (2013). UPb LA-(MC)-ICP-MS dating of rutile : New reference materials and applications to sedimentary provenance. *Chemical Geology*, *347*, 82-101.

Brown, M., & Dallmeyer, R. D. (1996). Rapid Variscan exhumation and the role of magma in core complex formation : Southern Brittany metamorphic belt, France. *Journal of Metamorphic Geology*, *14*(3), 361-379. https://doi.org/10.1111/j.1525-1314.1996.00361.x

Brown, M., & Johnson, T. (2018). Secular change in metamorphism and the onset of global plate tectonics. *American Mineralogist*, *103*(2), 181-196. https://doi.org/10.2138/am-2018-6166

Brown, M., Johnson, T., & Spencer, C. J. (2022). Secular changes in metamorphism and metamorphic cooling rates track the evolving plate-tectonic regime on Earth. *Journal of the Geological Society*, *179*(5), jgs2022-050. https://doi.org/10.1144/jgs2022-050

Byerly, G. R., Kröner, A., Lowe, D. R., Todt, W., & Walsh, M. M. (1996). Prolonged magmatism and time constraints for sediment deposition in the early Archean Barberton greenstone belt : Evidence from the Upper Onverwacht and Fig Tree groups. *Precambrian Research*, *78*(1-3), 125-138.

Byrne, T., Chojnacki, M., Lewis, J., Lee, J.-C., Ho, G.-R., Yeh, E.-C., Lee, Y.-H., Tsai, C.-H., Evans, M., & Webb, L. (2024a). Tectonic exhumation of a metamorphic core in an arc-continent collision during oblique convergence, Taiwan. *Progress in Earth and Planetary Science*, *11*(1), 23. https://doi.org/10.1186/s40645-024-00627-w

Byrne, T., Chojnacki, M., Lewis, J., Lee, J.-C., Ho, G.-R., Yeh, E.-C., Lee, Y.-H., Tsai, C.-H., Evans, M., & Webb, L. (2024b). Tectonic exhumation of a metamorphic core in an arc-continent collision during oblique convergence, Taiwan. *Progress in Earth and Planetary Science*, *11*(1), 23. https://doi.org/10.1186/s40645-024-00627-w

Cagnard, F., Durrieu, N., Gapais, D., Brun, J.-P., & Ehlers, C. (s. d.). *Crustal thickening and lateral flow during compression of hot lithospheres, with particular reference to Precambrian times*. Consulté 10 octobre 2025, à l'adresse https://onlinelibrary.wiley.com/doi/10.1111/j.1365-3121.2005.00665.x

Catling, D. C., & Zahnle, K. J. (2020). The Archean atmosphere. *Science Advances*, *6*(9), eaax1420. https://doi.org/10.1126/sciadv.aax1420

Chardon, D., Gapais, D., & Cagnard, F. (2009). Flow of ultra-hot orogens : A view from the Precambrian, clues for the Phanerozoic. *Tectonophysics*, *477*(3), 105-118. https://doi.org/10.1016/j.tecto.2009.03.008

Cherniak, D. J. (2000). Pb diffusion in rutile. *Contributions to Mineralogy and Petrology*, *139*(2), 198-207. https://doi.org/10.1007/PL00007671

Chew, D. M., & Spikings, R. A. (2015). Geochronology and thermochronology using apatite : Time and temperature, lower crust to surface. *Elements*, *11*(3), 189-194.

Chew, D. M., & Spikings, R. A. (2021). Apatite U-Pb Thermochronology : A Review. *Minerals*, *11*(10), Article 10. https://doi.org/10.3390/min11101095

Chew, D. M., Sylvester, P. J., & Tubrett, M. N. (2011). U–Pb and Th–Pb dating of apatite by LA-ICPMS. *Chemical Geology*, *280*(1-2), 200-216.

Clemens, J. D., Belcher, R. W., & Kisters, A. F. (2010). The Heerenveen batholith, Barberton Mountain Land, South Africa : Mesoarchaean, potassic, felsic magmas formed by melting of an ancient subduction complex. *Journal of Petrology*, *51*(5), 1099-1120.

Cloete, D. (1993). *Processing Remotely Sensed Data for Geological Content Over a Part of the Barberton Greenstone Belt, Republic of South Africa* [Master's Thesis, University of the Witwatersrand, Johannesburg (South Africa)]. https://search.proquest.com/openview/5cfcd55e3605de82a0efba46f3e2c020/1?pq-origsite=gscholar&cbl=2026366&diss=y

Cloete, M. (1999). *Aspects of volcanism and metamorphism of the Onverwacht group lavas in the South-Western portion of the Barberton greenstone belt.* [PhD Thesis]. https://wiredspace.wits.ac.za/items/cd520741-8d50-41a3-851e-bbc95bf82b2b

Collins, W. J. (2002). Hot orogens, tectonic switching, and creation of continental crust. *Geology*, *30*(6), 535-538. https://doi.org/10.1130/0091-7613(2002)030%253C0535:HOTSAC%253E2.0.CO;2

Compston, W., & Kröner, A. (1988). Multiple zircon growth within early Archaean tonalitic gneiss from the Ancient Gneiss Complex, Swaziland. *Earth and Planetary Science Letters*, *87*(1-2), 13-28.

Condie, K. C., Macke, J. E., & Reimer, T. O. (1970). Petrology and geochemistry of early Precambrian graywackes from the Fig Tree Group, South Africa. *Geological Society of America Bulletin*, *81*(9), 2759-2776.

Cutts, J. A., Smit, M. A., Kooijman, E., & Schmitt, M. (2019). Two-Stage Cooling and Exhumation of Deeply Subducted Continents. *Tectonics*, *38*(3), 863-877. https://doi.org/10.1029/2018TC005292

Cutts, K. A., Maneiro, K. A., Stevens, G., & Baxter, E. F. (2021). Metamorphic evolution for the Inyoni shear zone : Investigating the geodynamic evolution of a 3.20 Ga terrane boundary in the Barberton granitoid greenstone terrane, South Africa. *South African Journal of Geology*, *124*(1), 163-180. https://doi.org/10.25131/sajg.124.0009

Cutts, K. A., Stevens, G., Hoffmann, J. E., Buick, I. S., Frei, D., & Münker, C. (2014). Paleo-to Mesoarchean polymetamorphism in the Barberton Granite-Greenstone Belt, South Africa : Constraints from U-Pb monazite and Lu-Hf garnet geochronology on the tectonic processes that shaped the belt. *Bulletin*, *126*(3-4), 251-270.

De Wit, M. J., Armstrong, R., Hart, R. J., & Wilson, A. H. (1987). Felsic igneous rocks within the 3.3- to 3.5-Ga Barberton Greenstone Belt : High crustal level equivalents of the surrounding Tonalite-Trondhjemite Terrain, emplaced during thrusting. *Tectonics*, *6*(5), 529-549. https://doi.org/10.1029/TC006i005p00529

de Wit, M. J. (1982). Gliding and overthrust nappe tectonics in the Barberton Greenstone Belt. *Journal of Structural Geology*, *4*(2), 117-136.

de Wit, M. J., Furnes, H., & Robins, B. (2011). Geology and tectonostratigraphy of the Onverwacht Suite, Barberton greenstone belt, South Africa. *Precambrian Research*, *186*(1-4), 1-27.

Diener, J. F. (2004). *The tectono-metamorphic evolution of the Theespruit Formation in the Tjakastad schist belt and surrounding areas of the Barberton Greenstone Belt, South Africa* [PhD Thesis, Stellenbosch: University of Stellenbosch]. https://scholar.sun.ac.za/handle/10019.1/16309

Diener, J. F. A., & Dziggel, A. (2021). Can mineral equilibrium modelling provide additional details on metamorphism of the Barberton garnet amphibolites? *South African Journal of Geology*, *124*(1), 211-224. https://doi.org/10.25131/sajg.124.0003

Diener, J. F., Stevens, G., Kisters, A. F., & Poujol, M. (2005). Metamorphism and exhumation of the basal parts of the Barberton greenstone belt, South Africa : Constraining the rates of Mesoarchaean tectonism. *Precambrian Research*, *143*(1-4), 87-112.

Dodson, M. H. (1973). Closure temperature in cooling geochronological and petrological systems. *Contributions to Mineralogy and Petrology*, *40*(3), 259-274. https://doi.org/10.1007/BF00373790

Dziggel, A., Armstrong, R. A., Stevens, G., & Nasdala, L. (2005). Growth of zircon and titanite during metamorphism in the granitoid-gneiss terrane south of the Barberton greenstone belt, South Africa. *Mineralogical Magazine*, *69*(6), 1019-1036.

Dziggel, A., Knipfer, S., Kisters, A. F. M., & Meyer, F. M. (2006). P-T and structural evolution during exhumation of high-T, medium-P basement rocks in the Barberton Mountain Land, South Africa : METAMORPHIC EVOLUTION, BARBERTON MOUNTAIN LAND. *Journal of Metamorphic Geology*, *24*(7), 535-551. https://doi.org/10.1111/j.1525-1314.2006.00653.x

Dziggel, A., Stevens, G., Poujol, M., Anhaeusser, C. R., & Armstrong, R. A. (2002). Metamorphism of the granite–greenstone terrane south of the Barberton greenstone belt, South Africa : An insight into the tectono-thermal evolution of the 'lower' portions of the Onverwacht Group. *Precambrian Research*, *114*(3), 221-247. https://doi.org/10.1016/S0301-9268(01)00225-X

Eglington, B. M., & Armstrong, R. A. (2004). The Kaapvaal Craton and adjacent orogens, southern Africa : A geochronological database and overview of the geological development of the craton. *South African Journal of Geology*, *107*(1-2), 13-32.

England, P. C., & Thompson, A. (1986). Some thermal and tectonic models for crustal melting in continental collision zones. *Geological Society, London, Special Publications*, *19*(1), 83-94. https://doi.org/10.1144/GSL.SP.1986.019.01.05

England, P. C., & Thompson, A. B. (1984). Pressure—Temperature—Time paths of regional metamorphism I. Heat transfer during the evolution of regions of thickened continental crust. *Journal of Petrology*, *25*(4), 894-928.

Ewing, T. A., Rubatto, D., Beltrando, M., & Hermann, J. (2015). Constraints on the thermal evolution of the Adriatic margin during Jurassic continental break-up : U–Pb dating of rutile from the Ivrea–Verbano Zone, Italy. *Contributions to Mineralogy and Petrology*, *169*(4), 44. https://doi.org/10.1007/s00410-015-1135-6

Ferry, J. M., & Watson, E. B. (2007). New thermodynamic models and revised calibrations for the Ti-in-zircon and Zr-in-rutile thermometers. *Contributions to Mineralogy and Petrology*, *154*(4), 429-437. https://doi.org/10.1007/s00410-007-0201-0

Floess, D., & Baumgartner, L. P. (2015). *Constraining magmatic fluxes through thermal modelling of contact metamorphism*. https://doi.org/10.1144/SP422.8

Force, E. R. (1980). The provenance of rutile. *Journal of Sedimentary Research*, *50*(2), 485-488. https://doi.org/10.1306/212F7A31-2B24-11D7-8648000102C1865D

Gardien, V., Martelat, J.-E., Leloup, P.-H., Mahéo, G., Bevillard, B., Allemand, P., Monié, P., Paquette, J.-L., Grosjean, A.-S., & Faure, M. (2022). Fast exhumation rate during late orogenic extension : The new timing of the Pilat detachment fault (French Massif Central, Variscan belt). *Gondwana Research*, *103*, 260-275.

Giuntoli, F., Viola, G., & Villa, I. M. (2024). Dating syn-orogenic exhumation of subducted continental crust : The case of the Northern Apennines. *Lithos*, *488-489*, 107801. https://doi.org/10.1016/j.lithos.2024.107801

Hacker, B. R., Ritzwoller, M. H., & Xie, J. (2014). Partially melted, mica-bearing crust in Central Tibet. *Tectonics*, *33*(7), 1408-1424. https://doi.org/10.1002/2014TC003545

Hart, E., Storey, C., Harley, S. L., & Fowler, M. (2018). A window into the lower crust : Trace element systematics and the occurrence of inclusions/intergrowths in granulite-facies rutile. *Gondwana Research*, *59*, 76-86. https://doi.org/10.1016/j.gr.2018.02.021

Herzberg, C., Condie, K., & Korenaga, J. (2010). Thermal history of the Earth and its petrological expression. *Earth and Planetary Science Letters*, *292*(1-2), 79-88.

Heubeck, C. (2019). The Moodies Group—A High-Resolution Archive of Archaean Surface Processes and Basin-Forming Mechanisms. In A. Kröner & A. Hofmann (Éds.), *The Archaean Geology of the Kaapvaal Craton, Southern Africa* (p. 133-169). Springer International Publishing. https://doi.org/10.1007/978-3-319-78652-0_6

Heubeck, C., Drabon, N., Byerly, G., Leisgang, I., Linnemann, U., Lowe, D., Mertz-Kraus, R., Gonzalez-Pinzon, A., Thomsen, T. B., & Zeh, A. (2022). Detrital zircon provenance of the Archean Moodies Group, Barberton Greenstone Belt, South Africa and Eswatini. *American Journal of Science*, *322*(2), 65-107.

Heubeck, C., & Lowe, D. R. (1994). Depositional and tectonic setting of the Archean Moodies Group, Barberton greenstone belt, South Africa. *Precambrian Research*, *68*(3-4), 257-290.

Hofmann, A. (2005). The geochemistry of sedimentary rocks from the Fig Tree Group, Barberton greenstone belt : Implications for tectonic, hydrothermal and surface processes during mid-Archaean times. *Precambrian Research*, *143*(1), 23-49. https://doi.org/10.1016/j.precamres.2005.09.005

Horstwood, M. S. A., Košler, J., Gehrels, G., Jackson, S. E., McLean, N. M., Paton, C., Pearson, N. J., Sircombe, K., Sylvester, P., Vermeesch, P., Bowring, J. F., Condon, D. J., & Schoene, B. (2016). Community-Derived Standards for LA - ICP - MS U-(Th-)Pb Geochronology – Uncertainty Propagation, Age Interpretation and Data Reporting. *Geostandards and Geoanalytical Research*, *40*(3), 311-332. https://doi.org/10.1111/j.1751-908X.2016.00379.x

Huet, B., Le Pourhiet, L., Labrousse, L., Burov, E., & Jolivet, L. (2011). Post-orogenic extension and metamorphic core complexes in a heterogeneous crust : The role of crustal layering inherited from collision. Application to the Cyclades (Aegean domain). *Geophysical Journal International*, *184*(2), 611-625. https://doi.org/10.1111/j.1365-246X.2010.04849.x

Jamieson, R. A., & Beaumont, C. (2013). On the origin of orogens. *GSA Bulletin*, *125*(11-12), 1671-1702. https://doi.org/10.1130/B30855.1

Jochum, K. P., Weis, U., Stoll, B., Kuzmin, D., Yang, Q., Raczek, I., Jacob, D. E., Stracke, A., Birbaum, K., Frick, D. A., Günther, D., & Enzweiler, J. (2011). Determination of Reference Values for NIST SRM 610–617 Glasses Following ISO Guidelines. *Geostandards and Geoanalytical Research*, *35*(4), 397-429. https://doi.org/10.1111/j.1751-908X.2011.00120.x

Kamo, S. L., & Davis, D. W. (1994). Reassessment of Archean crustal development in the Barberton Mountain Land, South Africa, based on U-Pb dating. *Tectonics*, *13*(1), 167-192. https://doi.org/10.1029/93TC02254

Kato, D., Aoki, K., Komiya, T., Yamamoto, S., Sawaki, Y., Asanuma, H., Sato, T., Tsuchiya, Y., Shozugawa, K., & Matsuo, M. (2018). Constraints on the P–T conditions of high-pressure metamorphic rocks from the Inyoni shear zone in the mid-Archean Barberton Greenstone Belt, South Africa. *Precambrian Research*, *315*, 1-18.

Kelsey, D. E., & Hand, M. (2015). On ultrahigh temperature crustal metamorphism : Phase equilibria, trace element thermometry, bulk composition, heat sources, timescales and tectonic settings. *Geoscience Frontiers*, *6*(3), 311-356. https://doi.org/10.1016/j.gsf.2014.09.006

Kisters, A. F., Belcher, R. W., Poujol, M., & Dziggel, A. (2010). Continental growth and convergence-related arc plutonism in the Mesoarchaean : Evidence from the Barberton granitoid-greenstone terrain, South Africa. *Precambrian Research*, *178*(1-4), 15-26.

Kisters, A. F. M., Stevens, G., Dziggel, A., & Armstrong, R. A. (2003). Extensional detachment faulting and core-complex formation in the southern Barberton granite–greenstone terrain, South Africa : Evidence for a 3.2 Ga orogenic collapse. *Precambrian Research*, *127*(4), 355-378. https://doi.org/10.1016/j.precamres.2003.08.002

Kohler, E. A., & Anhaeusser, C. R. (2002). Geology and geodynamic setting of Archaean silicic metavolcaniclastic rocks of the Bien Venue Formation, Fig Tree Group, northeast Barberton greenstone belt, South Africa. *Precambrian Research*, *116*(3-4), 199-235.

Kohn, M. J. (2016). Metamorphic chronology—a tool for all ages : Past achievements and future prospects. *American Mineralogist*, *101*(1), 25-42. https://doi.org/10.2138/am-2016-5146

Kohn, M. J. (2020). A refined zirconium-in-rutile thermometer. *American Mineralogist*, *105*(6), 963-971. https://doi.org/10.2138/am-2020-7091

Kohn, M. J., Penniston-Dorland, S. C., & Ferreira, J. C. S. (2016). Implications of near-rim compositional zoning in rutile for geothermometry, geospeedometry, and trace element equilibration. *Contributions to Mineralogy and Petrology*, *171*(10), 78. https://doi.org/10.1007/s00410-016-1285-1

Kooijman, E., Mezger, K., & Berndt, J. (2010). Constraints on the U–Pb systematics of metamorphic rutile from in situ LA-ICP-MS analysis. *Earth and Planetary Science Letters*, *293*(3-4), 321-330.

Korenaga, J. (2018). Crustal evolution and mantle dynamics through Earth history. *Philosophical Transactions of the Royal Society A: Mathematical, Physical and Engineering Sciences*, *376*(2132), 20170408.

Korenaga, J. (2021). Was there land on the early Earth? *Life*, *11*(11), 1142.

Korhonen, F. J., Clark, C., Brown, M., Bhattacharya, S., & Taylor, R. (2013). How long-lived is ultrahigh temperature (UHT) metamorphism? Constraints from zircon and monazite geochronology in the Eastern Ghats orogenic belt, India. *Precambrian Research*, *234*, 322-350. https://doi.org/10.1016/j.precamres.2012.12.001

Kröner, A., Hegner, E., Wendt, J. I., & Byerly, G. R. (1996a). The oldest part of the Barberton granitoid-greenstone terrain, South Africa : Evidence for crust formation between 3.5 and 3.7 Ga. *Precambrian Research*, *78*(1-3), 105-124.

Kröner, A., Hegner, E., Wendt, J. I., & Byerly, G. R. (1996b). The oldest part of the Barberton granitoid-greenstone terrain, South Africa : Evidence for crust formation between 3.5 and 3.7 Ga. *Precambrian Research*, *78*(1), 105-124. https://doi.org/10.1016/0301-9268(95)00072-0

Kröner, A., Hoffmann, J. E., Xie, H., Wu, F., Münker, C., Hegner, E., Wong, J., Wan, Y., & Liu, D. (2013). Generation of early Archaean felsic greenstone volcanic rocks through crustal melting in the Kaapvaal, craton, southern Africa. *Earth and Planetary Science Letters*, *381*, 188-197.

Labrousse, L., Huet, B., Le Pourhiet, L., Jolivet, L., & Burov, E. (2016). Rheological implications of extensional detachments : Mediterranean and numerical insights. *Earth-Science Reviews*, *161*, 233-258. https://doi.org/10.1016/j.earscirev.2016.09.003

Lana, C., Tohver, E., & Cawood, P. (2010). Quantifying rates of dome-and-keel formation in the Barberton granitoid-greenstone belt, South Africa. *Precambrian Research*, *177*(1), 199-211. https://doi.org/10.1016/j.precamres.2009.12.001

Laurent, O., Björnsen, J., Wotzlaw, J.-F., Bretscher, S., Pimenta Silva, M., Moyen, J.-F., Ulmer, P., & Bachmann, O. (2020). Earth's earliest granitoids are crystal-rich magma reservoirs tapped by silicic eruptions. *Nature Geoscience*, *13*(2), 163-169.

Laurent, O., Couzinié, S., & Doucet, L. S. (2023). Timescales of ultra-high temperature metamorphism and crustal differentiation : Zircon petrochronology from granulite xenoliths of the Variscan French Massif Central. *Earth and Planetary Science Letters*, *611*, 118133. https://doi.org/10.1016/j.epsl.2023.118133

Lowe, D. R. (1999). *Geologic evolution of the Barberton Greenstone Belt and vicinity*. https://pubs.geoscienceworld.org/gsa/books/edited-volume/486/chapter-pdf/967261/i0-8137-2329-9-329-0-287.pdf

Lowe, D. R., & Byerly, G. R. (1999). *Stratigraphy of the west-central part of the Barberton Greenstone Belt, South Africa*. https://pubs.geoscienceworld.org/gsa/books/edited-volume/486/chapter-pdf/967200/i0-8137-2329-9-329-0-1.pdf

Lowe, D. R., & Byerly, G. R. (2007). An overview of the geology of the Barberton Greenstone Belt and vicinity : Implications for early crustal development. *Developments in Precambrian geology*, *15*, 481-526.

Luvizotto, G. L., Zack, T., Triebold, S., & Von Eynatten, H. (2009). Rutile occurrence and trace element behavior in medium-grade metasedimentary rocks : Example from the Erzgebirge, Germany. *Mineralogy and Petrology*, *97*(3-4), 233-249. https://doi.org/10.1007/s00710-009-0092-z

Maslov, A. V. (2007). Archean metaterrigenous rocks : Major geochemical constraints. *Geochemistry International*, *45*(4), 327-344. https://doi.org/10.1134/S0016702907040027

Matsumura, R. (2014). *The petrogenesis of the Nelshoogte pluton : The youngest and most compositionally variable TTG pluton in the Barberton Granite-Greenstone Terrain* [PhD Thesis, Stellenbosch: Stellenbosch University]. https://scholar.sun.ac.za/handle/10019.1/86589

Meinhold, G., Anders, B., Kostopoulos, D., & Reischmann, T. (2008). Rutile chemistry and thermometry as provenance indicator : An example from Chios Island, Greece. *Sedimentary Geology*, *203*(1-2), 98-111.

Mezger, K., Hanson, G. N., & Bohlen, S. R. (1989). High-precision UPb ages of metamorphic rutile : Application to the cooling history of high-grade terranes. *Earth and Planetary Science Letters*, *96*(1-2), 106-118.

Moyen, J. F., Zeh, A., Cuney, M., Dziggel, A., & Carrouée, S. (2021). The multiple ways of recycling Archaean crust : A case study from the ca. 3.1 Ga granitoids from the Barberton Greenstone Belt, South Africa. *Precambrian Research*, *353*, 105998.

Moyen, J.-F., Stevens, G., & Kisters, A. (2006). Record of mid-Archaean subduction from metamorphism in the Barberton terrain, South Africa. *Nature*, *442*(7102), 559-562.

Moyen, J.-F., Stevens, G., Kisters, A. F., & Belcher, R. W. (2007). TTG plutons of the Barberton granitoid-greenstone terrain, South Africa. *Developments in Precambrian Geology*, *15*, 607-667.

Mühlberg, M., Stevens, G., Moyen, J.-F., Kisters, A. F., & Lana, C. (2021). Thermal evolution of the Stolzburg Block, Barberton granitoid-greenstone terrain, South Africa : Implications for Paleoarchean tectonic processes. *Precambrian Research*, *359*, 106082.

Nédélec, A., Chevrel, M. O., Moyen, J.-F., Ganne, J., & Fabre, S. (2012). TTGs in the making : Natural evidence from Inyoni shear zone (Barberton, South Africa). *Lithos*, *153*, 25-38.

Nelson, K. D., Zhao, W., Brown, L. D., Kuo, J., Che, J., Liu, X., Klemperer, S. L., Makovsky, Y., Meissner, R., Mechie, J., Kind, R., Wenzel, F., Ni, J., Nabelek, J., Leshou, C., Tan, H., Wei, W., Jones, A. G., Booker, J., … Edwards, M. (1996). Partially Molten Middle Crust Beneath Southern Tibet : Synthesis of Project INDEPTH Results. *Science*, *274*(5293), 1684-1688. https://doi.org/10.1126/science.274.5293.1684

Parman, S. W., Dann, J. C., Grove, T. L., & De Wit, M. J. (1997). Emplacement conditions of komatiite magmas from the 3.49 Ga Komati Formation, Barberton greenstone belt, South Africa. *Earth and Planetary Science Letters*, *150*(3-4), 303-323.

Peng, T., Wang, G.-D., Wang, H. Y., Liu, J.-H., Zhang, H. C., Chen, H.-X., & Wu, C.-M. (2019). Metamorphic PT path and geochronology of garnet-bearing amphibolite of the Inyoni Shear Zone, southwestern Barberton Greenstone Belt, South Africa. *Precambrian Research*, *321*, 261-276.

Percival, J. A. (1994). Archean high-grade metamorphism. In *Developments in Precambrian Geology* (Vol. 11, p. 357-410). Elsevier.

Pereira, I., Bruand, E., Koga, K., Nicollet, C., & Brovarone, A. V. (s. d.). *Stability and chemistry of rutile and titanite in metamafic rocks*. Consulté 10 septembre 2025, à l'adresse http://christian.nicollet.free.fr/page/Publications/Lherzolite2024_Pereira_et_al.pdf

Pereira, I., & Storey, C. D. (2023). Detrital rutile : Records of the deep crust, ores and fluids. *Lithos*, *438-439*, 107010. https://doi.org/10.1016/j.lithos.2022.107010

Pereira, I., Storey, C. D., Darling, J. R., Moreira, H., Strachan, R. A., & Cawood, P. A. (2021). Detrital rutile tracks the first appearance of subduction zone low T/P paired metamorphism in the Palaeoproterozoic. *Earth and Planetary Science Letters*, *570*, 117069.

Pereira, I., Storey, C., Darling, J., Lana, C., & Alkmim, A. R. (2019). Two billion years of evolution enclosed in hydrothermal rutile : Recycling of the São Francisco Craton Crust and constraints on gold remobilisation processes. *Gondwana Research*, *68*, 69-92.

Petrus, J. A., & Kamber, B. S. (2012). VizualAge : A Novel Approach to Laser Ablation ICP-MS U-Pb Geochronology Data Reduction. *Geostandards and Geoanalytical Research*, *36*(3), 247-270. https://doi.org/10.1111/j.1751-908X.2012.00158.x

Ring, U., Brandon, M. T., Willett, S. D., & Lister, G. S. (1999). Exhumation processes. *Geological Society, London, Special Publications*, *154*(1), 1-27. https://doi.org/10.1144/GSL.SP.1999.154.01.01

Rivers, T. (2008). Assembly and preservation of lower, mid, and upper orogenic crust in the Grenville Province—Implications for the evolution of large hot long-duration orogens. *Precambrian Research*, *167*(3), 237-259. https://doi.org/10.1016/j.precamres.2008.08.005

Robb, L. J., Barton Jr, J. M., Kable, E. J. D., & Wallace, R. C. (1986). Geology, geochemistry and isotopic characteristics of the Archaean Kaap Valley pluton, Barberton mountain land, South Africa. *Precambrian Research*, *31*(1), 1-36.

Santos Leandro, M. V., Stevens, G., Moyen, J.-F., Kisters, A., & Ferreira, A. (s. d.). Archean Syenites by Intracrustal Processes : The Boesmanskop Alkaline Complex, Eastern Kaapvaal Craton. *Eastern Kaapvaal Craton*. Consulté 16 mai 2025, à l'adresse https://papers.ssrn.com/sol3/papers.cfm?abstract_id=4972697

Schirra, M., & Laurent, O. (2021). Petrochronology of hydrothermal rutile in mineralized porphyry Cu systems. *Chemical Geology*, *581*, 120407. https://doi.org/10.1016/j.chemgeo.2021.120407

Schmitt, A. K., & Zack, T. (2012a). High-sensitivity U–Pb rutile dating by secondary ion mass spectrometry (SIMS) with an O2+ primary beam. *Chemical Geology*, *332-333*, 65-73. https://doi.org/10.1016/j.chemgeo.2012.09.023

Schmitt, A. K., & Zack, T. (2012b). High-sensitivity U–Pb rutile dating by secondary ion mass spectrometry (SIMS) with an O2+ primary beam. *Chemical Geology*, *332*, 65-73.

Schoene, B., De Wit, M. J., & Bowring, S. A. (2008). Mesoarchean assembly and stabilization of the eastern Kaapvaal craton : A structural-thermochronological perspective. *Tectonics*, *27*(5), 2008TC002267. https://doi.org/10.1029/2008TC002267

Schoene, B., Dudas, F. O. L., Bowring, S. A., & De Wit, M. (2009). Sm–Nd isotopic mapping of lithospheric growth and stabilization in the eastern Kaapvaal craton. *Terra Nova*, *21*(3), 219-228. https://doi.org/10.1111/j.1365-3121.2009.00877.x

Schulmann, K., Lexa, O., Štípská, P., Racek, M., Tajčmanová, L., Konopásek, J., Edel, J.-B., Peschler, A., & Lehmann, J. (2008). Vertical extrusion and horizontal channel flow of orogenic lower crust : Key exhumation mechanisms in large hot orogens? *Journal of Metamorphic Geology*, *26*(2), 273-297. https://doi.org/10.1111/j.1525-1314.2007.00755.x

Scibiorski, E., Tohver, E., & Jourdan, F. (2015). Rapid cooling and exhumation in the western part of the Mesoproterozoic Albany-Fraser Orogen, Western Australia. *Precambrian Research*, *265*, 232-248. https://doi.org/10.1016/j.precamres.2015.02.005

Sciuba, M., & Beaudoin, G. (2021). Texture and trace element composition of rutile in orogenic gold deposits. *Economic geology*, *116*(8), 1865-1892.

Smye, A. J., & Stockli, D. F. (2014). Rutile U–Pb age depth profiling : A continuous record of lithospheric thermal evolution. *Earth and Planetary Science Letters*, *408*, 171-182. https://doi.org/10.1016/j.epsl.2014.10.013

Stevens, G., Droop, G. T. R., Armstrong, R. A., & Anhaeusser, C. R. (2002). Amphibolite facies metamorphism in the Schapenburg schist belt : A record of the mid-crustal response to∼ 3.23 Ga terrane accretion in the Barberton greenstone belt. *South African Journal of Geology*, *105*(3), 271-284.

Stevens, G., & Moyen, J.-F. (2007). Metamorphism in the Barberton Granite Greenstone Terrain : A record of Paleoarchean accretion. *Developments in precambrian geology*, *15*, 669-698.

Taylor, S. R., & McLennan, S. M. (1983). Geochemistry of Early Proterozoic sedimentary rocks and the Archean/Proterozoic boundary. In L. G. Medaris Jr., C. W. Byers, D. M. Mickelson, & W. C. Shanks (Éds.), *Proterozoic Geology : Selected Papers from an International Proterozoic Symposium* (p. 0). Geological Society of America. https://doi.org/10.1130/MEM161-p119

Triebold, S., von Eynatten, H., Luvizotto, G. L., & Zack, T. (2007). Deducing source rock lithology from detrital rutile geochemistry : An example from the Erzgebirge, Germany. *Chemical geology*, *244*(3-4), 421-436.

Triebold, S., von Eynatten, H., & Zack, T. (2012). A recipe for the use of rutile in sedimentary provenance analysis. *Sedimentary Geology*, *282*, 268-275.

Tual, L., Möller, C., & Whitehouse, M. J. (2018). Tracking the prograde P–T path of Precambrian eclogite using Ti-in-quartz and Zr-in-rutile geothermobarometry. *Contributions to Mineralogy and Petrology*, *173*(7), 56. https://doi.org/10.1007/s00410-018-1482-1

Van Kranendonk, M. J., Kröner, A., Hegner, E., & Connelly, J. (2009). Age, lithology and structural evolution of the c. 3.53 Ga Theespruit Formation in the Tjakastad area, southwestern Barberton Greenstone Belt, South Africa, with implications for Archaean tectonics. *Chemical Geology*, *261*(1-2), 115-139.

Van Kranendonk, M. J., Kröner, A., Hoffmann, J. E., Nagel, T., & Anhaeusser, C. R. (2014). Just another drip : Re-analysis of a proposed Mesoarchean suture from the Barberton Mountain Land, South Africa. *Precambrian Research*, *254*, 19-35.

Vanderhaeghe, O., & Teyssier, C. (2001). Partial melting and flow of orogens. *Tectonophysics*, *342*(3), 451-472. https://doi.org/10.1016/S0040-1951(01)00175-5

Vanderhaeghe, O., Teyssier, C., McDougall, I., & Dunlap, W. J. (2003). Cooling and exhumation of the Shuswap Metamorphic Core Complex constrained by 40Ar/39Ar thermochronology. *Geological Society of America Bulletin*, *115*(2), 200-216.

Vermeesch, P. (2018). IsoplotR : A free and open toolbox for geochronology. *Geoscience Frontiers*, *9*(5), 1479-1493.

Virgo, S., von Hagke, C., & Urai, J. L. (2018). Multiphase boudinage : A case study of amphibolites in marble in the Naxos migmatite core. *Solid Earth*, *9*(1), 91-113. https://doi.org/10.5194/se-9-91-2018

Wang, H., Yang, J.-H., Kröner, A., Zhu, Y.-S., & Li, R. (2019). Non-subduction origin for 3.2 Ga high-pressure metamorphic rocks in the Barberton granitoid-greenstone terrane, South Africa. *Terra Nova*, *31*(4), 373-380.

Willigers, B. J. A., van Gool, J. a. M., Wijbrans, J. R., Krogstad, E. J., & Mezger, K. (2002). Posttectonic Cooling of the Nagssugtoqidian Orogen and a Comparison of Contrasting Cooling Histories in Precambrian and Phanerozoic Orogens. *The Journal of Geology*, *110*(5), 503-517. https://doi.org/10.1086/341595

Wong, L., Davis, D. W., Krogh, T. E., & Robert, F. (1991). UPb zircon and rutile chronology of Archean greenstone formation and gold mineralization in the Val d'Or region, Quebec. *Earth and Planetary Science Letters*, *104*(2), 325-336. https://doi.org/10.1016/0012-821X(91)90213-2

Wong, M. S., Williams, M. L., McLelland, J. M., Jercinovik, M. J., & Kowalkoski, J. (2012). Late Ottawan extension in the eastern Adirondack Highlands : Evidence from structural studies and zircon and monazite geochronology. *GSA Bulletin*, *124*(5-6), 857-869. https://doi.org/10.1130/B30481.1

Zack, T., & Kooijman, E. (2017). Petrology and geochronology of rutile. *Reviews in Mineralogy and Geochemistry*, *83*(1), 443-467.

Zack, T., Luvizotto, G. L., Barth, M., & Stockli, D. F. (2007). U/Pb rutile dating in granulite-facies rocks by LA-ICP-MS. *AGU Fall Meeting Abstracts*, *2007*, V34C-05. https://ui.adsabs.harvard.edu/abs/2007AGUFM.V34C..05Z/abstract

Zack, T., Moraes, R., & Kronz, A. (2004). Temperature dependence of Zr in rutile : Empirical calibration of a rutile thermometer. *Contributions to Mineralogy and Petrology*, *148*(4), 471-488. https://doi.org/10.1007/s00410-004-0617-8

Zack, T., Stockli, D. F., Luvizotto, G. L., Barth, M. G., Belousova, E., Wolfe, M. R., & Hinton, R. W. (2011). In situ U–Pb rutile dating by LA-ICP-MS : 208Pb correction and prospects for geological applications. *Contributions to Mineralogy and Petrology*, *162*(3), 515-530. https://doi.org/10.1007/s00410-011-0609-4

Zack, T., von Eynatten, H., & Kronz, A. (2004). Rutile geochemistry and its potential use in quantitative provenance studies. *Sedimentary Geology*, *171*(1-4), 37-58.

Zeh, A., Cabral, A. R., Koglin, N., & Decker, M. (2018). Rutile alteration and authigenic growth in metasandstones of the Moeda Formation, Minas Gerais, Brazil – A result of Transamazonian fluid–rock interaction. *Chemical Geology*, *483*, 397-409. https://doi.org/10.1016/j.chemgeo.2018.03.007

Zeh, A., Gerdes, A., & Barton Jr, J. M. (2009). Archean accretion and crustal evolution of the Kalahari Craton—The zircon age and Hf isotope record of granitic rocks from Barberton/Swaziland to the Francistown Arc. *Journal of Petrology*, *50*(5), 933-966.

Zou, Y., Chu, X., Li, Q., Mitchell, R. N., Zhai, M., Zou, X., Zhao, L., Wang, Y., & Liu, B. (2020). Local Rapid Exhumation and Fast Cooling in a Long-lived Paleoproterozoic Orogeny. *Journal of Petrology*, *61*(10), egaa091. https://doi.org/10.1093/petrology/egaa091

5. Chapter 5: Conclusion

5.1. Main results from this work

The present work has outlined the lack of preservation of potentially voluminous segments of the Archean Crust and shows that the preserved geological record from that time suffers from substantial biases. The Barberton Greenstone Belt in South Africa illustrates this phenomenon as, like most Archean terranes of that age, it mainly shows a juxtaposition of a binary set of rocks with supracrustal greenstone sequences on the one hand and the granitoids of dominantly TTG composition that intruded them, on the other hand (Anhaeusser, 1981, 2014). However, the following results from our accessory mineral inventory support a more complex history:

1) Zircons deposited in felsic volcano-clastic rocks of the Theespruit Formation are richer in Nb, Ti and Hf than zircons of the Barberton TTGs. They have a consistently sub-chondritic $\varepsilon Hf_{(t)}$ that matches that of ca. 3.4 – 3.5 Ga zircons hosted in granite/rhyolite clasts from the Moodies basal conglomerate (Sanchez-Garrido, 2012).
2) The detrital zircons of different clastic sediments taken at every level of the Barberton stratigraphy, produced comparable ages, yet distinct chemistry but more often Hf isotopic differences, with plutonic zircons of the TTG suite. Zircons from the Hooggenoeg Formation have Ti and Hf content higher than that of zircons crystallized in the ca. 3.45 Ga trondhjemites whereas Schapenburg zircons produced a ca. 3.4 Ga age component that has no known plutonic equivalent in the northern part of the BGGT (from where the sediments are derived). Both samples, however, show supra-chondritic Hf isotopic signatures (i.e. $\varepsilon Hf_{(t)}$ > CHUR).

3) In contrast, ca. 90% of the Moodies zircons sampled in this work have a sub-chondritic $\varepsilon Hf_{(t)}$ i.e. not matching that of BTTG zircons. Combining this data with literature results, it comes out that ~ 40% of the Moodies zircon record show negative $\varepsilon Hf_{(t)}$ and must derive from felsic crustal components of significant volume, that are now missing out from the rock record. These missing sources to Moodies sediments presumably resembled granitic clasts of the Moodies basal conglomerate as well as felsic volcanic schists from the Theespruit Formation as both rock units revealed zircons with similarly sub-chondritic $\varepsilon Hf_{(t)}$ (at least for the ca. 3.4-3.5 Ga generations, Sanchez-Garrido, 2012; Sanchez-Garrido et al., 2011).
4) Apatites extracted from the same samples as zircons of the ca. 3.43 Ga Hooggenoeg volcano-sediments and ca. 3.23 Ga Schapenburg turbidites allowed to better constrain the chemical identity of the missing felsic source of these clastic sediments, as suspected from the zircon data. As shown in Chapter 3, detrital apatites from both samples possess halogen, trace and REE characteristics that clearly distinguish them from apatites crystallized in the BTTGs and rather resemble those of apatites crystallized in Neoarchean sanukitoids or post-Archean Basalt-Andesite-Dacite-Rhyolite rocks (BADR) from convergent margin settings.
5) The U-Pb and trace elements data extracted from rutiles belonging to the Theespruit-age felsic volcano-clastic sediments document the two metamorphic episodes undergone by the Stolzburg Terrane (at ca. 3.45 and ca. 3.20 Ga). The preservation of ca. 3.47 Ga U-Pb ages in small rutiles from one sample of the Theespruit felsic schists argues for a fast cooling rate of the Stolzburg Terrane following the main metamorphic event at ca. 3.20 Ga, that is between 22 and 60°C/Ma. Therefore, the upper crustal rocks that sourced the sediments were not only compositionally more diverse than TTGs but were also characterized by low geothermal gradients.

5.2. The importance of combining multiple accessory minerals to constrain the compositional diversity of the Paleoarchean crust

The case of the Hooggenoeg and Schapenburg sediments illustrates the limits of a zircon-focused study to constrain sediment provenance. Indeed, while Hooggenoeg and Schapenburg zircons revealed ages or trace element differences that do not match those of BTTG zircons, the chemical identity of their felsic source remains difficult to untangle solely using zircons, due to their modest chemical variability between different granitoid types (Grimes et al., 2015; Hoskin & Schaltegger, 2003; J.-F. Moyen et al., 2017). However, apatites extracted from the same samples helped me fill the gap, as postulated by previous studies (Belousova et al., 2001, 2002; Chu et al., 2009; Kieffer et al., 2024; O'Sullivan et al., 2020). Combining both accessory minerals (**Figure 5-1**), I stress that the missing (and local) source of Hooggenoeg sediments must be isotopically supra-chondritic (zircon) and resemble chemically intermediate Neoarchean sanukitoids (apatite). In the case of the Schapenburg turbidites, the source must contain a ca. 3.4 Ga felsic component that is supra-chondritic (zircon), more chemically evolved than the source of Hooggenoeg sediments (apatite), i.e. a silicic sanukitoid-like source. The contrasting Sr contents measured in both detrital populations (ca. 600-1200 ppm for Hooggenoeg apatites, ca. 200 ppm for Schapenburg apatites), as well as their distinct Cl and F contents (high Cl, low F for Hooggenoeg, high F, low Cl for Schapenburg), highlight different degrees of differentiation of the source rock (Bruand et al., 2016, 2017; Kendall-Langley et al., 2021). Specifically, Hooggenoeg apatites crystallized in an intermediate to mafic melt of dioritic composition, which is a common lithology in sanukitoid suites (L. P. Bédard, 1996; Shirey & Hanson, 1984; Stern et al., 1989), whereas the Schapenburg apatites would have likely formed in a more evolved melt of granodioritic or granitic composition, e.g. similar to the evolved end-members of the sanukitoid suites (Jayananda et al., 1995; Laurent et al., 2013).

As I did not find detrital apatites in samples from the Moodies Group, from which the isotopically sub-chondritic zircons were extracted, I could not further assess the chemical identity of the voluminous felsic component (sourcing ca. 40% of the Moodies zircons from this work + literature) that produced the negative-$\varepsilon Hf_{(t)}$-zircons. However, and luckily, Lu-Hf data on zircons of ca. 3.5-3.2 Ga

Moodies granitic/rhyolitic clasts from (Agangi et al., 2018; Sanchez-Garrido, 2012; Sanchez-Garrido et al., 2011) and Lu-Hf data and trace element in zircons of the Theespruit felsic volcanic rocks presented in chapter 2, helped me fill the gap in that case. The isotopically similar zircons analyzed by (Sanchez-Garrido, 2012) in the ca. 3.4-3.5 Ga granitic clasts does suggests that those 40% Moodies zircons with sub-chondritic Hf isotopic signature were crystallized in Paleoarchean K-rich, Ca-poor granitic magmas presumably derived from melting of meta-sedimentary rocks (Sanchez-Garrido et al., 2011). Additionally, the fact that sanukitoid-like magmas that produced the Hooggenoeg and Schapenburg detrital apatites must also have been isotopically supra-chondritic (to agree with zircons $\varepsilon Hf_{(t)}$ from the same samples, **Figure 5-1A&B**) indicates that perhaps, even Moodies detrital zircons with supra-chondritic signature are in fact, not derived from TTGs but from other Paleoarchean granites that are isotopically supra-chondritic. Agangi et al., 2018 documented some ca. 3.3 Ga Moodies granitic clasts with supra-chondritic zircons which suggests that this hypothesis might have significance and requires further testing. Therefore, the 40% of non-TTG detrital zircons deposited in Moodies sandstones should be taken only as a minimum estimate of the proportion of missing sources of clastic sediments in the BGGT.

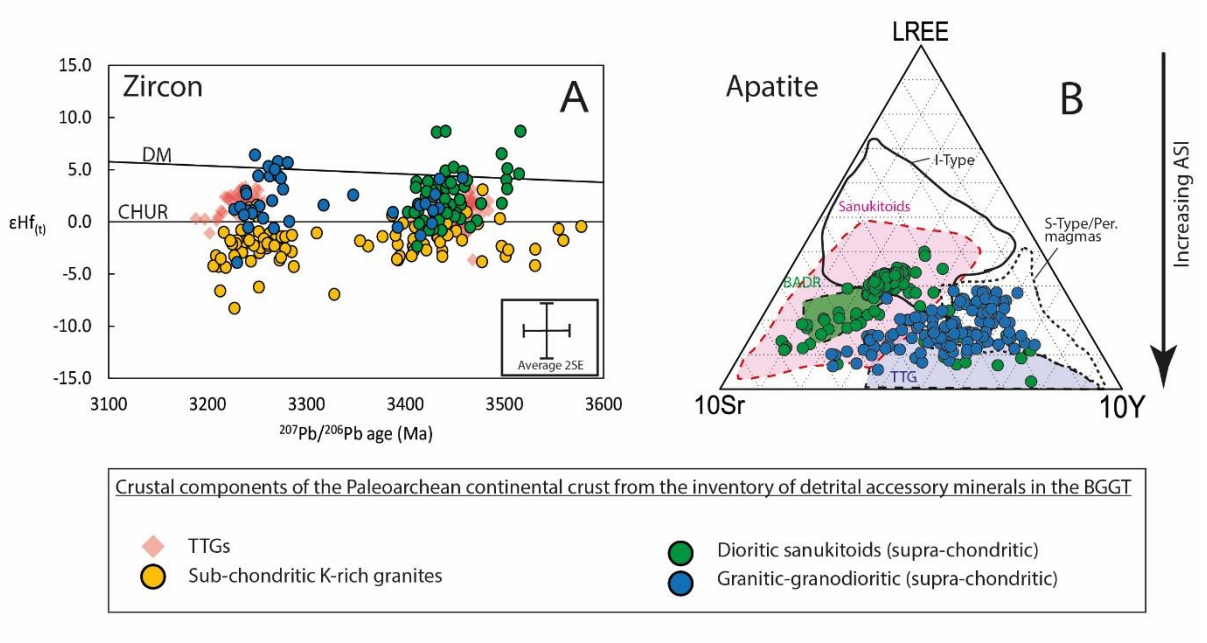

Figure 5-1 : Crustal components of the Paleoarchean continental crust and main results from this study.

Collectively, the conclusions drawn from the zircon and apatite inventory of Barberton supracrustal sequences point towards a compositionally diverse Paleoarchean upper continental crust containing:

1) TTGs i.e. similar to those exposed in the preserved geological record.
2) Granites whose zircon ages cover the Paleoarchean history of the BGGT i.e. from ca. 3.55 Ga to 3.20 Ga (see chapters 2 and 3).
3) Dioritic sanukitoids with a supra-chondritic Hf isotopic signature. These were crystallized broadly coevally (ca. 3.50-3.45 Ga, see chapter 2 and 3) with the Steynsdorp tonalites and Theespruit/ Stolzburg trondhjemites. They sourced the detrital zircons and apatites of the Hooggenoeg sediments.
4) Granitic-to-granodioritic sanukitoids with a supra-chondritic Hf isotopic signature in the Northern Terrane of the BGGT. These crystallized at ca. 3.40 Ga and 3.25 Ga and eventually sourced the detrital zircons and apatites of the SSB.

5.3. Coeval production of diverse granitoids in the Paleoarchean BGGT

The occurrence of compositionally diverse granitoids in the BGGT before 3.2 Ga, as evidenced from detrital zircons and apatites, suggests that they did not start forming at the Neoarchean-Proterozoic transition as previous models proposed (Bibikova et al., 2005; Cassidy et al., 2006; Champion & Smithies, 2001; Fowler & Rollinson, 2012; Halla, 2005; Jayananda et al., 1995, 2006, 2018, 2020; Jiang et al., 2016; Laurent et al., 2011, 2014; McLaren & Powell, 2014; J. F. Moyen et al., 2021; J.-F. Moyen et al., 2003; Stern et al., 1989; Y. Wang et al., 2009). Instead, these granitoids were formed broadly coevally with documented TTG magmatic events in the Paleoarchean (at ca. 3.50, 3.45 and 3.20 Ga). The simultaneous production of different granitoid types is a well-known phenomenon of Phanerozoic-Proterozoic orogenic belts (e.g. the coeval I and S-type and TTG granites of the Famatinian Belt of the Western margin of Gondwana, Pankhurst et al., 2000; Rapela et al., 2018 or the Lachlan Fold Belt in Eastern Australia, Chappell & White, 1992), where the contrasting chemical compositions of granites are ascribed to either 1) partial melting of different source rocks both in mantle and crust (Castro, 2020;

Chappell et al., 2012; Chappell & Stephens, 1988; J.-F. Moyen et al., 2017) and/or 2) diversity in later differentiation mechanisms (see contributions from Clemens et al., 2011; Stevens et al., 2007 for peritectic entrainment of clinopyroxene). Here, the granites that produced the isotopically sub-chondritic zircons of the Moodies Group would form as a result of partial melting of an older sialic basement, possibly reworking higher-grade equivalents of felsic volcanic schists of the Theespruit formation (Sanchez-Garrido et al., 2011) (consistently with similarly sub-chondritic $\varepsilon Hf_{(t)}$-in-zircon signature present in both lithologies and K_2O-enrichment, cf. Agangi et al., 2018), whereas apatite- and supra-chondritic, zircon-bearing sanukitoids would result from the partial melting of a metasomatized mantle component mixed with juvenile mafic crust (consistent with supra-chondritic $\varepsilon Hf_{(t)}$-in-zircon signature, entailing shorter crustal residence time, Fisher et al., 2014; C. J. Spencer et al., 2020). Different tectonic frameworks, both non-uniformitarian and uniformitarian, have been proposed to explain the near-coeval production of TTGs, silicic sanukitoids, intermediate-to-mafic sanukitoids, and granites, and are further explored below.

5.3.1. Non-uniformitarian models

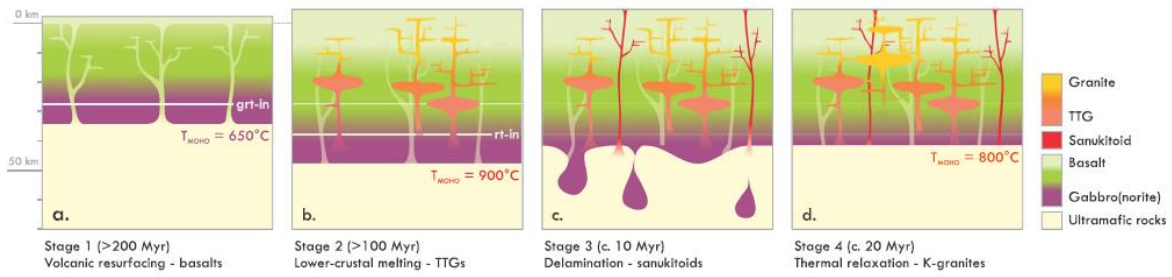

Figure 5-2: Scenario of successive production of compositionally different granitoids in a magmatically overthickened composite crust (Smit et al., 2024).

Recent numerical models from (Smit et al., 2024) proposed that, because of voluminous basaltic resurfacing (constant volcanic activity), an Archean composite crust (consisting of mafic lower crust + felsic middle crust) would vertically thicken up to 50 km over 200 Myr. The resulting burial of mafic rocks to these depths, associated with higher mantle heat flow in Archean time would warm up the Moho to ca. 900°C (**Figure 5-2**) and eventually trigger partial melting of the cumulate-gabbroic lower crustal rocks to produce TTG melts. Intense melt extraction from that mafic lower crust would result in

the formation of dense, eclogitic solid residuum that would likely founder into the asthenospheric mantle (see also J. H. Bédard, 2018) and interact with it (see also Smithies et al., 2019). The resulting metasomatized asthenosphere would melt to produce sanukitoids, following (J. H. Bédard, 2006) while the concomitant thermal relaxation of the crustal isotherms would trigger partial melting of the felsic middle crust (Theespruit-like felsic volcanics) and generate K-rich magmas. In this model, an incubation period of ca. 200 Ma is necessary for sufficient burial of gabbroic rocks (through top-down stacking of volcanic rocks) to pressure conditions that enables partial melting. Then a period of ca. 30-to-100 Myr takes place when TTG, sanukitoids and granites are produced together. Accounting for uncertainties of ± 40 Ma that were documented on zircon Pb-Pb ages in this work, this would make these magmas look coeval, at least from a detrital zircon perspective.

5.3.2. Semi-uniformitarian models

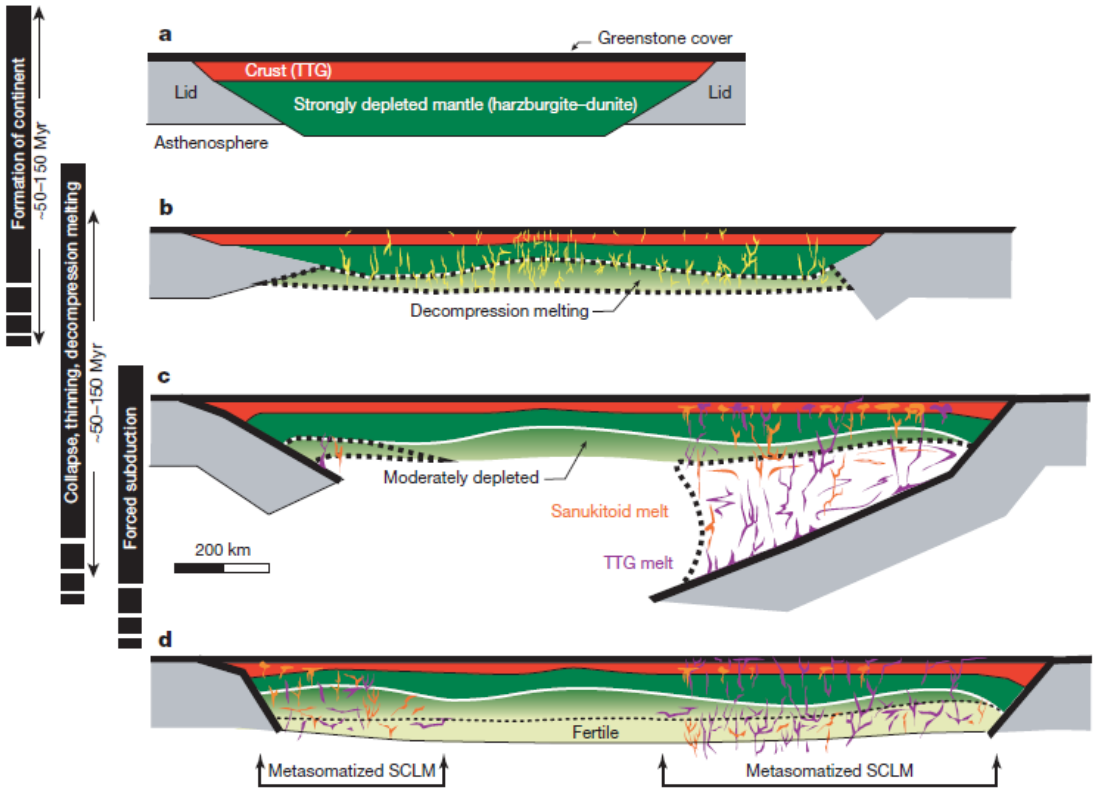

Figure 5-3 : Gravitational instability of an Archean continent (from Rey et al., 2014). Higher mantle heat flow in the Archean triggered the production of voluminous basaltic melts, translating into a thick basaltic continent that further differentiates into TTGs (~50-150 Myr). The growth of this continent eventually leads to an overweight which triggers gravitational collapse of

the overthickened crust. The downflow of crustal material pushes the continental margins against the oceanic crust, leading the latter to subduct. The subduction down to eclogite facies conditions triggers partial melting of the oceanic slab which rises through the mantle wedge and metasomatize it (i.e. sanukitoid magmatism for ~50-150 Myr).

The model of (Rey et al., 2014) discusses Archean continental growth through 1) partial melting of the deep mantle, producing thick basaltic crust (oceanic plateau-like) which further differentiates into TTGs (**Figure 5-3**). 2) With the continent growing in thickness, it becomes gravitationally unstable leading to collapse and horizontal compression of margins (at the contact with oceanic lids). During that stage, isostatic rebound of the Moho triggers further partial melting of the subcontinental mantle. 3) As a result of the horizontal compression happening at the continent margins, the oceanic lids subduct underneath the TTG-like continental crust, down to eclogite facies thereby producing HP-TTG melts (**Figure 5-3**). These TTG melts metasomatize the mantle wedge, triggering the production of sanukitoid-like magmas. 4) The subducted slab eventually breaks off, and the continental crust stabilizes through thermal relaxation and cooling. Quite similarly to the model of (Smit et al., 2024), in this model, a period of TTG-dominated magmatism, lasting for 50 to 150 Myr (**Figure 5-3**), is ultimately followed by another period of 50-150 Myr of more diverse granitoid magmatism . This model can be considered “semi-uniformitarian” as it starts with an episode of vertical magmatic thickening (which does not require any operation of subduction i.e. non-uniformitarian) and is eventually followed by a second episode of horizontal motion of oceanic plates underneath a thick continent i.e. akin to subduction-accretion processes.

5.3.3. Uniformitarian models

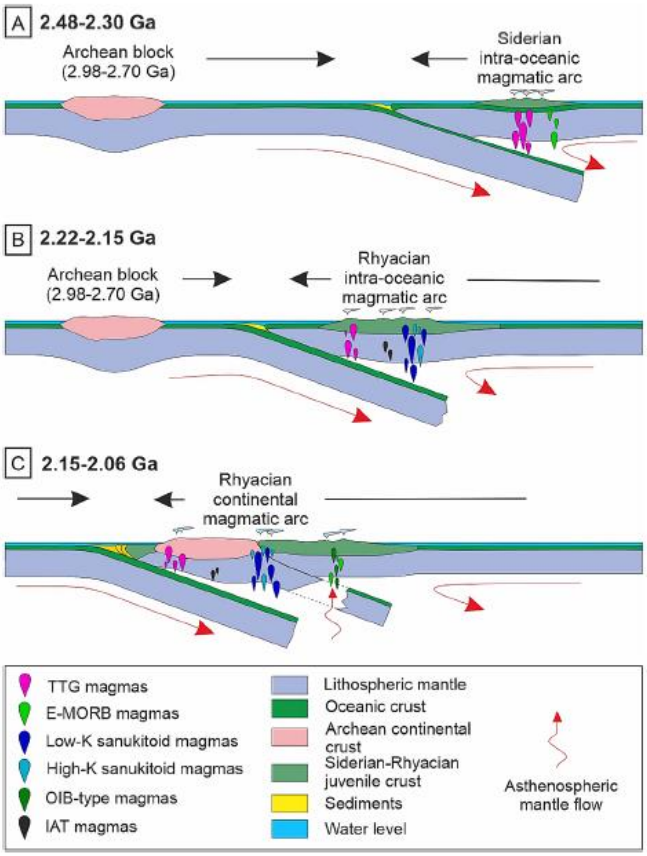

Figure 5-4: Simultaneous production of TTG and various sanukitoid magmas in the Neoarchean Juiz de Fora Complex (from Mauri et al., 2024). The generation of TTGs occurs close to the subduction trench where little to no mantle wedge is present whereas the production of sanukitoid melts occurs further inland from the trench and at higher pressure.

The contribution from (Mauri et al., 2024) has described coeval TTG, granites and sanukitoids occurring in the ca. 2.2-2.0 Ga Juiz de Fora Complex (São Francisco Craton, Brazil) and proposed the partial melting of an oceanic slab (containing basaltic rocks + overlying sediments) at different distances from the trench in an island arc setting (**Figure 5-4**). Partial melts of the slab rocks close to the trench, where little mantle wedge is developed, would generate TTG melts, whereas partial melts of the same rocks at greater distance from the trench (and at greater depth, so likely less fertile than their lower pressure equivalent after significant TTG melt production has occurred) would produce TTG-like melts that interacts with a thick mantle wedge and thus, produce sanukitoids. Hybrid granitoids, enriched in K, would then form during collision of island arcs and recycle isotopically evolved felsic material (like Theespruit felsic volcano-clastic sediments). In contrast with the two previous models, this scenario allows for coeval formation of both TTG and sanukitoids albeit at varying distance from the trench.

In every model of TTG or sanukitoid magma production, variable interaction of these magmas with felsic country rocks during the rise to the surface could explain variable degrees of differentiation, hence potentially explaining the different Sr contents (correlated to whole-rock SiO_2) recorded in each apatite sample of the BGGT (advanced interactions for Schapenburg granodioritic-granitic magma source, limited interactions for Hooggenoeg dioritic magma source).

5.3.3. Merits and drawbacks from all models

The magmatic thickening models of (Smit et al., 2024) and (Rey et al., 2014) requires that TTG and sanukitoid-granitic magmatism happen rapidly with sanukitoid and granites forming rapidly (10-30 Myr) in the case of (Smit et al., 2024) and over a longer timespan of ca. 100 Ma in the case of (Rey et al., 2014). In contrast, the present work documents production of TTGs and other compositionally different magma over an extended period of ca. 300 Ma (between 3.5 to 3.2 Ga see chapter 2), which contradicts the models of (Rey et al., 2014) and (Smit et al., 2024). In contrast, the model of (Mauri et al., 2024) strongly supports coeval generation of compositionally diverse granitoids over long periods of time, i.e. more akin to the duration of Barberton's Paleoarchean history. Additionally, non-uniformitarian models would not fit the structural grain of the Eastern Kaapvaal craton that shows parallel NE-SW orientation of greenstone belts thrust against competent TTG-gneisses which suggests progressive lateral accretion of different tectonic blocks along suture zones (Eglington & Armstrong, 2004; James et al., 2003; Luskin et al., 2019; Poujol, 2001; Schoene et al., 2008). While it is true that most Kaapvaal craton granitoid-greenstone terranes are younger than ca. 3.1 Ga (granitoid ages for Murchison greenstone belt are ca. 2.93-2.67 Ga, Francistown at ca. 2.70-2.65 Ga and Limpopo Central Zone ca. 3.2-2.03 Ga, J.-F. Moyen et al., 2024; Poujol, 2001; Zeh et al., 2009), the involvement of mantle and reworked felsic material in the source of granitoids formed as early as ca. 3.5 Ga favors that this represent an early increment of buoyant lithospheric-mantle formation that propagated to the NW with time (following successive tectonic collage documented by Zeh et al., 2009). Therefore, I argue that the accessory mineral record of the BGGT strongly supports the contribution of varying sources (subducted basaltic rocks producing TTGs, mantle rocks producing sanukitoids, felsic crustal rocks producing granites) to the early stabilization of the Eastern Kaapvaal craton.

5.4. Growth, reworking, recycling and structure of the Paleoarchean continental crust

The existence of K-rich granites at ages as old as ca. 3.5 Ga in the BGGT demonstrates the operation of intra-continental-crust reworking at that time while the existence of sanukitoid-like

magmas testifies to the onset of continental crustal growth through mantle depletion and recycling through subduction of surface material, confirming global $\varepsilon Hf_{(t)}$-in-zircon evolution documented in other studies (Bauer et al., 2020; Drabon et al., 2022; Mulder et al., 2021). This points towards an already differentiated and stable felsic crust at ca. 3.5 Ga and confirms models proposed by (Agangi et al., 2018) for the coeval formation of TTG and K-rich volcanic/plutonic rocks in the Paleoarchean Kaapvaal Craton. Finally, at least part of this Paleoarchean continental crust (i.e. the Stolzburg Terrane) behaved as a cold, mechanically strong block that experienced rapid orogenic thickening during the ca. 3.2 Ga event, followed by rapid extensional collapse and fast exhumation of lower crustal rocks (chapter 4).

Given the fact that clastic sediments mainly sample rocks of the upper crust (Ptáček et al., 2020; Spencer et al., 2022; Taylor et al., 1986; Taylor & McLennan, 1995), the present work suggests, that granites and granodiorite-like-sanukitoids were mostly concentrated in the upper portions of the Paleoarchean continental crust. This particular structural position could explain their removal from the geological record as a result of weathering and erosion (Agangi et al., 2018). This contradicts model of (Smithies et al., 2019) who ascribed the absence of sanukitoids from the upper crustal record before 2.95 Ga to their incapacity to rise through a rheologically ductile continental crust, thus stagnating in the middle crust and mixing with TTG melts. The authors proposed that the rise of sanukitoid magma at the end of the Archean was the result of stabilization of the continental lithosphere and the activation of crustal-scale tectonic breaks, providing migration pathways to the upper crust. Instead, the accessory mineral record, and especially that of detrital apatites, provides evidence for the existence of sanukitoids in the upper crustal, source area of clastic sediments at ages as old as ca. 3.43 Ga. TTGs on the other hand, likely emplaced at mid to lower crustal depth. Besides separate depth of melting discussed in chapter 2, a possible reason for the vertical stratification of the Paleoarchean continental crust into upper crustal granites and granodiorites-sanukitoïds could reside in the density contrasts between granitic-granodioritic suites (D ~ 2.67 g/cm3, see Gomah et al., 2021; Lipman & Bachmann, 2015) and underlying tonalitic rocks (D ~ 2.7-2.9 g/cm3) as is observed in Phanerozoic sub-volcanic batholith like the San Juan Batholith in the Western USA (Lipman & Bachmann, 2015).

5.5. Perspectives

As shown in this thesis, accessory minerals are a powerful tool to investigate the isotopic and chemical characteristics of rocks that are long gone to reworking or recycling. However, while revealing a more diversified Paleoarchean upper continental crust than previously conceived in the context of the BGGT, a few questions are still not fully solved and might benefit from future development on accessory minerals. Three main guidelines for future work are proposed below.

1) Fully assess the genetic link between Moodies sediments and potential Paleoarchean granites down to 3.3-3.2 Ga. Indeed, whereas ca. 3.40-3.55 Ga Moodies sub-chondritic zircons likely derived from granites carrying isotopically similar zircons, the same source-to-sink relationship is still ambiguous for Moodies zircons younger than ca. 3.3 Ga as all zircons from granitic clasts of that age that have been analyzed for Lu-Hf isotopes are supra-chondritic (Agangi et al., 2018). Sure thing, these supra-chondritic granites could represent the source of isotopically similar zircons of Moodies and Fig Tree Groups documented in other studies (Drabon et al., 2024; H. Wang et al., 2022; Zeh et al., 2013) but in the case of the Moodies zircons of the present work, a sub-chondritic component is requested. Possibly, this sub-chondritic, < 3.3 Ga, felsic source might be present in the granitic clasts but not yet identified (besides Sanchez-Garrido, 2012 and Agangi et al., 2018, I am not aware of any other publication that produced Lu-Hf-in-zircons in the ca. 3.3-3.2 Ga Moodies granitic clasts, especially on the ca. 3.2 Ga generation). Therefore, more analytical work is warranted on the Moodies granitic clasts, especially on the younger generation. This could involve zircon Lu-Hf analysis (in addition to U-Pb dating!) as well as apatite trace element profiling to further establish possible differences and resemblances with detrital apatites of Moodies, Hooggenoeg and Schapenburg samples
2) Testing the premise that Paleoarchean sanukitoids and granites crystallized at shallow levels in the upper crust before sourcing clastic sediments would require to look into pressure-sensitive minerals or fluid inclusions trapped in minerals from the Moodies granitic clasts. Due to CO_2's higher solubility in silicic melts at higher pressures (Hansteen & Klügel, 2008), finding CO_2-

poor fluid inclusions in Moodies granitic quartz for example would strongly support an emplacement of Paleoarchean granites close within a few kbar of the surface. Finding CO_2-rich fluid inclusions in quartz crystallized in BTTGs would further support their emplacement at deeper level than granites.

3) A key question raised in this work is that of the cooling rate achieved by Archean mid-to-lower crustal rocks which, following rutile data described in chapter 4, might approximate those encountered during the latest stages of exhumation of Phanerozoic metamorphic core complexes. (Mühlberg et al., 2021) conducted an extensive work on apatites of the Stolzburg pluton and identified the non-resetting of the U-Pb clock in apatite cores during the main metamorphic event of the BGGT at ca. 3.2 Ga. However, actual cooling rates experienced by the pluton after peak metamorphic conditions are still not fully quantified and would likely benefit from a more detailed study of apatite's geochronological systems in the TTGs, i.e. Sm-Nd, Lu-Hf and U-Pb, all having different closure temperatures from > 700°C to < 500°C (Cherniak, 2000, 2010; Cherniak et al., 1991; Cherniak & Ryerson, 1993; Chew & Spikings, 2015, 2021; Gillespie et al., 2022) thus covering the range of maximum temperatures recorded by rocks of the Stolzburg Terrane. In addition to this, other thermo-chronometric systems such as Rb-Sr-in-biotite (a mineral that is abundant in TTGs, see J.-F. Moyen, 2011; J.-F. Moyen et al., 2007) or U-Pb-in-titanite would help strengthen the thermal history and calculation of cooling rates (building up on data from Kamo & Davis, 1994; Schoene et al., 2008). To determine whether the cooling rates calculated from a single sample of metamorphic rutile has regional application, I could apply this procedure to both felsic schists and intruding trondhjemitic samples of Stolzburg from locations close to the Komati River fault to the center of the pluton and thereby answer the question of the representativity of cooling rates calculated only in one spot (cf chapter 4).

References

Agangi, A., Hofmann, A., & Elburg, M. A. (2018). A review of Palaeoarchaean felsic volcanism in the eastern Kaapvaal craton : Linking plutonic and volcanic records. *Geoscience Frontiers*, *9*(3), 667-688.

Anhaeusser, C. R. (1981). Geotectonic evolution of the Archaean successions in the Barberton Mountain land, South Africa. In *Developments in Precambrian Geology* (Vol. 4, p. 137-160). Elsevier. https://www.sciencedirect.com/science/article/pii/S0166263508700112

Anhaeusser, C. R. (2014). Archaean greenstone belts and associated granitic rocks–a review. *Journal of African Earth Sciences*, *100*, 684-732.

Bauer, A. M., Reimink, J. R., Chacko, T., Foley, B. J., Shirey, S. B., & Pearson, D. G. (2020). Hafnium isotopes in zircons document the gradual onset of mobile-lid tectonics. *Geochemical Perspectives Letters*, *14*, 1-6.

Bédard, J. H. (2006). A catalytic delamination-driven model for coupled genesis of Archaean crust and sub-continental lithospheric mantle. *Geochimica et Cosmochimica Acta*, *70*(5), 1188-1214. https://doi.org/10.1016/j.gca.2005.11.008

Bédard, J. H. (2018). Stagnant lids and mantle overturns : Implications for Archaean tectonics, magmagenesis, crustal growth, mantle evolution, and the start of plate tectonics. *Geoscience Frontiers*, *9*(1), 19-49.

Bédard, L. P. (1996). Archean high-Mg quartz-monzodiorite suite : A re-evaluation of the parental magma and differentiation. *The Journal of Geology*, *104*(6), 713-728.

Belousova, E. A., Griffin, W. L., O'Reilly, S. Y., & Fisher, N. I. (2002). Apatite as an indicator mineral for mineral exploration : Trace-element compositions and their relationship to host rock type. *Journal of Geochemical Exploration*, *76*(1), 45-69.

Belousova, E. A., Walters, S., Griffin, W. L., & O'Reilly, S. Y. (2001). Trace-element signatures of apatites in granitoids from the Mt Isa Inlier, northwestern Queensland. *Australian Journal of Earth Sciences*, *48*(4), 603-619. https://doi.org/10.1046/j.1440-0952.2001.00879.x

Bibikova, E. V., Petrova, A., & Claesson, S. (2005). The temporal evolution of sanukitoids in the Karelian Craton, Baltic Shield : An ion microprobe U–Th–Pb isotopic study of zircons. *Lithos*, *79*(1-2), 129-145.

Bruand, E., Fowler, M., Storey, C., & Darling, J. (2017). Apatite trace element and isotope applications to petrogenesis and provenance. *American Mineralogist*, *102*(1), 75-84. https://doi.org/10.2138/am-2017-5744

Bruand, E., Storey, C., & Fowler, M. (2016). An apatite for progress : Inclusions in zircon and titanite constrain petrogenesis and provenance. *Geology*, *44*(2), 91-94.

Cassidy, K. F., Champion, D. C., & Smithies, R. H. (2006). Origin of Archean late potassic granites : Evidence from the Yilgarn and Pilbara cratons. *Geochimica et Cosmochimica Acta Supplement*, *70*(18), A88-A88.

Castro, A. (2020). *The dual origin of I-type granites : The contribution from experiments*. https://pubs.geoscienceworld.org/books/edited-volume/2289/chapter/127762777

Champion, D. C., & Smithies, R. H. (2001). Archaean granites of the Yilgarn and Pilbara cratons, Western Australia. *KF Cassidy, JM Dunphy and MJ Van Kranendonk (Eds.)*, *4*, 134-136.

Chappell, B. W., Bryant, C. J., & Wyborn, D. (2012). Peraluminous I-type granites. *Lithos*, *153*, 142-153. https://doi.org/10.1016/j.lithos.2012.07.008

Chappell, B. W., & Stephens, W. E. (1988). Origin of infracrustal (I-type) granite magmas. *Earth and Environmental Science Transactions of the Royal Society of Edinburgh*, *79*(2-3), 71-86.

Chappell, B. W., & White, A. J. R. (1992). I- and S-type granites in the Lachlan Fold Belt. *Earth and Environmental Science Transactions of The Royal Society of Edinburgh*, *83*(1-2), 1-26. https://doi.org/10.1017/S0263593300007720

Cherniak, D. J. (2000). Rare earth element diffusion in apatite. *Geochimica et Cosmochimica Acta*, *64*(22), 3871-3885.

Cherniak, D. J. (2010). Diffusion in accessory minerals : Zircon, titanite, apatite, monazite and xenotime. *Reviews in mineralogy and geochemistry*, *72*(1), 827-869.

Cherniak, D. J., Lanford, W. A., & Ryerson, F. J. (1991). Lead diffusion in apatite and zircon using ion implantation and Rutherford backscattering techniques. *Geochimica et cosmochimica acta*, *55*(6), 1663-1673.

Cherniak, D. J., & Ryerson, F. J. (1993). A study of strontium diffusion in apatite using Rutherford backscattering spectroscopy and ion implantation. *Geochimica et Cosmochimica Acta*, *57*(19), 4653-4662.

Chew, D. M., & Spikings, R. A. (2015). Geochronology and thermochronology using apatite : Time and temperature, lower crust to surface. *Elements*, *11*(3), 189-194.

Chew, D. M., & Spikings, R. A. (2021). Apatite U-Pb Thermochronology : A Review. *Minerals*, *11*(10), Article 10. https://doi.org/10.3390/min11101095

Chu, M.-F., Wang, K.-L., Griffin, W. L., Chung, S.-L., O'Reilly, S. Y., Pearson, N. J., & Iizuka, Y. (2009). Apatite composition : Tracing petrogenetic processes in Transhimalayan granitoids. *Journal of Petrology*, *50*(10), 1829-1855.

Clemens, J. D., Stevens, G., & Farina, F. (2011). The enigmatic sources of I-type granites : The peritectic connexion. *Lithos*, *126*(3), 174-181. https://doi.org/10.1016/j.lithos.2011.07.004

Drabon, N., Byerly, B. L., Byerly, G. R., Wooden, J. L., Wiedenbeck, M., Valley, J. W., Kitajima, K., Bauer, A. M., & Lowe, D. R. (2022). Destabilization of Long-Lived Hadean Protocrust and the Onset of Pervasive Hydrous Melting at 3.8 Ga. *AGU Advances*, *3*(2), e2021AV000520. https://doi.org/10.1029/2021AV000520

Drabon, N., Kirkpatrick, H. M., Byerly, G. R., & Wooden, J. L. (2024). Trace elements in zircon record changing magmatic processes and the multi-stage build-up of Archean proto-continental crust. *Geochimica et Cosmochimica Acta*, *373*, 136-150.

Eglington, B. M., & Armstrong, R. A. (2004). The Kaapvaal Craton and adjacent orogens, southern Africa : A geochronological database and overview of the geological development of the craton. *South African Journal of Geology*, *107*(1-2), 13-32.

Fisher, C. M., Vervoort, J. D., & Hanchar, J. M. (2014). Guidelines for reporting zircon Hf isotopic data by LA-MC-ICPMS and potential pitfalls in the interpretation of these data. *Chemical geology*, *363*, 125-133.

Fowler, M., & Rollinson, H. (2012). Phanerozoic sanukitoids from Caledonian Scotland : Implications for Archean subduction. *Geology*, *40*(12), 1079-1082.

Gillespie, J., Kirkland, C. L., Kinny, P. D., Simpson, A., Glorie, S., & Rankenburg, K. (2022). Lu–Hf, Sm–Nd, and U–Pb isotopic coupling and decoupling in apatite. *Geochimica et Cosmochimica Acta*, *338*, 121-135.

Gomah, M. E., Li, G., Bader, S., Elkarmoty, M., & Ismael, M. (2021). Damage Evolution of Granodiorite after Heating and Cooling Treatments. *Minerals*, *11*(7), 779. https://doi.org/10.3390/min11070779

Grimes, C. B., Wooden, J. L., Cheadle, M. J., & John, B. E. (2015). "Fingerprinting" tectono-magmatic provenance using trace elements in igneous zircon. *Contributions to Mineralogy and Petrology*, *170*(5-6), 46. https://doi.org/10.1007/s00410-015-1199-3

Halla, J. (2005). Late Archean high-Mg granitoids (sanukitoids) in the southern Karelian domain, eastern Finland : Pb and Nd isotopic constraints on crust- mantle interactions. *Lithos*, *79*(1-2), 161-178.

Hansteen, T. H., & Klügel, A. (2008). Fluid Inclusion Thermobarometry as a Tracer for Magmatic Processes. *Reviews in Mineralogy and Geochemistry*, *69*(1), 143-177. https://doi.org/10.2138/rmg.2008.69.5

Hoskin, P. W., & Schaltegger, U. (2003). The composition of zircon and igneous and metamorphic petrogenesis. *Reviews in mineralogy and geochemistry*, *53*(1), 27-62.

James, D. E., Niu, F., & Rokosky, J. (2003). Crustal structure of the Kaapvaal craton and its significance for early crustal evolution. *Lithos*, *71*(2-4), 413-429.

Jayananda, M., Aadhiseshan, K. R., Kusiak, M. A., Wilde, S. A., Sekhamo, K., Guitreau, M., Santosh, M., & Gireesh, R. V. (2020). Multi-stage crustal growth and Neoarchean geodynamics in the Eastern Dharwar Craton, southern India. *Gondwana Research*, *78*, 228-260.

Jayananda, M., Chardon, D., Peucat, J.-J., & Capdevila, R. (2006). 2.61 Ga potassic granites and crustal reworking in the western Dharwar craton, southern India : Tectonic, geochronologic and geochemical constraints. *Precambrian Research*, *150*(1), 1-26. https://doi.org/10.1016/j.precamres.2006.05.004

Jayananda, M., Martin, H., Peucat, J.-J., & Mahabaleswar, B. (1995). Late Archaean crust-mantle interactions : Geochemistry of LREE-enriched mantle derived magmas. Example of the Closepet batholith, southern India. *Contributions to Mineralogy and Petrology*, *119*(2), 314-329. https://doi.org/10.1007/BF00307290

Jayananda, M., Santosh, M., & Aadhiseshan, K. R. (2018). Formation of Archean (3600–2500 Ma) continental crust in the Dharwar Craton, southern India. *Earth-Science Reviews*, *181*, 12-42.

Jiang, N., Guo, J., Fan, W., Hu, J., Zong, K., & Zhang, S. (2016). Archean TTGs and sanukitoids from the Jiaobei terrain, North China craton : Insights into crustal growth and mantle metasomatism. *Precambrian Research*, *281*, 656-672.

Kamo, S. L., & Davis, D. W. (1994). Reassessment of Archean crustal development in the Barberton Mountain Land, South Africa, based on U-Pb dating. *Tectonics*, *13*(1), 167-192. https://doi.org/10.1029/93TC02254

Kendall-Langley, L. A., Kemp, A. I. S., Hawkesworth, C. J., Craven, J., Talavera, C., Hinton, R., Roberts, M. P., & EIMF. (2021). Quantifying F and Cl concentrations in granitic melts from apatite inclusions in zircon. *Contributions to Mineralogy and Petrology*, *176*(7), 58. https://doi.org/10.1007/s00410-021-01813-5

Kieffer, M. A., Dare, S. A., & Gendron, M. (2024). Trace element discrimination diagrams to identify igneous apatite from I-, S-and A-type granites and mafic intrusions : Implications for provenance studies and mineral exploration. *Chemical Geology*, *649*, 121965.

Laurent, O., Martin, H., Doucelance, R., Moyen, J.-F., & Paquette, J.-L. (2011). Geochemistry and petrogenesis of high-K "sanukitoids" from the Bulai pluton, Central Limpopo Belt, South Africa : Implications for geodynamic changes at the Archaean–Proterozoic boundary. *Lithos*, *123*(1-4), 73-91.

Laurent, O., Martin, H., Moyen, J.-F., & Doucelance, R. (2013). *Geochemical diversity of late-Archaean Mg-K-rich mafic magmas (sanukitoids) and its implication for metasomatic processes between silicate melts and mantle peridotite*. EGU2013-2114. https://ui.adsabs.harvard.edu/abs/2013EGUGA..15.2114L

Laurent, O., Martin, H., Moyen, J.-F., & Doucelance, R. (2014). The diversity and evolution of late-Archean granitoids : Evidence for the onset of "modern-style" plate tectonics between 3.0 and 2.5 Ga. *Lithos*, *205*, 208-235.

Lipman, P. W., & Bachmann, O. (2015). Ignimbrites to batholiths : Integrating perspectives from geological, geophysical, and geochronological data. *Geosphere*, *11*(3), 705-743. https://doi.org/10.1130/GES01091.1

Luskin, C., Wilson, A., Gold, D., & Hofmann, A. (2019). The Pongola Supergroup : Mesoarchaean Deposition Following Kaapvaal Craton Stabilization. In A. Kröner & A. Hofmann (Éds.), *The Archaean Geology of the Kaapvaal Craton, Southern Africa* (p. 225-254). Springer International Publishing. https://doi.org/10.1007/978-3-319-78652-0_9

Mauri, S., Heilbron, M., Bruno, H., Bersan, S., Almeida, R., de Abreu Marques, R., Lacerda, S., Marra de Souza, A., Paravidini, G., Neto, C., de Morisson Valeriano, C., Chapman, G., Fowler, M., Mottram, C., Strachan, R., & Storey, C. (2024). Coeval TTG and sanukitoid magmatism during the Rhyacian tectonic evolution of the Juiz de Fora Complex (São Francisco Paleocontinent, SE-Brazil). *Precambrian Research*, *414*, 107585. https://doi.org/10.1016/j.precamres.2024.107585

McLaren, S., & Powell, R. (2014). Magmatism, orogeny and the origin of high-heat-producing granites in Australian Proterozoic terranes. *Journal of the Geological Society*, *171*(2), 149-152. https://doi.org/10.1144/jgs2013-040

Moyen, J. F., Zeh, A., Cuney, M., Dziggel, A., & Carrouée, S. (2021). The multiple ways of recycling Archaean crust : A case study from the ca. 3.1 Ga granitoids from the Barberton Greenstone Belt, South Africa. *Precambrian Research*, *353*, 105998.

Moyen, J.-F. (2011). The composite Archaean grey gneisses : Petrological significance, and evidence for a non-unique tectonic setting for Archaean crustal growth. *Lithos*, *123*(1-4), 21-36.

Moyen, J.-F., Laurent, O., Chelle-Michou, C., Couzinié, S., Vanderhaeghe, O., Zeh, A., Villaros, A., & Gardien, V. (2017). Collision vs. subduction-related magmatism : Two contrasting ways of granite formation and implications for crustal growth. *Lithos*, *277*, 154-177. https://doi.org/10.1016/j.lithos.2016.09.018

Moyen, J.-F., Martin, H., Jayananda, M., & Auvray, B. (2003). Late Archaean granites : A typology based on the Dharwar Craton (India). *Precambrian Research*, *127*(1-3), 103-123.

Moyen, J.-F., Stevens, G., Kisters, A. F., & Belcher, R. W. (2007). TTG plutons of the Barberton granitoid-greenstone terrain, South Africa. *Developments in Precambrian Geology*, *15*, 607-667.

Moyen, J.-F., Vezinet, A., Guitreau, M., Chauvet, A., Paquette, J.-L., Stevens, G., & Bruand, E. (2024, septembre). Long term melt-generation in the Archaean crust : A case study from the Northern Kaapvaal craton, South Africa. *Granulites & Granulites 2024*. https://hal.science/hal-04714679

Mühlberg, M., Stevens, G., Moyen, J.-F., Kisters, A. F., & Lana, C. (2021). Thermal evolution of the Stolzburg Block, Barberton granitoid-greenstone terrain, South Africa : Implications for Paleoarchean tectonic processes. *Precambrian Research*, *359*, 106082.

Mulder, J. A., Nebel, O., Gardiner, N. J., Cawood, P. A., Wainwright, A. N., & Ivanic, T. J. (2021). Crustal rejuvenation stabilised Earth's first cratons. *Nature Communications*, *12*(1), 3535.

O'Sullivan, G., Chew, D., Kenny, G., Henrichs, I., & Mulligan, D. (2020). The trace element composition of apatite and its application to detrital provenance studies. *Earth-Science Reviews*, *201*, 103044.

Pankhurst, R. J., Rapela, C. W., & Fanning, C. M. (2000). Age and origin of coeval TTG, I- and S-type granites in the Famatinian belt of NW Argentina. *Earth and Environmental Science Transactions of The Royal Society of Edinburgh*, *91*(1-2), 151-168. https://doi.org/10.1017/S0263593300007343

Poujol, M. (2001). U-Pb isotopic evidence for episodic granitoid emplacement in the Murchison greenstone belt, South Africa. *Journal of African Earth Sciences*, *33*(1), 155-163. https://doi.org/10.1016/S0899-5362(01)90096-X

Ptáček, M. P., Dauphas, N., & Greber, N. D. (2020). Chemical evolution of the continental crust from a data-driven inversion of terrigenous sediment compositions. *Earth and Planetary Science Letters*, *539*, 116090.

Rapela, C. W., Pankhurst, R. J., Casquet, C., Dahlquist, J. A., Mark Fanning, C., Baldo, E. G., Galindo, C., Alasino, P. H., Ramacciotti, C. D., Verdecchia, S. O., Murra, J. A., & Basei, M. A. S. (2018). A review of the Famatinian Ordovician magmatism in southern South America : Evidence of lithosphere reworking and continental subduction in the early proto-Andean margin of Gondwana. *Earth-Science Reviews*, *187*, 259-285. https://doi.org/10.1016/j.earscirev.2018.10.006

Rey, P. F., Coltice, N., & Flament, N. (2014). Spreading continents kick-started plate tectonics. *Nature*, *513*(7518), 405-408. https://doi.org/10.1038/nature13728

Sanchez-Garrido, C. J. (2012). *The petrogenesis of the older (> 3.0 Ga) potassic granitoids of eastern Mpumalanga (South Africa) and Swaziland : An investigation of crustal formation processes in the early Earth* [PhD Thesis, Stellenbosch: Stellenbosch University]. https://scholar.sun.ac.za/handle/10019.1/20044

Sanchez-Garrido, C. J., Stevens, G., Armstrong, R. A., Moyen, J.-F., Martin, H., & Doucelance, R. (2011). Diversity in Earth's early felsic crust : Paleoarchean peraluminous granites of the Barberton Greenstone Belt. *Geology*, *39*(10), 963-966.

Schoene, B., De Wit, M. J., & Bowring, S. A. (2008). Mesoarchean assembly and stabilization of the eastern Kaapvaal craton : A structural-thermochronological perspective. *Tectonics*, *27*(5), 2008TC002267. https://doi.org/10.1029/2008TC002267

Shirey, S. B., & Hanson, G. N. (1984). Mantle-derived Archaean monozodiorites and trachyandesites. *Nature*, *310*(5974), 222-224.

Smit, M. A., Musiyachenko, K. A., & Goumans, J. (2024). Archaean continental crust formed from mafic cumulates. *Nature Communications*, *15*(1), 692. https://doi.org/10.1038/s41467-024-44849-4

Smithies, R. H., Lu, Y., Johnson, T. E., Kirkland, C. L., Cassidy, K. F., Champion, D. C., Mole, D. R., Zibra, I., Gessner, K., Sapkota, J., De Paoli, M. C., & Poujol, M. (2019). No evidence for high-pressure melting of Earth's crust in the Archean. *Nature Communications*, *10*(1), 5559. https://doi.org/10.1038/s41467-019-13547-x

Spencer, C. J., Cavosie, A. J., Morrell, T. R., Lu, G. M., Liebmann, J., & Roberts, N. M. W. (2022). Disparities in oxygen isotopes of detrital and igneous zircon identify erosional bias in crustal rock record. *Earth and Planetary Science Letters*, *577*, 117248. https://doi.org/10.1016/j.epsl.2021.117248

Spencer, C. J., Kirkland, C. L., Roberts, N. M. W., Evans, N. J., & Liebmann, J. (2020). Strategies towards robust interpretations of in situ zircon Lu–Hf isotope analyses. *Geoscience Frontiers*, *11*(3), 843-853.

Stern, R. A., Hanson, G. N., & Shirey, S. B. (1989). Petrogenesis of mantle-derived, LILE-enriched Archean monzodiorites and trachyandesites (sanukitoids) in southwestern Superior Province. *Canadian Journal of Earth Sciences*, *26*(9), 1688-1712.

Stevens, G., Villaros, A., & Moyen, J.-F. (2007). Selective peritectic garnet entrainment as the origin of geochemical diversity in S-type granites. *Geology*, *35*(1), 9-12. https://doi.org/10.1130/G22959A.1

Taylor, S. R., & McLennan, S. M. (1995). The geochemical evolution of the continental crust. *Reviews of Geophysics*, *33*(2), 241-265. https://doi.org/10.1029/95RG00262

Taylor, S. R., Rudnick, R. L., McLennan, S. M., & Eriksson, K. A. (1986). Rare earth element patterns in Archean high-grade metasediments and their tectonic significance. *Geochimica et Cosmochimica Acta*, *50*(10), 2267-2279. https://doi.org/10.1016/0016-7037(86)90081-5

Wang, H., Yang, J.-H., Zhu, Y.-S., Huang, C., Xu, L., Wu, S.-T., & Liu, Y. (2022). Archean crustal growth and reworking revealed by combined U-Pb-Hf-O isotope and trace element data of detrital zircons from ancient and modern river sediments of the eastern Kaapvaal Craton. *Geochimica et Cosmochimica Acta*, *320*, 79-104.

Wang, Y., Zhang, Y., Zhao, G., Fan, W., Xia, X., Zhang, F., & Zhang, A. (2009). Zircon U–Pb geochronological and geochemical constraints on the petrogenesis of the Taishan sanukitoids (Shandong) : Implications for Neoarchean subduction in the Eastern Block, North China Craton. *Precambrian Research*, *174*(3-4), 273-286.

Zeh, A., Gerdes, A., & Barton Jr, J. M. (2009). Archean accretion and crustal evolution of the Kalahari Craton—The zircon age and Hf isotope record of granitic rocks from Barberton/Swaziland to the Francistown Arc. *Journal of Petrology*, *50*(5), 933-966.

Zeh, A., Gerdes, A., & Heubeck, C. (2013). U–Pb and Hf isotope data of detrital zircons from the Barberton Greenstone Belt : Constraints on provenance and Archaean crustal evolution. *Journal of the Geological Society*, *170*(1), 215-223.

6. Chapter 6 : Appendix

The supplementary materials for all three research manuscripts are available at the following link (please copy and paste in your favorite web browser in case the link does not work):

https://1drv.ms/f/c/b7e037edab15e973/IgD7eLE_HU9RSpmdxkw3-4aQAStaK0BjxJAb10GRkI86gGQ?e=eo8FgC

These contain:

1) MS Excel tables (with the full datatsets + metadata on standards utilized, LA-ICP-MS, SIMS, MC-ICP-MS analytical conditions, etc.).
2) PDF and PWP files with images of the grains analyzed with positions of the spots.
3) Additional information on either analytical conditions (chapter 2) or discussion on closure temperature for Pb diffusion in rutile (chapter 4).